

AD 741491

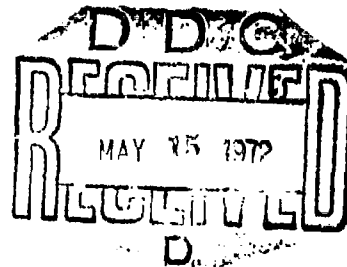
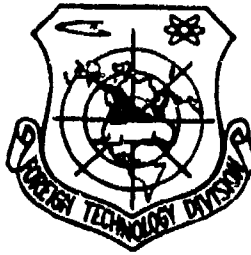
FOREIGN TECHNOLOGY DIVISION



TURBULENCE IN FREE ATMOSPHERE

by

N. K. Vinnichenko, N. Z. Pinus, et al.



Approved for public release;
Distribution unlimited.

Reproduced by
**NATIONAL TECHNICAL
INFORMATION SERVICE**
Springfield, Va. 22151

392

7

UNCLASSIFIED

Security Classification

DOCUMENT CONTROL DATA - R & D

(Security classification of title, body of abstract and included annotation must be entered when the overall report is classified)

1. ORIGINATING ACTIVITY (Corporate author) Foreign Technology Division Air Force Systems Command U. S. Air Force		2a. REPORT SECURITY CLASSIFICATION UNCLASSIFIED	
3. REPORT TITLE TURBULENCE IN FREE ATMOSPHERE		2b. GROUP	
4. DESCRIPTIVE NOTES (Type of report and inclusive dates) Translation			
5. AUTHOR(S) (First name, middle initial, last name) Vinnichenko, N. K. ; Pinus, N. Z. ; Shmeter, S. M. ; Shur, G. N.			
6. REPORT DATE 1968	7a. TOTAL NO. OF PAGES 380	7b. NO. OF REFS	
8. CONTRACT OR GRANT NO.	9c. ORIGINATOR'S REPORT NUMBER(S) FTD-MT-24-939-71		
9. PROJECT NO. 682E	9d. OTHER REPORT NUMBER(S) (Any other numbers that may be assigned this report)		
10. DISTRIBUTION STATEMENT Approved for public release; distribution unlimited.			
11. SUPPLEMENTARY NOTES		12. SPONSORING MILITARY ACTIVITY Foreign Technology Division Wright-Patterson AFB, Ohio	
13. ABSTRACT This monograph is concerned mainly with outlining the results of experimental investigations. Along with these, the authors discuss those questions in the theory of turbulence without which physical analysis of the presented data is difficult. The book also contains a description of instruments for measuring various parameters of turbulence in the free atmosphere. Since the majority of the instruments used in scientific research work undergo rapid modification, the authors did not feel it advisable to describe their construction in detail and limited themselves merely to outlining the physical principles of instrument operation and the functional diagrams required for an understanding of their operation. Aircraft methods of investigating turbulence are described in the greatest detail, since the overwhelming majority of experimental data were obtained in this manner.			

DD FORM 1 NOV 61 1473

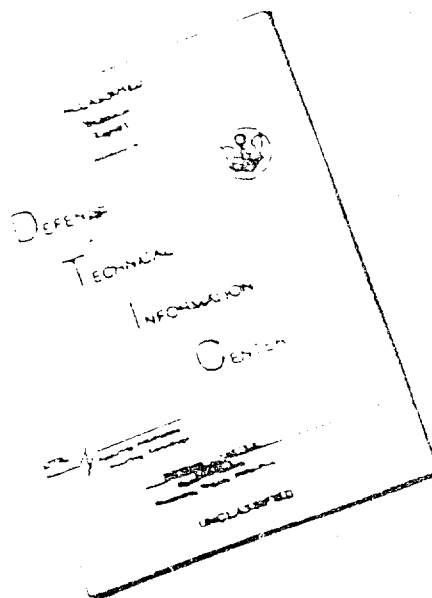
UNCLASSIFIED
Security Classification

UNCLASSIFIED
Security Classification

14. KEY WORDS	LINK A		LINK B		LINK C	
	ROLE	WT	ROLE	WT	ROLE	WT
Free Atmosphere Atmospheric Turbulence Storm Wind Velocity Atmospheric Density Atmospheric Physics Atmosphere Composition						

UNCLASSIFIED
Security Classification

DISCLAIMER NOTICE



THIS DOCUMENT IS BEST
QUALITY AVAILABLE. THE COPY
FURNISHED TO DTIC CONTAINED
A SIGNIFICANT NUMBER OF
PAGES WHICH DO NOT
REPRODUCE LEGIBLY.

REPRODUCED FROM
BEST AVAILABLE COPY

EDITED MACHINE TRANSLATION

TURBULENCE IN FREE ATMOSPHERE

By: N. K. Vinnichenko, N. Z. Pinus, et al.

English pages: 380

Source: Turbulentnost' v Svobodnoy Atmosfere,
Izd-vo Gidrometeorologicheskoye,
Leningrad, 1968, pp. 1-336.

This document is a SYSTRAN machine aided translation, post-edited for technical accuracy by: Dean Koolbeck.

Reproduced from
best available copy.

Approved for public release;
distribution unlimited.

UR/0000-68-000-000

THIS TRANSLATION IS A RENDITION OF THE ORIGINAL FOREIGN TEXT WITHOUT ANY ANALYTICAL OR EDITORIAL COMMENT. STATEMENTS OR THEORIES ADVOCATED OR IMPLIED ARE THOSE OF THE SOURCE AND DO NOT NECESSARILY REFLECT THE POSITION OR OPINION OF THE FOREIGN TECHNOLOGY DIVISION.

PREPARED BY:

TRANSLATION DIVISION
FOREIGN TECHNOLOGY DIVISION
WP-AFB, OHIO.

FTD-MT-24-939-71

Date 11 Feb. 1972

TABLE OF CONTENTS

U.S. Board on Geographic Names Transliteration System-----	iv
Designations of the Trigonometric Functions-----	v
Foreword-----	vi
Chapter 1. Some Questions of the Theory of Atmospheric Turbulence-----	1
§ 1. The Nature of Atmospheric Turbulence-----	1
§ 2. Structure and Energy Considerations of a Turbulent Flow-----	10
§ 3. Statistical Description of the Field of Turbulence-----	14
§ 4. Energy Spectrum of Turbulence-----	22
§ 5. Interaction of Averaged and Turbulent Fields of Temperature and Wind Velocity-----	28
Chapter 2. Methods of Experimental Investigation of Turbulence in the Free Atmosphere-----	33
§ 1. Aircraft Methods of Investigating Atmospheric Turbulence-----	33
§ 2. Radiosonde Method of Studying Atmospheric Turbulence-----	81
§ 3. Radar Methods of Studying Atmospheric Turbulence--	85
Chapter 3. Statistical Analysis of Measurements-----	89
§ 1. Calculation of Spectra From Continuous Recordings of Finite Length-----	90
§ 2. Calculation of Spectra According to Point Equidistant Recordings of Finite Length with the Use of Autocorrelation Functions-----	103
§ 3. Calculation of Spectra From Point Equidistant Recordings of Finite Length Using Mathematical Filters-----	118
§ 4. Instruments for Statistical Processing-----	129
Chapter 4. Spectral Structure of the Turbulence Field-----	140
§ 1. Spectral Characteristics of Turbulence at Low Altitudes-----	140

§ 2.	Intermittence of Turbulence. Spectrum of the External Boundary of Turbulized Layers of the Atmosphere-----	154
§ 3.	Spectrum of Turbulence in a Thermally Stratified Atmosphere-----	159
§ 4.	Transfer of Energy in the Spectrum and Generalized Spectrum of Turbulence of the Free Atmosphere-----	172
§ 5.	Some Particular Features of Experimental Spectra of Turbulence in Clear Air-----	182
§ 6.	Some Experimental Data on The Intensity of Turbulence at High Altitudes-----	184
Chapter 5.	Atmospheric Convection and Thermal Turbulence----	191
§ 1.	Disordered Atmospheric Convection-----	192
§ 2.	Cellular Convection-----	207
Chapter 6.	Waves and Atmospheric Turbulence-----	214
§ 1.	Gravitational-Shear Waves-----	215
§ 2.	Criteria of the Stability of Internal Gravitational-Shear Waves and the Connection of Turbulence with Degenerating Waves-----	232
§ 3.	Mountain Waves-----	236
Chapter 7.	Turbulence Which Influences Aircraft Flight-----	260
§ 1.	Methods of Evaluating the Intensity of Turbulence Which Influences the Flight of an Aircraft-----	260
§ 2.	Characteristics of Turbulence in the Troposphere and in the Lower Stratosphere-----	270
§ 3.	Turbulence in Jet Flow and in the Tropopause Zone-----	285
§ 4.	Connection of Turbulence Affecting Aircraft with Thermal and Dynamic Conditions in the Atmosphere--	298
Chapter 8.	Turbulence in Clouds-----	311
§ 1.	Turbulence in Stratiform Clouds-----	311
§ 2.	Turbulence in Cumuliform Clouds-----	319

Chapter 9. Local Structure of the Wind Velocity Field-----	346
§ 1. Local Heterogeneity of the Wind Velocity Field----	346
§ 2. Energy Spectra of Mesoscalar Turbulence-----	350
§ 3. Vertical Distributions of Wind Gusts and Their Spectra-----	354
§ 4. On the Local Meteorological Minimum of Energy in the Turbulence Spectrum-----	358

U. S. BOARD ON GEOGRAPHIC NAMES TRANSLITERATION SYSTEM

Block	Italic	Transliteration	Block	Italic	Transliteration
А а	<i>А а</i>	A, a	Р р	<i>Р р</i>	R, r
Б б	<i>Б б</i>	B, b	С с	<i>С с</i>	S, s
В в	<i>В в</i>	V, v	Т т	<i>Т т</i>	T, t
Г г	<i>Г г</i>	G, g	У у	<i>У у</i>	U, u
Д д	<i>Д д</i>	D, d	Ф ф	<i>Ф ф</i>	F, f
Е е	<i>Е е</i>	Ye, ye; E, e*	Х х	<i>Х х</i>	Kh, kh
Ж ж	<i>Ж ж</i>	Zh, zh	Ц ц	<i>Ц ц</i>	Ts, ts
З з	<i>З з</i>	Z, z	Ч ч	<i>Ч ч</i>	Ch, ch
И и	<i>И и</i>	I, i	Ш ш	<i>Ш ш</i>	Sh, sh
Й й	<i>Й й</i>	Y, y	Щ щ	<i>Щ щ</i>	Shch, shch
К к	<i>К к</i>	K, k	Ъ ъ	<i>Ъ ъ</i>	"
Л л	<i>Л л</i>	L, l	Ы ы	<i>Ы ы</i>	Y, y
М м	<i>М м</i>	M, m	Ь ь	<i>Ь ь</i>	'
Н н	<i>Н н</i>	N, n	Э э	<i>Э э</i>	E, e
О о	<i>О о</i>	O, o	Ю ю	<i>Ю ю</i>	Yu, yu
П п	<i>П п</i>	P, p	Я я	<i>Я я</i>	Ya, ya

* ye initially, after vowels, and after ъ, ь; e elsewhere.
 When written as ѐ in Russian, transliterate as yĕ or ĕ.
 The use of diacritical marks is preferred, but such marks
 may be omitted when expediency dictates.

FOLLOWING ARE THE CORRESPONDING RUSSIAN AND ENGLISH
DESIGNATIONS OF THE TRIGONOMETRIC FUNCTIONS

Russian	English
sin	sin
cos	cos
tg	tan
ctg	cot
sec	sec
cosec	csc
sh	sinh
ch	cosh
th	tanh
cth	coth
sch	sech
csch	csch
arc sin	sin ⁻¹
arc cos	cos ⁻¹
arc tg	tan ⁻¹
arc ctg	cot ⁻¹
arc sec	sec ⁻¹
arc cosec	csc ⁻¹
arc sh	sinh ⁻¹
arc ch	cosh ⁻¹
arc th	tanh ⁻¹
arc cth	coth ⁻¹
arc sch	sech ⁻¹
arc csch	csch ⁻¹
—	
rot	curl
lg	log

FOREWORD

Turbulence - chaotic disordered motion of volumes of air on radically different scales - is one of the characteristic properties of atmospheric air flows, and its study is necessary for solution of a number of theoretical and applied problems. Knowledge of the characteristics of turbulence at least over the entire troposphere and stratosphere is of great significance for many practical purposes. However, until recently experimental difficulties confined the study of turbulence mainly to the lower portion of the planetary boundary layer. Naturally, theoretical studies were also mainly based on these data.

The rapid development of aviation and the numerous cases of aircraft finding themselves in dangerous turbulent zones which have been observed in recent years made it necessary to take measures to sharply intensify study of the turbulence first in the atmospheric layer up to 10-12 km, and subsequently at greater altitudes. In the initial period such studies were limited to obtaining the simplest characteristics of the recurrence of gusts with different velocities and studying its dependence on altitude, geographic conditions, time of day and season of year, etc. Only since the end of the 1950's, following the development of the required measuring equipment and experimental methodology, was the attention of scientists drawn to more complete statistical characteristics of turbulence such as spectral densities of air flow velocity pulsations, structural functions, etc. In particular, when these data were obtained it became possible

to further develop theory with consideration of specific conditions of the free atmosphere.

Monograph literature on turbulence in the free atmosphere has not been published either in the USSR or abroad, if we do not count the small book edited by N. Z. Pinus, "Atmospheric Turbulence Causing Bumping of Aircraft," published in 1962.

This monograph is concerned mainly with outlining the results of experimental investigations. Along with these, the authors discuss those questions in the theory of turbulence without which physical analysis of the presented data is difficult. The book also contains a description of instruments for measuring various parameters of turbulence in the free atmosphere. Since the majority of the instruments used in scientific research work undergo rapid modification, the authors did not feel it advisable to describe their construction in detail and limited themselves merely to outlining the physical principles of instrument operation and the functional diagrams required for an understanding of their operation. Aircraft methods of investigating turbulence are described in the greatest detail, since the overwhelming majority of experimental data were obtained in this manner.

A special chapter is dedicated to outlining methods for statistical processing of measurement results, evaluation of their accuracy, and description of instruments for statistical analysis. The necessity for this section in the book was dictated by the absence of literature in the Russian language which describes procedures for such treatment with realizations of finite length.

In several chapters problems of the origin of turbulence in the free atmosphere, dependence of its structure on the stratification of the atmosphere, and also the connection of turbulence with such quasi-ordered mesoscale motions as waves and convection are discussed. These motions are given substantial attention, since they are important not only as one of the sources of turbulence energy, but are, in particular, important in connection with their effect on flight vehicles.

When outlining experimental data the authors have attempted wherever possible to give a physical analysis of the principles determining one or another peculiarity of the structure of turbulence. Along with the general characteristics of turbulence, peculiarities of its structure and such physical meteorological objects as clouds, jet flows, the tropopause, etc., are examined. Questions connected with the effect of turbulence on aircraft are examined in a separate chapter.

Naturally, the authors paid particular attention to those aspects of the problem connected with their personal scientific interests and their experience in scientific research work. In particular, therefore, the book does not contain reflections of data on those microscalar turbulent motions which influence the propagation of radio waves, light, and sound in the atmosphere. While the authors attempted during the writing of the text to use all data published and known to them on turbulent motions in a free atmosphere with a scale of several meters up to several tens of kilometers, those results which were obtained by the authors themselves are outlined most fully. These materials were obtained mainly in the course of numerous flight expeditions carried out by TsAO [Central Aerological Observatory] and the CAO together with the GOS NII [State Scientific Research Institute] of Civil Aviation, and particularly from data on free and captive balloons obtained at the CAO.

The authors recognize the fact that much of the material in this book, which represents a first effort at systematic outlining of data on atmospheric turbulence in the free atmosphere, is incomplete and must be refined in the future. The authors thank, in advance, all readers who assist them in their future work on the study of turbulence by advancing comradely criticism.

The authors consider it their pleasant duty to express their profound gratitude to Scientific Editor L. S. Gandin for his valuable critical remarks and advice, and also to V. D. Litvinov, V. I. Silayeva, and the other colleagues of the Laboratory of the Dynamics of the

Atmosphere of the Central Aerological Observatory, who rendered great assistance in the technical shaping of the manuscript.

October 1967

CHAPTER 1

SOME QUESTIONS OF THE THEORY OF ATMOSPHERIC TURBULENCE

§ 1. THE NATURE OF ATMOSPHERIC TURBULENCE

The majority of processes in the atmosphere, such as transfer of water vapor and atmospheric dust, heat exchange, and the formation of clouds and precipitation, are extremely closely tied to the turbulent nature of motion in the atmosphere. Atmospheric turbulence renders an essential influence on the propagation of sound, light, and radio waves. Finally, atmospheric turbulence influences flight conditions for aircraft.

In contrast to a laminar fluid, the turbulent motion of a viscous fluid is characterized by a nonconstant velocity field and by the presence of nonuniformities or the so-called turbulent eddies, which lead to mixing of the jets. By the term "turbulent eddy" we understand an element of turbulent flow with a certain characteristic dimension (eddy scale).

The instantaneous value of velocity in a turbulent flow, u , can itself represent the result of the imposition of small vibrations on an average motion. If we designate the average value of velocity as \bar{u} , then $u = \bar{u} + u'$, where u' is the so-called pulsation or eddy velocity. If $u' = 0$, the motion is laminar.

If we designate the characteristic dimension of a flow of viscous fluid as L , and the characteristic velocity of flow as U , then from L , U , and ν (ν is the kinematic viscosity of the fluid) it is possible to compile a dimensionless combination known as the Reynolds number:

$$Re = \frac{UL}{\nu}. \quad (1.1)$$

Laminar motion becomes turbulent only when the Reynolds number exceeds a certain critical value Re_{cr} , i.e.,

$$\frac{UL}{\nu} > Re_{cr} \quad (1.2)$$

[$Re_{cr} = cr$]

The following is the physical concept of Re_{cr} . Forces of inertia lead to the approach of volumes of liquid which are initially far removed from one another and which possess different rates of motion; at the same time these forces facilitate a situation in which velocities at close points are changed sharply. The forces of viscosity, on the other hand, lead to a leveling of velocities at close points - i.e., to the smoothing of small nonuniformities of flow. At small Re values, when the forces of viscosity predominate over the forces of inertia, the flow has a laminar character.

With an increase in Re the smoothing action of the forces of viscosity is weakened and the flow is turbulized, i.e., disordered pulsations of velocity Re_{cr} appear in it, exactly corresponding to the conditions when the forces of inertia become so great in comparison with the forces of viscosity that a stable turbulent regime is formed.

Experimental studies in tunnels showed that laminar flow converts to turbulent flow at Re equaling 2500-5000.

With application to the atmosphere the Reynolds number becomes indeterminate to a substantial degree because of the difficulty in determining the scale of the flow as a whole. The indeterminate

geometry of atmospheric flows makes it necessary to introduce new concepts: thus, for example, the distance from the surface of the earth to the level of maximum wind speed or the altitude of the tropopause are sometimes introduced as the characteristic dimension. If the value of Re is calculated formally for the atmosphere, it turns out that it exceeds the critical by many times and, consequently, motion in the atmosphere is always turbulent. Actually, if a sufficiently sensitive and low-inertia instrument is used to measure wind velocity it is always possible to detect disordered fluctuations of velocity around a stable average value.

However, in certain cases these fluctuations become so small that it is possible to consider motion in the atmosphere to be quasi-laminar.

The principal causes of turbulization of air flows in the atmosphere are contrasts in the temperature and wind-velocity fields which arise for one or another reason.

The atmospheric processes which shape these contrasts include the following.

a) Friction of the air flow over the surface of the earth and the formation in its lower portion of a wind velocity profile with large vertical gradients.

b) Unequal heating of different segments of the underlying surface of the earth and the development of thermal convection in this convection.

c) Processes of cloud formation, during which there is liberation of heat of condensation and crystallization and also a change in the nature of the temperature and wind-velocity fields.

d) The approach and interaction of air masses with different characteristics along atmospheric fronts and altitude frontal zones, where there are great horizontal contrasts in temperature and wind speed.

e) Loss of stability by waves which form in inversion layers, on the tropopause, and close to other atmospheric interfaces.

f) Deformation of air flows by mountainous obstacles and the appearance of wave perturbations and rotor motions on their lee sides.

The indicated processes can operate simultaneously and thus intensify or weaken one another, and thus can weaken or intensify turbulization of the air flow.

The existence of viscosity of the air causes a continuous conversion of the kinetic energy of turbulent air flows into heat. It is obvious that if there is no external source of the energy required for continuous excitation of turbulent motion, this motion will sooner or later degenerate.

A particular property of turbulent motion is the disordered nature of the velocity field in time and space; therefore the classical problem of hydromechanics concerned with discovering the position of all particles of a fluid at any moment of time t according to the given position and velocities of particles at the moment of time t_0 and by the boundary conditions for turbulent motion becomes meaningless.

Even with a constant field of external forces and constant boundary conditions, during a turbulent flow the velocity at a given point will undergo substantial changes with time. This circumstance gives rise to the need for applying statistical methods to the investigation of turbulent flows.

As was already indicated, the development of atmospheric turbulence is conditioned by the effect of not only dynamic, but also thermal factors; as a consequence of this the Re number turns out to be inadequate for describing its appearance even in those cases when it is possible to evaluate the scale of the flow.

This problem was examined theoretically by L. F. Richardson (1920), who gave a criterion for the growth and diminishing of kinetic energy of turbulent motions in a thermally stratified medium. Richardson proposed that loss of turbulent energy due to work counter to a stable vertical stratification (against the force of gravity) significantly exceeds the loss of energy due to molecular viscosity, which converts turbulent kinetic energy into heat. Therefore Richardson limited himself to examining only turbulent dissipation.

Richardson obtained his criterion of stability of the atmosphere from the equation of the balance of turbulent energy:

$$\frac{dE'}{dt} = K \left(\frac{d\bar{u}}{dz} \right)^2 - K_T \frac{g}{\theta} \frac{d\theta}{dz} - \epsilon + D, \quad (1.3)$$

where E' is the kinetic energy of turbulent pulsations; $d\bar{u}/dz$ is the vertical gradient of average wind speed; θ is the potential temperature; g is the acceleration of gravity; K is the coefficient of turbulent exchange of momentum; K_T is the coefficient of turbulent heat exchange; ϵ is the rate of dissipation of turbulent energy into heat; and D is the diffusion of turbulent energy in the presence of a gradient of the energy of turbulence.

If dissipation and turbulent diffusion are ignored, the inflow of kinetic energy of turbulence equals

$$\frac{dE'}{dt} = K \left(\frac{d\bar{u}}{dz} \right)^2 - K_T \frac{g}{\theta} \frac{d\theta}{dz}. \quad (1.4)$$

The quantity

$$RI = \frac{K}{K_T} \frac{\frac{d\theta}{dz}}{\left(\frac{d\bar{u}}{dz} \right)^2} \quad (1.5)$$

is called the Richardson number. Since $\frac{1}{\theta} \frac{d\theta}{dz} = \frac{1}{T} (\gamma_s - \gamma)$, expression (1.5) can be written in the form

$$Ri = \frac{g}{T} \frac{(\gamma_a - \gamma)}{\left(\frac{du}{dz}\right)^2} \quad (1.6)$$

where γ_a is the adiabatic and γ is the actual vertical temperature gradient.

The quantity

$$Ri = \alpha \frac{g}{T} \frac{(\gamma_a - \gamma)}{\left(\frac{du}{dz}\right)^2} \quad (1.7)$$

is called the dynamic Richardson number. In (1.7) $\alpha = \frac{K_z}{K}$. From (1.6) and (1.7) it follows that

$$Ri = \frac{1}{\alpha} Ri \quad (1.8)$$

The dynamic Richardson number defines the role of thermal convection in the generation of turbulent energy, as compared with dynamic factors which cause the transfer of energy of turbulence from averaged motion, since the quantity Ri can be interpreted as the ratio of Archimedean forces to the forces of inertia.

From (1.4) and (1.7) it follows that

$$\frac{dE^t}{dt} = K \left(\frac{du}{dz}\right)^2 [1 - \alpha Ri] \quad (1.9)$$

and, consequently, stationary (nonattenuating) turbulence is possible only when $Rf = 1$, or with account taken of the dissipation of the energy of turbulence, when $Rf < 1$.

The effect of Archimedean forces on the turbulent regime depends on the vertical gradient of potential temperature. With a positive value of $d\theta/dz$ (stable thermal stratification) Archimedean forces counteract the development of turbulence; a portion of the turbulent energy is expended on overcoming the action of Archimedean forces. At negative values of $d\theta/dz$ (unstable thermal stratification, facilitating the development of convection), Archimedean forces

facilitate the appearance and development of turbulence. Thermal instability is of essential significance in clouds and also at low altitudes in the cloudless troposphere. In the middle and upper troposphere without clouds vertical shift of the average wind velocity apparently plays a major role in the excitation of turbulence. On cloudless days with strong heating of the underlying surface, superadiabatic temperature gradients are observed from the surface of the earth up to 500-1000 m, and sometimes even higher. At high altitudes such temperature gradients can be observed only in very thin layers, having thicknesses of a few tens or hundreds of meters.

Finally, at values of $d\theta/dz$ which are close to zero (neutral thermal stratification), Archimedean forces do not influence the turbulent regime.

As the investigations by H. W. Panus (1960) showed, the turbulizing action of the vertical gradient of average wind velocity in the atmosphere is compensated to a significant degree by the stabilizing of its thermal stratification.

In the general case turbulence in a thermally nonuniform atmosphere can be developed when the Ri number is less than a certain critical value which, as follows from (1.9), should be less than $\alpha_1 = K/K_T$. The critical value of the Richardson number characterizes conditions of the development and attenuation of turbulence in a thermally stratified atmosphere. A tendency toward growth of turbulence when $Ri < Ri_{cr}$ should, apparently, be manifested more or less sharply, just as in the case of excitation of turbulence as a function of Re number in conditions when Archimedean forces have no influence.

The value of the critical Richardson number has been evaluated by many investigators, mainly on the basis of theoretical considerations. The magnitude of Ri_{cr} depends, as follows from (1.9), on the ratio taken for K and K_T . As is known, in the classical theory of turbulence it is postulated that the substance carried is passive, i.e., its addition to the air does not influence the turbulence regime.

From this it follows that the magnitude of the coefficient of turbulence does not depend on the type of substance and, consequently, $K = K_T$, which means that $Ri_{cr} = 1$.

In actuality, the exchange of momentum between two masses of air can occur thanks to dynamic interaction without substantial mixing of these masses - i.e., with disruption of the postulate of indestructibility. Furthermore, the nature of the temperature distribution can have an effect such that the postulate of passivity is violated. For example, in an isothermal layer of the atmosphere in which a vertical gradient of wind velocity is observed, apparently $K \neq K_T$. In a thermally stable atmosphere exchange of momentum occurs more rapidly than that of the quantity of heat (Obukhov, 1954). Therefore there is no basis to assert that $Ri_{cr} = 1$ for conditions of a free atmosphere.

In the meteorological literature frequent use is made of the assumption that the coefficients of turbulence for different substances (for heat and momentum) are proportional to one another and that the ratio between their values is a constant quantity. Meanwhile laboratory investigations (Millison and Turner, 1960) and also studies in the lowest atmospheric layer (see Priestley, 1964; Monin and Yaglom, 1965) showed that α depends significantly on the thermal and wind stratification. In particular, with a reduction in Ri the value of α increases; this increase is particularly sharp in the region of values $Ri < 1$. Under convective conditions $\alpha > 1$, while in cases of temperature inversion $\alpha < 1$. According to data from Proudman (1957), $\alpha = 0.03-0.05$ at $r < Ri < 10$. We will note that the dynamic Richardson number Rf for these conditions is substantially less than unity. Thus, turbulence can be excited also with comparatively large Ri numbers. This must be kept in mind when studying turbulence, especially in the upper troposphere and in the stratosphere, where stable thermal stratification rules.

We will now examine the role of diffusion of turbulent energy. It is possible to consider that the magnitude of diffusion transfer of turbulent energy, D , depends on the coefficient of turbulence K

and on the gradient of eddy energy dE'/dr . If we consider the dimensionality of these quantities, the diffusion consumption of turbulent energy can be determined with an accuracy to a constant factor by the following expression:

$$D = K^{\frac{1}{3}} \left[\frac{dE'}{dr} \right]^{\frac{4}{3}}. \quad (1.10)$$

Thus, D depends on the coefficient of turbulence K to a smaller degree and is determined in significant measure by the degree of nonuniformity of the turbulence field.

With consideration of (1.10), and also assuming that $K_T = K$, we obtain

$$Ri_{cr} = 1 = \frac{\left[\frac{dE'}{dr} \right]^{\frac{4}{3}}}{K^{\frac{1}{3}} \left(\frac{du}{dz} \right)^{\frac{4}{3}}}. \quad (1.11)$$

[$ur = cr$]

From (1.11) it follows that the critical Richardson number depends, other conditions being equal, on the degree of nonuniformity of the turbulence field, i.e., dE'/dr , which in turn depends on the conditions of turbulization of the flow. From (1.11) it also follows that the critical Ri number cannot be a constant quantity for a nonuniform field of turbulence.

The Richardson number characterizes conditions of transformation of kinetic energy of average motion and the energy of instability into the kinetic energy of turbulent motion; however, it does not provide the possibility of evaluating such important characteristics of turbulence as the magnitude of pulsation velocities and the thickness of the turbulized layer of the atmosphere.

The intensity of turbulence depends not on the Ri number alone, though it is a function of this number. If $Ri < Ri_{cr}$, this fact can serve as a qualitative indication that, first, development of

turbulence is proceeding and, second, that the smaller is R_1 the greater the quantity of accumulated turbulent energy that can be observed under steady-state conditions.

§ 2. STRUCTURE AND ENERGY CONSIDERATIONS OF A TURBULENT FLOW

From hydrodynamics it is known that as the Reynolds number increases, large-scale pulsations are manifested first. At very large Reynolds numbers pulsations exist in a turbulent flow with scales which are comparable to the characteristic lengths which determine the dimensions of the flow as a whole and with the scales at which turbulent energy dissipates into heat due to molecular viscosity. According to A. N. Kolmogorov (1941), turbulent motion in the atmosphere may be visualized as follows. Since Reynolds numbers are very great in the atmosphere, the average flow is unstable and perturbations arise in it - "turbulent eddies of the first order" - characterized by disordered displacement with respect to one another of individual volumes of the fluid with diameters on the order of the characteristic dimensions of the flow. The rate of these relative displacements is less than the average velocity of the flow. Since the Reynolds numbers are still very great for eddies of the first order and since such eddies are also unstable, "eddies of the second order" with even smaller characteristic dimensions and velocities will arise.

The process of the successive reduction in size of turbulent eddies will continue until the Reynolds number

$$Re^{(n)} = \frac{U^{(n)} L^{(n)}}{\nu} \quad (1.12)$$

for eddies of some sufficiently great order n becomes so small that the influence of viscosity on eddies of the order n will be perceptible and will prevent the formation of eddies of the $(n + 1)$ -th order.

The problem of energy characteristics of turbulent motion deserves special attention. Contemporary hydrodynamics gives the

following presentation on the dissipation of energy during turbulent motion.

From eddies with large scales, which derive their energy from the main flow, energy transfers to eddies with smaller scales; there is virtually no dissipation during this process. Thus, the kinetic energy of turbulence transfers continually from large eddies to small ones - i.e., from small frequencies to high. This flow of energy dissipates (kinetic energy converts to heat) in eddies of the very smallest scales. Since the transfer of energy from large-scale to small-scale eddies occurs without losses, the quantity of energy which dissipates under the action of viscosity into heat can be determined (with respect to order of magnitude) by means of the characteristics of the basic flow.

Maintenance of the "stationary" state requires external sources which continually transmit energy to the basic large-scale motion. And, on the other hand, if the external source of energy ceases to operate turbulent flows will be attenuated. It is obvious that along with stationary sources of turbulent energy which are constant or which operate over a fairly long period, it is possible to encounter in the atmosphere comparatively short-term sources of this energy.

When studying the energy properties of a turbulent flow it is necessary first of all to clarify the method by which turbulent eddy motions are maintained in the air flow, the source from which energy of fluctuating motions is taken, and just how it is consumed. In the work of A. M. Obukhov (1954) use was made of the basic equation of the energy balance of turbulence in the form

$$\begin{aligned} \frac{\partial E_t}{\partial t} + \sum_{k=1}^3 \bar{u}_k \frac{\partial E_t}{\partial x_k} - \sum_{k=1}^3 \sum_{j=1}^3 \overline{u_j u_k} \frac{\partial \bar{u}_j}{\partial x_k} - \\ - \frac{1}{\rho} \sum_{k=1}^3 \sum_{j=1}^3 \left(\overline{\epsilon_{kj} \frac{\partial u_j}{\partial x_k}} + \overline{\epsilon_{jk} \frac{\partial u_k}{\partial x_j}} \right) + \frac{1}{\rho} \sum_{j=1}^3 \frac{\partial}{\partial x_j} \left[- \overline{F' u_j} + \right. \\ \left. + \sum_{k=1}^3 \left(\overline{u_k^2 u_j} - \rho \frac{\overline{u_k^2 u_j}}{\rho} \right) \right] \end{aligned} \quad (1.13)$$

Equation (1.13) has the same physical concept as equation (1.3), but it is written under somewhat different assumptions.

The left side of equation (1.13) contains the individual increment of fluctuation energy

$$\frac{dE'}{dt} = \frac{\partial E'}{\partial t} + \sum_{k=1}^3 u_k \frac{\partial E'}{\partial x_k}$$

The first term on the right side represents the quantity of kinetic energy of average motion which is converted per unit time into kinetic energy of fluctuation motion. A. M. Obukhov called this quantity the transformation energy:

$$T^* = \sum_{k=1}^3 \sum_{j=1}^3 u_j u_k \frac{\partial u_j}{\partial x_k} \quad (1.14)$$

The second component of the right side represents the rate of dissipation of energy of fluctuation motion, ϵ :

$$\begin{aligned} \epsilon &= \frac{1}{2\nu} \sum_{k=1}^3 \sum_{j=1}^3 \left(\overline{\sigma_{kj} \frac{\partial u_j}{\partial x_k}} + \sigma_{jk} \frac{\partial u_k}{\partial x_j} \right) = \\ &= \frac{\nu}{2} \sum_{j=1}^3 \sum_{k=1}^3 \left(\frac{\partial u_j}{\partial x_k} + \frac{\partial u_k}{\partial x_j} \right)^2 \end{aligned} \quad (1.15)$$

The third component is the average power of all fluctuations of surface forces (pressure, viscous and turbulent stresses) during displacement with the fluctuation velocity:

$$A = \frac{1}{\rho} \sum_{j=1}^3 \frac{\partial}{\partial x_j} \left[-\overline{p' u_j} + \sum_{k=1}^3 \left(\overline{u_k \sigma_{jk}} - \rho \frac{\overline{u_k^2 u_j}}{2} \right) \right] \quad (1.16)$$

Thus,

$$\frac{dE'}{dt} = T^* - \epsilon + A \quad (1.17)$$

i.e., the instability of average motion leads to an increase in the energy of fluctuation motion, while the major source of losses is dissipation of fluctuation energy into heat. The work of surface forces is not of special significance in the energy picture of the turbulent flow; therefore

$$\frac{dE}{dt} = -T \dots \quad (1.18)$$

Here it should be noted that outside the boundary layer of the atmosphere dissipation into heat is the basic loss of turbulent energy only in a limited interval of scales. Below it will be demonstrated that in a free atmosphere a noticeable fraction of kinetic energy of turbulent motions can be expended on an increase in potential energy.

As was already pointed out, turbulent motions have a very broad spectrum of scales ranging from primary eddies, which may be hundreds or even thousands of kilometers in diameter, down to eddies in which molecular viscosity is manifested. At present adequate theoretical studies have been made of the properties of turbulence whose scale is much less than the major scale and at the same time much greater than those scales in which dissipation of turbulent energy into heat occurs. In this region of scales, which has come to be called the inertial interval, the property of isotropy is ascribed to turbulence - i.e., independence of the properties of turbulent motion from the selected direction.

The theory of locally isotropic turbulence developed by A. N. Kolmogorov (1941) makes it possible to obtain valuable results on the local properties of turbulence in the inertial interval directly from considerations of dimensionality.

Local properties of turbulence cannot be determined by viscosity, since its influence is substantial only in the very smallest-scale motions. The characteristic dimension and rate of motion as a whole also cannot influence the properties of turbulence in the inertial interval. According to the Kolmogorov hypothesis, a continuous flow

of energy exists from the very largest (primary) eddies down to the very smallest. In the inertial interval energy is transmitted from eddy to eddy without losses and, consequently, the rate of energy transfer should be numerically equal to the rate of dissipation ϵ .

Changes in the rate of turbulent motion u_l at a distance on the order l should be determined only by ϵ and by the actual value of l . Utilizing the theory of dimensionality, Kolmogorov obtained the expression

$$u_l \sim (\epsilon l)^{\frac{1}{3}}, \quad (1.19)$$

i.e., the change in speed over the extent of distance l is proportional to the cube root of this distance. A. M. Obukhov arrived at this same result simultaneously, but by a different method (1941).

The quantity u_l can be examined qualitatively as the speed of a turbulent eddy having a characteristic scale on the order of l . Since $\epsilon = \text{const}$ in the inertial interval, from (1.19) the conclusion of self-similarity of turbulent eddies follows directly. This means that eddies of all scales included in the inertial interval exist in the development of turbulent flow. Each eddy, decaying, generates eddies similar to itself - i.e., also subordinate to (1.19) - but having smaller dimensions.

§ 3. STATISTICAL DESCRIPTION OF THE FIELD OF TURBULENCE

Despite the complexity and disordered nature of the field of velocities in a turbulent flow, turbulent motion should obey the basic equations of hydrodynamics:

Navier-Stokes equation

$$\frac{du}{dt} + u \nabla u = - \frac{1}{\rho} \nabla p + \nu \Delta u, \quad (1.20)$$

continuity equation

$$\nabla u = 0. \quad (1.21)$$

The equation of continuity is written for an incompressible fluid, which is true under the condition

$$\frac{(\overline{u})^2}{a^2} \ll 1. \quad (1.22)$$

where a is the speed of sound, since in this case, as is known, density pulsations can be ignored.

The system of equations (1.20) and (1.21) is sufficient for determination of u as a function of x and t if the initial and boundary conditions are given. Thus, for example, in the case of uniform turbulence the boundary conditions with respect to x are determined by the presence of statistical uniformity in space. The initial conditions consist in the fact that at a certain moment of time t_0 speed is a random function of a point and the probability laws characterizing this function are given.

It is obvious that if the initial conditions are given in probability form, at subsequent moments of time the field of velocities may be determined only in probability form. One of the basic characteristics of a random quantity is its distribution function $P(u)$. Interpretation of u as a random function relates to each point x, t . In this case, generally speaking, a statistical connection should exist between the random values at different space-time points. The function of consistent distribution of probabilities for the values of u at several given space-time points can serve as the characteristic of this statistical connection.

A turbulence field of infinite extent is defined statistically by the total set of consistent distributions of probabilities for values of the velocity vector $u(x, t)$ at any n space-time points. In this case one must take into account the fact that the statistical characteristics of the turbulence field at various values of t are

uniquely connected with one another by the hydrodynamic equations (1.20) and (1.21).

Ordinarily during description of a turbulence field we are limited by average values, which correspond to small n . Among these average values with small n , the following are of particular value in the theory of turbulence: the correlation tensor of the velocity field (i.e., a two-point moment of the second order) and the tensor obtained from it as a result of Fourier transformation.

The correlation tensor of a field of velocities for two points connected by the vector r has the form

$$R_{jk}(r) = \overline{u_j(x) \cdot u_k(x+r)}, \quad (1.23)$$

where $u(x)$ is a continuous function of x in view of the fact that discontinuities under the action of viscous forces cannot be retained in time. From this it follows that $R_{jk}(r)$ is continuous at all values of r . When $j = k$ we have

$$R_{jj}(r) \leq R_{jj}(0). \quad (1.24)$$

A theory developed by A. Ya. Khinchin (1938) exists for the entire class of random processes which are called stationary.

A random process which is defined by the totality of variables $Y_k(t)$ is called stationary in the case when the laws of distribution of probabilities of two groups of values of these variables

$$\{Y(t_1), Y(t_2), \dots, Y(t_n)\} \text{ and} \\ \{Y(t_1+\tau), Y(t_2+\tau), \dots, Y(t_n+\tau)\}$$

are identical to one another, where n , t and τ can be selected completely arbitrarily.

On the basis of Khinchin's theory (1938), G. Kramer (1948) arrived at the following conclusion. In order for the tensor $R_{jk}(r)$

to be a correlation tensor for a continuous stationary random process it is necessary and sufficient that this tensor allow presentation in the form

$$R_{jk}(r) = \int_{-\infty}^{\infty} S_{jk}(\Omega) e^{i\Omega r} d\Omega, \quad (1.25)$$

where Ω is the wave vector and $l = \sqrt{-1}$, under the condition that

$$\int_{-\infty}^{\infty} S_{jk}(\Omega) d\Omega < \infty. \quad (1.26)$$

From the Fourier transform which is the reciprocal of (1.25), it also follows that

$$S_{jk}(\Omega) = \frac{1}{2\pi^3} \int_{-\infty}^{\infty} R_{jk}(r) e^{-i\Omega r} dr. \quad (1.27)$$

When $r = 0$ formula (1.25) takes the form

$$R_{jk}(0) = \overline{u_j(x) \cdot u_k(x)} = \int_{-\infty}^{\infty} S_{jk}(\Omega) d\Omega. \quad (1.28)$$

From formula (1.28) it is clear that $S_{jk}(\Omega)$ represents the density of the quantity $u_j u_k$ in a wave space.

The tensor $\overline{u_j(x) u_k(x)}$ determines the energy per unit mass of fluid and is called the energy tensor.

The tensor $S_{jk}(\Omega)$ describes the distribution of energy with respect to different wave numbers in expansion of the velocity field into harmonic components and is called the spectral tensor of energy.

Thanks to its explicit physical concept, the tensor $R_{jk}(r)$, and also the tensor $S_{jk}(\Omega)$, which connects it with the Fourier transform, represent the most important quantities describing the field of turbulence.

The spectral and correlation tensors are functions of vector arguments. In a real experiment it is most frequently necessary to carry out measurements of only one of the velocity components. The correlation and spectral functions, depending on one scalar argument, can be obtained by averaging $R_{jk}(r)$ and $S_{jk}(\Omega)$ over all directions of the vector arguments r and Ω . In the case of isotropic turbulence these tensor functions of the vector modulus play an important role.

Besides the correlation and spectral functions, the structural functions introduced by A. N. Kolmogorov are applied as characteristics of the external properties of a locally isotropic and uniform turbulent flow:

$$D_j(r) = \overline{[u_j(x_1 + r_1, x_2 + r_2, x_3 + r_3, t) - u_j(x_1, x_2, x_3, t)]^2}, \quad (1.29)$$

where u_j is the velocity component in the direction j .

Thus, $D(r)$ is the mean square of the difference in the values of u_j at two points located at the distance r :

$$r = \sqrt{r_1^2 + r_2^2 + r_3^2}$$

That is, in terms of structural functions the dependence of the velocity of fluctuating motions on the scales of the fluctuations has become widely known as the "law of two-thirds" of Kolmogorov-Obukhov:

$$D_j(r) = A(\delta_j) \cdot \frac{2}{3} r^{2/3}, \quad (1.30)$$

where $A(\delta_j)$ is a dimensionless coefficient dependent upon the angle between x_j and r .

If a studied random process satisfies the condition of stationarity, the statistical characteristics which characterize this process turn out to be uniquely connected with one another:

$$D(r) = 2[R(0) - R(r)]. \quad (1.31)$$

and, since $R(\infty) = 0$, and, consequently, $D(\infty) = 2R(0)$, then

$$R(r) = \frac{1}{2}[D(\infty) - D(r)]. \quad (1.32)$$

The correlation function can be expressed as follows on the basis of (1.25):

$$R(r) = \int_{-\infty}^{\infty} S(\Omega) e^{i\Omega r} d\Omega. \quad (1.33)$$

From the determination of uniformity $R(r) = R(-r)$; consequently,

$$R(r) = \int_{-\infty}^{\infty} S(\Omega) \cos(\Omega r) d\Omega. \quad (1.34)$$

We can obtain an expression for the spectral function from (1.33):

$$S(\Omega) = \frac{1}{2\pi} \int_{-\infty}^{\infty} R(r) e^{-i\Omega r} dr. \quad (1.35)$$

The spectral function $S(\Omega)$ represents the spectral density of energy of a unit of mass. In the literature on turbulence $S(\Omega)$ is frequently called the energy spectrum of turbulence. The structural function and energy spectrum are connected with one another by the relationship

$$D(r) = 2 \int_{-\infty}^{\infty} (1 - e^{i\Omega r}) S(\Omega) d\Omega. \quad (1.36)$$

This connection is valid also when a random process has a linearly varying average value (Tatarskiy, 1967).

It was already pointed out above that in a real experiment, as a rule, only one component of velocity is measured; therefore the statistical characteristics which are obtained as the result of processing experimental data characterize the totality of projections of the velocity vector to a selected direction.

The development of the energy spectrum of turbulence from experimental data is frequently hampered by the impossibility of realizing a sufficiently extensive series of independent measurements, and also by equipment difficulties. In this case it is necessary to limit oneself to the simpler statistical characteristics of turbulence, such as the dispersion of velocities $\overline{u'^2}$ and the mean square value of the velocity $\sigma_u = \sqrt{\overline{u'^2}}$. The latter quantity is frequently used for quantitative evaluation of the integral intensity of turbulence. For a quantitative description of the relative intensity of turbulence, the turbulence literature uses the relationship

$$\psi = \frac{\sigma_u}{\overline{u}}$$

which is sometimes called the gustiness of velocity. The quantities $\overline{u'^2}$ and σ_u can, in particular, be obtained from the energy spectrum, where in this case the intervals of scales (frequencies) for which the corresponding characteristics are calculated will be given. Thus, for example, the dispersion of velocities is determined as

$$\overline{u'^2} = \int_{\lambda}^{\infty} S(\alpha') d\alpha'$$

The quantity obtained as the result of such calculation characterizes the intensity of fluctuations which have fully defined scales. It is necessary that the interval of scales for which one or another integral characteristic of turbulence intensity is determined must be known when comparing data obtained by different investigators. As will be shown in Chapter 2, each experimental method of investigation permits measurement of only a limited segment of the turbulence spectrum. For comparison of turbulence intensities in regions of different scales it is more convenient to use not the integral characteristics, but the rate of energy transfer in the turbulence spectrum. This problem will be considered below.

An essential peculiarity of experimental investigations of the structure of the turbulence field in the atmosphere is the fact that

measurements are conducted either at one point in space over a prolonged period of time or by moving the measurement instrument in space at a comparatively high speed. If a single measurement instrument is used the result of the experiment is always the realization of a random process measured in the course of some interval of time; however, this time interval has a completely different meaning for each case. In the first case this is the time during which the studied process occurs, while in the second case it is the time of "instantaneous" measurement of the spatial picture along some particular direction.

In the first case the measuring instrument is moved relative to the flow with the average velocity of the flow. In order to transfer from time concepts to spatial, it is possible to use the hypothesis of J. Taylor (1938) on the so-called frozen turbulence - i.e., the hypothesis that the shape of perturbations can be retained without essential changes in appearance during motion of these perturbations together with an air flow at the average velocity of the flow. This hypothesis, put forward under the assumption that the average velocity of the flow is sufficiently great in comparison with velocity fluctuations, has been experimentally confirmed for turbulent perturbations from comparatively small scales up to scales of several kilometers. It has not been verified for perturbations of larger scales. One may assume that for scales which are close to the synoptic, the Taylor hypothesis on frozen turbulence may not be fulfilled. In particular, substantial errors can be tolerated in the case when this hypothesis is applied to turbulent motions when the energy of turbulent pulsations is commensurate with the energy of average motion. Thus, numerical transition from time presentations to spatial is not possible in all cases. In the opinion of A. S. Monin, however, such a transition on the basis of the hypothesis of frozen turbulence is permissible for oscillations with a period up to four days. These questions will be examined in more detail later in the appropriate sections of the book.

If the measuring instrument is displaced at a velocity many times greater than the average velocity of the flow, transition from

time characteristics to spatial does not require fulfillment of the hypothesis of frozen [turbulence]; it is sufficient to know only the speed of motion of the instrument. We should only note that in order to justify examining the realization obtained in this way as a stationary random process and using the relationships derived above it is necessary that the field of turbulence in the direction of motion of the instrument satisfy the condition of uniformity.

§ 4. ENERGY SPECTRUM OF TURBULENCE

As was already stated in § 3, the energy spectrum represents the expansion of kinetic energy in the Fourier interval in terms of the wave numbers $\Omega = \frac{2\pi}{L}$. In other words, $S(\Omega)d\Omega$ is the quantity of kinetic energy calculated per unit mass retained or transferrable by eddies with dimensions which are characterized by wave numbers from Ω to $\Omega + d\Omega$.

Thus,

$$S(\Omega) = \frac{1}{2} \frac{d\overline{v^2}}{d\Omega}. \quad (1.37)$$

It is simplest to determine the expression for the energy spectrum of turbulence in that region of wave numbers where turbulence satisfies the condition of uniformity and local isotropy. According to the definition of A. N. Kolmogorov (1941), in this region (called the inertial interval) the velocity v_Ω depends on the wave number Ω and on the dissipation rate ϵ . An analytical expression for the spectrum of the velocity vector in the inertial interval can be obtained from considerations of dimensionality:

$$S(\Omega) = c\epsilon^{\frac{2}{3}} \Omega^{-\frac{5}{3}}. \quad (1.38)$$

In the inertial interval the three-dimensional spectrum of turbulence and, correspondingly, the one-dimensional spectra of the components u (along the main flow), v , and w (across the main flow) are described by the formulas:

$$S_u(\Omega) = c_1 \Omega^{-\frac{5}{3}},$$

$$S_v(\Omega) = S_w(\Omega) = c_1' \Omega^{-\frac{5}{3}}. \quad (1.39)$$

For the coefficients c , c_1 and c_1' , which have the nature of universal constants, the following relationships are fulfilled:¹

$$c = \frac{55}{18} c_1, \quad (1.40)$$

$$c_1' = \frac{4}{3} c_1.$$

According to contemporary data (Gurvien et al., 1967), the coefficient c_1 equals 0.45-0.50 with an accuracy to 20-15% if Ω is measured in radians per unit length.

Relationship (1.38) can also be obtained from the "two-thirds law" for a structural function. Expression (1.38) has found the name Kolmogorov spectrum or "spectral law minus five-thirds." The "minus five-thirds" law is valid only for the inertial interval - i.e., for the region of wave numbers which are greater than those at which the energy of the main flow reaches the turbulence spectrum due to stability and smaller than those where the "consumer" of turbulent energy - dissipation into heat under the action of molecular viscosity - is operative. Only a single mechanism for energy transfer exists within the inertial interval - inertial transfer from eddies with lesser Ω to eddies with greater Ω . Proceeding from precisely these considerations, Kolmogorov and Obukhov equated the rate of energy transfer through point Ω in the spectrum to the dissipation rate ϵ .

Thus, the spectrum of the field of wind velocities in the initial interval is uniquely determined by the quantity ϵ and by single unique universal constant c . The quantity c can be calculated on the basis of (1.39), if the spectral density for any wave number belonging to the inertial interval is known.

¹Between the universal constants A for structural functions u , v and w in expression (1.30) and the universal constants for the spectrum the following relationships are fulfilled: $A_1 = 4c_1$, and $A_1' = \frac{4}{3} A_1$.

Heisenberg (1948), proceeding from the idea that the process of energy transfer from large to small eddies is similar to the process of transformation of mechanical energy into heat under the action of molecular motions, introduced into the equation for energy (besides a term describing molecular dissipation) a term describing the transfer of energy from motions of large scales to motions of small scales:

$$-\frac{\partial}{\partial t} \int_0^{\infty} S(\Omega') d\Omega' = 2\nu \int_0^{\infty} S(\Omega') \Omega'^2 d\Omega' + 2a \int_0^{\infty} |S(\Omega')|^2 \Omega'^{-3} d\Omega' \int_0^{\infty} S(\Omega'') \Omega''^2 d\Omega'' \quad (1.41)$$

The left side of the equation represents the total dissipation of kinetic energy in a unit mass per unit time in motions with scales greater than $L = \frac{2\pi}{\Omega}$, while the right side contains terms which describe different mechanisms for dissipation and conversion of energy.

The term $2\nu \int_0^{\infty} S(\Omega') \Omega'^2 d\Omega'$ determines the dissipation of kinetic energy directly into thermal energy as a consequence of molecular viscosity. The term $2a \int_0^{\infty} |S(\Omega')|^2 \Omega'^{-3} d\Omega' \int_0^{\infty} S(\Omega'') \Omega''^2 d\Omega''$ (a is an absolute constant on the order of unity) describes the transfer of kinetic energy from motions of large scales to motions of smaller scales. This transition is, actually, a characteristic feature of turbulence.

Since viscosity ν equals the product of the length of the free path times the velocity of molecules with an accuracy to the numerical factor, by analogy turbulent viscosity should represent also the product of the path length $L = \frac{2\pi}{\Omega}$ of small eddies times their velocity

$$\nu_t \sim l \overline{S(\Omega) d\Omega}.$$

The transfer of energy from motions with scales greater than l to motions with smaller scales is accomplished, as Heisenberg proposed, by all eddies with scales smaller than l . Therefore turbulent viscosity is defined by the expression

$$v_{rms} = a \int |S(\Omega')|^{\frac{1}{2}} \Omega'^{-\frac{3}{2}} d\Omega'. \quad (1.42)$$

The solution of the Heisenberg equation (Batchelor, 1955) has the form

$$S(\Omega) = \left(\frac{8\epsilon}{9a}\right)^{\frac{2}{3}} \Omega^{-\frac{5}{3}} \left[1 + \frac{8\nu^3}{3a^2\epsilon} \Omega^4\right]^{-\frac{4}{3}}. \quad (1.43)$$

When $\Omega \ll \left(\frac{3a^2\epsilon}{8\nu^3}\right)^{\frac{1}{4}}$, i.e., at comparatively small Ω where viscosity has no influence, the expression (1.43) converts to the spectral law "minus five-thirds." When $\Omega > \left(\frac{3a^2\epsilon}{8\nu^3}\right)^{\frac{1}{4}}$, where molecular dissipation plays a significant role, the expression for the energy spectrum at the limit takes the form

$$S(\Omega) \sim \Omega^{-7}. \quad (1.44)$$

The physical idea at the basis of the Heisenberg formula is more suitable for the case of exchange of energy between widely spaced wave numbers than for the more important case of energy exchange between wave numbers of one and the same order of magnitude. Experimental data do not confirm relationship (1.44); however, on the basis of this relationship it is possible to draw certain qualitative conclusions. In particular, the introduction of an additional "consumer" of energy at large Ω - dissipation into heat - leads to an increase in the modulus of the exponent at Ω if the energy spectrum is expressed by a power function of Ω in the form $S(\Omega) \sim \Omega^{-n}$.

From the outlined presentations it follows that a turbulent flow represents the superposition of eddies of different dimensions from a certain minimum dimension L_0 up to the dimension L_0 , which is comparable in scale with the flow as a whole. Thanks to the influence of viscosity the size of the eddy cannot be reduced infinitely. Generally speaking, the smaller the eddy the greater the gradient of velocities across the eddy - i.e., the greater the viscous shear stresses which counteract the eddy motion. Thus, in any turbulent flow there should exist a statistical lower limit of

the size of the smallest eddy. In the region of turbulent scales where $l \leq l_0$, direct dissipation of kinetic energy of turbulence into heat will occur.

Figure 1.1 shows the curve of spectral density of turbulent energy (the energy spectrum) for a flow in which the forces of gravity can be ignored. In the real atmosphere this corresponds to the case of neutral thermal stratification. The region a on this figure is the region of large (anisotropic) eddies in which energy of turbulence arrives from the energy of the basic motion, and there is also transfer of energy from large eddies to small eddies. Region b is a region of dissipation of turbulent energy to viscosity; this is the so-called viscous interval. The intermediate region c is the so-called inertial interval. In this region the appearance and dissipation of energy of turbulence are small in comparison with the arrival and consumption of energy connected with the transfer of energy over the spectrum during the "crushing" of eddies.

The lower, high-frequency boundary of the inertial interval is the region where the spectra should be defined by the rate of energy dissipation ϵ and by the magnitude of kinematic viscosity ν . On the basis of dimensionality considerations, it is possible to construct from these quantities a linear scale of turbulence in the region of which dissipation of turbulent energy is accomplished:

$$l_0 = \left(\frac{\nu^3}{\epsilon} \right)^{1/4}. \quad (1.45)$$

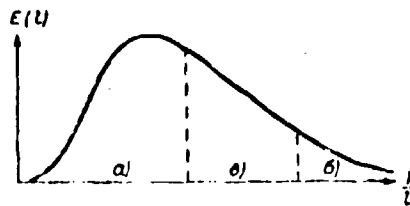


Fig. 1.1. Spectral density of turbulent energy.

Dissipation is greatest along this scale l_0 , called the Kolmogorov microscale. In the region of scales which are smaller than l_0 the curve of spectral density drops sharply because of viscous degeneration of the eddies. The quantity l_0' , approximately an order of magnitude larger than the Kolmogorov microscale l_0 , is taken as the lower boundary of the inertial interval. Even in the region l_0' the influence of viscosity becomes significant. The quantity l_0' in the lowest atmospheric layer equals approximately 5 mm; this has been shown by experimental studies. In the region of scales $l_0' \ll l \ll l_0$ the major factor is inertial transfer of turbulent energy over the spectrum without losses. It should be noted that in the free atmosphere (for which large Re numbers are characteristic, as has already been pointed out), the inertial interval is quite great. This is confirmed by experimental data.

Everything said above relates to the case of developed turbulence, when the source of turbulent energy operates continuously and compensates energy losses due to dissipation into heat and other factors. If the energy source ceases to operate, turbulence is degenerated. In this case the degeneration of turbulence can be broken down into three stages: initial, transition, and final (J. Batchelor, 1955).

If thermal stratification is not taken into account, the change in kinetic energy in a neutrally stratified atmosphere is described by expression (1.41). In the initial stage of degeneration of turbulence the scattering of energy under the action of viscosity is compensated by the inflow of energy from the direction of smaller wave numbers, which creates turbulent displacement. However, since the source of turbulent energy is no longer operating, in the end a moment arrives when maintaining the noted flow of energy from certain wave numbers to another which is comparable in magnitude to the rate of dissipation becomes impossible. In this final stage of degeneration the processes of redistribution of energy over the turbulent spectrum can actually be ignored in comparison with dissipation processes.

The flow has already ceased to be turbulent in the ordinary meaning of this word - turbulent displacement in it has terminated and there is only a quiet "laminar" attenuation of individual large-scale perturbations, retained from the time when there was developed turbulence in the flow (Mouin, Yaglom, 1967).

In the spectral theory of turbulence which was developed for flows in tunnels (Khintze, 1963) the energy spectrum in the final stage of degeneration is defined by the expression

$$S(\Omega, t) \sim \Omega^4 e^{-2\Omega^2 t}. \quad (1.46)$$

Here the law of degeneration of intensity of turbulence is expressed by the relationship

$$u'^2 \sim t^{-\frac{5}{2}}. \quad (1.47)$$

Although the applicability of these relationships to the atmosphere requires both theoretical and experimental verification, it is obvious that in the atmosphere in the degeneration stage eddies of small scales will attenuate rapidly, while large eddies, deprived of the ability to transfer their energy to smaller eddies, may exist for a comparatively prolonged period of time.

§ 5. INTERACTION OF AVERAGED AND TURBULENT FIELDS OF TEMPERATURE AND WIND VELOCITY

As was already pointed out, the basic source of turbulent energy is the energy of the main flow. The intensity of turbulence and the turbulent transfer of momentum or of any conservative additives in the atmosphere are determined not only by the velocity gradients of the main flow (vorticity)¹, but also by the nature of the interaction

¹Strictly speaking, vorticity $\text{curl } V$ (its component along the horizontal axis y , perpendicular to the main flow) is defined by the formula $\text{curl } V = (\partial u/\partial z - \partial w/\partial x)$. But, since the second term is significantly smaller than the first, the velocity gradient $\partial u/\partial z$ (wind shear) is frequently called vorticity.

of vorticity ($d\bar{u}/dz$) of the main flow with the vorticity of turbulent motions (du'/dz).

C. Tchen (1953) singled out the case when the vorticity of the main motion is small compared with the vorticity of turbulence in the considered range of frequencies (or scales), and the case when they are mutually comparable. In the first case a barely noticeable interaction should be observed and vorticity of the main motion fulfills only the function of "pumping" of kinetic energy of average motion into energy of turbulence. If the vorticities of the main and turbulent motions are mutually comparable, very strong interaction between them is possible. Under certain conditions this interaction, according to Tchen, can lead to the appearance of strong resonance. We will note that strong interaction can be observed in the region of fractures of the vertical profile of wind speeds. In the real atmosphere the effect of the interaction (weak or strong) is determined not only by vertical gradients of average wind speed, but also by vertical gradients of air temperature.

We will examine the spectral characteristics of turbulence with consideration of the influence of the degree of the interaction of vorticities of the main and turbulent motions. Proceeding on the basis of the work of E. A. Gisinia (1966), we will use for determination of spectral characteristics of turbulence an equation obtained from the equations of motion and continuity by means of averaging and expansion in Fourier Integrals. On the assumption of local uniformity of turbulence, this equation has the following form for the equilibrium region of the spectrum, $\Omega \gg L_0^{-1}$:

$$\begin{aligned}
 & \epsilon = 2 \cdot \int_0^{\Omega} \Omega'^2 S(\Omega') d\Omega' - \frac{d\bar{u}}{dz} \int_0^{\Omega} \tau(\Omega') d\Omega' + \\
 & + F(\Omega) + \beta \int_0^{\Omega} H(\Omega') d\Omega', \quad (1.48)
 \end{aligned}$$

where $\tau(\Omega)$ is the spectrum of turbulent stress of friction; $F(\Omega)$ is a function which characterizes the transfer of energy of turbulence in the range of wave numbers from 0 to Ω - i.e., to pulsations with higher wave numbers; $H(\Omega)$ is the spectrum of the vertical heat flow, while $\beta = g/\theta$ is the buoyancy parameter.

After Heisenberg (1948), one can assume that

$$F(\Omega) = K(\Omega) \cdot 2 \int_0^{\Omega} \Omega'^2 S(\Omega') d\Omega', \quad (1.49)$$

where

$$K(\Omega) = a \int_0^{\Omega} |S(\Omega')|^2 \Omega'^{-\frac{3}{2}} d\Omega', \quad (1.50)$$

is the coefficient of turbulent viscosity, and a is a numerical coefficient.

In the case of weak interaction of the main and turbulent motions in the region of wave numbers $\Omega \gg L_0^{-1}$

$$\int_0^{\Omega} \tau(\Omega') d\Omega' = -K(\Omega) \frac{du}{dx}, \quad (1.51)$$

and

$$\int_0^{\Omega} H(\Omega') d\Omega' = -\alpha K(\Omega) \frac{dT}{dx}, \quad (1.52)$$

where α is the ratio of the coefficients of turbulent mixing for heat and momentum.

In the case of strong interaction of the main and turbulent motions,

$$\int_0^{\Omega} H(\Omega') d\Omega' = -\alpha K(\Omega) \cdot \left[\int_0^{\Omega} \Omega'^2 C(\Omega') d\Omega' \right]^{\frac{1}{2}}, \quad (1.53)$$

and

$$\nu = 2(\nu + K(\Omega)) \int_0^{\Omega} \Omega'^2 S(\Omega') d\Omega' + \alpha_1 K(\Omega), \quad (1.54)$$

where $C(\Omega)$ is the spectrum of temperature pulsations.

By substituting the expressions (1.49), (1.51) and (1.52) into (1.48) we obtain the spectral equation for the case of weak interaction of the main and turbulent motions:

$$\int_0^{\infty} \varepsilon(\Omega') d\Omega' = K(\Omega) \left[2 \int_0^{\infty} \Omega'^2 S(\Omega') d\Omega' \right]^{\frac{1}{2}}, \quad (1.55)$$

where

$$a_1 = \left(\frac{d\bar{u}}{dz} \right)^2 - 2\beta \frac{dT}{dz}.$$

Solving (1.55) with consideration of expression (1.50) gives

$$S(\Omega) = \left(\frac{8}{9a} \right)^{\frac{2}{3}} (\varepsilon + a_1 \nu)^{\frac{2}{3}} \Omega^{-\frac{5}{3}} \left[1 + \frac{8\nu^2 \Omega^4}{3a^2 (\varepsilon + a_1 \nu)} \right]^{-\frac{4}{3}} \quad (1.56)$$

As we see, in the case of weak interaction the nature of the energy spectrum is described by the "minus five-thirds" law. The influence of nonuniformities of the fields of average temperature and average wind speed, defined by the quantity $a_1 \nu$, is manifested in a change in the magnitude of dissipation of the energy of turbulence. The gradients of temperature and average wind speed create an additional source of energy.

Strong interaction of the main and turbulent motions can be observed only in the region of turbulence scales which are commensurate with scales of the changes in the average fields of temperature and wind speed or which are greater. Therefore it is possible to limit ourselves to consideration of the interval of wave numbers: $L_0^{-1} \ll \Omega \ll L_1^{-1}$.

For this wave number interval it is possible to ignore the influence of viscosity. Substituting expressions (1.49), (1.53), and (1.56) into (1.48), we obtain

$$\begin{aligned} \varepsilon = K(\Omega) \cdot 2 \int_0^{\infty} \Omega'^2 S(\Omega') d\Omega' + \frac{d\bar{u}}{dz} K(\Omega) \left[2 \int_0^{\infty} \Omega'^2 S(\Omega') d\Omega' \right]^{\frac{1}{2}} - \\ - 2\beta K(\Omega) \left[\int_0^{\infty} \Omega'^2 C(\Omega') d\Omega' \right]^{\frac{1}{2}}. \end{aligned} \quad (1.57)$$

Assuming that in the region of wave numbers indicated above interaction between the main and turbulent motions plays a greater role than interaction between eddies of different scales, we can ignore the function $F(\Omega)$. Solution of (1.57) under the indicated assumptions and with consideration of (1.50) gives the following expression for the energy spectrum:

$$S(\Omega) = \frac{N}{\alpha \frac{d\bar{u}}{dz}} \left(1 + \frac{N}{\alpha \frac{dT}{dz}} \right) \Omega^{-1}, \quad (1.58)$$

where N is the rate at which temperature nonuniformities are leveled (see § 3, Chapter 4). This assumption is fulfilled for the wave numbers

$$\Omega \ll \frac{d\bar{u}}{dz} \left[\frac{N}{\alpha \frac{d\bar{u}}{dz}} \left(1 + \frac{N}{\alpha \frac{dT}{dz}} \right) \right]^{-\frac{1}{2}}. \quad (1.59)$$

From (1.58) it follows that strong interaction of the main and turbulent fields of temperature and of wind speeds will lead to a change in the form of the energy spectrum as compared with the form of the spectrum for conditions when the "minus five-thirds" law is fulfilled. We will note that the assumption made above concerning local uniformity is, as F. A. Gisina showed, applicable also in the case when vertical gradients of wind speed are changed with altitude.

CHAPTER 2

METHODS OF EXPERIMENTAL INVESTIGATION OF TURBULENCE IN THE FREE ATMOSPHERE

§ 1. AIRCRAFT METHODS OF INVESTIGATING ATMOSPHERIC TURBULENCE

A characteristic feature of methods of studying turbulence in the lowest layer of the atmosphere is the installation of measuring instruments on special structures (towers, masts, etc.) which are immobile with respect to the earth - i.e., motions of air measured by such instruments in a system of coordinates connected with the ground will be absolute. On the other hand, measurement of the speed of air at high altitudes is most frequently accomplished by balloon probes, which are easily moved about by the air flow. By measuring the speed of displacement of the balloons from the ground by radar or other methods it is possible to determine the speed of displacement of the air flow itself.

The aircraft occupies a certain intermediate position: on the one hand it can be used as a "platform" for the arrangement of measuring instruments, and on the other hand the aircraft is carried along by the air flow and in this sense is in itself a measuring instrument.

It is obvious that the aircraft will be drawn along the more by atmospheric motions, the greater the scale of these motions, while on the other hand for very small-scale motions the aircraft will be, as it were, a platform which is fixed or, more exactly, which moves at a constant speed.

Atmospheric turbulence is characterized by the existence of unordered motions of very different scales, some of which move the aircraft easily while others have virtually no effect on the aircraft as a whole.

Aircraft investigations of turbulence are extremely complex and expensive procedures; therefore it is advisable that such experiments be made multipurpose - i.e., that the aircraft be used both as a sensor and as a platform.

The majority of experimental data on turbulence in the free atmosphere have been obtained by means of specially equipped aircraft - flying laboratories. In order to measure the average values of the basic meteorological parameters the aircraft (flying laboratories) are equipped with electrometeorographs - instruments which make it possible to obtain quantitative thermal and dynamic characteristics of the medium in which turbulent motions exist. An airborne electrometeorograph is described in the work by S. M. Shmeter and G. N. Shur (1957).

In the following paragraphs of this section aircraft methods of measuring the characteristics inherent to turbulence will be examined. As a rule, unique equipment is used during the measurements.

During the outline of aircraft methods of investigating turbulence we will use the system of coordinates connected with the center of gravity of the aircraft which is accepted in aerodynamics. The x-axis coincides with the direction of flight and is called the longitudinal axis of the aircraft; for an aircraft in horizontal flight, the y-axis coincides with the direction of the force of gravity and the z-axis (transverse) is perpendicular to the plane xoy.

a. Method Utilizing the Reaction of the Aircraft to an Atmospheric Gust (Overload Method)

Upon reaching a zone with developed turbulence the aircraft is subjected to action by a perturbed flow and begins to oscillate,

experiencing a change in overloading (bumping)¹. The very fact of the appearance of bumping during flight of an aircraft in a perturbed flow led to the concept of using data on its intensity to evaluate the intensity of atmospheric turbulence. The magnitude of aircraft overload is measured in this case by special instruments - accelerometers.

The simplest single-component accelerometer, depicted on Fig. 2.1, represents inert mass m suspended on spring Π to the housing of the instrument. The accelerometer is equipped with a damper \mathcal{D} , which counteracts the displacement of mass m with respect to the housing of the instrument with a force which is proportional to the speed of this displacement. The equation of free motion of the accelerometer has the form

$$m \frac{d^2x}{dt^2} + D \frac{dx}{dt} + Kx = 0, \quad (2.1)$$

where D is the damping factor; K is spring rigidity; x is the displacement of the lower end of the spring from a position corresponding to $m = 0$. The system described by equation (2.1) is an oscillatory system with damping and when it is removed from the equilibrium state it will attempt to return to it. The nature of the attenuating oscillations will vary as a function of the degree of damping. In a critically damped system when $D_{cr} = 2\sqrt{mK}$ attenuation will be aperiodic; when $D = 0$ nondamping oscillations with a frequency $\omega_0 = \sqrt{\frac{K}{m}}$ will arise. As a rule, $0 < D < D_{cr}$ in accelerometers. Since the free vibrations of an accelerometer attenuate, the steady-state elongation of the spring, x_0 will be proportional to the force which is stretching it. Thus, in a state of rest the force $F = mg$ will act on the spring of an accelerometer with a vertical working axis; therefore

$$x_0 = \frac{m}{K} g. \quad (2.2)$$

¹Overloading of an aircraft is the name given to the ratio $n = A/G$, where A is lift and G is the weight of the aircraft. It is obvious that in quiet horizontal flight at a constant speed $n = 1$. Ordinarily overloads are measured in fractions of a gravity, g .

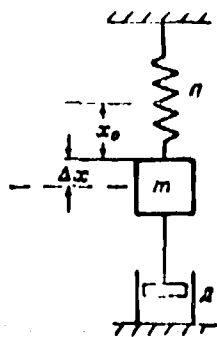


Fig. 2.1. Diagram of accelerometer.

During vertical motion of the accelerometer with constant acceleration a we will have

$$x = x_0 + \Delta x = \frac{m}{K}(g + a), \quad (2.3)$$

from which

$$\Delta x = \frac{m}{K} a. \quad (2.4)$$

Since the accelerometer represents an oscillatory system with attenuation whose motion is described by a linear differential equation, when an external periodic force acts on it forced oscillations will appear in it with a frequency equal to the frequency of the action of the external force. The frequency characteristic of the accelerometer is uniform at frequencies from 0 to ω_0 , and then drops. The accelerometer "logs" frequencies which are greater than the frequency of its natural oscillations.

In contemporary aircraft accelerometers the natural frequencies lie within the limits 8-14 Hz. Aircraft accelerometers have an electrical output: displacement of mass m is converted into displacement of the pointer of a potentiometer. Methods and instruments for measuring acceleration were outlined in detail in the work by N. K. Kobrinskiy (1942).

Besides mechanical accelerometers, piezoelectric instruments exist. They have a higher natural frequency and possess good

sensitivity. V. I. Skatskiy (1957) developed a piezoelectric aircraft accelerometer and applied it to studies of thermal turbulence at low altitudes.

Study of atmospheric turbulence by means of aircraft can be carried out according to a variety of plans. First of all it is possible to study the spatial characteristics of zones in which an aircraft experiences bumping during flight; the duration of existence of these zones, their connection with fields of averaged meteorological parameters, etc., can be studied. With such a "macroscopic" approach to the study of turbulence, its intensity is taken as equal to the intensity of bumping; the latter is evaluated in scale marks and is broken down into weak, moderate, strong, and very strong (see Chapter 4). Naturally, such evaluations are basically qualitative and, in particular, do not take into account differences in the reaction of the aircraft to gusts with different velocity and duration.

Secondly, it is possible to study the microstructure of turbulence. In this case the object of study is the quantitative characteristics of turbulent pulsations in the atmosphere and, consequently, it is necessary to accomplish the strictest possible transition from the reaction of the aircraft to a turbulent gust to the parameters of the gust itself; in other words, in this case the aircraft becomes a meter for measuring turbulence.

Strictly speaking, the "instrument" for measuring turbulence consists of the system aircraft/accelerometer. This instrument has a completely determined passband in terms of the scales of perturbations. The aircraft perceives the effects due to perturbations of different scales as actions of different frequencies. The frequency of the actions is determined by the scale of the perturbations and the flight speed of the aircraft. We will note that by using the aircraft as a turbulence meter it is possible to study a segment of the spectrum which, although quite broad, is nonetheless limited.

The overload experienced by the aircraft in a disturbed air flow will depend essentially on the type of the aircraft and on its flight

regime. In order to judge the true magnitudes of turbulent wind gust velocities in terms of aircraft overloads it is necessary to have some methods of converting from overloads of the center of gravity or another point in the aircraft structure where the instrument is installed to gust speed - i.e., to obtain an analytical, graphic, or tabular relationship connecting these two quantities by calculation or experimental means.

The strictest analytical method of converting from reaction of the aircraft to a gust to the characteristics of the gust itself is the use of equations of the dynamics of the aircraft, by means of which it is possible to connect the readings of a measuring instrument (accelerometer) installed on the aircraft with a turbulent gust acting on the aircraft. Of course, the system of dynamic equations should include the equation of the accelerometer.

By using the method of small perturbations it is possible to describe the behavior of an aircraft by means of linear differential equations. It is known that if any dynamic system can be described by a differential equation, and also if the action on the system can be written analytically, then by solving this equation (whose right side includes the action) we obtain a complete picture of the behavior of the system. However, analytical solution of such an equation is not always possible. Even if the system is described by a linear differential equation with constant coefficients and with a simple right side, solution of such an equation at an order above the fourth requires very laborious calculations.

Methods exist in the theory of harmonic analysis which permit making judgements about the behavior of a system without solving the differential equation (see Solodovnikov, 1952). A function which connects the reaction of a linear dynamic system to an action with the action itself is called a transfer function and can be defined as the ratio of the Fourier transform $x(\omega)$ (where ω is the angular frequency) for the quantity on the system output to the Fourier transform $F(\omega)$ for the action $f(t)$ on its input. In this case the transfer function $\Phi(\omega)$ or, as it is sometimes called, the complex

gain factor, takes on a completely defined independent physical meaning. Its modulus is none other than the amplitude gain factor for each individual harmonic component.

Determination of transfer functions of systems with a large number of degrees of freedom requires very laborious calculations and is possible only by using electronic computers.

Using the methods of harmonic analysis, it is possible to solve the reverse problem - i.e., if the reaction of the system to any disturbance is known, it is possible to find the disturbance itself. During investigation of atmospheric turbulence the problem is stated in precisely this form; however, in this case the actual effect of turbulent gusts on the aircraft and, consequently, the reaction of the aircraft to the gusts (overload increment) represent random functions of time.

It is possible to impose certain limiting assumptions on these random functions. We will consider that the investigated process (atmospheric turbulence) is a quasi-stationary random process; in other words, the shape of the probability distribution function does not depend on displacement of the readout origin along the time axis.

As was already indicated, the spectral theory of stationary random processes developed by A. Ya. Khinchin (1938) makes it possible to extend the method of harmonic analysis to cover the study of random processes. In this case the object of study is not an individual, completely determined oscillatory process, but the law of distribution of probabilities of different possible variants of the flow of such a process.

The results of experimental investigations of atmospheric turbulence to solve many problems, both theoretical and applied, can be presented most conveniently in the form of correlation and structural functions or energy spectra (see Chapter 1). If a stationary random process $f(t)$ acts on a linear dynamic system, then if the energy spectrum of this process $S_{11}(\omega)$ and the transfer

function of the system $\Phi(\omega)$ are known, it is possible to calculate the energy spectrum of the reaction of the system to the action, $S_{out}(\omega)$:

$$S_{out}(\omega) = S_{in}(\omega) |\Phi(\omega)|^2, \quad (2.5)$$

[out = out; in = in]

To solve the reverse problem, i.e., to determine the spectral density (energy spectrum) of the action, it is possible to write

$$S_{in}(\omega) = S_{out}(\omega) |\Phi(\omega)|^{-2}. \quad (2.6)$$

This very important conclusion of the theory of stationary random processes was used as a basis for the method of obtaining the energy spectrum of turbulence by means of an aircraft. The quantity $|\Phi(\omega)|^{-2}$ for each specific frequency ω_k represents the numerical factor k_{ω_k} ; consequently,

$$S_{in}(\omega_k) = S_{out}(\omega_k) k_{\omega_k}. \quad (2.7)$$

Calculation of the transfer function of such a complex system as an aircraft is carried out under certain limiting assumptions. The first of these is the assumption of the smallness of oscillations of the aircraft around a stable horizontal flight regime; this makes it possible to solve a linear problem.

If the elastic properties of the aircraft structure are not taken into account and if the oscillations of the aircraft are considered to be small, calculation of the transfer function can be carried out by using a system of linear equations derived by M. I. Yudin (1946), describing longitudinal oscillations of the aircraft in a turbulent atmosphere:

$$\left. \begin{aligned} \varphi_1 + a_{11}\varphi_1 + a_{12}\varphi_2 + a_{13}\varphi_3 &= a_{14}u_1 + a_{15}u_2 \\ \varphi_2 + a_{21}\varphi_1 + a_{22}\varphi_2 + a_{23}\varphi_3 &= a_{24}u_1 + a_{25}u_2 \\ \varphi_3 + a_{31}\varphi_1 + a_{32}\varphi_2 + a_{33}\varphi_3 &= \\ &= a_{34}u_1 + a_{35}u_2 + a_{36}u_3 \end{aligned} \right\} \quad (2.8)$$

where ϕ_1 is the pulsation of the horizontal velocity of the aircraft center of gravity, referred to the average flight speed \bar{v} ; ϕ_2 is the pulsation of the vertical velocity of the center of gravity, referred to \bar{v} ; ϕ_3 is the pulsation of the pitch angle; u_1 is the pulsation of the horizontal wind speed, referred to \bar{v} ; u_2 is the pulsation of the vertical wind velocity, referred to \bar{v} ; a_{jk} are dimensionless coefficients which depend on the aircraft structure and the flight regime.

During the derivation of the equations it was assumed that flight occurs without intervention of the pilot in control of the aircraft and that the undisturbed flight regime is horizontal.

We will consider the development of the transfer function of the aircraft from the M. I. Yudin system of equations by the A. S. Dubov method. Considering that the following are used as characteristic quantities in the system of equations written in dimensionless form: $\tau = \frac{m}{\rho S v}$ - characteristic time and $\mu = \frac{m}{\rho S b_a}$ - characteristic mass, where b_a is the mean aerodynamic chord, Dubov introduces the designations

$$n_2 = \frac{d^2 \tau_1}{d\tau^2}; \quad n_1 = \frac{d \tau_1}{d\tau} = a \tau_1,$$

where $a = \frac{\tau_0 g}{v} = \frac{c_y}{2}$. Here he assumes that deflections of the flight from the horizontal are small and, consequently, the vertical axis of the accelero-graph is deflected very little from the true vertical. The aircraft is considered to be an oscillatory system with six degrees of freedom and it is assumed that it accomplishes oscillations as a rigid body.

Using these relationships, it is possible to bring system of equations (2.8) to the form

$$\left. \begin{aligned} n_1' + a_{11}n_1 + a_{12}n_2 + aa_{13}\varphi_3 + (a_{14} + a)\varphi_3' &= a_{11}u_1 + a_{12}u_2 \\ n_2' + a_{21}n_1 + a_{22}n_2 + aa_{23}\varphi_3 - a_{22}\varphi_3' &= a_{21}u_1 + a_{22}u_2 \\ \varphi_3' + a_{31}\varphi_3 - a_{32}\varphi_3' + a_{33}\tau_1 + a_{34}n_1 + a_{35}n_2 &= a_{31}u_1 + a_{32}u_2 + \\ &+ a_{33}\tau_1 \end{aligned} \right\} \quad (2.9)$$

Giving the reaction of the aircraft (to overload) in the form of Fourier series

$$u_1 = \sum_N B_{1N} e^{iN\omega t}, \quad (2.10)$$

$$u_2 = \sum_N B_{2N} e^{iN\omega t}, \quad (2.11)$$

we will find the solution of the system in the form

$$u_1 = \sum_N A_{1N} e^{iN\omega t}, \quad (2.12)$$

$$u_2 = \sum_N A_{2N} e^{iN\omega t}, \quad (2.13)$$

$$z_3 = \sum_N B_{3N} e^{iN\omega t}, \quad (2.14)$$

Subsequently the following assumption is made. We will present A_{2N} in the form of the sum of two components: $A_{2N}^{(2)}$, causing vertical overloads of the aircraft, and $A_{2N}^{(1)}$, causing longitudinal overloads. Considering that a vertical gust will cause mainly vertical overloads, we arrive at the relationship

$$|B_{2N}|^2 = \frac{(c_2 - b_1 N^2 \omega^2)^2 + c_1^2 N^4 \omega^4}{(c_0 + c_7 N^2 \omega^2)^2 + (c_4 + c_6 N^2 \omega^2)^2 N^4 \omega^2} |A_{2N}|^2, \quad (2.15)$$

where

$$\begin{aligned} c_1 &= b_2 a_{43} - b_1 a_{34}, \\ c_2 &= c_0 = a_{42} (b_2 + b_1) + b_2 a_{11}, \\ c_3 &= a_{11}, \\ c_4 &= b_1 + a_{44} a_{11}, \\ c_5 &= a_{12} a_{11} + a_{31} (a_{13} + a) + b_1 a_{44}, \\ c_6 &= a_{12} a_{21} - a_{22} a_{11}, \\ c_7 &= (a_{13} + a) a_{21} + a_{22} a_{11}, \\ c_8 &= -a_{22} (a_{12} + a_{13} + a). \end{aligned}$$

To evaluate the error which arises because longitudinal accelerations are ignored, Dubov proposes the formula

$$\left| \frac{A_{2N}^{(1)}}{A_{2N}^{(2)}} \right|^2 = \lambda_c^2 (N\omega) \left| \frac{B_{1N}}{B_{2N}} \right|^2. \quad (2.16)$$

Then

$$\lambda_0^2(N\omega) = \frac{c_1^2 N^2 \omega^2 + (c_3 + c_3 N^2 \omega^2)^2}{(c_2 + c_7 N^2 \omega^2)^2 + (c_4 + c_6 N^2 \omega^2)^2 N^2 \omega^2} N^2 \omega^2, \quad (2.17)$$

where

$$c_3 = a_{21}, \quad c_4 = a_{11} a_{11}, \quad c_5 = a_{21} a_{11} = a_{11} a_{21}.$$

Inspection of a large quantity of recordings of vertical and longitudinal overloads during flights in zones of turbulence showed that on the average the longitudinal components of acceleration are an order of magnitude smaller than the vertical components.

From formula (2.15) we can obtain the square of the modulus of the aircraft transfer function:

$$|\Phi(N\omega)|^2 = \left| \frac{B_{2N}}{A_{2V}} \right|^2 = \frac{(c_2 + b_1 N^2 \omega^2)^2 + c_1^2 N^2 \omega^2}{(c_2 + c_7 N^2 \omega^2)^2 + (c_4 + c_6 N^2 \omega^2)^2 N^2 \omega^2} N^2 \omega^2. \quad (2.18)$$

The transfer function for an elastic aircraft was calculated by O. A. Kuznetsov. Aircraft oscillations, simulated by a system of elastic beams, were expanded in series with respect to a system of orthogonal functions, which represent the shapes of natural vibrations of the aircraft in a void. With the given forms, using the hypothesis of stationarity, the aerodynamic forces and coefficients of the equations of motion of the aircraft are determined. The motion of the aircraft is considered during the action of a vertical gust of wind whose intensity varies in space by a sinusoidal law with a wavelength equal to λ . The frequency of the action ω of such a gust on an aircraft flying at speed v is determined as

$$\omega = \frac{2\pi v}{\lambda}. \quad (2.19)$$

The steady-state motion of the aircraft is determined during the action of a gust of the given frequency with amplitude A ; in this case the maximum amplitudes of overloads are determined. Figure 2.2 gives the transfer function for overloads in various sections of the

fuselage of an elastic aircraft. The corresponding sections are shown on the drawing of the aircraft.

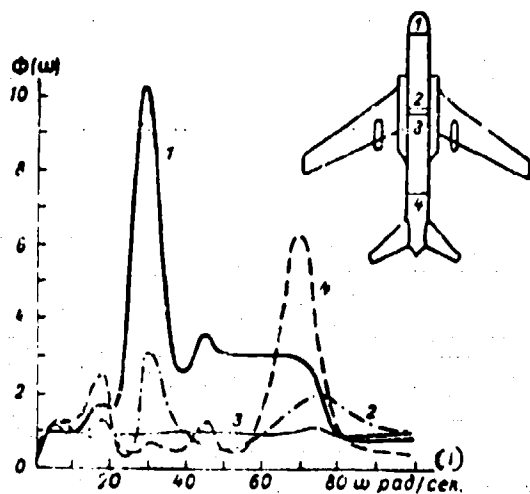


Fig. 2.2. Transfer functions of various sections of the fuselage of an elastic aircraft.

KEY: (1) rad/s.

From Fig. 2.2 it is clearly evident that the aircraft will react quite differently to gusts of different frequencies (scales). As is known, an aircraft is carried along well by motions of large scales and, consequently, does not react to these motions with any noticeable overload. At the maximum during flight of an aircraft in a flow which has a vertical component of velocity with zero frequency the aircraft will have a corresponding vertical component of velocity and will not experience any overload. The transfer function $\Phi(0)$ will therefore equal zero. As the frequency of the action increases the aircraft reacts ever better and better to a gust with an overload, which corresponds to a smooth growth in the value of the transfer function in the frequency interval from 0 to ω_1 . In the region of high frequencies the transfer function of a rigid aircraft is virtually invariable.

The figure shows the transfer function of the instantaneous center of gravity (curve 3) - a certain fictitious point which is not connected with the structure of the aircraft and for which its elastic properties are not essential. Therefore it is possible to consider the transfer function of the instantaneous center of gravity to be the transfer function of an equivalent rigid aircraft.

In contrast to a rigid aircraft, an elastic aircraft has a whole series of natural resonance frequencies, where the resonance properties are different in different sections of the aircraft. As is evident from the figure, this leads to a very complex shape of transfer functions, differing substantially from $\Phi(\omega)$ for the equivalent rigid aircraft. But in the region of high frequencies the aircraft will not react to gusts as a whole, since there is an influence of its linear dimensions and, in addition, of the inertial properties of the measuring instrument - the accelerometer, which should react to overload by displacement of a certain mass. Naturally, such displacement cannot occur instantaneously and the measuring instrument will "clog up" the high frequencies.

All of the above means that the aircraft/accelerometer system will react with a noticeable overload only to gusts of a certain range of frequencies (scales).

By using the transfer function it is possible, as it were, to "restore" the real distribution of gusts in terms of frequencies also in the region of small frequencies, down to a certain frequency ω_{\min} for which the value of the transfer function can also be determined correctly. In the region of large frequencies one should limit oneself to the frequency ω_{\max} , corresponding to the horizontal dimension of the aircraft itself:

$$\omega_{\max} = \frac{2\pi v}{L_c} \quad (2.20)$$

[max = max]

where v is the speed and L_c is the horizontal dimension of the aircraft.

Transfer functions can be obtained experimentally. For electrical systems the problem of experimental determination of transfer functions is solved comparatively simply: a sinusoidal input signal is supplied to the system input and after attenuation of the transient the amplitude and phase of the voltage on the output are measured.

Such measurements are conducted for the entire range of investigated frequencies. The experimental determination of the aircraft transfer function requires complex special equipment and the preparation of a dynamic model of the aircraft. Sensors for the measured parameters - overloads at various points of the structure, bending and torsion moments, etc. - are installed on the model. The model is placed in the working section of a wind tunnel and tested in the usual method. Then by means of a special device sinusoidal transverse perturbations are imposed on the main flow; the frequency of these perturbations can be varied. Exactly as in the case of electrical systems, after attenuation of the transient process the amplitudes of oscillations of the investigated parameters are measured. If the elastic properties of the aircraft are considered it is impossible to be limited to the study of the motion of a single point - the aircraft center of gravity. An elastic system can be likened to a multipole with a single input and numerous outputs, i.e., different points behave differently under one and the same action. During experimental determination of the transfer functions phase shifts, as a rule, are not measured - i.e., a model of the transfer function is obtained as the result of the experiment. As was shown above, to study the structure of turbulence it is necessary to have precisely the modulus of the transfer function.

Using the model, it is possible to "solve" the problem of the behavior of an aircraft under the effect of any action. There is only a single limitation here: it is necessary that during any action the natural oscillations of the system be attenuated with time. In this case the actual behavior of the aircraft will be the solution to the problem.

There exist other experimental methods for determining transfer functions of aircraft which do not require the preparation of a dynamic model. If independent measurements are used to obtain the energy spectrum of the velocities of turbulent gusts and the energy spectrum of overloads of the aircraft center of gravity, their ratio, as follows from (2.6), will equal the square of the modulus of the aircraft transfer function. B. M. Kopyov (1955) carried out flights

on an aircraft equipped with instruments permitting determination of the spectrum of vertical overload on the level and close to a tower on which anemometers measuring the vertical component of velocities had been installed. Considering turbulence to be frozen and calculating the average velocity, Koprov calculated the spatial energy spectrum of the vertical component of turbulent gusts. Dividing the spectrum of gusts by the spectrum of the overloads, Koprov obtained the value of the square of the modulus of the transfer function.

G. N. Shur (1959) developed a method which makes it possible to obtain automatically the energy spectrum of the vertical component of velocity pulsations. The method is based on the following limiting assumptions:

- 1) turbulence in the atmosphere is a stationary random process;
- 2) turbulence is uniform and frozen and therefore by considering the speed of the aircraft v in the period of the measurement regime to be constant, it is possible to convert from the scale of time to the scale of length (from angular frequency ω to wave number $\Omega = \omega/v$)¹;
- 3) the aircraft with an accelerator installed on it is a linear system and therefore the relationship

$$S_v(\Omega) = |\Phi(\Omega)|^2 \cdot S_n(\Omega), \quad (2.21)$$

which is easily obtained from formula (2.6), is applicable.

The equipment for this method consists of two sets: airborne and ground. All processing is carried out on the ground under stationary conditions.

Figure 2.3 shows the functional diagram of the method.

¹During aircraft investigations the requirement that the [turbulence] be frozen is apparently too strong, since the great speed of the aircraft permits making a virtually instantaneous cross section.

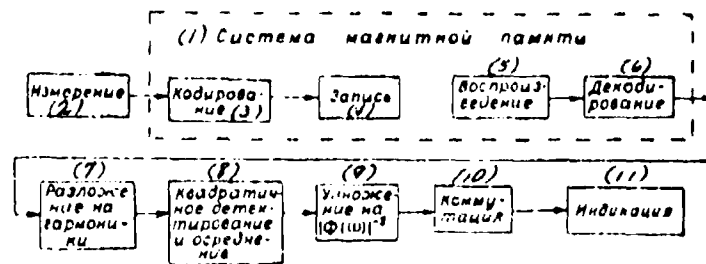


Fig. 2.3. Functional diagram of the method of obtaining the energy spectrum of atmospheric turbulence.

KEY: (1) Magnetic memory system; (2) Measurement; (3) Coding; (4) Recording; (5) Reproduction; (6) Decoding; (7) Expansion to harmonics; (8) Square-law detection and averaging; (9) Multiplication by $|\Phi(\omega)|^{-2}$; (10) Switching; (11) Readout.

The essence of the method is as follows. The overloads experienced by the aircraft are measured by an instrument having an electrical output and are coded by a pulse-frequency modulator and recorded on magnetic tape. During processing (on the ground) the recording is reproduced, deciphered in a pulse decoder and fed to the input of a spectral analyzer. The circuit of the spectral instrument includes an electrical model of the quantity reciprocal to the square of the modulus of the transfer function of the aircraft/accelerometer system. The voltage on the input of each filter is multiplied by the coefficient

$$K_{\omega_k} = |\Phi(\omega_k)|^{-2}. \quad (2.22)$$

Then the outputs of all channels are switched in a determined sequence to an electronic indicator. The use of a magnetic memory system makes it possible to change the time scale and to match the frequency bands of the investigated process and the spectral instrument. The method described above is statistical in its very nature; therefore its application requires statistical stability of the series of measurements - i.e., sufficiently prolonged realization under conditions when the hypothesis of stationarity is applicable. In this case individual (in particular extremal) values of turbulent gusts cannot be manifested from the final result.

As follows from the above description of the method, the signal containing information on the overload is subjected to numerous conversions and to spectral processing; also, multiplying by a factor which with the magnitude of the reciprocal of the square of the transfer function modulus, determined analytically with certain allowances, is introduced into the calculation scheme. Therefore the basic sources of error in the method are first the units of the measuring, converting, and processing equipment and secondly the actual transition from overload to gust - i.e., the transfer function of the aircraft/accelerometer system. Besides this, since the transfer function is calculated for horizontal flight without pilot intervention in aircraft control, intervention of this type is an additional source of error.

The mean square relative error of measurement of vertical overload amplitude equals ± 0.01 .

Frequency distortions introduced by the overload meter have a systematic nature and are taken into account by the transfer function of the aircraft/accelerometer system.

The magnetic memory system, consisting of a pulse-frequency modulator, a recording magnetograph, a reproducing magnetograph, and a demodulator, introduces a relative mean square error equal to ± 0.06 ; basically this error is determined by the nonuniformity in the rate of travel of the magnetic tape in the magnetographs (so-called "detonation").

The spectral equipment used for statistical processing - a subsonic frequency spectrometer (see Chapter 3, § 4) - consists of units which carry out a number of successive operations with a similar signal: amplification, expansion to harmonics, square-law detection, and averaging. The averaging time is identical for all channels; however, if we consider that the amplitude of each oscillation singled out by the filter is an independent measurement, it turns out that averaging with respect to the quantity of these measurements will depend on the average pass frequency of the

corresponding filter. Therefore the mean square error for the spectrum, with consideration of errors introduced by the overload meter and the magnetic memory system, is a function of frequency. On the smallest frequency it equals ± 0.08 , while for the maximum frequency it is ± 0.01 .

The transfer function of a real aircraft is different from the theoretically calculated quantity. Errors in its determination are connected with the fact that calculation is carried out under certain simplifying assumptions. To evaluate the obtained errors, measurements were carried out at two points of the aircraft for which the analytically calculated transfer functions differ substantially. As might be expected, the overload spectra obtained experimentally differ strongly from one another; however, after consideration of transfer functions of the corresponding points of the structure the relative difference in the obtained values did not exceed $\pm 0.2-0.3$.

The errors introduced by pilot intervention in aircraft control are not subject to analytical determination; therefore measurements are carried out, as a rule, with the aircraft controls locked. If the pilot nonetheless finds it necessary to intervene in aircraft control during flight in a turbulent flow, when the measurement data are being processed the segments of the recording made during the time when data from instruments installed on the aircraft indicate deviation of the elevator of greater than one degree are excluded.

Along with the statistical characteristics of turbulence, measurements on an aircraft make it possible to find the speed of individual wind gusts. During the calculations use is made of the ratios between the speed of the gust and the reaction of the aircraft to it; these ratios are found from the equations of flight dynamics. Thus, A. S. Dubov (1961) used the system of equations (2.8) to obtain the following formula for determination of the speed of a vertical gust w :

$$w = \frac{2G\Delta n}{S C_y \rho n^2 V} \sqrt{\frac{I_0}{I_a}} \int_0^t \Delta n d\tau = \frac{v_w \sqrt{\frac{I_0}{I_a}}}{205.2} \Delta \tau. \quad (2.23)$$

Here w is given in m/s; the overload increment $\Delta n = n - 1$ is given in fractions of a gravity; the equivalent airspeed (i.e., reduced to a pressure of 760 mm Hg) v_u is given in km/h; the deflection of the pitch angle $\Delta\phi$ is given in degrees; aircraft weight G , in kilograms; wing area S , in square meters; $c_y^\alpha = \frac{dc_y}{d\alpha}$ is the derivative of the lift coefficient c_y with respect to angle of attack α ; ρ_0 and ρ_H are the density of air at the 760 mm Hg level and at the altitude of flight. The second term in formula (2.23) equals the vertical velocity imparted to the aircraft as a result of its being pulled along by a gust.

As A. S. Dubov showed, formula (2.23) can also be used in those cases when the pilot intervenes in control of the aircraft. This makes it very convenient, since it is impossible to carry out a flight in a zone of strong bumping with locked controls.

During derivation of formula (2.23) a number of simplifying assumptions were made; to be precise, it was considered that there are no horizontal air gusts, the aircraft is absolutely rigid, and finally that the aerodynamic factors entering into (2.23) are unchanged during flight in a zone where vertical flows exist.

The largest errors are introduced by ignoring horizontal wind gusts. We will carry out an approximate evaluation of these errors, assuming the aircraft to be rigid.

Aircraft lift is

$$A = c_y \frac{\rho v^2}{2} S, \quad (2.24)$$

while aircraft overload is

$$n = \frac{A}{G} = c_y \frac{S}{G} \frac{\rho v^2}{2}. \quad (2.25)$$

Since n is a function only of α and v , the change in the overload can be described by the formula

$$\Delta n = \frac{1}{2} \rho \frac{S}{\sigma} (v^2 c_y^2 \Delta z + 2c_y v \Delta v). \quad (2.26)$$

It is obvious that formula (2.24) is valid only under the assumption that while inside a gust of air the aircraft does not manage to acquire a noticeable speed in the direction of the gust. Hence in this case $w/v = \Delta \alpha$, then

$$\Delta n = \frac{1}{2} \rho \frac{Sv}{\sigma} (wc_y^2 + 2c_y \Delta v). \quad (2.27)$$

It is obvious that the first term in formula (2.27) corresponds to the overload arising because of the action of a vertical gust w , while the second represents the overload arising under the influence of a change in airspeed Δv (for example, such as might be caused by a horizontal gust of air). The ratio of the overload caused by the horizontal gust with speed Δv (Δn_H) to the overload in a vertical gust with speed w (Δn_V) equals

$$\frac{\Delta n_H}{\Delta n_V} = \frac{2c_y \Delta v}{c_y^2 w}. \quad (2.28)$$

The quantity $\Delta n_H/\Delta n_V$ usually comprises from 0.05 to 0.25%.

The equipment used for calculation of the velocities of turbulent gusts by the Dubov formula is significantly simpler than the equipment required to obtain the spectrum of turbulence and it is installed directly on the aircraft. As is evident from the formula, to obtain the vertical speed of air it is necessary, along with measurement of Δn , to calculate the rate at which the aircraft is carried along by a gust - i.e., it is necessary to integrate the vertical overload in time:

$$v_y = g \int \Delta n dt + c. \quad (2.29)$$

We will consider that prior to the beginning of the action of the gust on the aircraft the latter was flying horizontally, i.e., $c = 0$. This corresponds to assigning zero initial conditions.

The principles and devices for integrating electrical signals are widely known and are based on the integrating properties of certain circuits. An electronic overload integrator based on an amplifier with feedback in terms of the derivative was used by G. N. Shur (1957) to study turbulence in mountainous regions. A special device which simulates the Dubov formula was first used in the study of turbulence in frontal zones (Shur, 1958). A functional diagram of this instrument is shown on Fig. 2.4. Overload of the aircraft center of gravity is measured and converted into an electrical signal by an electrical accelerometer (inside the broken line on the diagram). Then a voltage proportional to the overload passes to the indicator and to a unit for multiplication by the coefficient b . The coefficient b is set manually in accordance with readings of the instruments which measure the altitude and speed of the aircraft and also the flight weight (fuel consumption). Since according to formula (2.23) the calculation of w also requires consideration of the oscillation of the pitch angle, the set of airborne (so-called overload) equipment includes a gyroscopic pitch and roll deflection sensor (vertical gyroscope) (see § 1, pt. g).

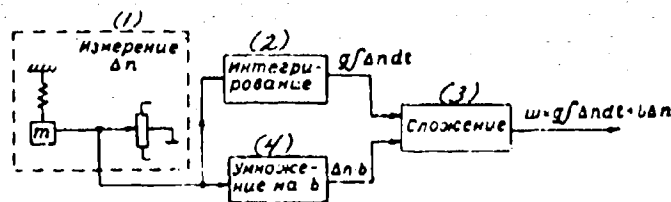


Fig. 2.4. Functional diagram of the method of obtaining w_z according to the Dubov formula (2.25).

KEY: (1) Measurement of Δn ; (2) Integration; (3) Addition; (4) Multiplication by b .

b. Method Using Measurement of the Absolute and Relative Speed of the Aircraft (Doppler Method)

An aircraft in flight moves within a current of air which itself is moving relative to the ground. When studying atmospheric turbulence,

in order to determine wind speed and the fluctuations of the horizontal component of turbulent pulsations it is necessary to know the instantaneous value of the speed and direction of motion of the aircraft with respect to the ground and the speed of motion of the aircraft with respect to the surrounding air.

Measurement of the aircraft speed vector in a system of coordinates tied to the earth is accomplished using instruments which utilize the Doppler effect. The Doppler effect is the name given to the phenomenon of a change in frequency of oscillations emitted by a specific source and picked up by a receiver during mutual relative displacement of the source and the receiver. The Doppler effect will also be observed when the source and receiver are located in the same place, but the receiver picks up a reflected rather than a direct signal. Here the Doppler effect will be observed during mutual relative displacement of the transceiver and the reflecting object. Aircraft Doppler stations emit oscillations in a highly directional beam toward the ground; they determine the speed of motion of the aircraft relative to the ground in terms of the change in frequency of the reflected signal.

In a system of coordinates tied to the ground this speed is the absolute speed of the aircraft. If the direction to the reflecting object (the ground) coincides with the direction of flight of the aircraft, the frequency of the oscillations picked up by the receiver, f_d , would be determined by the relationship

$$f_d = f_0 \left(1 + \frac{2v_a}{c} \right) = f_0 + F_d, \quad (2.30)$$

where f_0 is the frequency of emitted oscillations; v_a is the flight speed of the aircraft (absolute); c is the speed of light; F_d is the Doppler frequency,

$$F_d = \frac{2v_a}{c} f_0 = \frac{2v_a}{\lambda}, \quad (2.31)$$

where λ is the transmitter wavelength.

In actuality the direction of the beam comprises a certain angle γ with the direction of flight of the aircraft and, consequently,

$$F_{\text{Dop}} = \frac{2v_a}{\lambda} \cos \gamma. \quad (2.32)$$

Formula (2.32) does not consider the fact that the air medium in which the aircraft is moving is itself moving with respect to the earth. In the general case the direction of flight of the aircraft does not coincide with the direction of the wind. This leads to a situation in which the direction of the absolute motion of the aircraft does not coincide with its longitudinal axis but differs by a certain angle β , called the drift angle. In order to determine β it is necessary that it be possible to change the direction of the beam or, more exactly, the direction of its projection in the horizontal plane. When the horizontal projection of the beam coincides with the direction of absolute motion of the aircraft, the Doppler frequency F_{D} will be maximum. Expression (2.32) is more correctly presented in the form

$$F_{\text{D,max}} = \frac{2v_a}{\lambda} \cos \gamma. \quad (2.33)$$

The angle between the horizontal projection of the beam and the longitudinal axis of the aircraft will equal the drift angle β . If the direction of the longitudinal axis of the aircraft in some system of coordinates - for example, geographic - is known, complete determination of the vector of absolute aircraft velocity in this system of coordinates is possible.

Figure 2.5 shows the functional diagram of a single-beam Doppler meter for measuring the ground speed and drift angle of the aircraft. The transmitter generates sinusoidal oscillations of frequency f_0 , which pass through the antenna switch to the antenna and are emitted by it toward the ground. Oscillations reflected from irregularities on the ground surface, having a Doppler shift in frequency, are picked up by the antenna and passed through the antenna switch to the receiver mixer. Attenuated direct oscillations from the transmitter, with frequency f_0 , are also passed to the mixer through the antenna

switch. As a result of the interaction of these oscillations a difference voltage is formed on the mixer output, i.e., the Doppler frequency F_d , which is then amplified by an amplifier.

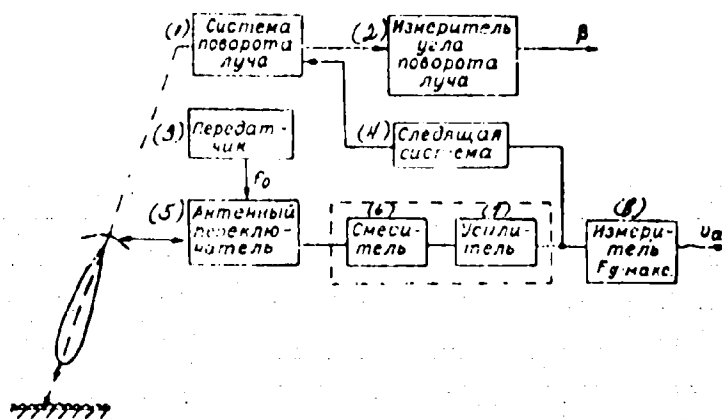


Fig. 2.5. Functional diagram of a Doppler ground speed and drift angle meter (DISS).

KEY: (1) beam rotation system; (2) beam rotation angle meter; (3) Transmitter; (4) Tracking system; (5) Antenna switch; (6) Mixer; (7) Amplifier; (8) F_d meter.

The amplified Doppler frequency signal passes to a special tracking system, which acts on the antenna rotation system in such a way that the beam is turned in the horizontal plane along the direction of the ground-speed vector. In this case the Doppler frequency F_d will be maximum; the frequency meter converts $F_{d, \max}$ into a signal proportional to ground speed v_a , while the beam rotation angle meter emits a signal which is proportional to the angle between the horizontal projection of the beam and the longitudinal axis of the aircraft - drift angle β .

The principle described above for measuring v_a and β by means of a single rotating beam has not found practical application due to the low accuracy in measuring ground speed and drift angle. At present multibeam Doppler speed and drift meters (DISS) are applied. The operating principle of multibeam DISS is based on the fact that the components of the ground speed vector in a linear system of coordinates connected with the aircraft are determined and are used for automatic

computation of the modulus of the ground speed vector v_g and drift angle β . A detailed description of the operating principle and the structure of a Doppler speed and drift meter was given in the work by G. K. Dudko and G. B. Reznikov (1964).

In aviation Doppler speed and drift meters (DISS), as a rule, are used in combination with navigation computers and course systems; in this case they make up Doppler navigation systems (DNS). The basic mission accomplished by the navigation computer of the DNS is computation of the path traveled by the aircraft.

At present a large number of types of DISS and DNS have been developed; these differ from one another in the number of beams, their type, radiation regimes, methods of measuring Doppler frequencies, etc. Table 2.1 gives some basic characteristics of a number of non-Soviet Doppler meters and Doppler navigation systems. The table was compiled from materials given in the works of N. V. Sytina (1957), P. B. Berger (1959), and by J. Holahan (1957).

Of particular interest are the data given in this table on the accuracy of determining ground speed of the aircraft (or, for certain systems, the components of the ground-speed vector) and in determining drift angle. For contemporary, fairly perfected DISS the probable relative error in determining ground speed during flight over dry land may be $\leq \pm 0.002$ of the maximum value. Errors in determining aircraft drift angle lie within the limits $\pm 0.15^\circ$.

In order to investigate the statistical characteristics of the horizontal component of wind speed it is necessary that it be possible to measure the instantaneous value of the wind vector. For this, besides ground speed and drift angle of the aircraft, it is obviously necessary to measure the airspeed of the aircraft v and the direction of the longitudinal axis of the aircraft in the geographic system of coordinates. Manometric speed pickups are used to measure the airspeed of the aircraft; these utilize the relationship between the speed of aircraft motion with respect to the air and the resultant dynamic impact pressure:

$$\Delta p = \rho \frac{v^2}{2}, \quad (2.34)$$

Table 2.1. Basic data on foreign DISS and DMS.

	AN/APN-66 AN/APN-61	AN/APN-78	AN/APN-79	AN/APN-86	AN/APN-87	AN/APN-88	AN/APN-85	AD-200
(1) Рассматриваемые системы								
(2) Число лучей антенной системы, шт.	(4) 4	(5) 3	(5) 3	(4) 4	(5) 2	(5) 3	(6) 4	
(3) Установки антенной системы	Полоротная, ус- табилизированная на вальной плат- форме	Фиксирован- ная	Фиксирован- ная	Полоротная, ус- табилизированная в вальной плат- форме	Фиксированная	Фиксированная	Полоротная, ус- табилизированная	
(7) Частота передатчика, МГц	8900	9799	11500	8800	13500	9799	8800	
(8) Режим излучения	(9) Импульсный	Квазими- пульс- ный	Непрерывный	Квазими- пульс- ный	Непрерывный	Квазими- пульс- ный	Импульсный	
(12) Длительность импульсов, мксек.	0.9			1.25—3			0.45	
(13) Частота повторений импульсов, кГц	(14) 50 при ме- дленном 130—1300, путе- вая скорость	15.6—125		83—200		4—125	50	(16) 185—1300, путе- вая скорость
(15) Предустановка измерения скорости, км/час		(17) 92—555, про- центная со- ставляющая скорости	(18) 185—2000, про- центная со- ставляющая скорости	(16) 140—1400, путе- вая скорость	(17) 148—1480, путе- вая скорость	(18) 155—2760, про- центная со- ставляющая скорости	(19) Не измеряет	
(18) Предустановка измерения вертикальной составляющей скорости, мксек.	(19) Не измеряет	±15	Не измеряет	Не измеряет	Не измеряет	±250	Не измеряет	
(20) Юшка измерения скорости в процентах от максимального показания шкалы; результаты усреднены на этапе, равном 18.5 км	±0.5, путе- вая скорость	±0.7, про- центная со- ставляющая росты	(21) ±0.7, про- центная со- ставляющая росты	(21) ±0.1, путе- вая скорость	(21) ±0.25, путе- вая скорость	(22) ±0.7, про- центная со- ставляющая скорости	(22) ±0.1, усреднен- ная на этапе, равном 18.5 км, путевая ско- рость	
(23) Предустановка измерения угла сноса, град.	±50	(24) Не измеряет по- перечную со- ставляющую скорости	(24) Не измеряет по- перечную со- ставляющую скорости	±30	±40	(24) Не измеряет по- перечную со- ставляющую скорости	±20	
(25) Точность измерения угла сноса	±0.15°	Точность изме- рения попе- речной со- ставляющей скорости ±0.7% (26)	Точность изме- рения попе- речной со- ставляющей скорости ±0.7% (26)	±0.15°			0.1°	
(27) Юшка определения места самолета, в процентах от пройсностиго расстояния	(28) ± гидрометрическим комплексом, 0.5 астрокомплексом (для AN/APN-66)	0.4 при точно- сти задания курса 0.25°	±0.5 при точно- сти задания курса 0.25°		(29) ±0.5 при точно- сти задания кур- са 0.1°	(29) ±0.5 при точно- сти задания кур- са 0.25°	1	

Reproduced from best available copy.

Table 2.1 (Cont'd).

Распределение данных	AN/APN-66 AN/APN-81	AN/APN-78	AN/APN-79	AN/APN-86	AN/APN-87	AN/APN-105	AD-100
(30) Предельные высоты, м. а) максимальная б) минимальная (31) Потребляемая мощность	21 000 150 (32) AN/APN-66 по постоянной ТОНУ 91-205 Вт. по переменному ТОНУ 2630-2950 Вт. AN/APN-81 а) по постоянной ТОНУ 67-95 Вт. б) по переменному ТОНУ 1650-1760 Вт. AN/APN-66 338 AN/APN-81 175	7500 0 600	21 000 0 850	21 000 60 700	21 000 0 900	24 000 0 850	21 000 120 (33) 24 (по переменному ТОНУ 750 Вт)
(34) Вес, кг	45	76.5	78.8	82	29.3	108.5	

KEY: (1) Data considered; (2) No. of antenna system beams, ea.; (3) Installation of antenna system; (4) Rotating, installed on a stabilized platform; (5) Fixed; (6) Rotating, not stabilized; (7) Transmitter frequency, MHz; (8) Radiation regime; (9) Pulse; (10) Quasi-pulse; (11) Continuous; (12) Pulse duration, us; (13) Pulse repetition rate, kHz; (14) With modulation; (15) Speed measurement limits, km/h; (16) Ground speed; (17) longitudinal speed component; (18) Limits of measurement of vertical speed component, ft/s; (19) Not measured; (20) Error in determining speed (as % of maximum scale reading); results averaged at level equal to 18.5 km; (21) Ground speed; (22) averaged on stage equaling 125 km, ground speed; (23) Drift angle measurement limits, deg.; (24) Measures transverse component of speed; (25) Drift angle measurement accuracy; (26) Accuracy in measuring transverse speed component 10.7%; (27) Error in determining aircraft location as % of distance traveled; (28) 1 with hydromagnetic compass, 0.5 with astrocompass (for AN/APN-66); (29) with accuracy of setting course of; (30) Limiting altitudes, m: a) maximum; b) minimum; (31) Power requirement; (32) AN/APN-66 on direct current 21-205 W, on alternating current 2620-2950 VA, etc.; a) on direct current; b) on alternating current; (33) (on alternating current, 750 VA); (34) weight, kg.

The basic relationships between elements of the navigation triangle are expressed as follows:

$$(v_a \cos \beta - v)^2 + v_a^2 \sin^2 \beta = u^2, \quad (2.36)$$

$$\delta = \psi + \beta, \quad (2.37)$$

$$\beta = \arctg \frac{v_a \sin \psi}{v_a \cos \psi - v}, \quad (2.38)$$

$$\delta = \frac{v}{v_a} + \varphi, \quad (2.39)$$

where

$$\varphi = \arctg \frac{v_a \cos(\psi + \beta) - v \cos \psi}{v_a \sin(\psi + \beta) - v \sin \psi}, \quad (2.40)$$

$$\mathbf{u} = [v_a \sin(\psi + \beta) - v \sin \psi] \cos \varphi + [v_a \cos(\psi + \beta) - v \cos \psi] \sin \varphi. \quad (2.41)$$

As was already indicated above, a Doppler speed and drift meter, DISS, and an airspeed sensor DVS, in combination with a gyroscopic course system make it possible to conduct continuous determination of v_a , β , v and ψ . Knowledge of these quantities makes it possible to solve the navigation triangle with respect to the wind vector parameters u and δ . In the course of designing equipment for automatic solution of this problem it was found to be more convenient to convert expressions (2.36)-(2.41) to a form convenient for calculation by means of automatic devices:

$$u = v_a \sqrt{1 + \left(\frac{v}{v_a}\right)^2 - 2 \frac{v}{v_a} \cos \beta}, \quad (2.42)$$

$$\delta = \psi + \arctg \frac{v_a \sin \beta}{v_a \cos \beta - v}, \quad (2.43)$$

$$u_1 \sin \varphi - u_2 \cos \varphi = 0, \quad (2.44)$$

$$u_1 \cos \varphi + u_2 \sin \varphi = u, \quad (2.45)$$

where

$$u_1 = v_a \cos(\psi + \beta) - v \cos \psi, \quad (2.46)$$

$$u_2 = v_a \sin(\psi + \beta) - v \sin \psi. \quad (2.47)$$

Figure 2.7 shows the functional diagram of a device for continuous measurement of current values of wind vector. Equations (2.46), (2.47), (2.44), (2.45) and (2.39) lie at the basis of the operating principle of the device. Solutions of equations (2.36) and (2.37) is not required in the explanations, since all of the quantities entering into these equations are given by the appropriate sensors. These equations are independent and the solution of each of them consists in successive fulfillment of the operations entering into them. As is evident from the functional diagram, these operations are fulfilled by means of functional units which carry out addition (subtraction) and sine-cosine conversion. Functional units of this type are standard and are used in analog computers (Kazakov, 1965).

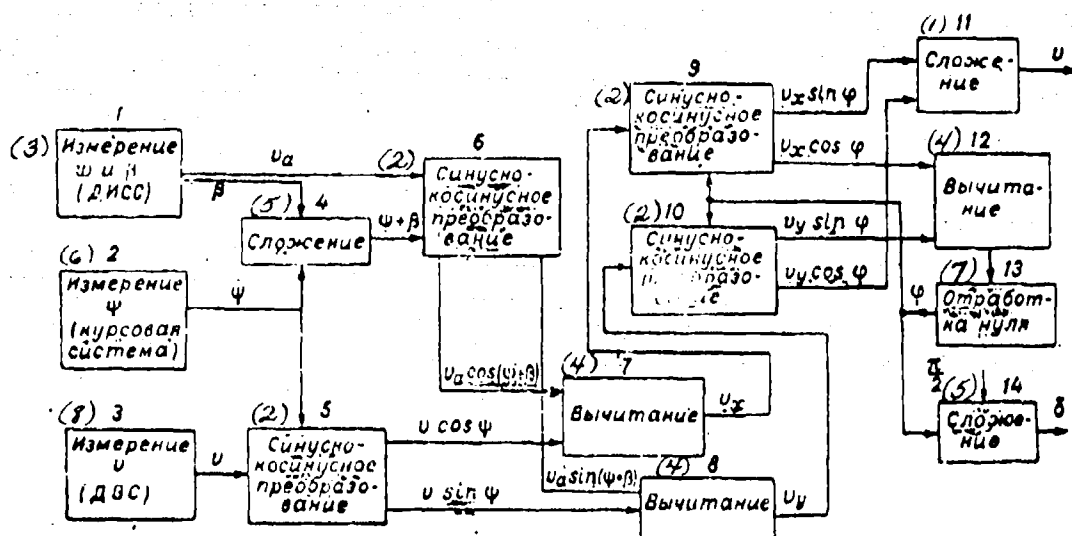


Fig. 2.7. Functional diagram of the measurement of the wind vector.

KEY: (1) Addition; (2) Sine-cosine conversion; (3) Measurement of w and v (DISS); (4) Subtraction; (5) Addition; (6) Measurement of ψ (course system); (7) Final null adjustment; (8) Measurement of v (DVS).

Equations (2.44) and (2.45) are mutually dependent and should be solved simultaneously. To determine u and v , the quantity ϕ should be known. This quantity is developed by unit 13. To clarify the operation of the circuit, we will assume that ϕ is given arbitrarily. In this case

$$u_1 \sin \varphi - u_2 \cos \varphi \neq 0,$$

(2.48)

i.e., a quantity different from zero appears on the output of unit 12. The function of unit 13 consists in changing φ until the signal on the input of unit 12 becomes equal to zero, i.e., until equation (2.44) is solved. Solution of equations (2.45) and (2.59) is clear from the functional diagram without additional explanations. Thus, the method described above makes it possible to determine the vector of wind speed and its fluctuations, using measurements of the vectors of absolute and relative speeds of the aircraft. We should also add that in practice several more complex systems are utilized; besides the wind vector, these permit obtaining its components in the aircraft system of coordinates. This last process is necessary during comparison with data on fluctuations of the horizontal component of aircraft airspeed as measured by methods which in principle single out the longitudinal (in the aircraft coordinate system) component (see § 1).

c. Method Utilizing Measurement of Pulsations in the Velocity of the Oncoming Flow (Hot-Wire Anemometric Method)

The major difference between this equipment and that described above lies in the fact that here the aircraft is used not as a sensor but as a platform for the installation of equipment. Of course, in this case also it is necessary to calculate carefully the natural behavior of the aircraft in a turbulent atmosphere; however, it has now been converted from an object of study into a certain disturbing factor.

One of the methods in which the aircraft plays the role of a measurement platform is the hot-wire anemometric method. The hot-wire anemometer long ago became the most widely used instrument in carrying out studies in wind tunnel (Shintee, 1963) and in the lowest layer of the atmosphere. The works of S. I. Knochner (1954) and S. S. Zulkovskiy (1955) describe a procedure for using hot-wire anemometers in studying turbulence in the lowest layer of the atmosphere; they also present the principal results obtained with these

instruments. This procedure was first applied as an aircraft method relatively recently (Vianichenko, 1964; Lumley and Pain, 1966).

The operating principle of the hot-wire anemometer is based on the fact that the heat removal from a heated filament placed in a flow of liquid or gas perpendicular to the flow direction depends on the speed of the flow (King, 1914):

$$Q = l(T_w - T_0)(K + \sqrt{2\pi K \rho d c_p v}), \quad (2.49)$$

where Q is the filament heat loss per unit time; l is the length of the filament; d is the filament diameter; T_w is the filament temperature; T_0 is the flow temperature; K is the coefficient of heat conductivity of the flow; ρ is the density of the medium; c_p is the heat capacity of the medium; v is the speed of the flow. In all hot-wire circuits used in practice the filament is heated by an electric current and, therefore, by connecting filament heat loss Q with current I or voltage U applied to the filament it is possible to write King's law in the form

$$U^2 = A + B\sqrt{v}. \quad (2.50)$$

where the coefficients A and B are determined by the filament parameters (length, diameter, material) and, in addition, are functions of the temperature T_0 and the density ρ of the air.

In studies of atmospheric turbulence the aircraft hot-wire anemometer is used to measure small-scale pulsations of the horizontal component of wind speed (perpendicular with respect to flight direction). During experiments in wind tunnels the hot-wire anemometer is, as a rule, immobile. Generally speaking the aircraft hot-wire anemometer moves arbitrarily with respect to the wind direction at a given altitude of flight, where the average speed of the flow encountered by the filament is determined only by the flight regime and is in no way connected with the average wind speed. Therefore the aircraft instrument cannot, in principle, measure the average wind speed (this problem is solved by the latter methods described above), but can

only measure the average airspeed of the aircraft and its pulsations (it is assumed that the filament is located perpendicular to the longitudinal axis of the aircraft).

However, it can be shown that in a certain region of scales the pulsations of the aircraft airspeed as a whole are determined by pulsations of the horizontal component of the wind speed. Actually, from analysis of the equations in (2.8), which describe the longitudinal motion of the aircraft, it follows that large-scale pulsations of the wind "pull along" the aircraft, changing its ground speed (speed with respect to the ground), while airspeed remains constant. On the other hand, small-scale pulsations of the wind cannot pull the aircraft along because of its inertia, and they therefore create pulsations of the flight air speed. Thus, the aircraft is characterized by a certain function which shows the reaction of the aircraft to the action of horizontal pulsations of the wind, depending upon their scale. The curve of such a function, called the longitudinal transfer function of the aircraft, is shown on Fig. 2.8, where Δv represents pulsations of air speed, Δu represents longitudinal wind pulsations, while L is the spatial scale of the pulsations. It is therefore obvious that the aircraft hot-wire anemometer can measure, without distortions, horizontal pulsations of wind speed with scales ranging from zero to a certain l_{rp} (thus, for the aircraft TU-104 the quantity $l_{rp} \approx 1-2$ km).

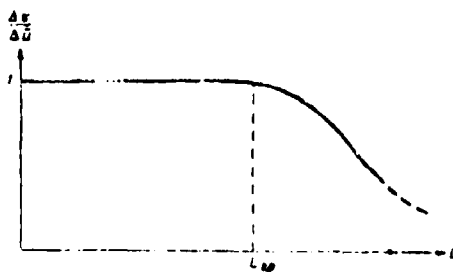


Fig. 2.8. Longitudinal transfer function of an aircraft.

In a turbulent atmosphere pulsations in windspeed exist in all directions. It is therefore necessary to show that the aircraft

hot-wire anemometer will measure only horizontal pulsations which are longitudinal with respect to the flight direction. If the hot-wire anemometer filament is arranged parallel to the transverse axis z of the aircraft, the instrument will measure the magnitude of any velocity vector v located in the plane xoy - i.e., perpendicular to the filament. It is obvious that the component v_x of vector v is the instantaneous airspeed of the aircraft, while v_y corresponds to vertical gusts of wind (it is assumed here that the aircraft is in a steady-state horizontal flight regime). Therefore \bar{v}_x equals the average airspeed, while \bar{v}_y is, generally speaking, equal to zero.

Now let the aircraft be subjected to the effect of a longitudinal (along the x -axis) gust with an amplitude of $+v_x$. Then the instrument will measure a quantity of velocity equal to $(\bar{v}_x + \Delta v_x)$. If the aircraft encounters a vertical gust with the magnitude $\Delta v_y = \Delta v_x$, a speed equal to

$$\left[(\bar{v}_x)^2 + (\Delta v_x)^2 \right]^{\frac{1}{2}} \quad (2.51)$$

will be measured.

Obviously, in the first case the magnitude of measured velocity pulsation will equal Δv_x , while in the second case it equals

$$\left\{ \left[(\bar{v}_x)^2 + (\Delta v_x)^2 \right]^{\frac{1}{2}} - \bar{v}_x \right\} \quad (2.52)$$

and goes to zero when $\bar{v}_x/\Delta v_x \rightarrow \infty$. Thus, at a sufficiently great average airspeed \bar{v}_x a hot-wire anemometer will, for practical purposes, measure only the longitudinal pulsations Δv_x and will virtually not react to vertical gusts Δv_y . For example, when $\bar{v}_x = 150$ m/s, which corresponds to the speeds of aircraft of the TU-104 type, a vertical wind gust with an amplitude of 5 m/s will be recorded as a pulsation with a magnitude of 4.07 m/s. We will note also that if the above reasoning is valid also for a filament located parallel to the y -axis, in practice it follows to locate the filament actually along the z -axis, since in this case the natural motions of

the aircraft in the pitch plane xoy will not affect the quality of measurement.

Actual circuits of hot-wire anemometers are very diverse. It is, however, possible to divide them into two basic types: direct current circuit and constant-temperature circuit. In the first case the filament is heated by a current whose magnitude is independent of speed, and the temperature of the filament or the filament resistance, uniquely connected with it, is measured. In the second case the temperature itself (or the resistance) remains constant, while the heating current required to maintain the filament temperature constant is measured as a function of speed. The constant-temperature hot-wire anemometer has a number of advantages as compared with the direct current circuit. The greatest of these is the extremely good frequency characteristic, which is particularly important in studying flows with large velocities. Since a hot-wire anemometer installed on a modern aircraft will always operate in a high-speed flow ($\bar{v} \geq 100$ m/s), it is better to use the constant-temperature setup. Figure 2.9 shows a block diagram of such an instrument.

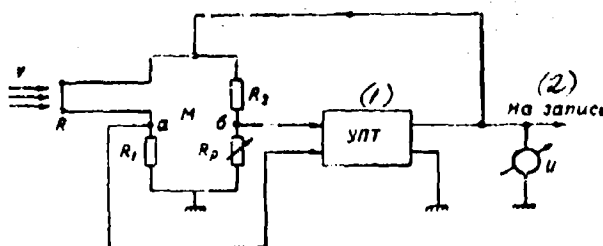


Fig. 2.9. Block diagram of a constant-temperature hot-wire anemometer.

KEY: (1) UPT; (2) To recording.

The operating principle of the constant-temperature hot-wire anemometer is as follows. At a certain constant speed of flow, let the measuring bridge M (consisting of resistance R of the anemometer filament, controllable resistor R_p , and fixed resistors R_1 and R_2) be in balance. This means that the voltage V which supplies bridge M ensures a magnitude of current through the filament such that its resistance equals $R = R_1 R_2 / R_p$ and there will be no voltage difference

between points a and b of the bridge. With a change in speed v resistance R of the filament is changed and an "error" voltage appears on the input of the controllable d-c amplifier (UPT), since bridge M is disbalanced and a voltage difference appears between points a and b. This entails a change in output voltage U of amplifier UPT and, consequently, a change in the current passing through the filament. The filament changes its temperature and, as a result, its resistance sufficiently to restore balance to the bridge. Controllable resistor R_p serves to assign the required temperature (resistance) of the filament, which is automatically maintained by the device in the course of the entire experiment.

One of the major features in the utilization of a hot-wire anemometer on an aircraft is the fact that the thermal and dynamic characteristics of the investigated flow are not constant. Actually, with a change in flight altitude from zero to 10-12 km the temperature and density of the air are essentially changed, a fact which must be taken into account during measurement. Generally speaking, by calibrating a given filament on the ground at constant temperature T_0 , constant air density ρ , and different v , it is possible to determine the coefficients A and B in formula (2.50); then, knowing the dependence of these coefficients on T_0 and ρ (Krechmer, 1954), it is possible to calculate corrections to A and B in terms of the measured T and ρ at a given flight altitude. Such a procedure is very tempting, since first of all the instrument becomes an absolute and, secondly, an independent method of measuring the average airspeed of the aircraft. However, at present this procedure is virtually inapplicable. First of all, the functional dependence of A and B on T_0 and ρ is quite complex and therefore the introduction of corrections without the use of automatic computers is extremely laborious. Secondly, the accuracy of contemporary aircraft methods of measuring T_0 and ρ is completely inadequate for accurate calculation of the correction. Thirdly, the hot-wire anemometer filament is usually so short-lived that the time spent on ground calibration frequently exceeds its "lifetime." Therefore when a hot-wire anemometer is used on an aircraft it is necessary to take the following approach. We will note first of all that the magnitude of average airspeed \bar{v} in itself

is necessary only for determination of the "working point" on the anemometer characteristic (formula (2.50)) and is, in this sense, an auxiliary quantity. Study of pulsations requires knowledge only of instrument sensitivity, which is determined by the expression

$$\alpha = \left(\frac{dU}{dv} \right)_v. \quad (2.53)$$

which gives the tangent of the slope of the instrument characteristic at working point \bar{v} . Differentiating (2.29) with respect to v , we find

$$\alpha = \frac{dU}{dv} = \frac{B}{4U\gamma v}. \quad (2.54)$$

At the same time, it follows from (2.50) that $B = \frac{U^2 - A}{\gamma v}$. We will note that A equals a certain U_0^2 when $B = 0$. Finally, we have

$$\alpha = \left(\frac{dU}{dv} \right)_v = \frac{U^2 - U_0^2}{4Uv}. \quad (2.55)$$

Thus, determination of α requires knowledge of the filament supply voltage U at a certain average flight speed \bar{v} , filament supply voltage U_0 at zero airspeed, and the quantity \bar{v} . The quantity U is measured by the hot-wire anemometer, while \bar{v} is determined with sufficient accuracy by means of standard aircraft instruments (see 1, pt. 5). The situation with regard to the quantity U_0 is more complex, since it is of course impossible to obtain a zero aircraft airspeed. Therefore, during installation of a hot-wire anemometer on an aircraft it is necessary to place the filament in a special strut (Vinnichenko, 1964), which makes it possible to remove the filament from the working position on command of the experimenter and place it in a protective housing manufactured in such a way that the airspeed in it equals zero. The described procedure makes it possible to conduct unique calibration of the instrument directly in the air at a given altitude (and, consequently, at given T_0 and ρ), which is very convenient.

The airborne hot-wire anemometer can be used only for studying turbulence in clear air, since the mechanical strength of the filaments used does not permit conducting measurements in clouds. Despite this serious limitation, the hot-wire anemometer allows obtaining valuable information on the microstructure of the wind field, thanks to the good frequency characteristic and high resolution in terms of scales. It is a natural supplement for the Doppler equipment, essentially expanding the spectrum of horizontal pulsations of the wind field which can be studied. The use of the hot-wire anemometer as an auxiliary apparatus during measurements of pulsations of temperature on high-speed aircraft is apparently very promising, since only highly accurate measurements of velocity pulsations make it possible to eliminate the influence of the dynamic pressure on the temperature sensors.

The aircraft hot-wire anemometer developed by N. K. Vinnichenko (1964) has the following basic characteristics. The sensor is a platinum wire 20 μm in diameter (or platinum-plated tungsten 18 μm in diameter); filament length is 2 mm and the working temperature is 250-400°C. The sensor operates at flight speeds up to 200 m/s at altitudes of 0 to 12 km in a clear sky. The upper limit of the frequency characteristic is no less than 1 kHz. The scales of pulsations which can be measured range from 50 cm to 1-2 km (for aircraft of the TU-104 type). Sensitivity (in the range of flight speeds 100-200 m/s) is 50-70 mV/m/s. Accuracy in measuring velocity pulsations (using standard aircraft sensors for measuring average airspeed) is about 10%. The instrument is equipped with an automatic stand for deployment of the sensor; this stand can be installed on any pressurized subsonic aircraft.

d. Method Using Measurement of Pressure at Different Points of the Body in the Flow (Anemoclinometer Method)

Measurement of the speed of motion of the aircraft in air (air-speed) is accomplished with manometric gauges in combination with the Pitot tube. As is known, the Pitot tube has an opening directed

parallel to the longitudinal axis of the aircraft and against the oncoming air flow. Another opening (or system of openings) is located along the side of the tube where the pressure is equal to the static pressure. The difference in the dynamic and static pressure is proportional to the square of the velocity of the oncoming flow (see (2.14)). The Pitot tube is used to measure the projection of velocity in the direction of flight. Measurement of the velocity vector in wind tunnels is accomplished with spherical fittings with a system of dynamic openings on the hemisphere which is directed against the main flow - so-called anemoclinometers.

L. A. Pakhomov (1962) used an anemoclinometer in measuring the vector of airspeed on an aircraft in clouds. A similar apparatus was used by A. Burns (1964) to study turbulence in clear air at altitudes up to 300 meters above Great Britain and North Africa. The sensor of the aircraft anemoclinometer is also a spherical fitting with a system of openings on the hemisphere directed against the oncoming flow.

The aircraft anemoclinometer has two pairs of openings arranged in the vertical and horizontal planes; they are arranged symmetrically with respect to a central opening which, like the dynamic opening of the Pitot tube, perceives the pressure of the total dynamic head.

Figure 2.10 gives a schematic section of a fitting in the plane xoy , where x is the longitudinal axis of the aircraft and y is the vertical axis. The pressure p on the inlet of the opening will be determined by the expression

$$p = p_0 + \frac{1}{2} \rho v^2 \left[1 - \frac{9}{4} \sin^2(\phi_0 + \Delta\phi) \right]. \quad (2.56)$$

where p_0 is static pressure; ρ is air density; v is the speed of the oncoming flow; $\phi_0 + \Delta\phi$ is the angle between the radius-vector connecting the center of the opening with the center of the sphere and the vector of the velocity of the oncoming flow. The longitudinal component of airspeed is measured in the usual way in terms of the difference between the total head sensed by the central opening and

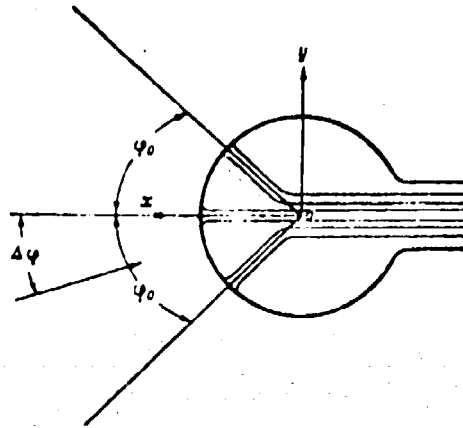


Fig. 2.10. Schematic cross section of an anemoclinometer fitting in the plane xoy (x - longitudinal aircraft axis; y - vertical axis).

the static pressure. If formula (2.56) is used, with substitution of $\psi_0 = 0$ and $\Delta\psi = 0$ in it, a known relationship is obtained:

$$\Delta p = p - p_0 = \frac{1}{2} \rho v^2. \quad (2.34)$$

[sic]

In order for the condition $\Delta\psi \approx 0$ to be fulfilled, before the beginning of measurement the entire fitting is oriented along the direction of the velocity of the oncoming flow. It can be shown (see § 1) that at an average velocity of the oncoming flow equal to 200 m/s (corresponding to the airspeed of the TY-104) the presence of a gust which is perpendicular to this velocity and which has a magnitude of 10 m/s will deflect the instantaneous vector of airspeed by an angle of less than 3° . In this case the error in determining the longitudinal component of airspeed does not exceed 0.5%. As was shown in the work by L. A. Pakhomov (1962), the difference in pressures on the inlet of the vertical and horizontal pairs of openings is proportional, respectively, to the corresponding vertical and transverse components of the airspeed vector. A differential manometer with an electrical output is used to measure the pressure difference. The aircraft anemoclinometer developed by Pakhomov (1962) is equipped with a computer which introduces corrections for air density, change in pitch angle, and the effect of carrying the

aircraft along by a gust of air. The true values of the components of the airspeed vector are obtained on the computer output. The measurement results are recorded by an optical automatic recorder. According to the data of A. Burns (1964), the instrument accuracy of measuring longitudinal and vertical pulsations of windspeed comprises about 10%. Owing to the natural transverse oscillations of the aircraft it is impossible to measure transverse pulsations of wind velocity by means of the anemometer.

c. Method Utilizing Measurements of the Angle of Attack (Anomoscope Method)

Sometimes an angle of attack anemoscope is used to measure pulsations of the vertical component of wind velocity on an aircraft (Ridland, 1964). The essence of this method consists in the fact that vertical pulsations of windspeed lead to pulsations in the angle of attack of the aircraft.

Instantaneous values of the angle of attack are measured by means of a special anomoscope, which is usually installed on an extension rod at a distance of 1.5-2.0 m ahead of the aircraft nose. Thanks to its low inertia, the anomoscope can react to comparatively small-scale gusts whose amplitudes are so small that their action does not lead to bumping of the aircraft.

It is obvious that for calculating the speed of vertical gusts from the readings of the anomoscope, α , it is necessary to pay attention to the motion of the aircraft itself along the vertical. First of all, it is necessary to calculate the instantaneous position of the aircraft - i.e., its pitch angle θ . Secondly, it is necessary to correct the readings of the anomoscope to the vertical velocity of the aircraft v_y , if it is carried along by the gust. Thirdly, it is necessary to consider the possible rotation of the aircraft around the transverse axis, which will lead to the appearance of a fictitious gust velocity.

Finally, in order to calculate pulsations of the vertical component of wind speed u_y it is possible to use the formula (Ridiand, 1964)

$$u_y = (x - l)v - v_y - l\theta' \quad (2.57)$$

where v is the true average airspeed; l is the distance from the aircraft center of gravity to the anemoscope; θ' is the rate of change of the pitch angle (angular velocity of aircraft rotation).

The quantity v_y is determined by integration of the vertical overload of the aircraft (see § 1). Ordinary and differential gyroscopes are used to obtain θ and θ' . It is clear that the given formula takes into account all corrections for any actions of the pilot with respect to control of the aircraft. This is especially significant, since the pilot ordinarily will interfere energetically in the behavior of the aircraft when intensive bumping is encountered.

It should be noted that the practical application of the described method can be successful only when the process of calculating u_y is automated, since in the opposite case the treatment becomes impermissibly lengthy.

The accuracy of measuring vertical pulsations of wind velocity by means of an angle of attack anemoscope comprises 10%, according to Ridiand.

f. Method Utilizing Measurement of the Speed of Sound (Acoustic Method)

The acoustic method is also used for aircraft investigations of the fine structure of atmospheric turbulence. It is known that the speed of propagation of sound in a flow of liquid or gas depends on its speed. This physical law is the basis of the instruments which are called ultrasonic (or acoustic) anemometers. Acoustic anemometers have been used to obtain important results touching on the properties of turbulence in the lowest layer of the atmosphere (Bovsheverov

et al., 1959). Comparatively recently B. M. Koprov and L. R. Tsvang (1965) and B. M. Koprov (1965) succeeded in applying the acoustic anemometer to the study of pulsations of wind velocity on an aircraft.

The sensor of the aircraft acoustic anemometer consists of an omnidirectional emitter of ultrasonic oscillations and two pairs of microphones located symmetrically with respect to the emitter along vertical axis y and transverse axis z of the aircraft. By measuring the pulsations in the propagation rate of sound from the emitter to the microphone it is possible to determine pulsations and windspeed along the respective axes.

In the coordinate system xyz , with the emitter located in its center, the x -axis corresponds to the longitudinal axis of the aircraft, the y -axis to the vertical, and the z -axis to the transverse; the vector of the velocity of the flow encountered by the aircraft can be broken down into the components v_x , v_y and v_z . The quantity v_x is the instantaneous airspeed of the aircraft, while v_y and v_z correspond to the vertical and transverse pulsations in wind velocity, respectively. We will designate the coordinates of the receiving microphones as $(0, l, 0)$ and $(0, -l, 0)$ for pairs which are arranged along the vertical axis y , and as $(0, 0, l)$ and $(0, 0, -l)$ for pairs which are located along the horizontal axis z . The propagation time for sound from the emitter to the microphone $(0, l, 0)$ equals

$$t_1 = \frac{l \left[(c^2 - v_0^2)^{\frac{1}{2}} - v_y \right]}{c^2 - v^2}, \quad (2.58)$$

where $v_0^2 = v_x^2 + v_z^2$, $v^2 = v_x^2 + v_y^2 + v_z^2$. Analogously, the time t_2 required for a sound wave to propagate to symmetrical microphone $(0, -l, 0)$ equals

$$t_2 = \frac{l \left[(c^2 - v_0^2)^{\frac{1}{2}} + v_y \right]}{c^2 - v^2}. \quad (2.59)$$

The difference between the times t_1 and t_2 will, obviously, characterize the vertical pulsations in windspeed (along the y-axis), since

$$t_1 - t_2 = - \frac{2l y}{c^2 - v^2}, \quad (2.60)$$

from which

$$v_y = (t_2 - t_1) \frac{c^2 - v^2}{2l}. \quad (2.61)$$

The same relationship is valid for a pair of microphones located along the transverse z-axis; consequently, these will measure the transverse pulsations of wind speed. Unfortunately, an acoustic anemometer installed on an aircraft does not permit measurement of longitudinal pulsations of windspeed, since a microphone located in front of the emitter (along the x-axis) will "shade" it, while the turbulent noise arising in the wake behind the microphone and emitter will disrupt operation of the second microphone.

The acoustic anemometer is used successfully on aircraft of the LI-2 and IL-14 types to study turbulence at altitudes of 50 to 4000 meters. The instrument includes a device which automatically inserts corrections for oscillation of the aircraft in the pitch plane xoy and for pulling along of the aircraft by vertical gusts.

The instrument has the following characteristics: the ultrasonic reference frequency equals 100 kHz; the upper limit of the frequency characteristic is 0.5 kHz; the scales of measurable pulsations range from 10 cm to 1 km (for the IL-14 type aircraft). Accuracy in measuring vertical pulsations of windspeed is about 10%. Owing to the strong distorting influence of aircraft yawing, transverse pulsations of the wind cannot be correctly measured by the acoustic method.

At present there is not yet any experience in using acoustic anemometers on high-speed high-altitude aircraft, and the technical and procedural difficulties which might arise in this case are as yet unclear.

g. Gyroscopic Instruments for Determining the Position of the Aircraft in Space

Without exception, methods of investigating atmospheric turbulence using an aircraft require detailed calculations of the actual position of the aircraft in space and its oscillation around this middle position. In certain cases, when the aircraft is used as a sensor, these data make up a useful "signal," carrying information on the state of the atmosphere (the overload method); in other cases, when the aircraft plays the role of an instrument platform, its natural vibrations become a disturbing factor, distorting the measurements (hot-wire anemometer, anemoclinometer, angle of attack anemoscope).

By the term position of the aircraft in space we understand in this case the angular distribution of a system of coordinates which is rigidly attached to the aircraft with respect to a system of coordinates tied to the ground - i.e., the relative motion of the centers of the systems of coordinates is eliminated from the consideration. The angular location of the aircraft system of coordinates with respect to the coordinate system which is tied to the ground can be given by means of three angles: pitch θ , bank ϕ , and course ψ . Here θ is the angle between the longitudinal axis of the aircraft and the plane of the true horizon, ϕ is the angle between the transverse axis of the aircraft and the horizon, and ψ is the angle between the vertical plane passing through the longitudinal axis of the aircraft and the meridional plane. These angles are determined on the aircraft by means of gyroscopic sensors (Braslavskiy and Logunov, 1954). The course angle ψ is also measured by means of magnetic compasses and astrocompasses.

As a rule, during investigation of atmospheric turbulence the principal attention is turned to measuring the angles of pitch, θ , and bank, ϕ , and their pulsations. These quantities are measured by means of a gyroscopic instrument which is called a vertical gyroscope (Fig. 2.11). The vertical gyroscope records deflections of the longitudinal axis x and transverse axis y of the aircraft from the plane of the true horizon. Operation of the instrument is based on

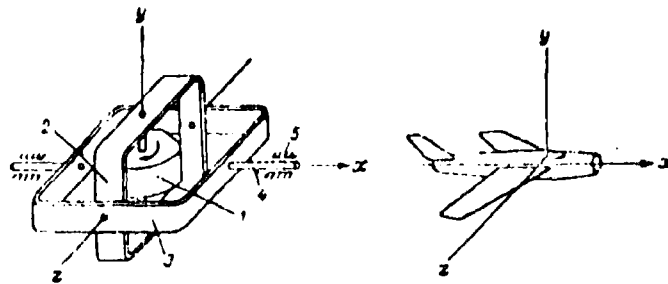


Fig. 2.11. Diagram of vertical gyroscope.

the property of a free gyroscope to retain an unchanging position of the axis of spin (arranged vertically along the y-axis) relative to outer space. The term gyroscope is applied to rotor 1, which rotates rapidly around its axis of symmetry and which is suspended in two cardan frames: internal 2 (pitch frame) and external 3 (bank frame). Axis 4 ties frame 3 to the gyroscope housing 5, which is rigidly attached to the aircraft. Such a gyroscope has three degrees of freedom, since the rotor can rotate around three mutually perpendicular axes x, y, and z. Cardan suspension 2, 3 permits the rotor axis to retain a vertical position in space at any angles of pitch θ and bank ϕ . For transmission of data on the angles θ and ϕ , potentiometers (or stator windings of relays) are attached to gyroscope housing 5, while potentiometer arms (or rotor windings of relays) are attached to cardan suspension frames 2 and 3. If the aircraft changes angles of pitch and bank, the relative position of the gyroscope housing and cardan frames change correspondingly; in its turn, this leads to a change in the output voltages on the potentiometers (or relays) of pitch and bank.

Contemporary airborne vertical gyroscopes provide accuracy in measuring angles of bank and pitch equal to $\pm 0.5^\circ$; their sensitivity is no less than 0.1° and makes it possible to trace angular displacements of the aircraft occurring at rates up to 360° per second.

While for the overwhelming majority of aircraft instruments described in 5.1 of this chapter the readings of pitch and bank gyroscopes are most essential, for Doppler computers of windspeed exact measurements of course ψ are also necessary for calculation of

the true wind direction. Gyroscopic instruments in which the gyroscope axis of rotation is arranged horizontally in the meridional plane are called course instruments.

In § 1, pt. b formulas are given for calculating the vector of the wind; these formulas include course angle ψ as measured by a course gyroscope.

In those cases when angular displacements of the aircraft are a "disturbing" factor, it is sometimes advisable to arrange the measuring instruments on a special platform whose position is stabilized in space by means of gyroscopic systems and thus does not depend on the evolutions of the aircraft. The widest use is made of platforms which are stabilized only with respect to angles of pitch and bank - i.e., platforms which remain parallel to the plane of the true horizon. Such platforms are used in certain Doppler navigation systems for stabilization of system position (see § 1, pt. b).

4. Combined Table of Aircraft Methods of Studying Turbulence

The methods examined in this section are intended for measurement of motions in a turbulent flow. In a turbulent flow not only the velocity field, but also the fields of temperature, density, etc., are nonuniform. With the presence of a conservative impurity in the atmosphere its distribution will also be determined by the structure of the field of turbulence. A variety of methods exist for measuring such atmospheric parameters as pulsations of temperature, pulsations of the dielectric constant, etc., by means of which it is possible to study the structure of an atmospheric flow. Airborne meters of temperature pulsations and also aircraft refractometers have been developed and applied to investigations of turbulence.

In this book, however, we have limited ourselves to consideration of methods which only measure directly the speed of turbulent motions. Table 2.2 presents comparative characteristics of the aircraft methods

Table 2.2. Comparative characteristics of aircraft methods for investigating atmospheric turbulence.

(1) Авиация	(2) Измеряемые составляющие скорости относительно направления полета ¹	(3) Частотный диапазон, Гц	(4) Разрешающая способность по высоте, км, м	(5) Чувствительность, м/сек.	(6) Диапазон измерений воздушной турбулентности, м/сек.	(7) Характеристики аппаратуры	(8) Примечание к аппаратуре
(9) Истребительный	y	0 - (~10)	~50	~0,5	50-5000	15	(10) Илет
(10) Дальновоздушный	x, z	0 - (~0,1)	~1000	~0,3	>3000	5	(12) Горы, штилевая вода, морская поверхность
(13) Турбореактивный	x	0 - (~1000)	~0,1	~0,05	10-1000	10	(14) Облака, пыль
(15) Аэробаллистический*	x, y, z ²	0 - (~50)	~1	~0,1	10-500	10	(16) Илет
(16) Фотонера угла атаки	y	0 - (~20)	~5	~0,1	10-3000	10	(17) Облачные
(18) Акустический*	y, z ²	0 - (~10000)	~0,1	~0,1	10-500	10	(19) Высокочастотный шум

¹Designations are given in the aircraft coordinate system: x-axis, longitudinal; y-axis, vertical; z-axis, transverse.

²Transverse components (along the z-axis) are practically impossible to measure owing to the strong distorting influence of aircraft yaw.

³Characteristics are given with respect to the aircraft И-2 and И-14 (airspeed 50-70 m/s). Characteristics of the remaining methods are given with respect to aircraft of the types И-18 and ТУ-104 (airspeed ~120-200 m/s).

KEY: (1) Method; (2) Components of wind velocity with respect to flight direction which can be measured; (3) Frequency range, Hz; (4) Scale resolution, m; (5) Sensitivity, m/s; (6) Range of measurement scales of wind velocity pulsations, m; (7) Accuracy, %; (8) Limitations in application; (9) Overload; (10) None; (11) Doppler; (12) Mountains, still water surface; (13) Hot-wire anemometric; (14) Clouds, dust; (15) Anemoclinometric; (16) Angle of attack anemoscope; (17) Icing; (18) Acoustic; (19) High-frequency noise.

examined above. Neither the table nor this entire § 1 pretend to an exhaustively complete survey of aircraft methods. The methods presented in Table 2.2 represent the major procedures and were used to obtain the majority of the results presented in the following chapters of this book.

5.2. RADIOSONDE METHOD OF STUDYING ATMOSPHERIC TURBULENCE

During ascent in unperturbed air a radiosonde has a constant vertical velocity or one which changes very little and monotonically. If the balloon arrives in a turbulized layer chaotic fluctuations of the velocity field will be perceived by the balloon and will disrupt the monotonic nature of its motion. As S. N. Shmeter showed (1957), the motion of a balloon probe in an accelerated airflow is determined by the expression

$$m_1 \frac{dv}{dt} = m_2 \frac{dw}{dt} + m_{sp} \frac{d}{dt} (w - v) - \frac{3}{8} \frac{c_x}{r} m_2 (w - v)^2 + (m_2 - m_1)g - N. \quad (2.62)$$

where m_1 is the mass of the balloon; m_2 is the mass of the air in the balloon volume; v is the speed of the balloon; w is the vertical speed of the flow; m_{sp} is the associated mass; r is the balloon radius; c_x is the aerodynamic drag factor; N is the vertical component of the reaction of the suspension, if the balloon is loaded.

Analyzing equation (2.62) for certain particular cases of a change in flow velocity, Shmeter showed that a rising balloon will trace changes in the vertical component of the speed of flow quite well if the scale of these changes is greater than the characteristic dimension of the balloon. For the particular case of an instantaneous jump in vertical velocity it was found that a balloon carrying a weight of 1 kg on a suspension will pick up almost completely the changing velocity of the flow as quickly as 1.5 seconds.

Thus, by measuring the change in the rate of ascent of the balloon it is possible to obtain information on the change in velocity (acceleration) of the airflow. An accelerometer suspended to a balloon probe was used for the first time to measure turbulence by C. Junge (1938). In subsequent years independent probe and parachute overload instruments were created in the Soviet Union and in the United States of America. V. P. Velyayev and G. N. Shar (1960, 1961) developed a method and created equipment for continuous measurement of overloads in flight of lot-produced aerological radiosondes, simultaneously with measurements of the basic meteorological parameters. The operating principle of the sounding overload device is as follows. The balloon probe, upon entering an accelerated air current, is easily carried along by this flow, since its mass is small and its dimensions comparatively large. At the same time the radiosonde itself possesses comparatively great mass. The radiosonde with mass M is suspended to the balloon on a spring, as depicted on Fig. 2.12. The magnitude of initial displacement x_0 , corresponding to rest or uniform motion of the balloon, can be determined from the relationship

$$Kx_0 = Mg, \quad (2.63)$$

where K is spring rigidity and M is the mass of the radiosonde. With a change in the speed of the balloon $dw/dt = a$, we obtain

$$M(g + a) = K(x_0 + \Delta x). \quad (2.64)$$

Subtracting (2.63) from (2.64), we have

$$K\Delta x = Ma = M \frac{dw}{dt}. \quad (2.65)$$

Consequently, the change in the length of the spring is connected linearly with acceleration of the balloon. As is known, by means of coded signals of its radio transmitter the radiosonde accomplishes discrete transmission of meteorological information to the ground. However, information on accelerations of the balloon must be transmitted virtually continuously. V. P. Velyayev and G. N. Shar introduced a variable resistor, kinematically connecting the

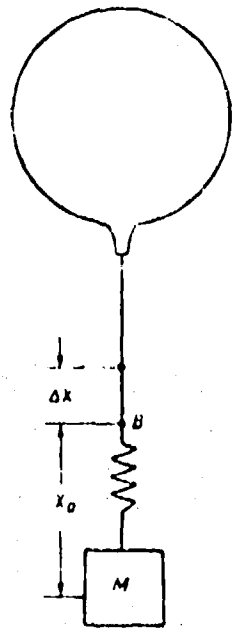


Fig. 2.12. Diagram of overload radiosonde.

potentiometer arm with the upper end of the spring, into the circuit of the transmitter tube grid. The change in the resistance of the transmitter tube grid circuit changes the duty cycle of the coded pulser, while at the same time the repetition rate of these pulses varies as a function of pressure, temperature, and humidity of the air. On the ground an instrument called the probe overload meter (POM) is connected to the output of a radio theodolite receiver. The operating principle of this instrument is based on the measurement of the duty cycle of video pulses in the low-frequency radiotheodolite receiver channel. Figure 2.13 shows a block diagram of the equipment used in this method.

Acceleration of the balloon probe is converted into relative displacement of the balloon and the radiosonde. By means of the spring and the potentiometer which is connected into the radio transmitter tube grid circuit, this displacement is converted into a change in the duty cycle of pulses which modulate the carrier frequency of the radio transmitter. The transmitter emits high-frequency pulses of variable duty factor; the radiotheodolite receiver separates the video signal with variable duty cycles; the

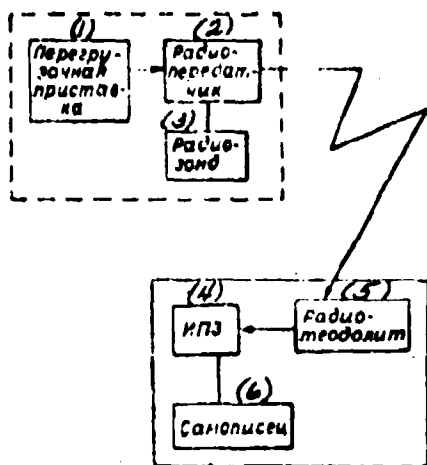


Fig. 2.13. Block diagram of the method of measuring overloads of a radiosonde.

KEY: (1) Overload attachment; (2) Radio transmitter; (3) Radiosonde; (4) POM; (5) Radiotheodolite; (6) Automatic recorder.

probe overload meter converts the change in video signal duty cycle into a change in current force. An automatic recorder records the current, which is proportional to the duty cycle of the video signal and, consequently, to the acceleration of the balloon probe.

The method developed by Belyayev and Shur permits measurement with high accuracy of the g-forces on a balloon probe in flight; however, transition from acceleration of the balloon to acceleration of the flow is connected with substantial difficulties. First of all, a balloon with a radiosonde suspended from it is not a sphere, but has a complex and usually irregular shape; therefore the analytical formulas proposed by Shmeter cannot be used for quantitative description of the behavior of the balloon in an accelerated air flow. Besides this, as kinotheodolite observations have shown, during ascent a balloon accomplishes unordered rotational oscillations caused, it is assumed, by nonuniform stretching of the elastic shell during ascent. These oscillations can act on the suspension and can be picked up by the instrument as vertical accelerations. Theodolite observations also have shown that the radiosonde swings on the suspension, describing complex curves. In this case forces arise which act on the instrument in the same way as acceleration of the flow.

All of the above indicates that as yet the sounding method cannot be used for quantitative measurements of accelerations and velocities of turbulent pulsations in windspeed.

However, despite this the method made it possible to obtain a large quantity of interesting data on the turbulent stratification of the atmosphere up to altitudes of 25-30 km - i.e., at those altitudes at which measurements of turbulence are not carried out by aircraft, radar, or other methods. Special comparisons of data obtained by the radiosonde method with results of measurements by specially equipped aircraft (as described in the work by V. P. Belyayev et al., 1965) showed good coincidence in the altitudes and thicknesses of detected turbulent layers. Despite the present impossibility of constructing any sort of strict theory of the method, all of this permits us to consider it an extremely useful tool during the study of turbulent stratification of the atmosphere up to altitudes of 25-30 km.

§ 3. RADAR METHODS OF STUDYING ATMOSPHERIC TURBULENCE

The application of radar devices to the measurement of movements in the atmosphere was undertaken comparatively recently, and the obtained results relate mainly to the lowest layer of the atmosphere. However, the promise in radar methods is extremely great and in the future these methods will make it possible to obtain data on the structure of turbulence in the free atmosphere as well.

The basic distinction between radar methods and aircraft methods lies in the fact that while an aircraft acting as a measuring instrument is located directly in the flow, the radar is located on the ground and particles which will reflect the radar signal are introduced into the turbulent flow.

During investigation of turbulence in clouds and precipitation, drops and crystals are used as passive radar signal reflectors. The further development of radar technology, accompanied by a rapid growth in radar set potentials, will undoubtedly permit using particles of atmospheric dust, zones characterized by sharp changes in the coefficient of refraction, etc., as reflecting and scattering objects.

Several methods exist for measuring the motions of scattering objects; all of them are based on analysis of the characteristics of the signal reflected from a certain volume filled with scattering objects which are easily carried along by motions of the ambient air.

The first method is the so-called method of pulse-by-pulse analysis proposed by A. G. Gorelik, V. V. Kostarev, and A. A. Chernikov (1958).

The transmitter of a pulse incoherent station emits electromagnetic waves in a narrow beam, which penetrates a cloud of scattering objects. Radio waves which are reflected by the objects are recovered by the set antenna; however, the radar receiver is switched on only for a brief time segment - in the interval between packets of sounding pulses. The volume which is singled out during observation is limited by beam diameter and the duration of receiver on-time. In the period between successive sounding pulses the mutual position of the scattering objects within the selected volume changes. In this connection the phase ratio in the received signal is changed and, consequently, there is a change in its magnitude on the receiver output. Fluctuations in the amplitude of the output signal are determined by the relative rates of motion of the scattering objects within the selected volume, where the frequency of the output signal fluctuations grows with an increase in relative velocity.

After isolating the envelope of the output signal it is possible to use the number of maxima n in observation period Δt for approximate determination of the rate of relative motion of the scattering objects, u_s :

$$u_s = \frac{n\lambda}{2\Delta t}. \quad (2.66)$$

where λ is the transmitter wavelength. This, of course, requires that the transmitter frequency be adequately stable. If the scattering objects are carried along by the flow so easily that their rate of gravitational fall can be ignored, the spectrum of radar signal

intensity fluctuations will be determined by the relationship

$$G(F) = \bar{A} P_r\left(\frac{\lambda F}{2}\right), \quad (2.67)$$

where \bar{A} is the average power of the signal reflected from the totality of objects; F is the frequency of signal intensity fluctuations on the radar receiver output; $P_r(u_s) = P_r\left(\frac{\lambda F}{2}\right)$ is the distribution of projections of relative velocities of the scattering objects in the direction of the beam.

The use of Doppler stations made it possible to obtain data on the absolute velocities of the scattering objects. Using a pulse Doppler radar, it is possible to measure both the average wind speed (from the average Doppler frequency) and also its fluctuations (from the nature of the signal spectrum on the output of the Doppler radar set phase detector). Certainly, all of this is valid only in the case when the scattering objects are easily carried along by the flow. Yu. V. Mel'nichuk (1964) showed that the spectrum of Doppler frequencies is connected with the distribution of projections of absolute velocities of scattering objects in the direction of the beam by the relationship

$$G_s(F) = \bar{A} P_r(u), \quad (2.68)$$

where $P_r(u)$ is the distribution of radial components of absolute velocity of scattering objects in the selected volume.

Along with their unquestioned advantages, radar methods of investigating turbulence possess a whole series of deficiencies. Thus, for example, due to the low potentials of contemporary radar the correct measurement of turbulent motions requires scattering objects with high reflectivity and, consequently, comparatively large dimensions. Such objects are poorly carried along by an airflow and their motion will be determined mainly by gravitational fall. Another substantial drawback of radar methods is the fact that the method itself is based on averaging over a scattering volume. This leads to

a very complex connection between the statistical characteristics of the Doppler signal and the statistical characteristics of turbulent pulsations of velocity.

In the work by A. G. Gorelik and A. A. Chernikov (1964), and also in that by A. G. Gorelik (1965), an attempt was made to measure the structure of turbulent pulsations of wind velocity in clouds. As regards investigations of turbulence in the free atmosphere in clear air, works published in the Soviet Union and abroad at present show only the possibility, in principle, of such measurements.

When speaking of the study of clear-air turbulence by means of radar, one should emphasize that the most promising approach is the application of lidars - laser locaters. Already several approaches have been outlined for solution of the problem of measuring turbulent motions in clear air by this method. The work by Collis (1964) presents data on the detection of two turbulent layers in the clear air by means of a lidar. The application of modulated laser emission for studying atmospheric turbulence holds vast possibilities. It is obvious that the procedure for measuring the structure of turbulence which has been developed with application to radar methods may be used also during the study of clear-air turbulence by means of lidars.

CHAPTER 3

STATISTICAL ANALYSIS OF MEASUREMENTS

In recent years statistical analysis has been used ever more frequently for processing observation materials. The statistical nature of many phenomena in the atmosphere makes such analysis necessary, while the appearance of a variety of computer equipment (analog and digital) creates a real possibility for carrying it out. Therefore it is necessary to pause, however briefly, on methods of statistical analysis and, no less important, on the accuracy of the obtained results. It must be noted that while the actual methods of statistical analysis are comparatively well known, the question of the accuracy of the obtained statistical characteristics is represented in meteorological literature comparatively weakly. This, in its turn, hampers (and frequently makes simply impossible) comparison of experimental data of different types and in addition can lead to erroneous conclusions on the nature of phenomena.

The most frequent results of statistical processing are dispersions, structural and correlation functions, and also spectral densities, which are simple and at the same time the most important characteristics of meteorological fields.

This chapter will outline methods of calculating spectra of meteorological parameters and also will point out errors arising during these calculations. The preference which the authors have assigned to spectra is explained by the ease of physical interpretation of spectral characteristics and the comparative simplicity of spectral conversions, a very important factor for practical applications.

We will also note that the scope of this book does not permit us to stop to consider the derivations of the majority of the formulas which will be introduced. Readers can find them in special monographs (see, for example, Blackman and Tukey, 1958).

§ 1. CALCULATION OF SPECTRA FROM CONTINUOUS RECORDINGS OF FINITE LENGTH

a. Some Definitions

Although the basic concepts of the statistical characteristics which describe the field of random velocities in a turbulent flow were already formulated in Chapter 1, it will be useful to repeat here certain of these while, generally speaking, digressing from the connection of these characteristics with turbulence.

The function $u(t)$ is called a random function of time if its value at any moment of time is a random quantity characterized by a certain probability distribution. Virtually everywhere below we will consider that the random process which generates $u(t)$ is Gaussian - i.e., for any set t_1, t_2, \dots, t_n the combined distribution of probability $u(t_1), \dots, u(t_n)$ is an n -dimensional Gaussian (normal) distribution. Each such distribution is completely defined by the average values of $\overline{u(t_i)}$ and by covariances

$$R_{ij} = \overline{\{[u(t_i) - \overline{u(t_i)}] \cdot [u(t_j) - \overline{u(t_j)}]\}}.$$

The line over the top indicates averaging in terms of the statistical ensemble, i.e., over an infinite set of functions $u(t)$, each of which is a particular manifestation of a single random process.

For convenience we shall assume that all $\overline{u(t_i)} = 0$. Besides this, it will be assumed everywhere below that the process is stationary (i.e., uniform with respect to time). Then

$$R_{ij} = \overline{u(t_i) \cdot u(t_j)} = R(t_i - t_j).$$

Thus, a stationary random process is completely determined by a unique function of a single variable $\tau = t_1 - t_2$.

However, it is obvious that during experimental study of random processes in the atmosphere it is most frequently necessary to deal with a unique function of time and not with a group of functions. This is precisely why it is extremely important that averaging over the group (the so-called ergodicity) is equivalent to averaging in time under the condition that the process is stationary and Gaussian and has a zero average value and a continuous energy spectrum. In other words, we can write

$$R(\tau) = \overline{u(t)u(t+\tau)} = \lim_{T \rightarrow \infty} \frac{1}{T} \int_{-T/2}^{+T/2} u(t)u(t+\tau) dt.$$

A. Ya. Khinchin (1938) showed that $R(\tau)$ can be presented in the form of a Fourier transform¹ from a certain function $S(f)$:

$$R(\tau) = \int_{-\infty}^{+\infty} S(f) e^{i2\pi f \tau} df. \quad (3.1)$$

where

$$S(f) = \lim_{T \rightarrow \infty} \frac{1}{T} \left| \int_{-T/2}^{+T/2} u(t) e^{-i2\pi f t} dt \right|^2.$$

Here and throughout this chapter $f = \omega/2\pi$. The function of frequency $S(f)$ is called the energy spectrum of the stationary random process being considered. The quantity $S(f)df$ is the contribution to dispersion of the process from frequencies between f and $(f + df)$. Besides (3.1), there exists the inverse Fourier transform, which makes it possible to express the energy spectrum through the autocorrelation function

$$S(f) = \int_{-\infty}^{+\infty} R(\tau) e^{-i2\pi f \tau} d\tau. \quad (3.2)$$

¹Under the term "Fourier transform" we understand a function obtained as the result of a Fourier transformation.

Since $R(\tau)$ and $S(f)$ are even functions, formulas (3.1) and (3.2) can be written in the form

$$R(\tau) = \int_{-\infty}^{+\infty} S(f) \cos 2\pi f \tau df, \quad (3.3)$$

$$S(f) = \int_{-\infty}^{+\infty} R(\tau) \cos 2\pi f \tau d\tau \quad (3.4)$$

or, even more simply,

$$R(\tau) = 2 \int_0^{\infty} S(f) \cos 2\pi f \tau df, \quad (3.5)$$

$$S(f) = 2 \int_0^{\infty} R(\tau) \cos 2\pi f \tau d\tau. \quad (3.6)$$

b. Calculation Procedure

In an actual experiment it is possible to obtain only a limited number of realizations of the function $u(t)$, each of which has a finite length. Therefore it is possible to obtain from available data only estimates (i.e., approximate values) of the autocorrelation function and the energy spectrum.

Actually, with a continuous recording of finite length it is impossible to estimate the values of $R(\tau)$ for τ which are greater than the length of the recording. Besides this, as will be shown below, it is usually undesirable to use τ which are greater than 5-10% of the length of the recording.

Thus, instead of

$$R(\tau) = \lim_{T \rightarrow \infty} \frac{1}{T} \int_{-T/2}^{+T/2} u(t) \cdot u(t + \tau) dt,$$

where $R(\tau)$ is meaningful for all τ , it is necessary to write

$$R_{00}(\tau) = \frac{1}{T_a - \tau} \int_{\tau/2}^{T_a - \tau/2} u\left(t - \frac{\tau}{2}\right) \cdot u\left(t + \frac{\tau}{2}\right) dt, \quad (3.7)$$

where $R_{00}(\tau)$ is meaningful only for $|\tau| \leq \tau_m < T_n$, where T_n is the length of the recording and τ_m is the maximum shift in time which it is desirable to utilize.

In view of the fact that the experimental autocorrelation function $R_{00}(\tau)$ is known only for $|\tau| \leq \tau_m$, generally speaking it is not possible to use one of the formulas (3.2), (3.4), or (3.6) for calculation of $S(f)$, since these formulas require values of $R(\tau)$ for all τ . In this case it is most natural to consider that when $|\tau| > \tau_m$, $R_{00}(\tau) = 0$, i.e., to assign a certain function $R_1(\tau)$ such that

$$R_1(\tau) = \begin{cases} R_{00}(\tau) & \text{при } |\tau| \leq \tau_m, \\ 0 & \text{при } |\tau| > \tau_m. \end{cases} \quad (3.8)$$

[при = when]

The symbol 1 is inserted in order to avoid entangling the obtained autocorrelation function with either the true $R(\tau)$ or with the experimental $R_{00}(\tau)$ function.

The function $R_1(\tau)$ is called a modified experimental autocorrelation function. Conversion from $R_{00}(\tau)$ to $R_1(\tau)$ is accomplished very simply; however, as will be shown below, it is reflected in a fairly complex manner in the form of the energy spectrum obtained from $R_1(\tau)$ by means of the Fourier transform.

Actually, formula (3.8) is equivalent to the notation

$$R_1(\tau) = D_1(\tau) R_{00}(\tau), \quad (3.9)$$

where

$$D_1(\tau) = \begin{cases} 1 & \text{при } |\tau| \leq \tau_m, \\ 0 & \text{при } |\tau| > \tau_m. \end{cases} \quad (3.10)$$

Since $R_1(\tau)$ is known for all τ , it is possible to fulfill the Fourier transform and to obtain

$$S_1(\omega) = Q_1(\omega) * S_{00}(\omega), \quad (3.11)$$

where $Q_1(f)$ is the Fourier transform from $D_1(\tau)$; $S_{00}(f)$ is the Fourier transform from $R_{00}(\tau)$, while the asterisk designates the mathematical operation of convolution¹.

Despite the fact that $S_{00}(f)$ is not determined (since $R_{00}(\tau)$ is known only for $|\tau| \leq \tau_m$), we can write (in view of ergodicity)

$$\overline{R_1(\tau)} = D_1(\tau) \cdot R(\tau), \quad (3.12)$$

where $R(\tau)$ is the true autocorrelation function. From (3.12) it follows immediately that

$$S_1(\omega) = Q_1(\omega) * S(\omega), \quad (3.13)$$

where $S(f)$ is now the true energy spectrum.

By interpreting the symbolism of convolution, it is possible to rewrite (3.13) in the form

$$\overline{S_1(\omega)} = \int_{-\infty}^{+\infty} Q_1(\omega - \eta) S(\eta) d\eta.$$

As is evident from (3.13), the average value of $S_1(f_1)$ is obtained by means of smoothing (averaging in terms of frequencies) the true energy spectrum close to f_1 with weights which are proportional to $Q_1(f_1 - f)$. It is therefore natural to call $Q_1(f)$ a spectral window, and to call the function $D_1(\tau)$ a time window.

It is clear that the quality of evaluations of the energy spectrum obtained by means of (3.13) depends to a great degree on the type of weighting function (or the spectral window) $Q_1(f)$, and

¹If the functions ϕ_1 and ϕ_2 are given, the operation of convolution of these functions is described in the form $\phi_1 * \phi_2 = \psi(y) = \int_{-\infty}^{+\infty} \phi_1(x-y) \phi_2(y) dy$.

consequently on the selection of the time window $D_1(\tau)$. Thus, it is necessary to strive not toward "simplicity" of $D_1(\tau)$, but toward a position in which the Fourier transform from a certain specially selected $D_1(\tau)$ will be concentrated close to $f = 0$ and would have small side maximums (as compared with the maximum on the frequency $f = 0$).

We will examine several specific examples of functions $D_1(\tau)$ and the $Q_1(f)$ corresponding to them. Let the time window be given by formula (3.10):

$$D_1(\tau) = \begin{cases} 1, & |\tau| \leq \tau_m; \\ 0, & |\tau| > \tau_m. \end{cases} \quad (3.14)$$

The symbol i is replaced here by 1 in order to show that the first pair of windows is being considered.

Then

$$Q_1(f) = \tau_m \frac{\sin 2\pi f \tau_m}{2\pi f \tau_m} \frac{1}{1 - (2\pi f \tau_m)^2}. \quad (3.15)$$

Figure 3.1 shows the curves of the functions $D_1(\tau)$ and $Q_1(f)$. From the figure it is clear that the seemingly simple and natural selection of $D_1(\tau)$ leads to a comparatively complex function $Q_1(f)$ in which, moreover, the first side extremum is negative and comprises almost 1/5 of the height of the main maximum.

Different authors have proposed several types of time windows $D_1(\tau)$ which have Fourier transform $Q_1(f)$ satisfactory for practical purposes.

We will pause on two generally accepted forms of assigning $D_1(\tau)$. The time window $D_2(\tau)$ proposed by W. von Hann [exact spelling not determined - translator] has the following form:

$$Q_1(f) = \int_{-\tau_m}^{\tau_m} D_1(\tau) e^{-i2\pi f \tau} d\tau = 2\tau_m \frac{\sin 2\pi f \tau_m}{2\pi f \tau_m}. \quad (3.16)$$

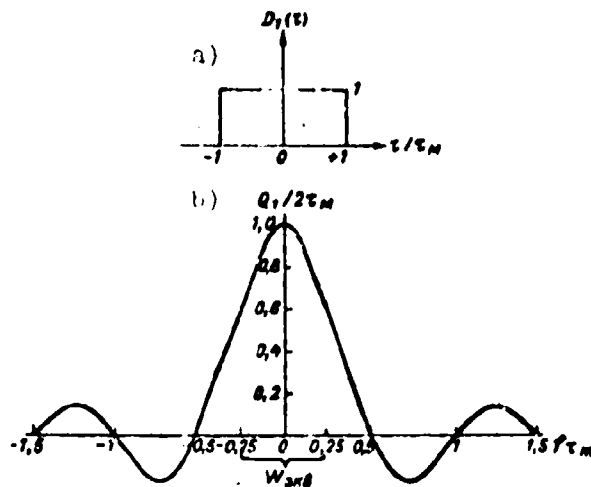


Fig. 3.1. a - time window, $D_1(\tau)$;
b - spectral window, $Q_1(f)$.

The corresponding spectral window $Q_2(f)$ is then written as follows:

$$D_2(\tau) = \begin{cases} \frac{1}{2} \left(1 + \cos \frac{\pi \tau}{\tau_m} \right), & |\tau| \leq \tau_m; \\ 0, & |\tau| > \tau_m. \end{cases} \quad (3.17)$$

And, finally, the time window proposed by R. V. Hamming,

$$D_3(\tau) = \begin{cases} 0.54 + 0.46 \cos \frac{\pi \tau}{\tau_m}, & |\tau| \leq \tau_m; \\ 0, & |\tau| > \tau_m. \end{cases} \quad (3.18)$$

has a spectral window of the type

$$Q_3(f) = 1.08 \tau_m \frac{\sin 2\pi f \tau_m}{2\pi f \tau_m} \frac{\pi^2 - 0.08(2\pi f \tau_m)^2}{\pi^2 - (2\pi f \tau_m)^2}. \quad (3.19)$$

Curves of the functions D_2 , D_3 and Q_2 , Q_3 are shown on Fig. 3.2. Comparing the curves of Q_2 and Q_3 with the curve of Q_1 (see Fig. 3.1), We note first of all that the side maxima for Q_2 and Q_3 are somewhat smaller than that for Q_1 . The magnitude of these maxima does not exceed 2% of the height of the main maximum, while for Q_1 the first side maximum is almost 10 times greater than that shown on Fig. 3.2.

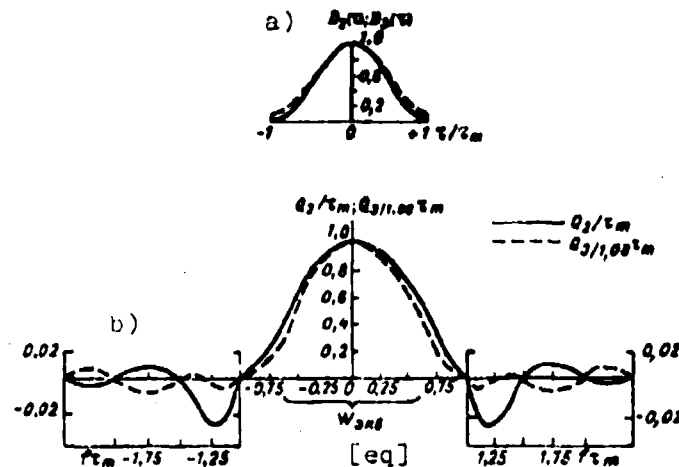


Fig. 3.2. a - time windows $D_2(\tau)$ and $D_3(\tau)$; b - spectral windows $Q_2(f)$ and $Q_3(f)$.

The difference between Q_2 and Q_3 is less noticeable and not so significant. We will only point out that the height of the side maxima for Q_2 diminishes more rapidly than that for Q_3 . Below during calculations of energy spectra we will use precisely these pairs (D_2, Q_2) and (D_3, Q_3). We must turn our attention to the following circumstance. As a result of multiplication of the experimental autocorrelation function $R_{00}(\tau)$ by the appropriate even function (let us say, by D_2 or D_3) the modified experimental autocorrelation function $R_1(\tau)$ was obtained; this function, certainly, is far from the true autocorrelation function. However, the Fourier transform from this modified function will yield a very satisfactory evaluation of the smoothed values of the true energy spectrum.

c. Stability of Energy Spectrum Evaluations

The method of calculating energy spectra and of deriving the formulas which make it possible to obtain average (smoothed) values of energy spectrum evaluations from experimental data were outlined above in general terms. Since the number of experimental data is limited, generally speaking the obtained evaluations will differ from the true values of energy spectrum by a certain quantity, called

the selective fluctuations. It is therefore necessary to know the magnitude of these fluctuations - i.e., the stability of the experimental spectrum. In the final accounting the accuracy of the obtained results can be evaluated if the limits at which the energy spectrum will be located with a certain probability are known.

Before moving on to quantitative analysis of the stability of energy spectrum evaluations, we will note that everything that has been and will be said concerning the average values of the energy spectrum is valid if the studied process is stationary and does not depend on whether or not the process is Gaussian. Strictly speaking, evaluations are valid only for Gaussian processes, although they are also approximately true for processes which are not precisely Gaussian.

The stability of certain fluctuating quantities (for example, $S_1(f_1)$) is determined most simply by the ratio of their dispersion σ^2 to the square of the average value.

It can be shown that the stability of spectral evaluation is determined by the formula

$$\frac{\sigma^2 |S_1(f_1)|}{|S_1(f)|^2} = \frac{1}{T_n' W_{\text{eq}}}, \quad (3.20)$$

where $T_n' = (T_n - 1/\sigma_m)$ is the so-called effective length of recording, while

$$W_{\text{eq}} = \frac{\left[\int_{-\infty}^{+\infty} Q_1(f_1 - f) S(f) df \right]^2}{\int_{-\infty}^{+\infty} |Q_1(f_1 - f) S(f)|^2 df} \quad (3.21)$$

is called the equivalent width of the function $Q_1(f_1 - f)S(f)$. Formula (3.20) is derived on the assumption that the true spectrum varies slowly as compared with $1/T_n'$.

Formula (3.21) has a simple meaning. We will assume that $S(f) = \text{const}$. Then, obviously, W_{eq} [W_{eq}] will represent the equivalent width of the spectral window $Q_1(f)$. In particular:

- 1) if Q_1 is a rectangle of width W , then $W_{eq} = W$;
- 2) if Q_1 is a triangle with base W , then $W_{eq} = 0.75 W$;
- 3) if $Q_1 \equiv Q_1$ (see formula (3.10)), then $W_{eq} = 0.5 W$, where W is the width of the main maximum;
- 4) when $Q_1 \equiv Q_2$ (see formula (3.16)), $W_{eq} = 0.67 W$, where W is the width of the main maximum (when $f_1 \geq 1/\tau_m$);
- 5) if $Q_1 \equiv Q_3$ (see formula (3.18)), then $W_{eq} = 0.63 W$, where W is the width of the main maximum (when $f_1 \geq 1/\tau_m$).

Values of W_{eq} for the spectral windows Q_1 , Q_2 and Q_3 are given on Figs. 3.1 and 3.2.

Thus, formula (3.20) shows that the greater the length of recording T_n and the greater the equivalent width of the spectral window, the more stable is the evaluation of the energy spectrum. It should be remembered, however, that an increase in W_{eq} leads to a situation in which the obtained evaluation is related to a broader band of frequencies.

It is obvious that unless the true form of $S(f)$ is known, exact determination of the value of W_{eq} by formula (3.21) is impossible. However, by assuming that $S(f)$ varies slowly along $Q_1(f)$, without great error it is possible to set

$$W_{eq} \approx \frac{1}{\tau_m}. \quad (3.22)$$

Then (3.20) is rewritten in the following form:

$$\frac{\sigma^2 |S_1(f_1)|}{|S_1(f_0)|^2} \approx \frac{\tau_m}{T_n}. \quad (3.23)$$

Thus if, for example, it is necessary that the mean square deviation (σ) in the value of the energy spectrum comprise no more than

1/3 of its average value, it is necessary that τ_m/T_n' be less than 1/9. Consequently, in order to guarantee stability of energy spectrum evaluations within the limits $\pm 30-40\%$ of the average value, it is necessary to obtain an experimental autocorrelation function up to the quantities τ_m which comprise no more than 10% of the entire length of recording T_n .

Below it will be convenient to examine the stability of spectral evaluations on the basis of the assumption that the distribution of values of the energy spectrum follows the so-called χ^2 -distribution. It is known (Fisher, 1958) that if y_1, y_2, \dots, y_k are independent normally distributed random quantities with zero averages and a unique dispersion, the quantity

$$\chi_k^2 = y_1^2 + y_2^2 + \dots + y_k^2.$$

which is obviously positive, follows, by definition, the χ^2 -distribution with k degrees of freedom. The stability of the quantity χ_k^2 , determined as the ratio of its dispersion to the square of its average value, equals $2/k$. Thus, with an increase in the number of degrees of freedom k the quantity χ_k^2 becomes relatively more stable, since its scatter with respect to the average value is reduced. This assertion is valid also for any square from χ_k^2 .

It is therefore convenient to regard stability of the evaluation of any positive quantity (and the energy spectrum is positive in its physical essence) in terms of the equivalent number of degrees of freedom. Here we understand the number of degrees of freedom of such a χ_k^2 distribution for which a certain multiple coincides with the evaluation being considered (with respect to its average value and dispersion).

The equivalent number of degrees of freedom is easily found by proceeding from its definition and from formula (3.20):

$$k = 2T_n' W_{\text{ave}}. \quad (3.24)$$

or, taking (3.23) into account, we obtain

$$k \approx \frac{2T'_a}{v_m}. \quad (3.25)$$

Table 3.1 shows how, if the number of degrees of freedom is known, one can determine with a certain given reliability the stability of a spectral evaluation - i.e., how to find those boundaries within which our evaluation of the magnitude of the energy spectrum will lie with a certain given probability. Table 3.1 is easy to use. We shall give several examples.

Example 1. If the average value of the energy spectrum of wind velocity pulsations is obtained as equal to $10 \text{ m}^2/\text{s}^3$ over a prolonged period of time, among the evaluations with 15 degrees of freedom 5% of the values will be less than $4.8 \text{ m}^2/\text{s}^3$, while 5% will exceed $16.6 \text{ m}^2/\text{s}^3$. Thus, the individual values of the energy spectrum will lie within the limits $4.8\text{-}16.6 \text{ m}^2/\text{s}^3$ with a reliability of 90%. If the reliability of determining stability limits is reduced to 80%, the individual values will lie within narrower limits - from 5.7 to $14.9 \text{ m}^2/\text{s}^3$.

Example 2. If the individual value of the energy spectrum possessing 30 degrees of freedom is obtained as equalling $5 \text{ m}^2/\text{s}^3$, we can state with 90% reliability that the true average value will lie within the limits $5/1.46 = 3.42 \text{ m}^2/\text{s}^3$ to $5/0.62 = 8.07 \text{ m}^2/\text{s}^3$. If the reliability is reduced to 80%, the true average value will now fall within the limits $5/1.34 = 3.74 \text{ m}^2/\text{s}^3$ to $5/0.69 = 7.25 \text{ m}^2/\text{s}^3$.

Example 3. We will assume that there is continuous recordings of wind velocity pulsations for a period of ten minutes. It is necessary to calculate the values of energy spectrum, where it is desirable to obtain sufficiently stable evaluations which will fall within the limits $\pm 25\%$ of the true value with a reliability of 80%. From Table 3.1 we find that in order to obtain such a stability it is necessary to have evaluations with at least 50 degrees of freedom. From

Table 3.1. Stability (scatter) of spectral evaluations as a function of the equivalent number of degrees of freedom and the reliability of determining the stability boundaries.

(2) Степени свободы	90% надежности (1)		90% надежности (1)	
	3 95% всех значений превышают данное	3 5% всех значений превышают данное	3 90% всех значений превышают данное	3 10% всех значений превышают данное
1	0,0039	3,8	0,016	2,7
5	0,23	2,2	0,32	1,85
10	0,39	1,83	0,49	1,60
15	0,48	1,66	0,57	1,49
20	0,55	1,57	0,62	1,42
25	0,59	1,50	0,66	1,38
30	0,62	1,46	0,69	1,34
40	0,66*	1,41*	0,73	1,30
50	0,69*	1,36*	0,76	1,28
70	0,74*	1,29*	0,80	1,20
100	0,76*	1,25*	0,82	1,18

KEY: (1) reliability; (2) Degrees of freedom; (3) of all values exceed the given.

Remark. We obtain the values marked with asterisks by extrapolation of standard data tables (see, for example, Fisher, 1958).

this, we can use formula (3.25) to determine the maximum shift τ_m to which it is necessary to calculate the autocorrelation function of wind pulsations:

$$\tau_m = \frac{2T_n'}{k} \approx \frac{2 \cdot 600 \text{ сек.}}{50} = 24 \text{ с.}$$

[сек = 3]

For simplicity we consider here that $T_n' = T_n$.

Thus, in the given case τ_m comprises a total of only 4% of the entire length of the recording.

An important property of the χ^2 distribution is the fact that if we have a quantity χ_k^2 with k degrees of freedom and a quantity χ_p^2 with p degrees of freedom, their sum $(\chi_k^2 + \chi_p^2)$ will possess $(k + p)$ degrees of freedom. This property must be remembered during calculations of stability of an averaged energy spectrum, when several

individual evaluations possessing different numbers of degrees of freedom enter into the averaging.

§ 2. CALCULATION OF SPECTRA ACCORDING TO POINT EQUIDISTANT RECORDINGS OF FINITE LENGTH WITH THE USE OF AUTOCORRELATION FUNCTIONS

Everything said above concerning methods of calculating energy spectra from continuous finite recordings can be realized in practice only by means of the appropriate analog computer equipment (correlometers and spectral analyzers). Below we will describe certain similar instruments and the principles involved in working with them. However, in meteorology very few measurements are processed by means of analog devices. First of all, in the overwhelming majority of cases standard meteorological measurements are of the "point" type, and not continuous. Secondly, even when continuous measurements are made we normally deal with very low-frequency processes; this permits accurate conversion of the analog code and processing of information in digital form by means of electronic digital computers (EDC). Therefore it is advisable to give special consideration here to the procedure of calculating spectra from recordings which represent a series of discrete points which are at equal distances from one another (equidistant). Although all of the formulas presented in § 1 for continuous recordings have their discrete analogs, digital calculation of energy spectra from point recordings possesses a number of specific features which require special examination.

a. The "Substitution" of Frequencies

Let the random process $u(t)$ be not a continuous function of time, but a set of discrete equidistant values arranged along the time axis at the points

$$t = 0, \pm \Delta t, \pm 2\Delta t, \dots, n\Delta t$$

in such a way that $R(\tau)$ can be calculated only for the values

$$|\tau| = 0, \Delta t, 2\Delta t, \dots, n\Delta t.$$

Moving for the moment away from the finite nature of the recording (i.e., considering $n = \infty$), we can write the discrete analog of the Fourier transform [compare with (3.2)]:

$$S_A(\omega) = \sum_{r=-\infty}^{+\infty} R(r\Delta t) e^{-i\omega r \Delta t} \Delta t, \quad (3.26)$$

where

$$r = 0, \pm 1, \pm 2, \dots$$

First of all, by substituting $f = 1/\Delta t$ into (3.26) it is possible to verify that $S_A(f)$ has the period Δt , and since the spectrum is symmetrical we can verify that its major portion is included within the frequency band from $f = 0$ to $f_N = 1/2\Delta t$, with the values of the spectrum being subsequently simply repeated with frequency $f = 1/\Delta t$ (Fig. 3.3). Thus, the highest frequency (the so-called Nyquist frequency) on which it is possible to obtain an evaluation of the energy spectrum with selection at intervals Δt will equal $f_N = 1/2\Delta t$.

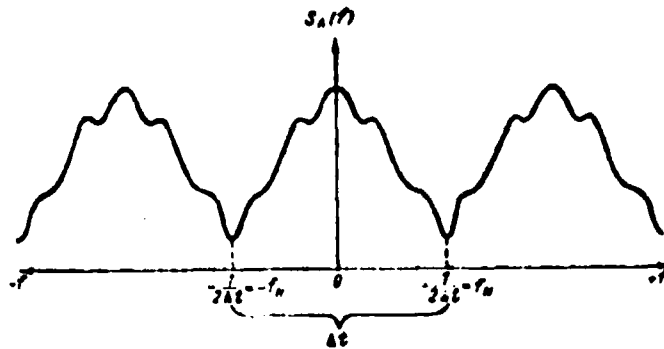


Fig. 3.3. Periodicity of the spectrum $S_A(f)$.

In addition, it is extremely important that we know whether or not the true spectrum $S(f)$ of the real process contains frequencies which are greater than f_N . If so, the problem of "substitution" of frequencies arises. This consists in the fact that if frequencies in the band $[0, f_N]$ are easily distinguished from one another, any frequency greater than f_N will be indistinguishable from a certain

frequency in the band $[0, f_N]$. This leads to a situation in which the calculation of the energy spectrum $S_A(f)$ will contain errors in all its values; these errors will be greater, the greater the energy of the process on frequencies higher than f_N . The nature of this phenomenon (which unfortunately cannot be avoided if $S(f > f_N) \neq 0$) can be explained by means of Fig. 3.4.

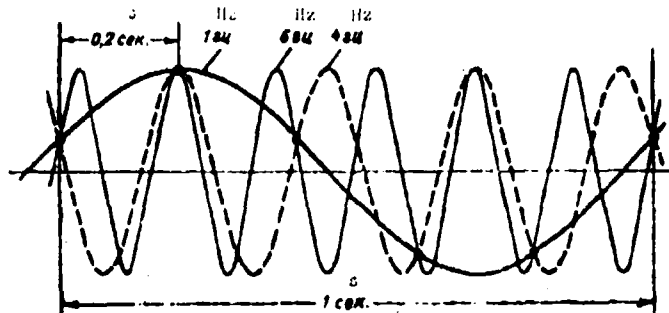


Fig. 3.4. Equidistant selection from sinusoids of different frequency.

Thus, for example, from Fig. 3.4 it is evident that with the beat interval $\Delta t = 0.2$ s it is impossible to state with confidence from the sinusoid of which frequency the selection is actually made: 1, 4, or 6 Hz. Therefore, it is natural that if it is necessary to calculate the value of $S_A(1 \text{ Hz})$ and if the true spectrum of the process extends, for example, up to 10 Hz, during selection with an interval $\Delta t = 0.2$ s the energy of the process on the frequencies 4, 6 and 9 Hz will be added to the true value $S(1 \text{ Hz})$ and a false presentation of the form of the energy spectrum will be obtained. The given figure also shows the derivation of the term "substitution" - frequencies greater than f_N will, as it were, substitute themselves for frequencies in the band $[0, f_N]$. The phenomenon of substitution of frequencies is written analytically in the form (Blackman and Tukey, 1958)

$$S_A(f) = S(f) + S(2f_N - f) + S(2f_N + f) + S(4f_N - f) + S(4f_N + f) + \dots \quad (3.27)$$

where $S_A(f)$ is the spectrum of the process calculated from a discrete recording, while $S(f)$ is the true spectrum.

For the example shown on Fig. 3.4, formula (3.27) gives

$$f_N = \frac{1}{2\Delta t} = \frac{1}{2 \cdot 0,2} = 2,5 \text{ ru.}$$

$$S_A(1 \text{ ru}) = S(1 \text{ ru}) + S(4 \text{ ru}) + S(6 \text{ ru}) + S(9 \text{ ru}) + S(11 \text{ ru}) + \dots$$

[ru = Hz]

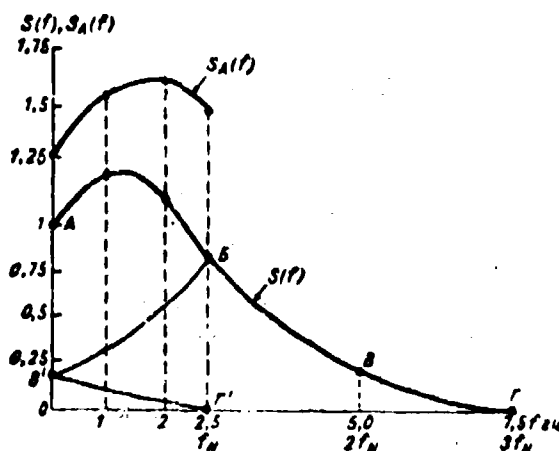


Fig. 3.5. Addition of the true spectrum $S(f)$.

$$\Delta t = 0,2 \text{ cek. } f_N = 2,5 \text{ ru. } S_A(0 \text{ ru}) = S(0 \text{ ru}) + S(5,0 \text{ ru}) + S(10,0 \text{ ru}).$$

$$S_A(1 \text{ ru}) = S(1 \text{ ru}) + S(4 \text{ ru}) + S(6 \text{ ru}). S_A(2 \text{ ru}) = S(2 \text{ ru}) + S(3 \text{ ru}) + S(7 \text{ ru}). S_A(2,5 \text{ ru}) = S(2,5 \text{ ru}) + S(2,5 \text{ ru}) + S(7,5 \text{ ru}).$$

[cek = s; ru = Hz].

The Nyquist frequency f_N is also often called the frequency of "addition," since from formula (3.27) it follows that the true spectrum $S(f)$ is, as it were, complicated by the accordion effect in multiples of f_N . Figure 3.5 shows how the true spectrum $S(f)$ is added together with the given f_N with transition to $S_A(f)$. The same figure also shows the calculated spectrum $S_A(f)$. It is clear that when selection is discrete and equal to $\Delta t = 0,2 \text{ s}$ and with a given $S(f)$, values of $S_A(f)$ will be obtained which are overstated by 30-50% with respect to the true spectrum. It is clear that for correct calculation of the

spectrum $S_A(f)$ in the case shown on Fig. 3.5 it is necessary to give $f_N = 7.5$ Hz; this corresponds to the selection interval $\Delta t = 1/2f_N = 0.07$ s. The above material makes it mandatory to focus the most serious attention on the phenomenon of substitution of frequencies during calculations of energy spectra from discrete recordings. To reduce (or totally eliminate) the influence of substitution, in the very earliest stages of the experiment (measurement, recording) it is necessary to filter out all high frequencies which may possibly exist in the process and which will not interest the investigator for any reason in subsequent calculations.

b. Preliminary Calculation Outline and the Stability of Spectral Evaluations

For convenience we will designate the obtained values of the random process u_0, u_1, \dots, u_n , which correspond to $u(0), u(\Delta t), \dots, u(n\Delta t)$. Subsequently, following the system described in § 1, it is necessary to calculate the values of experimental coefficients of autocorrelation (and not the continuous experimental function $R_{00}(\tau)$), to modify these values, and then to carry out Fourier transformation in order to obtain the spectrum. It is obvious that it is impossible to calculate experimental autocorrelation coefficients for shifts in time which are different from $0, \Delta t, \dots, n\Delta t$. Therefore it is convenient to write R_0, R_1, \dots, R_m instead of $R_{00}(0), R_{00}(\Delta t), \dots, R_{00}(m\Delta t)$. Here n is the quantity of available values of the random process, corresponding to T_n from § 1, while m is the quantity of shifts in time with a magnitude of Δt for which the autocorrelation coefficients are to be calculated. This quantity of shifts corresponds to τ_m from § 1.

If we now carry out Fourier transformation of all autocorrelation coefficients (the quantity of which equals $m + 1$), it is possible to obtain smooth evaluations of the energy spectrum for any frequency between 0 and $f_N = 1/2\Delta t$. However, it can be shown that in order to draw in all information included in the process it is sufficient to calculate only $m + 1$ values of the energy spectrum - i.e., one value of the spectrum for each R_r , where $r = 0, 1, \dots, m$. The calculated

values of the energy spectrum will be uniformly distributed over the frequency axis in the band $0 \leq f \leq f_N$ with the intervals $f_N/m = 1/2m\Delta t$.

For continuous recordings it is necessary first to modify the experimental autocorrelation function $R_{00}(\tau)$ by means of a certain time window $D_1(\tau)$ and then to carry out Fourier transformation of the modified function $R_1(\tau)$. In this way evaluations of smooth values of the energy spectrum are obtained as the result of passage of a true spectrum of the process $S(f)$ through a certain spectral window $Q_1(f)$ (see (3.14)). With transition to discrete recordings it turns out to be simpler first to carry out the Fourier transformation and only then to modify the obtained values of the energy spectrum. Actually, since D_2 and D_3 represent finite sums of cosines, their Fourier transforms will be simply sums of the delta-functions and therefore the convolution in formula (3.14) is reduction* to smoothing with the weights

$$\begin{array}{ccc} 0,25 & 0,5 & 0,25 \\ 0,23 & 0,54 & 0,23 \end{array} \quad \begin{array}{l} (\text{for } D_2) \\ (\text{for } D_3) \end{array}$$

[Данн = for]

Finally the following calculation scheme is assembled.

1. Calculation of experimental autocorrelation functions by the formula (compare with (3.7))

$$R_r = \frac{1}{n-r} \sum_{q=0}^{n-r} u_q u_{q+r} \quad (3.28)$$

for $r = 0, 1, \dots, m$, where $m \leq n$.

2. Calculation of the Fourier transform from R_r according to the formula (compare with (3.6))

$$P_r = \Delta t \left[R_0 + 2 \sum_{q=1}^{m-r} R_q \cos \frac{q\pi}{m} + R_m \cos r\pi \right]. \quad (3.29)$$

*[Translator's Note: Original wording unclear. Might be a typo for the verb "is reduced to".]

3. Smoothing the values of P_r to obtain evaluations of the energy spectrum according to the formulas:

$$\begin{aligned} S_0 &= 0,5P_0 + 0,5P_1, \\ 1 &\leq r \leq m-1, \\ S_r &= 0,25P_{r-1} + 0,5P_r + 0,25P_{r+1}, \quad 1 \leq r \leq m-1, \\ S_m &= 0,5P_{m-1} + 0,5P_m \end{aligned} \quad (3.30)$$

with application of the time window D_2 or

$$\begin{aligned} S_0 &= 0,54P_0 + 0,54P_1, \\ S_r &= 0,23P_{r-1} + 0,51P_r + 0,23P_{r+1}, \quad 1 \leq r \leq m-1, \\ S_m &= 0,54P_{m-1} + 0,54P_m \end{aligned} \quad (3.31)$$

with application of time window D_3 . The obtained values of S_r are related to the frequencies $f_r = r/2m\Delta t$, whereas $0 \leq f_r \leq f_N = 1/2\Delta t$.

The distance (on the frequency axis) between neighboring evaluations of the energy spectrum equals $1/2m\Delta t$. Analysis of the stability of the obtained spectral evaluations differs in no way from that described in § 1 and furthermore it is based on calculation of the equivalent number of degrees of freedom. The analog of formula (3.25) for calculation of the equivalent number of degrees of freedom k is written in the form

$$k = \frac{2n'}{m}, \quad (3.32)$$

where $n' = n - 1/3m$ is called the equivalent number of points. If k is known and if Table 3.1 is then used, it is possible to determine the stability of the obtained values of S_r of the energy spectrum.

c. Preliminary "Whitening" of the True Spectrum

The general methods of calculating energy spectra from equidistant recordings were described above. Now it is necessary to pause on certain special problems which, although they do not always appear, will require strict attention when they do arise.

We will assume that the curve of the true energy spectrum of the process $S(f)$ drops sharply with an increase in frequency. Then the situation explained by Fig. 3.6 can become extremely complicated. If the true spectrum $S(f)$ has the form shown on Fig. 3.6a, during evaluation of the value of the spectrum on frequency f_1 by means of spectral window $Q_1(f)$ (Fig. 3.5b) the influence of side maxima to the left of f_1 grows beyond permissible limits (Fig. 3.6c). In the end it is possible to find that the calculated value of the spectral evaluation $S_A(f_1)$ will relate more quickly to a lower frequency than to the actual frequency f_1 . From this it follows that it is desirable to deal with a spectrum whose magnitude varies with frequency, in order to avoid serious distortions. To obtain such a spectrum it is obviously necessary to introduce at a certain stage in the experiment an operation which would lead to emphasizing of high frequencies and to weakening of low frequencies. It is natural to call such an operation whitening, since in the end it is desirable to obtain a uniform energy spectrum, which is usually called a spectrum of "white" noise. It is most convenient to introduce the whitening operation at the very earliest stages of the experiment (measurement, recording) by appropriate selection of the frequency characteristics of the equipment used. However, for various reasons this is not always possible and therefore it is necessary to bleach the spectrum after the experimental data has been obtained.

One method of whitening a spectrum after obtaining the actual data is by compiling a certain linear sliding combination whose frequency characteristic is such that the resulting spectrum becomes more uniform than the initial. Actually, if there are a series of equidistant values of the process $u_l = u_0, u_1, \dots, u_n$, it is possible to compile a sliding linear combination of the type

$$\bar{u}_l = u_l - \alpha u_{l-1} - \beta u_{l-2} - \gamma u_{l-3}. \quad (3.33)$$

It can be shown (Blackman and Tukey, 1958) that the energy spectrum $\tilde{S}_A(f)$ of the obtained process \bar{u}_l is connected with the energy spectrum $S_A(f)$ of the initial process u_l by the relationship

$$\frac{\tilde{S}_A(f)}{S_A(f)} = \frac{\tilde{S}(f)}{S(f)} = |1 - \alpha e^{-i\omega\Delta t} - \beta e^{-i2\omega\Delta t} - \gamma e^{-i3\omega\Delta t}|^2. \quad (3.34)$$

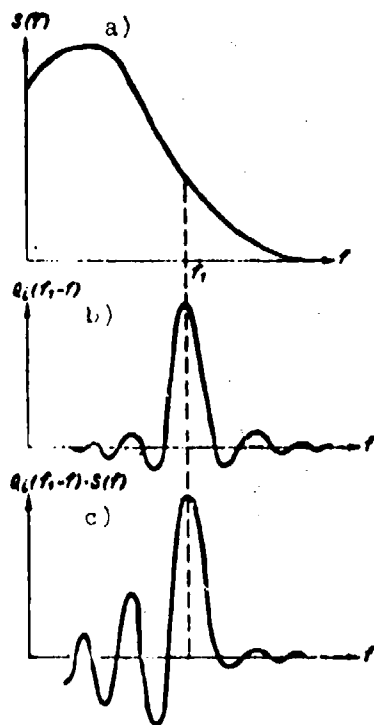


Fig. 3.6. The problem of "whitening" the true spectrum. a - sharply dropping true spectrum $S(f)$; b - spectral window $Q_1(f)$; c - result of passage of $S(f)$ through the window $Q_1(f)$.

where $\omega = 2\pi f$ and Δt is the interval between successive values of the process.

Expression (3.34) represents a non-negative polynomial of the third power from $\cos \omega \Delta t$. By appropriate selection of the coefficients α, β, γ it is possible to obtain the desired frequency dependence, leading to whitening of the true spectrum.

As an illustration we will introduce the simplest operation of whitening by means of a linear combination of the type

$$\tilde{u}_i = u_i - 0,6u_{i-1} \quad (3.35)$$

(where we will set $\Delta t = 1$). We will note that in (3.35) the values of i begin with unity and not with zero. For clarity we will demonstrate graphically that operation (3.35) actually leads to weakening of lower frequencies and intensification of high frequencies. For this purpose we will take two extreme cases: the zero frequency and the

highest frequency, which is obviously equal to the Nyquist frequency f_N . Figure 3.7a shows values of u_z which are all equal to +1 m/s (i.e., we are speaking of the zero frequency of the initial process) and also values of u_z obtained according to (3.35) and equal to +0.4 m/s.

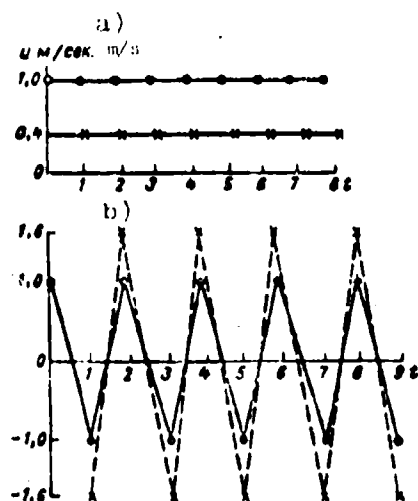


Fig. 3.7. Effect of the "whitening" operation (3.35) on the constant component (a) and on the high-frequency component (b) of the process.

It is obvious that on the zero frequency attenuation occurs which equals $\hat{S}_A(0)/S_A(0) = 0.4^2 / (1)^2 = 0.16$, i.e., by more than 6 times. Figure 3.7b shows values of u_z equal to ± 1 m/s (i.e., velocity pulsations with a frequency of $f_N = 1/2\Delta t = 0.5$) and it also shows values obtained according to (3.35) and equal in turn to ± 1.6 m/s.

It is evident that intensification equal to $\hat{S}_A(f_N)/S_A(f_N) = \frac{(1.6)^2}{(1)^2} = 2.56$, i.e., by more than 2.5 times, has occurred on frequency f_N . Formula (3.34) gives the following relationship for the linear combination (3.35):

$$\frac{\hat{S}_A(f)}{S_A(f)} = |1 - 0.6e^{-i\omega\Delta t}|^2 = 1.36 - 1.20 \cos 2\pi f. \quad (3.36)$$

whose curve is shown on Fig. 3.8.

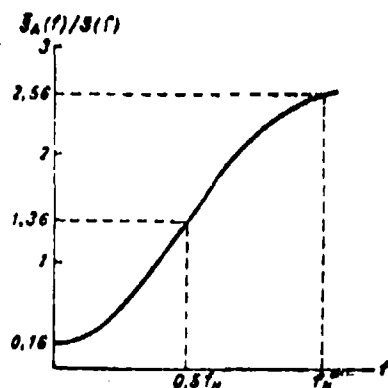


Fig. 3.8. Frequency characteristic of the "whitening" operation (3.35).

Thus during the study of processes with sharply falling spectra (to be exact, with processes of the type which are most frequently encountered by meteorologists), we can recommend the application of one or another procedure of whitening the real spectrum, which will lead to more reliable final results.

d. Elimination of Zero Frequencies

During digital processing of equidistant recordings yet another problem arises - one which does not normally exist during analog treatment of continuous recordings. As a rule, analog computers automatically filter out very low frequencies, which makes it possible to regard the process being treated as having a zero average value. However, when discrete data are being processed it is necessary to deal with all frequencies, right down to the zero frequencies. In this case it is very important to take measures to filter out zero frequencies in order to avoid obtaining distorted values of the energy spectrum.

In the example presented by Blackman and Tukey (1958) it is easy to see how such distortions arise and also to evaluate their order of magnitude. Let us assume that the majority (we will say 999 out of 1000) of processed values in a certain experiment vary from -100 to +100 (conditional units). Then, apparently, the standard deviation $\sigma = 30$ and the dispersion $\sigma^2 = 900$. If the average value equals 5 or even 10, it is quite difficult to determine visually that it is, in fact, not equal to zero. We will assume further that these experimental data were obtained for the period $T_n = 15$ min with a sampling interval of $\Delta t = 1$ s. Thus, there are 900 points in all. The Nyquist frequency equals $f_N = \frac{1}{2\Delta t} = 0.5$ Hz, and the distance (in terms of frequency) between neighboring spectrum values equals $\Delta f = \frac{1}{2T_n} = 5 \cdot 10^{-4}$ Hz, i.e., the band $[0, f_N]$ will be broken down into 900 elementary frequency bands.

The total power included in the process equals the sum of the square of the average value (the so-called power of the constant component) and of the dispersion. In the given example $P_{\text{obs}} = 5^2 + 900 = 925$ or $10^2 + 900 = 1000$. It is clear that the power of the constant component is contained in the actual low-frequency elementary band (i.e., in the first band adjacent to zero). And this leads to a value of the energy spectrum of this band equal to $\frac{100}{\Delta f} = \frac{100}{5 \cdot 10^{-4}} = 2 \cdot 10^5$ 1/Hz, while the average value of the energy spectrum for all of the remaining 899 elementary bands will equal in all only $\frac{900}{f_N} = \frac{900}{0.5} = 2 \cdot 10^3$ 1/Hz. Thus, the value of the spectrum in "zero" will be about 100 times greater than the average on the higher frequencies.

This example shows clearly the situation to which unfiltered zero frequencies may lead. When we speak of zero frequencies, we usually have in mind not only processes with a constant component (i.e., with a constant, but not zero, average), but also processes in which slow "drifts" of the average value (a so-called trend) will be observed. In meteorology it is most frequently necessary to deal with such processes, when rapid fluctuations are superimposed on

vastly slower pulsations which play the role of the trend. As a rule interest lies precisely in the rapid fluctuations and it is desirable to filter out the trend so that its influence will not affect the statistical properties of the high-frequency component of the process.

Such a problem is completely soluble but only in that case when the low-frequency (LF) and the high-frequency (HF) components lie in substantially different frequency ranges which do not overlap (Fig. 3.9). Actually, if the LF spectrum lies to the left of a certain limiting frequency f_1 , while the HF spectrum lies to the right of a certain limiting frequency f_2 , by constructing a filter which will pass all frequencies higher than a certain f_0 and which will extinguish all frequencies below f_0 , where $f_1 \leq f_0 \leq f_2$, it is possible to eliminate the trend completely without distorting the high-frequency component. However, such ideal cases are virtually never encountered in meteorological practice. The best that can be counted on (Van der Hoven, 1957) is the presence of a large or small dip between the maxima of the LF and HF spectra (broken line on Fig. 3.9). Most frequently even this condition is not fulfilled. Therefore, in each individual case during experimental investigations of any particular phenomena in the atmosphere it is necessary to develop unique specific methods of combatting the distorting influence of zero frequencies (Lumley [?] and Panofsky, 1966).

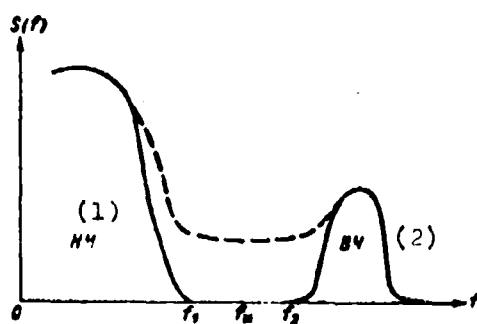


Fig. 3.9. $S(f)$ spectrum with complete or partial (broken line) dip between the high-frequency (HF) and the low-frequency (LF) components.

KEY: (1) LF; (2) HF.

Here we will point out only the common (and mandatory) method of eliminating the constant component. This is most simply done by subtracting from each value of the experimental autocorrelation function the square of the average value of the investigated quantity. Then formula (3.28) for calculation of R_r will be replaced by

$$R_r = \frac{1}{n-r} \sum_0^{n-r} u_q u_{q+r} - \left[\frac{1}{n} \sum_0^n u_q \right]^2. \quad (3.37)$$

e. Resultant Calculation System

The calculation system proposed below is not unique or universal. However, it provides a good illustration of the basic concepts of the method and will be useful in many practical cases.

Let there be a set of the values of the process u_q ($q = 0, 1, \dots, n$) and a separation interval $\Delta t = 1$. In this case it follows that one should:

1) Set value $\Delta t = 1$; it is ascertained that the true spectrum of the process, $S(f)$, is reduced for practical purposes to 0 with a change in frequency from 0 to $f_N = 0.5$. In the opposite case it is necessary to reduce Δt in order to avoid the distorting influence of substitution of frequencies.

2) Carry out the preliminary whitening of the real spectrum by means of the operation (see (3.35))

$$\tilde{u}_q = u_q - 0.6u_{q-1} \quad (3.38)$$

(the subscript q varies from unity and not from zero).

3) Calculate the experimental coefficients of autocorrelation of the whitening process with simultaneous filtering out of the constant component (see (3.37)):

$$R_r = \frac{1}{n-r} \sum_0^{n-r} \tilde{u}_q \tilde{u}_{q+r} - \left[\frac{1}{n-1} \sum_1^n \tilde{u}_q \right]^2 \quad (3.39)$$

for $r = 0, 1, \dots, m$, where $m \leq n$. If a trend is present it is necessary to use more complex filters (see Blackman and Tukey, 1958).

4) Carry out Fourier transformation from P_r^i according to the formula

$$P_r^i = \left[R_0^i + 2 \sum_{k=1}^{m-1} R_k^i \cos \frac{kr\pi}{m} + R_m^i \cos r\pi \right]. \quad (3.40)$$

5) Smooth the obtained values of P_r^i by means of the spectral window Q_2 (0.25; 0.5; 0.25) to obtain preliminary evaluations of the energy spectrum:

$$\begin{aligned} S_0^i &= 0.5P_0^i + 0.5P_1^i, \\ S_r^i &= 0.25P_{r-1}^i + 0.5P_r^i + 0.25P_{r+1}^i, \quad 1 \leq r \leq m-1, \\ S_m^i &= 0.5P_{m-1}^i + 0.5P_m^i. \end{aligned} \quad (3.41)$$

6) Take into account the whitening operation and the filtering out of the constant component to obtain the final evaluations of the energy spectrum (see (3.36)):

$$\begin{aligned} S_0 &= \frac{n}{n-m} \frac{1}{1.36 - 1.20 \cos \frac{2\pi}{6m}} S_0^i, \\ S_r &= \frac{1}{1.36 - 1.20 \cos \frac{2\pi r}{2m}} S_r^i, \quad 1 \leq r \leq m-1, \\ S_m &= \frac{1}{1.36 - 1.20 \cos \left(\frac{1}{2} - \frac{1}{6m} \right) 2\pi} S_m^i. \end{aligned} \quad (3.42)$$

The evaluation of the magnitude of the energy spectrum S_0 relates to a frequency which is somewhat greater than zero (here it is assumed that $f_0 = 1/6m$); the evaluation S_r relates to frequencies $r/2m$, while the evaluation S_m relates to frequencies which are somewhat lower than $f_N = 0.5$ (here it is assumed that $f_m = f_N - 1/6m$). All of the calculated evaluations have a stability which is no greater than the χ^2 distribution with $2n/m$ degrees of freedom (see Table 3.1).

§ 3. CALCULATION OF SPECTRA FROM POINT EQUIDISTANT RECORDINGS OF FINITE LENGTH USING MATHEMATICAL FILTERS

The procedure described in §§ 1 and 2 for calculating the energy spectrum of a process by means of the Fourier transform of its autocorrelation function is, in a certain sense, artificial. Naturally, it would be better to obtain the energy spectrum directly - for example, by means of a set of one or another sort of filters, i.e., without resorting to formal methods. In the case of continuous recording the procedure for obtaining the spectrum directly does not cause any difficulties (and in fact it is frequently used). When it is necessary to deal with equidistant point recordings the ordinary radio-engineering methods of obtaining the spectrum become inapplicable.

In this section we will show how an electronic digital computer can be used to realize operations which are equivalent to radio-engineering filtration and also how to obtain the spectrum of a process without intermediate calculation of its autocorrelation function.

In general form the filtration operation can be described as follows:

$$v(t) = \int_{-\infty}^{+\infty} h_p(t-t')u(t')dt' \quad (3.43)$$

where $u(t)$ and $v(t)$ are processes on the input and output of the filter, while $h_p(t)$ is the so-called transient or weighting function of the filter. The subscript p designates a specific form of the function $h(t)$.

The connection between the energy spectrum of the initial process S_u and the spectrum of the process on the filter output S_v is given by the expression

$$S_v = |\Phi_p(\omega)|^2 S_u \quad (3.44)$$

where $\Phi_p(f)$ is the transfer function of the filter, connected with $h_p(t)$ by the relationship

$$\Phi_p(f) = \int_{-\infty}^{+\infty} h_p(t) e^{-i2\pi ft} dt. \quad (3.45)$$

Let it be possible to select function $h_p(t)$ in such a way that $|\Phi_p(f)|^2$ has the form shown on Fig. 3.10. Then, obviously, the process $v(t)$ on the output of such a filter will contain only frequencies in the band $[f_1, f_2]$, and the energy of the process in this band will equal

$$\begin{aligned} \sigma_v^2 &= \int_{-\infty}^{+\infty} |\Phi_p(f)|^2 S_u(f) df = \int_{f_1}^{f_2} |\Phi_p(f)|^2 S_u(f) df = \\ &= S_u(f^*) (f_2 - f_1). \end{aligned} \quad (3.46)$$

From this the spectral density of the energy of the initial process $u(t)$ equals

$$S_u(f^*) = \frac{\sigma_v^2}{f_2 - f_1}. \quad (3.47)$$

where f^* is included between f_1 and f_2 . If S_u is changed slowly in the band $[f_1, f_2]$, it is possible to set $f^* = f_1 + f_2/2$.

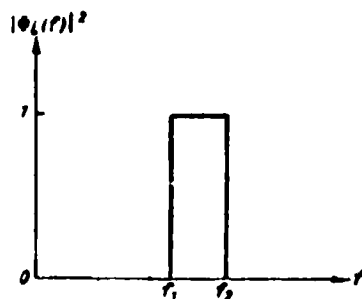


Fig. 3.10. Ideal band filter.

The filter shown on Fig. 3.10 is called a band filter because it passes only a certain band of frequencies of the initial process.

A similar effect can be achieved by successive application of simpler filters of low or high frequencies. Actually, let there be a filter $|\phi_p(f_1)|^2$ which passes all frequencies above a certain limiting frequency f_1 and which does not pass lower frequencies (see Fig. 3.11a). Such a filter is called a high-frequency filter. The energy of the process $v_1(t)$ on the output of such a filter equals

$$\sigma_1^2 = \overline{|v_1(t)|^2} = \int_{f_1}^{\infty} |\phi_p(f_1)|^2 S_u(f) df. \quad (3.48)$$

If we now pass the initial process $u(t)$ through a similar filter $|\phi_p(f_2)|^2$, with a limiting frequency $f_2 > f_1$ (Fig. 3.11b), for the process $v_2(t)$ we will have

$$\sigma_2^2 = \overline{|v_2(t)|^2} = \int_{f_2}^{\infty} |\phi_p(f_2)|^2 S_u(f) df. \quad (3.49)$$

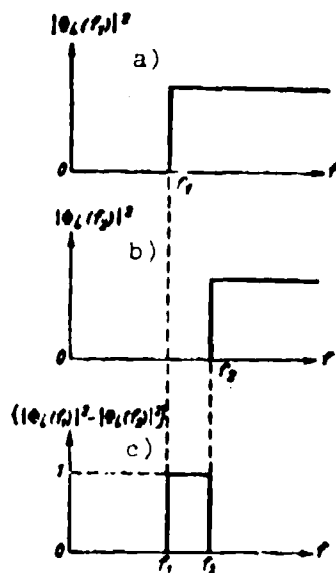


Fig. 3.11. Obtaining a band-filter effect (c) as a result of successive application of high-frequency filters with different (a and b) boundary frequencies.

It is evident that the difference in energies $(\sigma_1^2 - \sigma_2^2)$ will represent the energy of the initial process $u(t)$ in the frequency band $[f_1, f_2]$, since from (3.48) and (3.49) it follows that

$$\sigma_1^2 - \sigma_2^2 = \int_{f_1}^{f_2} (|\Phi_p(f_1)|^2 - |\Phi_p(f_2)|^2) S_e(f) df = -S_e(f^*) (f_2 - f_1), \quad (3.50)$$

from which

$$S_e(f^*) = \frac{\sigma_1^2 - \sigma_2^2}{f_2 - f_1}, \quad (3.51)$$

which is analogous to formula (3.47) for a band filter. Such a coincidence is natural, since the difference between the two high-frequency filters with different boundary frequencies will give the effect of a band filter (see Fig. 3.11c). It is obvious that a band filter can be obtained also as the difference between two low-frequency filters. As a rule, however, it is high-frequency filters which are used, since they make it possible to avoid the influence of zero frequencies on the calculation results. The procedure for calculating energy spectra based on the application of successive high-frequency filters can be realized by means of an electronic digital computer.

a. Mathematical High-Frequency Filters

We will now examine two pairs of functions $h_p(t)$, $\phi_p(f)$, which are most frequently used during calculations of energy spectra. The simplest transient function $h_p(t)$ represents an ordinary sliding average

$$h_1(t) = \begin{cases} \frac{1}{T} \text{ при } -\frac{T}{2} \leq t \leq +\frac{T}{2}. \\ 0 \text{ при } |t| > \frac{T}{2}. \end{cases} \quad (3.52)$$

[при = when]

The corresponding transfer function $|\phi_1(f)|^2$ has the form

$$|\phi_1(f)|^2 = \left(\frac{\sin \pi f T}{\pi f T} \right)^2. \quad (3.53)$$

The functions $h_1(t)$ and $|\phi_1(f)|^2$ are shown on Fig. 3.12. From the figure it is clear that $|\phi_1(f)|^2$ represents a low-frequency

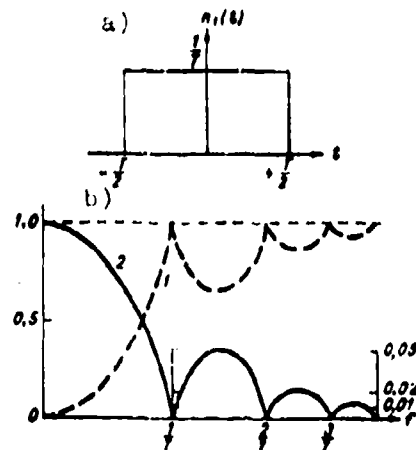


Fig. 3.12. "Sliding" average (a) and its transfer function (b). 1 - high-frequency filter; 2 - low-frequency filter.

filter with a boundary frequency $f_{\text{rp}} = 1/T$ (curve 2). It is obvious that the transfer function equal to $\{1 - |\Phi_1(f)|^2\}$ will also be a high-frequency filter with the same boundary frequency (curve 1). The form of this filter is far from ideal (compare with Fig. 3.11a). First of all, frequencies higher than f_{rp} are passed unevenly and, secondly, frequencies below f_{rp} are not completely extinguished. It is obvious that a band filter obtained as the difference between two $\{1 - |\Phi_1(f)|^2\}$ with different f_{rp} will have a fairly complex form. We will note that $\{1 - |\Phi_1(f)|^2\}$ filters with different f_{rp} correspond simply to different times of averaging in formula (3.52).

The best properties are found in the transient function $h_2(t)$, called the smoothed sliding average (Ozmidov, 1964):

$$h_2(t) = \begin{cases} \frac{1 + \cos \frac{2\pi}{T} t}{T} & \text{при } -\frac{T}{2} \leq t \leq +\frac{T}{2}, \\ 0 & \text{при } |t| > \frac{T}{2}. \end{cases} \quad (3.54)$$

The corresponding transfer function $|\Phi_2(f)|^2$ has the form

$$|\Phi_2(f)|^2 = \left(\frac{\sin \pi f T}{\pi f T}\right)^2 \cdot \frac{\pi^2}{|\pi^2 - (\pi f T)^2|^2} \approx$$

$$\approx |\Phi_1(f)|^2 \frac{\pi^2}{|\pi^2 - (\pi f T)^2|^2} \quad (3.55)$$

The functions $h_2(t)$, $|\Phi_2(f)|^2$ (curve 2) and $\{1 - |\Phi_1(f)|^2\}$ (curve 1) are shown on Fig. 3.13; $\{1 - |\Phi_2(f)|^2\}$ is the high-frequency filter with a boundary frequency $f_{\text{гп}} = 2/T$, where its basic distinction from and advantage over $\{1 - |\Phi_1(f)|^2\}$ consists in the fact that it has much smaller side maxima.

In subsequent calculations of the energy spectrum we will use band filters which represent the difference between $\{1 - |\Phi_2(f)|^2\}$ filters with different $f_{\text{гп}}$. Before moving to discussion of the calculation scheme, we will show that the distinction between the proposed filters and ideal filters leads to a requirement for a slight change in the form of formula (3.51).

The fact is that the boundary frequencies of the filters $|\Phi_1|^2$ and $|\Phi_2|^2$, pointed out above and equal to $1/T$ and $2/T$ respectively, are defined formally as the frequencies at which the filters achieve the first null (see Figs. 3.12 and 3.13). But formula (3.51) is written for the ideal band filter shown on Fig. 3.11c.

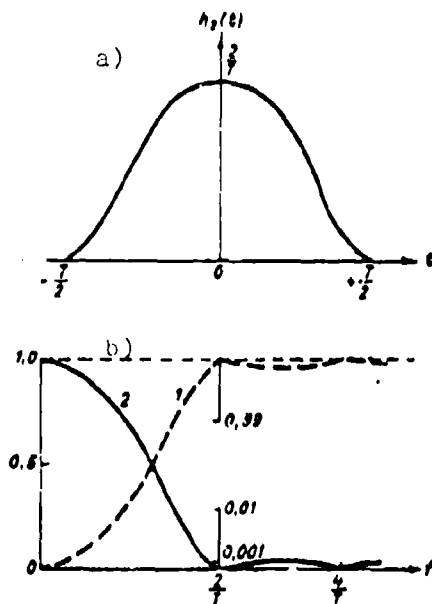


Fig. 3.13. Smoothed "sliding" average (a) and its transfer function (b). 1 - high-frequency filter; 2 - low-frequency filter.

Therefore when using a real filter it is necessary to find a certain equivalent boundary frequency which is defined as the boundary frequency of the equivalent ideal filter whose area is equal to the area of the real filter. Thus, to find the equivalent boundary frequency of the real filter it is possible to write the formula

$$f_{rp}^{eq} = \int_0^{\infty} |\Phi_p(f)|^2 df, \quad (3.56)$$

which gives $f_{rp}^{eq} = \frac{1}{2T} = \frac{1}{2} f_{rp}$ for the filter $|\Phi_1|^2$ and $f_{rp}^{eq} = \frac{3}{4T} = \frac{3}{8} f_{rp}$ for the filter $|\Phi_2|^2$.

Formula (3.51) is then rewritten in the form

$$S_p(f^*) = \frac{\sigma_1^2 - \sigma_2^2}{f_2^{*2} - f_1^{*2}}, \quad (3.57)$$

where

$$f^* = \frac{f_2^{*2} + f_1^{*2}}{2}.$$

b. Calculation Scheme

All of the formulas which were written above relate to the case of continuous recording, since in this form it is easier to manipulate them. In the calculation system outlined below discrete analogs of these formulas are presented with application to the treatment of point equidistant recordings.

Let there be a set of the values of the process u_q , where $q = 0, 1, \dots, n$, while the separation interval equals Δt . The length of the recording is $T_n = n\Delta t$.

1. We will determine the set of averaging times T_l entering into the formula for h_2^l . The notation h_2^l indicates that the transfer function h_2 will be used (see formula (3.54)); in this function $T \equiv T_l$, $T_l = 2l\Delta t$, where $l = 1, 2, \dots, m$. It is obvious that $(2l + 1)$ of the

initial process will enter each time into averaging with the given T_l . The maximum averaging time $T_m = 2m\Delta t$ should not, as a rule, exceed 10-15% of recording time T_n , in order to ensure suitable stability of the obtained evaluations of the spectrum.

2. The values of T_l uniquely determine the set of frequency bands for which the spectrum evaluations will be obtained:

$$\Delta f_l = f_l^{m_0} - f_{l+1}^{m_0} = \frac{3}{4T_l} - \frac{3}{4T_{l+1}}.$$

In all there will be m values of Δf_l .

3. We will calculate values of v_s^l on the output of each given filter h_2^l by the formula

$$v_s^l = \sum_{n=1}^{n=2l} u_{s-n} \frac{1 + \cos \frac{\pi}{l} n}{2}. \quad (3.58)$$

Here l is fixed for each h_2^l (or, which is the same thing, for each T_l), while s runs through the values $l, l+1, \dots, n-l$. Thus, for each T_l we will obtain $n-2l$ values of v_s^l - i.e., with an increase in averaging time the quantity of values of v_s on the filter output will be reduced.

Values of v_s^l are obtained on the output of the low-frequency filter $|\Phi_2|^2$. In order to obtain values of the process on the output of the high-frequency filter $(1 - |\Phi_2|^2)$ it is clearly necessary to calculate the quantities $u_s - v_s^l$.

4. We will find the energy of the initial process u_q in the frequency band $[f_l^{m_0}, f_n]$:

$$\sigma_l^2 = \frac{1}{n-2l} \sum_{s=1}^{s=n-2l} [u_s - v_s^l]^2. \quad (3.59)$$

where f_N is the Nyquist frequency.

5. We will calculate the values of estimates of the energy spectrum of the initial process u_q according to the formula (see formula (3.57)):

$$S_i(f^*) = \frac{\sigma_i^2 - \sigma_{i+1}^2}{f_{i+1}^{*m} - f_i^{*m}}. \quad (3.60)$$

The calculated m values of S_i are related to frequencies:

$$f^* = \frac{f_i^{*m} + f_{i+1}^{*m}}{2}.$$

During the description of the procedure for calculating the energy spectrum using mathematical filters, nothing at all was said about substitution of frequencies and preliminary whitening of the spectrum of the real process. This was done because those judgements relative to these problems which were presented in § 2 are also true in the case of the application of mathematical filters. The appropriate changes in the calculation scheme outlined above are easily accomplished by means of the methods outlined in § 2.

The situation is different with regard to the problem of filtering out "zero" frequencies (see § 2, point d). Actually, the described method makes it possible, at least normally, to estimate the value of the energy spectrum at zero, since the method of filters is limited from the low-frequency side by the value $f_m = 1/T_m$. This makes it possible to calculate the spectrum without turning special attention to the behavior of the process at low frequencies.

c. Stability of Evaluations of the Energy Spectrum

Analysis of the stability of energy spectrum evaluations obtained by the filter method differs in no way from the analysis presented in § 2, point b. The stability of the obtained evaluations will approximately equal the stability of the corresponding χ^2 distribution with k degrees of freedom.

As is known, the equivalent number of degrees of freedom is determined by formula (3.24):

$$k \approx 2T_n W_{\text{ЭНБ}}$$

where $W_{\text{ЭНБ}}$ is called the equivalent width and is determined by formula (3.21):

$$W_{\text{ЭНБ}} = \frac{\left[\int_{-T_n}^{+T_n} Q_p(f_1 - f) S(f) df \right]^2}{\int_{-T_n}^{+T_n} |Q_p(f_1 - f) S(f)|^2 df}$$

It is natural to consider that when the method of filters is used the band filter representing the difference $(|\Phi_p'|^2 - |\Phi_p^{i+1}|^2)$ is an analog of the spectral window $Q_p(f)$. Therefore the formula for $W_{\text{ЭНБ}}$ is rewritten in the form

$$W_{\text{ЭНБ}} = \frac{\left\{ \int_{-T_n}^{+T_n} [|\Phi_p'|^2 - |\Phi_p^{i+1}|^2] S(f) df \right\}^2}{\int_{-T_n}^{+T_n} [|\Phi_p'|^2 - |\Phi_p^{i+1}|^2] |S(f)|^2 df} \quad (3.61)$$

It can be shown that if $S(f)$ varies slowly in the band $[f_{i-1}^{\text{ЭНБ}}, f_{i+1}^{\text{ЭНБ}}]$, then

$$W_{\text{ЭНБ}} \approx \frac{1}{T_i} \quad (3.62)$$

Consequently,

$$k \approx \frac{2T_n}{T_i} \quad (3.63)$$

Thus, if the length of recording T_n and the time of averaging T_i used to construct the given filter $(1 - |\Phi_p'|^2)$ are known, it is possible to find k from formula (3.63), and then to use Table 3.1 to find (with given reliability) the boundaries of stability of the spectral evaluation.

d. Advantages and Deficiencies of the Method of Filters

The filter method has no advantages in principle over the method described in § 2, since neither method of calculating permits the extraction of information greater in scope than that which is inherent in the process itself (or in its final realization). However, incorrect selection of the calculation system can, and in fact frequently does, entail either a partial loss of information or the obtaining of evaluations that are so unstable that it is difficult to work with them.

The fact that the spectral evaluation is obtained without intermediate calculation of the autocorrelation function is a procedural advantage of the method of filters. Besides this, by using the method of filters the experimenter insures, to some degree, that he will avoid distortions of the spectrum due to the presence of zero frequencies.

The basic drawback to the filter method is the nonuniform distribution of the obtained spectrum evaluations on the frequency axis. Actually, if the width of the transient function h_p^L grows in proportion to T_L (see Figs. 3.12 and 3.13), the width of the transfer function $|G_p|$ is reduced in proportion to $1/T_L$ - i.e., nonuniformly. It is precisely for this reason that the width of elementary frequency bands $[f_{1}^{*}, f_{2}^{*}]$ is reduced with a growth in L , which means that the spectral evaluations are calculated over ever narrower bands of frequencies. A direct (and, possibly, most unfavorable) consequence of this is the dependence of the evaluation stability boundaries on frequencies, since in formula (3.63) k depends on T_L . This leads to a situation in which the first (high-frequency) elementary band $[f_{1}^{*}, f_{2}^{*}]$ gives a very stable evaluation, while at the same time this band is extremely wide (hence the stability) and consequently it is impossible to clarify any particular features of the energy spectrum of the real process if they are manifested in this band. On the other hand, with displacement towards the low-frequency side the elementary bands become ever narrower and the stability boundaries

are expanded. These deficiencies are not found in the method described in § 2. There the evaluations of the spectrum are actually distributed uniformly over the axis of frequencies, while the quantity k is constant - i.e., the boundaries of stability of spectral evaluations are constant on all frequencies. Consequently, the final selection of one or the other method of calculating the spectrum depends on the particular features of the spectrum of the real process - on the extent to which we are interested in one or another of these features and what degree of stability of the obtained evaluations is required.

§ 4. INSTRUMENTS FOR STATISTICAL PROCESSING

a. Types of Presentation of Information of Measurement Results

Recently, in connection with the fact that the volume of incoming information grows continuously and that without the use of computers various types of statistical processing cannot be realized operationally, oscillographic recording methods have begun to be supplemented by the development of methods and devices which accumulate information on measurement results in a form which is convenient for direct computer input. Such types of recording include recording measured quantities on magnetic tape in the form of an electrical analog or a digital code, and also recording of a digital code on perforated tape or punchcards. Machine processing of graphic recordings will obviously require conversion of the graphic recording into an electrical analog or a digital code; this conversion should also be automated.

We will examine in more detail existing forms of information presentation during investigations of atmospheric turbulence.

At present a graphic recording is the most widely used. An oscillogram of the studied parameter makes it possible to obtain a visual presentation of the nature of the process and to select both the method of processing and the sections of the recordings to be

subjected to treatment of one sort or another. Existing multichannel automatic recorders make it possible to compare synchronous values of a large number of simultaneously measured quantities. Any measuring instrument used at present can be matched to an automatic recorder which will guarantee recording of the result without substantial distortions. Low-inertia vibrators used in optical automatic recorders make it possible to record processes with frequencies up to 1000 Hz. The speed of the diagram during recording in contemporary automatic recorders can also be varied within wide limits - from 0.001 to 500 mm/s.

As was already pointed out above, the continuously growing volume of information and the need for machine statistical processing requires the use of other types of information recording along with oscillograms. The majority of measuring instruments have an electrical output and the devices for automatic processing have an electrical input. At the same time it is not always possible to connect the measuring instrument directly with the processing device. As a rule, the processing equipment, being of comparatively large size and weight, operates under stationary conditions, while the measuring instrument should be located in the investigated atmospheric flow. Under these conditions it is sensible to use magnetic automatic recorders for registration of data.

Although a recording of measurement results on magnetic tape is not in itself a visual display, during reproduction under stationary conditions it makes it possible to restore the primary information in its analog form. Besides this, the use of the magnetic recording method makes it possible to change the time scale during reproduction. Thus, for example, if a high-speed analog device is used for processing, by applying a speed reduction of 10:1 it is possible to carry out complete statistical processing of measurements made over a period of 30 min within a little more than 3 min. However, the magnetic recording method has its drawbacks. Without the use of special devices it is difficult to record and reproduce signals of very low frequency by means of a magnetic automatic recorder. In order to avoid this limitation it is necessary to

introduce an intermediate information carrier. A sequence of audio-frequency pulses is usually selected as the intermediate carrier; this sequence is modulated, for example, in terms of the frequency of the analog of the measured quantity. The application of frequency-pulse modulation makes it possible to record signals of very low frequency on magnetic tape - right down to a constant-component level. In this case, however, the band of frequencies of the investigated process will be limited from above because the lowest frequency of pulse repetition must be at least an order of magnitude greater than the highest frequency in the process spectrum. The use of a magnetic memory with intermediate frequency-pulse modulation was cited in § 1 of Chapter 2 in the description of the method for obtaining automatically the energy spectrum of a vertical component of atmospheric turbulence. The works of N. Z. Pinus et al. (1964) and N. K. Vinnichenko and G. N. Shur (1965) contain descriptions of an experimental multichannel system of magnetic storage for onboard recording of parameters which characterize atmospheric turbulence. The use of magnetic recording makes it possible to apply analog computers for processing the measurement results. However, in many cases it is advisable to use digital computers (EDC) for processing.

In contemporary digital computers information is input as a digital code either from perforated tape (punchcards) or from magnetic tape. Therefore during the experiment it is necessary to have a recorder which will permit recording parameters of the studied process on magnetic tape or on punch tape as a digital code. The basic unit of such a recorder is the analog-code converter, which converts the analog of the studied quantity into a binary or binary-decimal code. An experimental multichannel aircraft device for recording parameters measured during studies of aircraft turbulence in the form of a digital code on magnetic tape is described in the works by N. Z. Pinus et al. (1964) and V. I. Chernysh (1965).

b. Graph-Analog-Code Conversion

The application of analog and digital computers for processing experimental data requires that measurement results be presented in a

form which is suitable for computer input. Since graphic recordings cannot be input directly into electronic computers, there is a need for devices to convert these recordings into an electrical analog or into a digital code.

The work by N. K. Vinnichenko and G. N. Shur (1959) contains a description of the simplest semiautomatic device for conversion of a graphic recording into an electrical analog. Oscillographic tape carrying the recording travels at a constant speed, while the operator, tracking the path of the curve, matches an index to it. The index is kinematically connected with the moving arm of a potentiometer from whose output the electrical analog of the recorded process is taken. In the EASP-S electronic analyzer developed by the Vil'nyus plant "Schetmash" the role of the operator is filled by a television monitor. This permits a substantial increase in the oscillograph tape speed and eliminates subjective operator errors. The main drawback of existing television reading systems is the impossibility of treating oscillograms with intersecting curves.

Conversion of a graphic recording into digital code, as a rule, is included an intermediate stage of the transition from a graph to an electrical analog. This first stage can be realized by one of the methods discussed above. The analog-code conversion is usually based on discrete counting of time segments, which is required for the linearly growing voltage developed in the converter unit to achieve a value equal to the magnitude of the analog voltage. The magnitude of this time segment is determined from the quantity of high-frequency pulses (frequency is determined by the required accuracy of conversion) arriving in a system of binary counters from the moment when the auxiliary generator of the growing voltage is switched on up to the moment when this voltage coincides with the voltage which is an analog of the converted signal. In the work by V. I. Chernish (1965) there is a description of an experimental aircraft four-channel analog-code converter based on semiconductors; the work includes its schematic diagram and gives an accuracy analysis. It must be noted that although at present there are many experimental devices of various types for accomplishing the graph-analog-code

conversion, they are either excessively large and unreliable or are not intended for investigation of atmospheric turbulence.

c. Analog Devices for Automatic Statistical Processing

Correlometers. Analog devices for computing the autocorrelation (or correlation) function are so constructed as to realize the operations described by the formula (see formula (33.7) [sic])

$$R_{00}(\tau) = \frac{1}{T - |\tau|} \int_0^{T - |\tau|} u(t) \cdot u(t + \tau) dt,$$

where $u(t)$ is the studied random process; T is the length of the recording; τ is the time shift.

This formula can be used to construct the functional diagram of a correlometer which is shown on Fig. 3.14. Voltage u , which is an electrical analog of the studied process $u(t)$, arrives at the input of the high-frequency filter, which filters out null frequencies from the process (if any are present). Voltage u , containing only the frequencies of interest to the experimenter, passes from the output of the filter to the input of a multiplication block with two channels - a direct channel and one through a controllable delay device which accomplishes a shift of voltage $u(t)$ by time $\tau = \tau_1$. Thus, voltages equal to $u(t)$ (channel I) and $u(t + \tau_1)$ (channel II) enter the input of the multiplication block. A voltage proportional to $u(t)u(t + \tau_1)$ appears on the output of the multiplier; this voltage proceeds to an integrator which has an integration time greater than recording length T . Finally, a voltage proportional to $\int u(t)u(t + \tau_1) dt$ from the integrator output is multiplied in a scale unit by the coefficient $1/(T - |\tau_1|)$; a voltage proportional to the value of the experimental autocorrelation function $R_{00}(\tau_1)$ appears on the output of the device as a whole. Then the delay unit is returned to a new shift time $\tau = \tau_2$ and the entire operation is repeated to calculate $R_{00}(\tau_2)$. Finally we obtain a set of values $R_{00}(\tau)$ for $\tau = 0, \tau_1, \tau_2, \dots, \tau_m$, where τ_m is the maximum shift in time and ordinarily does not exceed 5-10% of the recording length T .

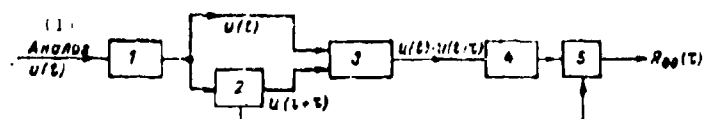


Fig. 3.14. Functional diagram of correlometer. 1 - low-frequency filter; 2 - delay unit; 3 - multiplier; 4 - integrator; 5 - scale unit.

KEY: (1) Analog.

From the above description of correlometer operation it clearly follows that the time required to obtain a single value of the autocorrelation function is virtually equal to the time of experiment T (considering that $T - t_m \approx T$). This means that, for example, to obtain ten values of $R_{00}(\tau)$ from an experimental recording 10 min in length it is necessary to spend almost 2 h. Therefore the analog voltage should usually be entered into the correlometer input with a speed several times greater than the speed of the recording during the actual experiment. The use of magnetic automatic recorders does permit such a time reduction.

When speaking of specific correlometer circuits it is necessary to note the following. Analog computers which carry out filtration, multiplication, integration, and coefficient input operations are well known and widely used in analog units for various purposes (Kazakov, 1965). It is only the delay unit which is specific for correlometers. The development of correlometer delay units suitable for treating processes which characterize atmospheric turbulence is, as a rule, tied to a need for ensuring extremely large time delays (up to several tens of seconds). Such delays cannot ordinarily be accomplished reliably by means of purely radio equipment.

A unique and promising method for obtaining large time delays is that used in the EASB-3 correlometer from the VIL'nyus plant "Schetmash" (Fig. 3.15). Analog voltage $u(t)$ is recorded synchronously on two tracks of the magnetic tape by means of recording heads ZI and ZII. Then the recording head of the first track, ZI, is shifted over the vernier by a certain distance Δl from its initial position. During reproduction the analog voltage taken from reading heads BI and

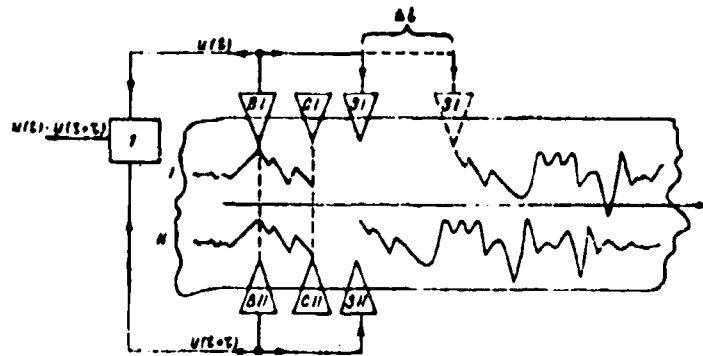


Fig. 3.15. Delay device using a magnetic memory. 1 - multiplier unit.

$U(t)$ is passed to the multiplier unit and simultaneously to recording heads ZI and ZII. Thus there is re-recording over both tracks (erasing heads CI and CII ensure erasing of the preceding recording). In this case, however, the relative positions of the recordings on tracks I and II is changed and in fact recording I is shifted with respect to recording II by the time $\tau = \frac{\Delta l}{v}$, where v is the magnetic tape speed. By repeating the re-recording process m times it is possible to obtain a shift equal to $m\tau$. Using relatively small displacements of head the ZI (up to 40 mm), with this method it is possible to achieve a substantial shift in time, such as is frequently necessary during calculation of autocorrelation functions.

d. Spectrometers

As a rule the autocorrelation functions which are obtained by means of analog computers are not used to calculate spectral densities, since this is connected with the problem of converting the autocorrelation function into an analog voltage and its input into some new unit. Usually energy spectra are calculated directly by means of analog devices called spectrometers.

Analog devices for calculating the energy spectrum (spectrometers) are usually constructed by the filter method (see Chapter 3, § 3). Figure 3.16 shows the functional diagram of a spectrometer with one filter; the operating principle of the device can be clarified on

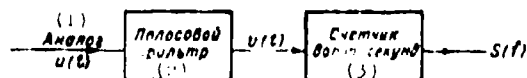


Fig. 3.16. Functional diagram of a spectrometer.

KEY: (1) Analog; (2) Band filter; (3) Watt-second counter.

this diagram. Let voltage u be an electrical analog of the random process $u(t)$, whose spectrum $S_u(f)$ must be found. If this voltage is passed through an electrical filter possessing the transfer function $\Phi(f)$, voltage $v(t)$ appears on the filter output; the spectrum of this voltage, $S_v(f)$, is connected with the spectrum of the initial process $u(t)$ by the relationship

$$S_v(f) = |\Phi(f)|^2 S_u(f).$$

If recording time equals T , the watt-second counter standing at the filter output and accomplishing square detection and integration operations will record a quantity equal to $\int_0^T [v(t)]^2 dt$; this quantity is connected with the spectrum of the initial process, $S_u(f)$, by the relationship

$$\sigma_v^2 = \frac{1}{T} \int_0^T [v(t)]^2 dt = \int_{-f}^{\infty} S_v(f) df = \int_{-f}^{\infty} |\Phi(f)|^2 S_u(f) df.$$

As a rule, in real spectrometers band filters with transfer functions $\Phi(f)$ concentrated in a certain frequency band $[f_1, f_2]$ are used (see Fig. 3.11). In this case the value of spectral density of the initial process $u(t)$ on the frequency $f = \frac{f_1 + f_2}{2}$ will equal

$$S_u(f^*) = \frac{\sigma_v^2}{f_2 - f_1}.$$

To obtain the entire spectrum of the studied process in a certain frequency band it is necessary, obviously, either to retune the characteristic of the filter shown on Fig. 3.10 or to use a set of such filters arranged in a certain way along the axis of frequencies. In the first case the spectral analysis is called successive, since the values of spectral density are obtained

successively, one after another, as the filter characteristic is adjusted. In the second case the spectral analysis is called parallel, since the values of spectral density are obtained simultaneously on the outputs of all filters. During investigation of the parameters which characterize atmospheric turbulence parallel-analysis spectrometers are most frequently used. The fact is that successive analysis naturally requires more time than the parallel process. Any increase in analysis time is extremely undesirable, since atmospheric turbulence is not a stationary random process in the strict definition of this concept (see Chapter 1).

The work by N. K. Vinnichenko and G. N. Shur (1964) contains a description of an industrial spectrometer for parallel analysis which uses the overload method (see Chapter 2, § 1) to obtain the spectra of vertical wind gusts. This instrument, called a subsonic-frequency spectrometer, consists of 22 three-octave filters which continuously intersect a frequency band of 1 to 125 Hz (octave is a term applied to the band of frequencies in which the highest frequency has a ratio of 2:1 to the lowest). The use of magnetic recording makes it possible to investigate energy spectra right down to 0.1 Hz by applying an analog voltage to the spectrometer input with increased speed. L. P. Tsvang (1962) developed a parallel-analysis aircraft spectrometer in which half-octave filters cover a frequency band from 0.001 to 100 Hz. This instrument makes it possible to obtain energy spectra directly on board the aircraft.

In conclusion we should pause briefly on the analysis of the accuracy of results obtained with spectrometers. This analysis, as in §§ 1-3, will be based on calculation of the number of degrees of freedom k of the corresponding χ^2 distribution. The number of degrees of freedom is determined by formula (3.24):

$$k = 2TW_{\text{eq}}$$

where T is the recording length and W_{eq} is the equivalent width, determined by formula (3.21).

It can be shown (see (3.61)) that when a band filter with transfer function $\Phi(f)$ is used the equivalent width $W_{\text{ЭKB}}$ is determined by the relationship

$$W_{\text{ЭKB}} = \frac{\left[\int_0^{\infty} |\Phi(f)|^2 \cdot S(f) df \right]^2}{\int_0^{\infty} [|\Phi(f)|^2 \cdot S(f)]^2 df} \quad (3.64)$$

In the case when the spectrum of the initial process changes little in the frequency band $[f_1, f_2]$, which determines the filter position, $W_{\text{ЭKB}}$ can be considered equal to the equivalent width $|\Phi(f)|^2$. Finally, to determine the number of degrees of freedom it is possible to use the formula

$$k = 2\Delta f T,$$

where Δf is the filter width.

Having determined k from this formula, one should use Table 3.1 and find, with the assigned reliability, the stability of the obtained energy spectrum evaluations. When the filter width equals a half octave the calculation of stability is particularly clear, since in this case the number of degrees of freedom simply equals the number of half-periods of the investigated frequency in the recording of the process. Actually, in this case

$$k = 2 \frac{f}{2} T = \frac{T}{T_n},$$

where $T_n = \frac{1}{f}$ is the period of the investigated frequency f . Thus, for example, to obtain evaluations of the magnitude of the energy spectrum with an accuracy of $\pm 30\%$ and a reliability of 80% it is necessary to have at least 40 complete periods of the investigated frequency in the experimental recording. For the frequency $f = 0.1$ Hz this corresponds to a recording length of approximately 7 min.

The above analysis indicates the inadvisability of using spectrometers with very narrow filters. The apparent advantage of the filters is usually wiped out by the practical impossibility of obtaining extremely long experimental recordings and, as a rule, leads to the obtaining of very unstable evaluations of the energy spectrum.

CHAPTER 4

SPECTRAL STRUCTURE OF THE TURBULENCE FIELD

§ 1. SPECTRAL CHARACTERISTICS OF TURBULENCE AT LOW ALTITUDES

In a number of cases turbulence in the middle and upper troposphere is determined by the influence of the underlying surface and also by the dynamics and thermodynamics of the planetary boundary layer. Therefore it is advisable to introduce some results of investigations of turbulence at low altitudes.

a. Spectral Characteristics of Pulsations in the Horizontal Wind Velocity Component

At present the largest quantity of available experimental data for low altitudes are concerned with pulsations of the longitudinal horizontal wind velocity component.

The experimental autocorrelation functions obtained by a number of investigators have, as a rule, an exponential or exponential-oscillatory character. The latter indicates that wind velocity pulsations at altitudes are apparently made up of pulsations of a turbulent character and periodic oscillations. As a result of this, "bursts" connected with the effect of wave perturbations are frequently observed on experimental functions of spectral density.

The studies by N. Z. Pinus and L. V. Shcherbakova (1966) showed that in the lower half of the troposphere the spectra of pulsations of the longitudinal wind velocity component depend on the thermal stratification of the atmosphere and on the nature of the boundaries between turbulized layers of the atmosphere. The functions of spectral density in logarithmic coordinates are linear - i.e., they are described by a power law.

The dependence of the energy spectra of the horizontal wind-velocity component pulsations on thermal and wind stratification of the atmosphere is shown on typical examples presented in Figs. 4.1 and 4.2.

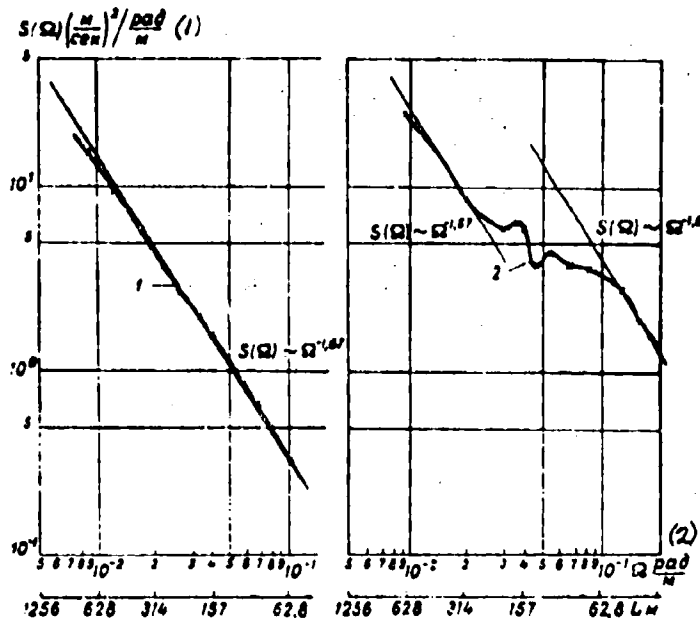


Fig. 4.1. Typical curves of the spectral density of pulsations in the horizontal wind-velocity component.

KEY: (1) $S(\Omega)(\text{m/s})^2/\text{rad/m}$; (2) rad/m .

Curve 1 on Fig. 4.1 characterizes the dependence of $S(\Omega)$ on Ω for an altitude of 500 m above the ground level with indifferent thermal stratification and a very small gradient of average wind speed.

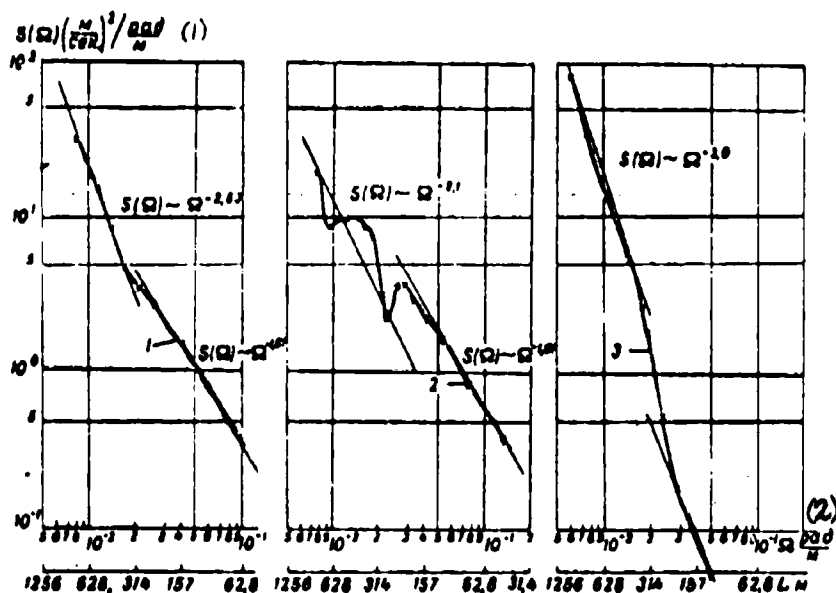


Fig. 4.2. Typical curves of spectral density of pulsations in the horizontal wind-velocity component.

KEY: (1) $S(\Omega)(\text{m/s})^2/\text{rad/m}$; (2) rad/m .

As we see, for scales ranging from several hundreds to several tens of meters the exponent at Ω equals -1.67 , i.e., it equals the theoretical value for the inertial interval.

Curve 2 on this figure characterizes $S(\Omega)$ for an altitude of 10 m, where the vertical temperature gradient in the lower 100-meter layer of the atmosphere was superadiabatic and the vertical gradient of average windspeed was close to zero. As we see, the left (low-frequency) and right (high-frequency) portions of the curve of $S(\Omega)$ correspond to the "minus $5/3$ " law. However, the right side of this curve falls in the region of higher values of spectral density.

Curve 1 on Fig. 4.2 characterizes the function $S(\Omega)$ for an altitude of 1000 m under conditions of stable thermal stratification and a small vertical wind-velocity gradient. As we see, this curve can be approximated by two rectilinear segments described by the power law. Up to scales approximately equal to 300 m, the modulus of the exponent equals 2.83, while for small scales it corresponds to the "minus $5/3$ " law.

Curve 2 on Fig. 4.2 characterizes $S(\Omega)$ at an altitude of 80 m during very stable thermal stratification and a significant vertical gradient of average wind speed. At scales from several hundred meters down to approximately 150 m there are bursts on the curve of $S(\Omega)$; these are apparently connected with the influence of short-period oscillations in windspeed caused by the high value of the vertical gradient of average windspeed in the stably stratified atmosphere.

We will turn to a theoretical explanation of the physical nature of the described spectra somewhat later (see § 3). We will note that for conditions of a stable atmospheric state the exponent can vary in broad limits. This is clear from the data presented in Table 4.1.

Table 4.1. Dependence of the exponent n at Ω on altitude.

(1) Высота, м	Число (2) спектров	β , 100 м	(3) н сев. β - 100 м	(4) Диапазон значений n	\bar{n}
400-700	9	0,65	1,84	2,0-2,9	2,43
700-1200	17	0,61	0,78	2,0-3,5	2,50
1200-1700	6	0,76	0,86	2,2-3,5	2,83
1700-2500	6	0,46	0,45	2,3-3,3	2,70
2500-3500	1	—	—	2,6	—
3500-4500	9	0,72	1,13	2,7-3,5	3,10

KEY: (1) Altitude, m; (2) Number of spectra; (3) β (m/s)/100 m; (4) Range of n values.

On the average the quantity n grows with altitude. This complicates obtaining averaged spectra, which might be regarded as standards for different applied problems.

Since on the average the troposphere is stably thermally stratified, the average spectra should be close in shape to the spectrum represented by curve 1 on Fig. 4.2. Considering that the stability of a thermally stratified atmosphere will, on the average, grow with altitude, it is possible to expect an increase in n for the region of scales exceeding several hundreds of meters.

Figure 4.3 shows averaged spectra for various altitudes in the lower half of the troposphere. As is evident from this figure, the

steepness of the curve of spectral density grows with altitude - i.e., the modulus of the exponent as a function of $S(\Omega) \sim \Omega^{-n}$ grows with altitude.

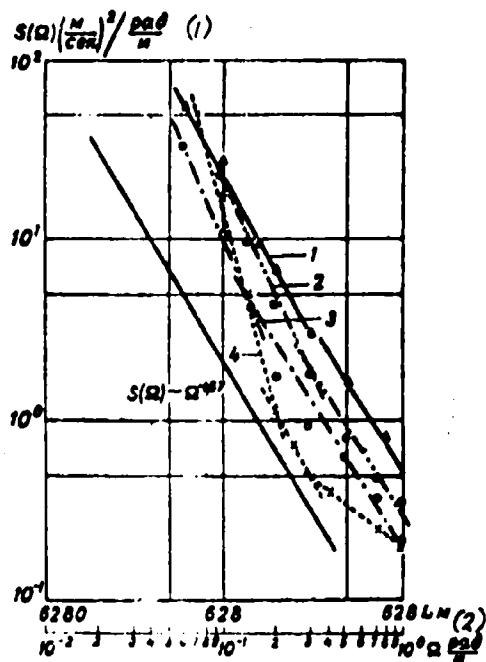


Fig. 4.3. Averaged spectra of pulsations of the horizontal wind-velocity component for different altitudes in the troposphere. 1) 500 m, 2) 1000 m, 3) 2000 m, 4) 3500 m.

KEY: (1) $S(\Omega)(\text{m/s})^2/\text{rad/m}$; (2) rad/m .

b. Spectral Characteristics of Pulsations in the Vertical Wind-Velocity Component

The distance from the earth's surface has an essential influence on pulsations in the vertical component of wind velocity. In particular, the limiting scale of these pulsations - the so-called turbulence scale - is bounded by this distance. Therefore the curve of the distribution of turbulent energy over the spectrum should have a maximum at a frequency corresponding to the limiting distance. Other

conditions being equal, its position should shift with altitude into the region of greater scales (lower frequencies). We will note that Archimedean forces should have a stronger influence on pulsations of the vertical component of wind velocity than on pulsations of the horizontal wind speed.

S. L. Zubkovskiy (1963) studied the spectral characteristics of pulsations in the vertical wind-velocity component; these pulsations were measured by means of an acoustic anemometer installed on an IL-14 aircraft. Flights were carried out by day over level terrain under conditions of strong thermal convection. Spectra were constructed for altitudes of 50, 100, 200, 500, 1000, and 2000 m. It was found that for perturbation scales ranging from 10^2 to 10^4 cm these spectra agree satisfactorily with the Kolmogorov-Obukhov "minus 5/3" law. Table 4.2 presents averaged characteristics of these spectra.

Table 4.2. The exponent n and the spectral density for the wave number 10^{-3} cm^{-1} as functions of altitude H .

(1) Высота H , м	(2) Количество спектров	n	(3) $S(\Omega) 10^{-3} \text{ cm}^3 \text{ сек.}^{-2}$	$\frac{S_H(\Omega)}{S_H(\Omega)_{H=50 \text{ м}}}$
50	20	1.72	6.46	1.00
100	22	1.74	6.31	0.98
200	19	1.68	4.90	0.76
500	18	1.57	5.18	0.80
1000	17	1.59	4.07	0.63
2000	18	—	0.68	0.11

KEY: (1) Altitude H , m; (2) Number of spectra; (3) cm^3/s^2 .

A tendency to a reduction in $S(\Omega)$ with altitude is noticeable, especially above 500-1000 m, where conditions of pure convection were apparently strongly disturbed during the period of the flight experiments.

Similar results for the above-indicated turbulent scale regions were obtained by P. A. Vorontsov and M. A. German (1964), who carried out measurements on a PO-2 aircraft equipped with an accelerograph.

We should point out the very interesting studies carried out by K. B. Notess (1957). These studies measured all three components of wind-velocity pulsations. The spectra in the region of scales from 20-30 to 400 m are approximated well by the "minus 5/3" law. However, the dispersions in pulsations u' , v' , and w' turned out to be different.

The article by B. M. Koprov (1965) presented data on the spectra of the pulsations in the vertical-wind velocity component obtained for the scale region ranging from a few meters up to 2-3 km. The spectra were measured at altitudes of 50, 100, 200, 500, 1000, and 2000 m during the day with developed convection above level terrain. The measurements were made on an IL-14 aircraft with an acoustic anemometer. Figure 4.4 shows the spectra which were obtained in experiments carried out from 1106 hours to 1417 hours on 31 August 1963. As we see, up to an altitude of approximately 1000 m the spectra are in good agreement with the "minus 5/3" law. At higher altitudes, where the atmosphere was stably stratified, the tangent to the slope of the spectrum constructed in logarithmic coordinates for perturbation scales exceeding 100-200 m is greater than 5/3 (in absolute value).

A. Burns (1964) published data on the spectra of pulsations in the vertical wind-velocity component measured on a "Canberra" aircraft during flights at low altitudes over different surfaces in England and North Africa. Velocity pulsations were measured with an anemoclinometer, supported on a rod ahead of the aircraft nose. The pulsation spectrum covered scales of pulsations ranging approximately from 15 to 2500 m. Certain characteristics of these spectra are given in Table 4.3.

From Table 4.3 it is clear that the values of the modulus of the exponent n have comparatively great scatter, especially at altitudes of 60-150 m, but on the average the values of n are close to 5/3.

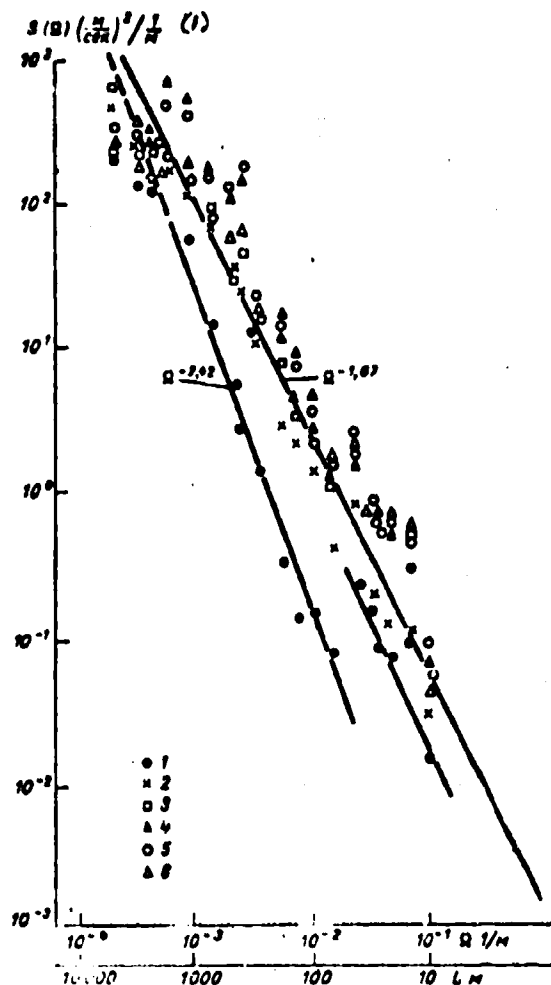


Fig. 4.4. Curves of the spectral density of pulsations in the vertical wind-velocity component (at various altitudes).

KEY: (1) (m/s)²/1/m.

Table 4.3. Characteristics $S_w(\Omega)$ as functions of altitude.

(1) Высота, м	(2) Количество спектров	(3) Средняя измененная n	(4) $ n $	σ_n	σ_w м/сек.
60	14	1,20—2,03	1,58	$\pm 0,32$	0,96
150	7	1,27—1,92	1,68	$\pm 0,23$	1,19
300	4	1,53—1,80	1,65	$\pm 0,16$	1,05

KEY: (1) Altitude, m; (2) Number of spectra; (3) Range of change in n; (4) m/s.

Unfortunately, there are very few data at present on the spectral density for scales of turbulence exceeding 2.5-3.0 km. This is connected with the fact that obtaining reliable data on the spectral density of pulsations in the vertical wind-velocity component on such large scales requires measurements over a horizontal flight segment no less than 90-100 km in extent. At the same time the horizontal extent of turbulent zones is, as a rule, less than 100 km. Besides this, it is difficult to assume that conditions of at least relative uniformity for which calculations of spectral density would be meaningful could be retained over a segment of such length.

The results of studies of the influence of the nature of the underlying surface on the spectrum are of definite interest. According to the experimental data of Burns (1964), spectral density is greater over the entire range of scales above hilly terrain than it is above a smooth surface. This difference grows with an increase in the scale of perturbations, beginning with scales approximately on the order of 100 m.

Spectra which he obtained during flights with and against the flow (wind) differ little from one another. This difference is particularly small if the groundspeed, and not the airspeed, of the aircraft is used for transition from time spectra to spatial spectra. This indicates that at low altitudes $S(\Omega)$ for the vertical component of wind velocity depends on the distance between orographic inhomogeneities. The spectra obtained by Burns during flight across the flow differ from those obtained during flights either with or counter to the flow. This difference is manifested particularly sharply in regions of small turbulence scales.

Not only turbulence intensity, but also the determined power and nature of the spectrum change with altitude. In particular, under conditions of indifferent or unstable stratification and small vertical gradients of average wind velocity, the spectral density of comparatively large scales of perturbations grows with altitude, while the spectral density of small scales of perturbations, on the contrary, diminishes. Intersection of curves of $S(\Omega)$ for different altitudes occurs at scales on the order of 600 m.

c. Relationship Between Spectra of Pulsations of the Vertical and Horizontal Components of Wind Velocity

As experimental investigations show, the magnitudes of the vertical and longitudinal components of velocity pulsations depend on the altitude above the surface of the earth and on the thermal and wind stratification of the atmosphere. Therefore they are subject to diurnal and annual variations. Table 4.4 gives experimental data obtained by P. A. Vorontsov (1966) which characterize this dependence for pulsations in the longitudinal and vertical components of wind velocity. He obtained these data over level terrain in the middle latitudes.

From Table 4.4 it is clear that in the summer and in the daylight hours, independently of the season, the mean square values of pulsations in the wind-velocity components σ_w and σ_u are greater than these characteristics for pulsations of the wind-velocity component in the winter and in the evening and night hours. Besides this, in the 100-meter atmospheric layer next to the ground the quantity σ_u grows in the warm season, while σ_w grows over the course of the entire year; at high altitudes, on the other hand, they diminish with altitude. The diurnal amplitudes of σ_w and σ_u vary similarly with altitude. In the cold season in the entire layer, not only the values of σ_u but also their diurnal amplitudes, diminish with altitude (Table 4.5).

Table 4.4 also gives the magnitude of the ratio σ_w/σ_u . From this table, which includes data on pulsations in wind velocity without distinction of the magnitude of the vertical gradient of average wind velocity, it is evident that even with an indifferent or thermally unstable state of the atmosphere the dispersion of pulsations of the vertical wind-velocity component is, on the average, less than that of pulsations of the longitudinal component. The anisotropy of pulsations of the wind velocity component is expressed particularly sharply in the winter, and also in the evening and night hours during the summer, when temperature inversions with comparatively

Table 4.4. Characteristics of pulsations in horizontal (u') and vertical (w') components of wind velocity.

(1) Высота, м	(2) Время суток, часы											
	00	13	17	21	01	03	09	13	17	21	01	03
	(3) σ_u м/сек (4)											
	Теплый период года						Холодный период года					
2	0.45	0.84	0.51	0.31	0.16	0.21	0.86	1.04	0.76	0.51	0.37	0.34
100	0.68	1.35	0.11	0.58	0.48	0.25	0.71	1.00	0.65	0.37	0.39	0.32
200	0.65	1.17	0.70	0.41	0.31	0.22	0.46	0.72	0.50	0.29	0.31	0.22
300	0.71	0.81	0.61	0.45	0.25	0.35	0.36	0.45	0.27	0.26	0.20	0.19
	σ_w м/сек											
2	0.26	0.61	0.34	0.10	0.05	0.06	0.20	0.34	0.21	0.08	0.10	0.10
100	0.41	0.98	0.40	0.18	0.18	0.09	0.30	0.60	0.29	0.12	0.12	0.16
200	0.39	0.81	0.34	0.14	0.10	0.10	0.26	0.41	0.20	0.09	0.14	0.09
300	0.30	0.60	0.29	0.12	0.07	0.12	0.21	0.26	0.09	0.07	0.09	0.07
	σ_w/σ_u											
2	0.58	0.72	0.65	0.36	0.30	0.29	0.23	0.31	0.28	0.29	0.30	0.30
100	0.62	0.76	0.56	0.32	0.38	0.35	0.42	0.49	0.44	0.32	0.31	0.42
200	0.60	0.75	0.48	0.31	0.32	0.34	0.16	0.52	0.38	0.30	0.36	0.38
300	0.42	0.74	0.47	0.27	0.30	0.35	0.42	0.52	0.39	0.32	0.37	0.40
	$\tau^{\circ}/100$ м											
2	---	---	---	---	---	---	---	---	---	---	---	---
100	0.9	1.5	0.9	-1.3	-3.4	-2.4	-0.0	0.6	0.4	-1.1	-2.3	-2.0
200	0.9	1.2	0.9	0.1	-0.2	-0.5	-0.4	0.2	0.3	-0.3	-0.8	-1.1
300	0.8	1.1	0.8	0.4	0.2	-0.2	-0.3	0.2	0.0	-0.1	-0.5	-0.7
	ρ м/сек / 100 м											
2	---	---	---	---	---	---	---	---	---	---	---	---
100	1.2	1.2	1.2	3.3	3.6	3.1	2.6	1.9	2.5	1.9	4.8	4.3
200	0.1	0.2	0.2	1.1	1.4	0.5	0.9	0.5	1.9	1.3	1.5	1.2
300	0.3	0.3	0.6	0.0	0.0	-0.1	1.0	0.4	0.0	0.9	0.6	0.0

KEY: (1) Altitude, m; (2) Time of day, hours;
(3) Warm season; (4) Cold season.

Designation: м/сек = m/s.

Table 4.5. Diurnal amplitudes of σ_u and σ_w , m/s.

(1) Время года	(2) Высота, м							
	σ_u				σ_w			
	2	100	200	300	2	100	200	300
(3) Теплое	0.63	1.10	0.95	0.56	0.56	0.89	0.71	0.53
(4) Холодное	0.70	0.68	0.50	0.26	0.26	0.48	0.32	0.19

KEY: (1) Season; (2) Altitude, m; (3) Warm;
(4) Cold.

small vertical gradients of average wind velocity are observed very frequently in the considered layer of the atmosphere. While the quantity σ_w/σ_u comprises an average 0.72-0.76 at noon in the summer and 0.30-0.36 at midnight in the summer, in the winter the values for these times of day are, respectively, 0.31-0.52 and 0.29-0.32.

One must bear in mind that with weak winds and small vertical gradients of average wind velocity, when conditions of free convection can exist, the sign and magnitude of the ratio σ_w/σ_u differ substantially from the average characteristics presented in Table 4.4.

Investigations by B. M. Koprov (1965) showed that in the summertime in the bottom layer of the atmosphere over level terrain and in cloudless weather the inflow of energy of turbulence is accomplished mainly due to the inflow from energy of average motion. Thus, for example, at a height of about a meter the inflow of energy from average motion $\left(-\frac{\partial \bar{u}}{\partial z} \overline{u'w'}\right)$ is one or two orders greater than the inflow of energy due to the work of forces of buoyancy $\left(\frac{g}{T} \overline{w'T'}\right)$. At a height of about 50 m the energy inflows are level and at higher altitudes the inflow of energy due to the work of buoyancy forces substantially exceeds that from average motion. Generally, the free-convection regime is realized in the daylight hours in the 50-200 m layer. According to Koprov's data, this regime is not observed in pure form at high altitudes. In particular, this is expressed in the fact that the decrease in the inflow of energy due to the work of buoyancy forces with altitude occurs substantially more rapidly than the decrease in the rate of dissipation of turbulent energy with altitude. Koprov considers that the growth in the role of vertical diffusion flows of energy of turbulence with altitude is the reason for this phenomenon.

We will examine in more detail the relationship between σ_w and σ_u with consideration of certain special features of the function of spectral density for pulsations of the vertical and longitudinal components of wind velocity. As was stated above, wind-velocity pulsation spectra depend on the nature of the thermal stratification

of the atmosphere, but spectra of pulsations of the vertical component of wind velocity at low altitudes also depend on the distance above the surface of the earth. With an increase in distance from the surface the observed break in the curve of $S(\Omega)$ for pulsations of the vertical wind-velocity component, constructed in logarithmic coordinates, is shifted into the region of larger scales (smaller Ω), as is clear from Fig. 4.5. Besides this, as Burns' studies showed, spectral density generally diminishes with altitude in the small-scale region, while in the region of large scales after the beginning of the break in the curve of $S(\Omega)$, on the other hand, it increases. Thus, the increase in the energy of vertical wind-velocity component pulsations with altitude occurs at the expense of the long-wave portion of the spectrum. Meanwhile the spectrum for pulsations of the horizontal wind-velocity component has one and the same slope for a broad range of scales and in this case spectral density diminishes with altitude. For these conditions the ratio between σ_w and σ_u at small altitudes has a characteristic vertical profile: up to 50-70 m, $\sigma_w < \sigma_u$; at higher altitudes $\sigma_w > \sigma_u$.

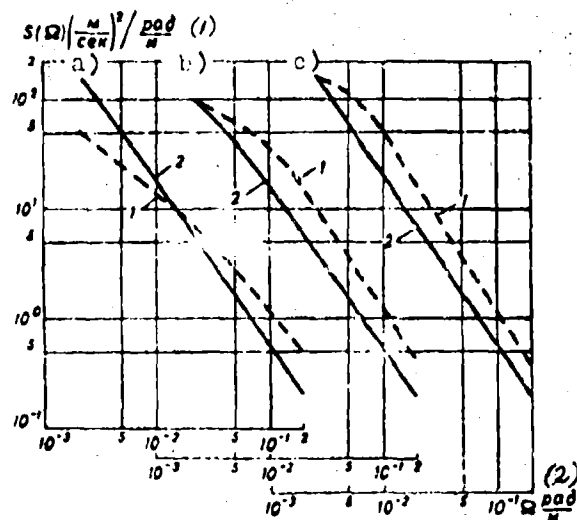


Fig. 4.5. Curves of spectral density for the vertical (1) and horizontal (2) components of wind velocity at altitudes of 60 m (a), 150 m (b), and 300 m (c).

KEY: (1) $(\text{m/s})^2/\text{rad/m}$; (2) rad/m .

As an example, Table 4.6 presents data from A. Burns (1964) for three flight experiments; during the first two experiments the vertical temperature gradient was $1.05^\circ/100$ m and during the third flight it was $1.11^\circ/100$ m. The wind speed at ground level was 6 and 3 m/s, respectively, while the vertical gradient of average wind speed was substantially less than 1 m/s per 100 m of altitude.

Table 4.6. σ_w/σ_u as a function of altitude.

(1) Altitude, m	σ_w/σ_u		
	1	2	3
30	---	---	0.80
60	0.99	0.73	1.29
150	1.23	1.06	1.33
300	1.20	1.46	---

KEY: (1) Altitude, m.

We will recall that the data in Table 4.6 relate to scales ranging from tens of meters up to 2500 meters. Thus, the nature of the anisotropy of wind-velocity component pulsations changes with altitude. At present there are no reliable data on the nature of anisotropy for high altitudes. However, it is possible to assume that at high altitudes, especially where stratification begins to become stable, σ_w is less than σ_u .

As the studies by A. F. Gurvich (1962) showed, in the lowest layer of the atmosphere the point at which a break in the curve of $S(\Omega)$ for pulsations of the vertical wind-velocity component occurs will depend on the thermal stratification of the atmosphere and is shifted into the region of large scales with an increase in the thermal instability of the atmosphere. Similar results were obtained by G. A. Panovskiy and R. A. Makkormik (1954) for altitudes up to 100 m above the surface. These studies showed that not only does the total energy of vertical wind-velocity component pulsations in the low-frequency region increase with an increase in altitude and thermal instability of the atmosphere, but there is also a growth in the displacement of the maximum toward the side of lower frequencies. Radar studies of the structural characteristics of pulsations of the

longitudinal and transverse components of wind velocity carried out by Yu. V. Mel'nichuk (1966) showed that with horizontal eddy scales which are smaller than the height of observations the structural functions of these components almost coincide. Beginning with scales which are close in magnitude to the value of the altitude of the observations, the structural function of transverse pulsations achieves saturation, while the structural function of longitudinal pulsations continues to grow. This indicates that the anisotropy of horizontal pulsations is shifted with altitude into the region of large perturbation scales.

§ 2. INTERMITTENCE OF TURBULENCE. SPECTRUM OF THE EXTERNAL BOUNDARY OF TURBULIZED LAYERS OF THE ATMOSPHERE

As indicated by the results of balloon and aircraft investigations of clear air turbulence, zones of intensive turbulence of great extent are encountered relatively rarely in the atmosphere. In a majority of cases it is possible to detect only individual zones of turbulence, localized in space; these move together with the average flow, where such local zones can arise spontaneously in the form of "flares." Flashes of turbulence can acquire comparatively great frequency, increase in size, and run together as they move along the flow. Gradually turbulent zones in the form of spots arise along the flow, so that a succession of quasi-laminar and turbulent regimes is observed. At a fixed point in space above which the airflow is moving, first the quasi-laminar regime and next the turbulent regime will predominate at the beginning of the described process.

The spontaneous nature of the appearance of, in particular, microturbulence in the free atmosphere was first detected by A. M. Obukhov, N. Z. Pinus, and S. I. Krechmer (1952) during experimental investigations of atmospheric turbulence on free balloons.

Under laboratory conditions it is possible to visualize the region of turbulent motions by the method of so-called shadow

photography. Considering the spatial scales of turbulent motions, this is virtually impossible to do in the atmosphere. To a certain degree it is possible to describe the geometry of turbulized layers, in particular at low altitudes, from the degree to which the space intersected by an aircraft in horizontal flight is filled with turbulent pulsations. In this case the most accurate description can be made if simultaneous measurements of wind-velocity pulsations are carried out by several aircraft at different levels. In practice flight experiments are, as a rule, carried out with a single aircraft and therefore the vertical section of the atmosphere can be obtained only by "cementing together" data from measurements during several different horizontal flights at different levels between fixed points on the surface. Besides this, during evaluation of experimental data on the presence or absence of turbulence in a flow of air it is necessary to consider the frequency characteristics and the initial sensitivity of the measuring equipment.

The diurnal variation of turbulence above level terrain is shown on Fig. 4.6, which was constructed from data of a flight experiment on a PO-2 aircraft carried out on 29 September 1946. Horizontal flights were made at levels of 100, 300, 500, 1000, 1500, and 2000 m. The segments on which aircraft overloads recorded by the SP-11¹ accelerograph were observed are traced on Fig. 4.6. During the first flight, carried out 15 min after sunrise, "solid turbulence" was observed at an altitude of 100 m, while at higher altitudes turbulence was noted only in isolated places in the form of flashes. In particular, individual flares of turbulence were noted at altitudes of 1000 and even 1500 m. A similar picture was observed during the second flight. Subsequently, as is evident from the figure, turbulence developed intensively and by 1100-1200 h it occupied a layer of the atmosphere up to 500 m; by 1200-1300 h it reached 1000 m. The greatest intensity was achieved at 1400 h. The last flight was carried out at 1625 h, i.e., 1-2 h before sunset. Turbulence at altitudes was weak and the perturbed sections of the flow had the

¹Initial instrument sensitivity 0.05 g.

nature of moving spots with horizontal dimensions ranging from several tens of meters to several hundred.

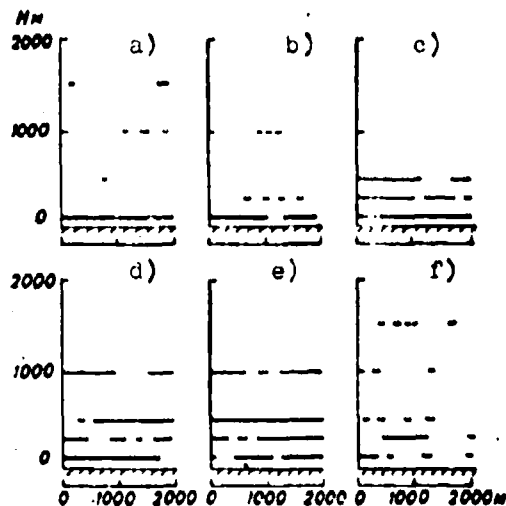


Fig. 4.6. Diurnal variation in the development of turbulence. a) 0640 h; b) 0830 h; c) 1029 h; d) 1238 h; e) 1433 h; f) 1625 h.

Thus, during the stages of development and attenuation of the turbulent regime in air flows turbulence can have an intermittent character. This same feature characterizes the transition zones between the turbulized zone and the unperturbed atmosphere. Experimental studies showed that turbulent layers in the atmosphere usually have a fairly clear-cut boundary, beyond which aircraft measurements indicate that there is no turbulence. The boundary between the turbulized and laminar segments of an air flow have irregular outlines which vary randomly in time and space. This stems from the fact that air can flow freely from the quasi-laminar region into the turbulent area, while turbulent pulsations can penetrate the quasi-laminar region of the flow only with substantial weakening on the path of penetration. According to L. D. Landau and Ye. M. Lifshits (1953), attenuation of velocity pulsation amplitude during penetration into a quasi-laminar region of the flow is described in the first approximation by the formula

$$A_H = A_0 e^{-\alpha H}, \quad (4.1)$$

where A_0 is the initial amplitude of pulsation velocity; Ω is the wave number, inversely proportional to the spatial scale of turbulent pulsations; H is the coordinate along the normal to the turbulized layer. From (4.1) it follows that the smaller the scale of turbulent pulsations, the smaller the distance from the turbulized layer at which they will attenuate. Therefore only comparatively large-scale turbulent pulsations can penetrate into the depth of the quasi-laminar region of the flow. These pulsations create irregular distortions of the boundary and a sequence of turbulent and quasi-laminar flow regimes. As an example, Fig. 4.7 shows the vertical section of a turbulized boundary layer of the atmosphere. This section was constructed by the "cementing" method from measurement data on aircraft overloads during flights above level terrain.

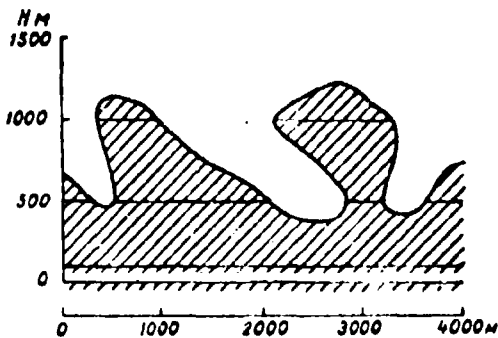


Fig. 4.7. Vertical section of the turbulized boundary layer of the atmosphere.

The degree of intermittence is evaluated according to the magnitude of the intermittence coefficient - i.e., from the magnitude of the ratio (α) of the total horizontal extent of the turbulized sections of the flow to the total length of the flow intersected by the aircraft or passing a given point. It is obvious that the distribution of the intermittence coefficient in altitude depends on the nature of the vertical distribution of air temperature and the average wind speed, while in the boundary layer it also depends on the distance from the surface. As an example Fig. 4.8 shows the curves of intermittence coefficient distributions; curve 1 was obtained for conditions of comparatively small vertical temperature

gradients but large gradients of average wind velocity (2 November 1963), curve 2 for conditions of convection (20 April 1962), and curve 3 for conditions of a disruptive surface temperature inversion (21 April 1962).

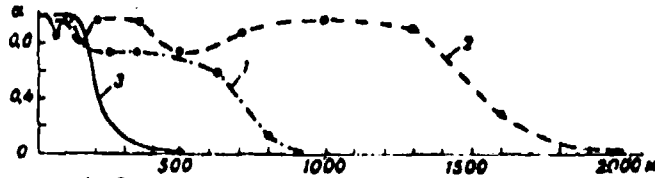


Fig. 4.8. Vertical profile of the intermittence coefficient of turbulence.

Laboratory studies show that in free turbulent flows the zone of intermittent turbulence is significantly deeper than in the boundary layers. In the boundary layers its depth can reach 0.4-1.2 of the thickness of the boundary layer, while in free turbulent flows it can reach 3.2 times the transverse dimension of the turbulized flow region. At present there are virtually no studies of the geometric characteristics of turbulence in the free atmosphere.

From (4.1) it follows that intermittent turbulent portions of the flow may exist at times, while at times small-scale turbulence may be absent. Thanks to this the function of spectral density for these flow regions should differ by very small values from the spectral density for a region of small-scale turbulence. As an example, Fig. 4.2 shows curve 3, characterizing $S(\Omega)$ for an altitude of 2000 m above the ground under conditions of stable thermal stratification of the atmosphere ($0.68^\circ/100$ m) and a small vertical gradient of average wind speed (0.20 m/s per 100 m). On the figure it is clear that the left part of the curve of spectral density has a slope which is characteristic for conditions of stable stratification with a small vertical gradient of average wind speed. The right portion of the curve has a very steep slope with a very small magnitude of spectral density for small-scale turbulence. Spectra having the same characteristic features as that on Fig. 4.2 were obtained by N. K. Vinnichenko (1966) at very high altitudes (up to 10 km).

It should be noted that the type of curve of spectral density $S(\Omega)$ depicted on Fig. 4.2 may characterize particular features of a spectrum of degenerating turbulence in the final period of degeneration (see Chapter 1). The greater the wave number Ω , the higher the rate at which spectral density $S(\Omega)$ diminishes in the process of turbulence degeneration.

Thus, besides the three basic types of energy spectra pointed out in § 1 and connected with thermal stratification, yet a fourth type is observed in the atmosphere; this type is characteristic for the region of the boundaries between turbulent layers of the atmosphere or conditions of degenerating turbulence. Interpretation of such spectra for turbulence of the free atmosphere in a clear sky, when it is virtually impossible to determine the boundaries of turbulent zones, represents a very complex problem.

§ 3. SPECTRUM OF TURBULENCE IN A THERMALLY STRATIFIED ATMOSPHERE

Experimental studies of the structure of turbulence in the troposphere and lower stratosphere were undertaken by the authors in 1958, when methods and equipment were available which permitted obtaining energy spectra of pulsations of the vertical wind-velocity component. The experimental data available at that time had been obtained mainly in the lowest and boundary layers of the atmosphere, where the underlying surface exerts an essential influence.

The first experimental energy spectra of atmospheric turbulence were obtained in zones of the jet stream (Shur, 1962). Figure 4.9 shows a typical energy spectrum of pulsations of the vertical wind-speed component obtained in the jet-stream zone. As is evident from the figure, the spectral curve constructed in a logarithmic scale can be approximated by two rectilinear segments. Each of these segments corresponds to the power law $S(\Omega) \approx \Omega^{-n}$. The segment BC can be approximated by the power law $S(\Omega) \approx \Omega^{-5/3}$, i.e., it corresponds to the inertial interval of the spectrum for which the Kolmogorov-Obukhov postulate about self-similarity and the transfer of energy from scale

to scale without losses is fulfilled. The line AD on the figure is drawn from point A with a slope of $-5/3$. If the spectrum were to pass along AD, this would mean that all the energy obtained by turbulent pulsations characterized by the wave number Ω_A , being gradually transferred without losses to turbulent formations with large Ω , would in the end dissipate into heat. Curve ABC passes below AD; consequently, less energy converts into heat per unit time than arrives at point A. Spectra which are similar to that shown in Fig. 4.9 are characteristic for the upper troposphere.

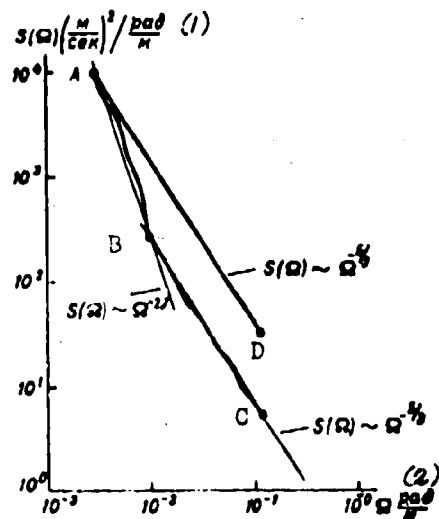


Fig. 4.9. Energy spectrum of turbulence (vertical component) in clear air in the jet-stream zone.

KEY: (1) $S(\Omega)(\text{m/s})^2/\text{rad/m}$;
(2) rad/m .

Figure 4.10 shows energy spectra normalized in terms of dispersion; they were obtained during flights in clear air in a zone of weakly expressed jet flow.

The overload method, which was used to obtain the spectra shown on Figs. 4.9 and 4.10, gives reliable results only when the intensity of turbulence exceeds a certain threshold value in the region of wave numbers to which the aircraft is sensitive (see § 1, Chapter 2).

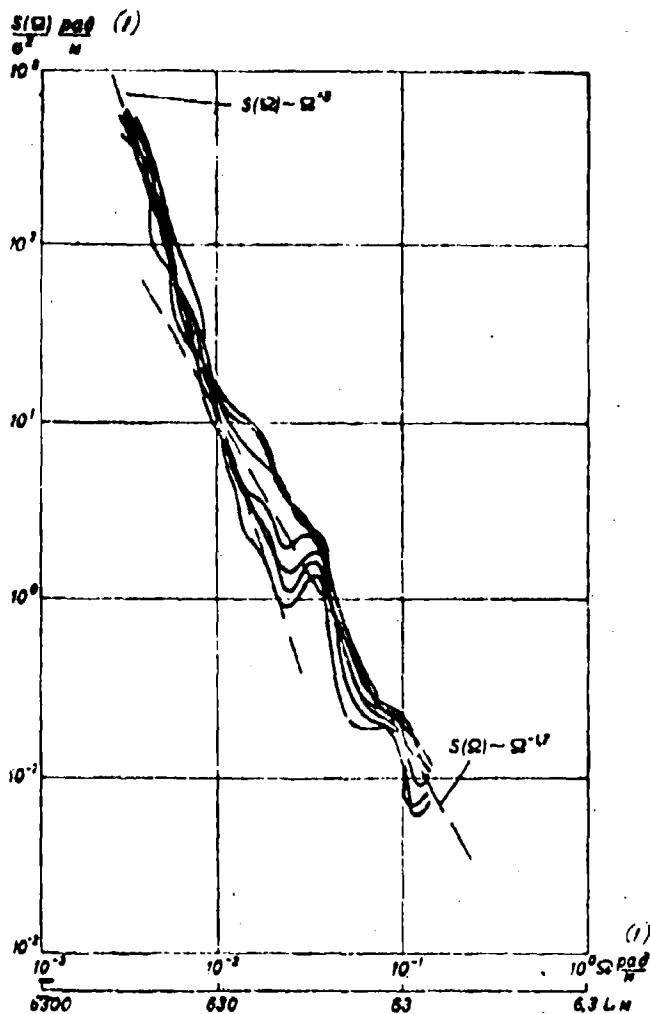


Fig. 4.10. Dispersion-normalized energy spectra of turbulence in clear air in a jet-stream zone above mountainous terrain.

KEY: (1) rad/m.

However, energy losses on scales corresponding to segment AB can be so significant that fluctuations in velocity with scales corresponding to segment BC (Fig. 4.9) will not be perceived by the aircraft as an overload meter. It is obvious that in those cases when the aircraft as a whole does not react to these velocity fluctuations, by using it as a platform it is possible to install on it more sensitive instruments and to study fluctuations lying below the

sensitivity threshold of the overload equipment. Such measurements, in particular pulsations of the horizontal wind-speed component, were carried out by the hot-wire anemometric method (Vinnichenko, 1964). In order to obtain the spectrum of the horizontal component in a broader range of wave numbers (scales), the measurements on the aircraft were carried out simultaneously by an airborne hot-wire anemometer and by the Doppler navigation system (see § 1, Chapter 2).

Figure 4.11 shows the energy spectrum of pulsations of the horizontal wind-speed component obtained in clear air in the jet-stream zone by N. K. Vinnichenko (1966). From comparison of Fig. 4.11 with Fig. 4.9 it is evident that the spectrum of the horizontal component has the same character as that of the vertical component. At the same time the magnitudes of spectral density on these figures differ by almost two orders of magnitude. In the case corresponding to Fig. 4.11, the aircraft did not experience noticeable overloads and only the use of sensitive equipment made it possible to obtain data on the turbulence spectrum. Figure 4.12 shows spectra of the horizontal component obtained by Vinnichenko (1966) during flights in clear air; they are similar in character to the spectrum on Fig. 4.11. The experimental data point to the fact that some mechanisms should exist for the absorption of the kinetic energy of turbulence present in the free atmosphere. This mechanism may be connected with peculiarities of the medium, that is either with the "absence of a solid wall" or with temperature stratification. The particular features of the structure a turbulent flow in a temperature-stratified medium were first pointed out by A. M. Obukhov (1946).

In the work by G. N. Shur (1962) the leakage of a portion of the energy of turbulent pulsations is explained by losses in resisting Archimedean forces. The basis for this explanation is as follows.

In the free atmosphere in the presence of stable stratification with respect to density the kinetic energy of an eddy obviously will not be transmitted to eddies with smaller scales without losses. In its lifetime an eddy must resist Archimedean forces of stable stratification. Part of the eddy energy will enter into an increase

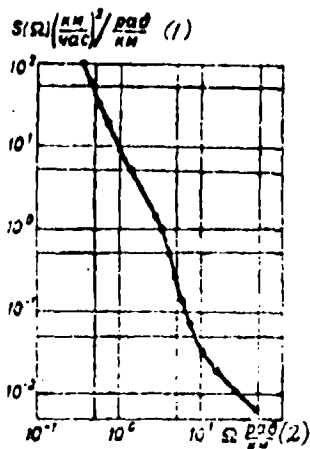


Fig. 4.11. Energy spectrum of turbulence (horizontal component) in clear air in a zone of jet flow.

KEY: (1) $(\text{km/h})^2$ per rad/km; (2) rad/km.

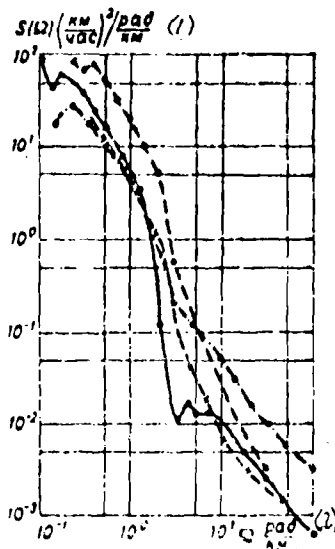


Fig. 4.12. Examples of the energy spectra of turbulence in clear air (horizontal component).

KEY: (1) $(\text{km/h})^2$ per rad/km; (2) rad/km.

in the potential energy of the flow, i.e., into a reduction in the stability reserve. It is also obvious that for eddies of small size losses of energy due to work expended resisting Archimedean forces will be negligibly small, while large-scale eddies may lose a

significant portion of their energy. The conversion of the kinetic energy of turbulent pulsations into potential energy should occur so long as stratification remains stable. In certain cases, as will be shown below, virtually all of the energy of turbulence may be expended on resisting the forces of stratification, and the turbulence spectrum can be limited from the side of large wave numbers (small scales).

We will examine certain quantitative relationships on the basis of the widely accepted assumption that in a turbulent flow energy is transferred from large-scale to small-scale eddies.

We will designate losses of energy due to resistance to Archimedean forces per unit time as dE'/dt :

$$\frac{dE'}{dt} = gv\Delta\rho = gv\frac{\Delta\theta}{\theta}\rho, \quad (4.2)$$

where v is the eddy velocity; ρ is density; g is the acceleration of gravity; θ is the potential temperature. We will have per unit mass

$$\frac{dE_p}{dt} = \frac{1}{\rho} \frac{dE'}{dt} = v \frac{g}{\theta} \frac{\partial\theta}{\partial z} l, \quad (4.3)$$

where $\frac{\partial\theta}{\partial z} = (\gamma_0 - \gamma)$ is the potential temperature gradient and l is the characteristic dimension of the eddy.

We will assume further that in the region of small l , as confirmed by many experiments, the Kolmogorov-Obukhov law is fulfilled well, and we will trace the tendency of the change in the spectral law "minus 5/3" during transition to large l with consideration of the effect being examined. Then

$$v_l = (nl)^{\frac{1}{3}}. \quad (4.4)$$

Substituting (4.4) into (4.3), we obtain

$$\frac{dE_p}{dt} \approx \frac{g}{\theta} \frac{\partial\theta}{\partial z} \frac{1}{3} l^{\frac{4}{3}}. \quad (4.5)$$

Expression (4.5) defines the rate of conversion of kinetic energy of turbulence into potential energy of the flow - i.e., the rate of loss of kinetic energy of turbulence per unit mass. The quantity dE_p/dt characterizes stable stratification of the flow as a certain consumer of turbulent energy. The larger the reserve of stability, the greater the quantity of turbulent energy which is pumped out of the spectrum. Expression (4.5) also shows that an unstably stratified flow can serve as a source of turbulent energy.

The total rate of transfer of turbulent energy, v_T , is made up of the rate of inertial transfer, numerically equal to the dissipation rate ϵ , and the rate of loss of turbulent energy dE_p/dt :

$$v_T = \epsilon + \frac{dE_p}{dt} = \epsilon \left(1 + \frac{\rho}{\theta} \frac{\partial \theta}{\partial z} z^{-\frac{2}{3}} l^{\frac{4}{3}} \right). \quad (4.6)$$

We will express the potential temperature θ through the average temperature of the turbulized layer T and we will designate

$$b = \frac{\rho}{\theta} \frac{\partial \theta}{\partial z} z^{-\frac{2}{3}} = \frac{\rho}{T} (\gamma_a - \gamma) z^{-\frac{2}{3}}. \quad (4.7)$$

Expression (3) is now rewritten in the form

$$v_T \propto z^{\frac{1}{3}} l^{\frac{1}{3}} \left(1 + bl^{\frac{4}{3}} \right)^{\frac{1}{3}}. \quad (4.8)$$

Raising (4.8) to the square, we obtain

$$v_T^2 \propto z^{\frac{2}{3}} l^{\frac{2}{3}} \left(1 + bl^{\frac{4}{3}} \right)^{\frac{2}{3}}. \quad (4.9)$$

According to (4.4), $bl^{\frac{4}{3}} \ll 1$; consequently,

$$v_T^2 \propto z^{\frac{2}{3}} l^{\frac{2}{3}} \left(1 + \frac{2}{3} bl^{\frac{4}{3}} \right). \quad (4.10)$$

By expressing the scale of l through the wave number, $\Omega = \frac{2\pi}{l}$, we obtain

$$v_0^2 \propto \Omega^{-\frac{2}{3}} \left[1 + \frac{2}{3} (2\pi)^{\frac{4}{3}} b_1 \Omega^{-\frac{4}{3}} \right]. \quad (4.11)$$

Differentiating (4.11) with respect to Ω , after simple conversions we obtain

$$S(\Omega) \propto \Omega^{-\frac{5}{3}} (1 + b_1 \Omega^{-\frac{4}{3}}), \quad (4.12)$$

where

$$b_1 = \frac{4}{3} (2\pi)^{\frac{4}{3}} \frac{g}{f} (\gamma_s - \gamma) \epsilon^{-\frac{2}{3}}.$$

The calculations used to obtain expression (4.12) are not strict; however, the conclusion which ensues from (4.12) that there is an increase in the modulus of the exponent at Ω in that region of wave numbers where stable stratification is influential is in good agreement with experimental results.

J. Lumley (1964) carried out a stricter solution of the problem of the spectrum of turbulence in a stably stratified atmosphere. He also proceeded from the assumption that the rate of transfer of energy in the spectrum is a function of the wave number Ω and depends on the degree of thermal stability of the atmosphere. For the spectrum of turbulence in a stably stratified atmosphere, Lumley obtained the expression

$$S(\Omega) \propto \Omega^{-\frac{5}{3}} \left[1 + \left(\frac{\Omega}{\Omega_A} \right)^{-\frac{4}{3}} \right], \quad (4.13)$$

where Ω_A is the wave number which characterizes the region of influence of Archimedeuan forces.

It is obvious that (4.13) converts to (4.12) if

$$\Omega_A^{\frac{4}{3}} = b_1 = c \frac{g}{T} (\tau_0 - \tau) \epsilon^{-\frac{1}{3}}. \quad (4.14)$$

On the basis of analysis of experimental results, R. Bolgiano (1959, 1962) proposed a model of the energy spectrum for a stably stratified atmosphere. He proposed that in a certain interval of wave numbers the rate of dissipation of mean square fluctuations of specific buoyancy forces has an essential influence on the shape of the spectrum. Bolgiano applied the name "buoyancy subrange" to the interval of wave numbers in which the shape of the spectrum is determined by thermal stratification.

It should be noted that the buoyancy subrange, if it exists, includes scales which fall in the inertial interval with indifferent temperature stratification. Therefore the buoyancy subrange is a segment of the inertial interval in which, besides transfer of energy over the spectrum, there is conversion of part of the kinetic energy of turbulence into potential energy.

For the spectrum in the buoyancy subrange, Bolgiano obtained the expression

$$S(\Omega) \sim \Omega^{-\frac{11}{3}}. \quad (4.15)$$

A. S. Monin (1962) arrived at the same result. He proposed that in the case of very strong stability the structure of the turbulent flow in the buoyancy subrange does not depend on the rate of energy dissipation, but is determined by only two parameters: the buoyancy parameter g/T and the average rate of levelling of temperature non-uniformities, N :

$$N = v_T \sum_{j=1}^3 \left(\frac{dT}{dx_j} \right)^2. \quad (4.16)$$

where v_T is the coefficient of molecular heat conductivity.

From dimensionality considerations, Monin obtained

$$S(\Omega) \propto \left(\frac{g}{T}\right)^{\frac{1}{2}} N^{\frac{1}{2}} \Omega^{-\frac{11}{4}}. \quad (4.17)$$

Further, from considerations of dimensionality it is possible to use the three parameters g/T , N , and ϵ to compile a scale of length L_B :

$$L_B = \epsilon^{-\frac{1}{3}} N^{-\frac{2}{3}} \left(\frac{g}{T}\right)^{-\frac{2}{3}}, \quad (4.18)$$

which has come to be called the Bolgiano-Obukhov scale. For inhomogeneities whose scale $L < L_B$, Archimedean forces do not influence turbulent motions. For $L > L_B$, the regime of turbulent motions in the inertial interval depends, as is evident from (4.18), on g/T and N . An expression for the turbulence spectrum in a thermally stratified atmosphere can also be obtained by using the interaction theory developed by Tchen (1953), for which the basic positions were outlined in Chapter 1.

F. A. Gisina (1966) examined the influence of thermal stratification on the nature of the energy spectrum as an effect of strong interaction of the temperature fields during weak interaction of average and turbulent fields of wind velocity (see Chapter 1). From the equations of motion and discontinuity, by averaging and expanding in Fourier integrals, Gisina obtained a spectral equation for the energy balance which takes into account the influence of buoyancy. To solve this equation she used a widely-known method. The parameters included in the spectral equation were used to compile certain scales of length on the basis of dimensionality considerations. Partial solutions were sought for these scales. For the scales corresponding to the buoyancy subrange, Gisina obtained an expression which coincides with the Bolgiano formula.

Thus it can be considered to be experimentally and theoretically established that the spectrum of developed turbulence during stable stratification of the atmosphere includes a buoyancy subrange which

is characterized by a spectral curve slope which is greater than $5/3$. In the region of large wave numbers both the Shur-Lumley and the Bolgiano-Monin formulas convert, as would be expected, into the spectral law "minus $5/3$." In the buoyancy subrange the very dependence $S(\Omega) = f(\Omega)$ is obtained as different; if it is difficult, by approximating experimental results, to give preference to one or another form of presentation for the spectrum of energy, as follows from the works of J. Lumley (1964), R. Bolgiano (1962), and A. S. Monin (1962), the difference becomes extremely substantial for spectra of temperature pulsations. Comparative analysis of the two theories describing the turbulence spectrum in the buoyancy subrange is given in the works by A. S. Monin (1965) and O. M. Phillips (1965).

Phillips showed that both expressions for the spectrum can be obtained from the spectral equation of the balance of turbulent energy. The final form of the expression for the spectrum in the buoyancy subrange will depend on certain initial hypotheses. If we assume that the magnitude of the turbulence spectrum $S(\Omega_1)$ is determined by the rate of energy transfer to the environment of Ω_1 and that the density of energy consumed on overcoming Archimedean forces is proportional to the average gradient of buoyancy forces $\frac{\partial}{\partial z} \left[\frac{g}{T} (\nu_* - \nu) \right]$, then as Phillips showed it is possible to obtain an expression coinciding with the Shur-Lumley formula.

If we assume that the structure of the turbulence of a stably stratified flow is determined by the rate of dissipation of mean square fluctuations of buoyancy forces $b' = -g \frac{\Delta \rho}{\rho}$ due to molecular diffusion, an expression coinciding with the Bolgiano-Monin formula is obtained.

The analytical expressions (4.12) and (4.17) are suitable for describing the energy spectrum of turbulence in a stably stratified atmosphere. With indifferent stratification the buoyancy forces equal zero and expressions (4.12) and (4.17) convert asymptotically into the spectral law "minus $5/3$." With unstable stratification of the atmosphere the expressions (4.12) and (4.17) have no physical

meaning. However, on the basis of simple physical presentations it is possible to show that the presence of unstable stratification can lead to a growth in the energy of turbulence.

Thermal instability, like thermal stability, can act in a certain interval of wave numbers (scales). If the loss of energy due to resistance to Archimedean forces leads to an increase in the modulus of the exponent (if we present the spectrum of the exponential function in the form $S_p \propto \Omega^{-n}$), the influx of energy due to thermal instability will lead to a reduction in $|n|$; in the case of strong instability it will lead to a change in the sign of n .

An experiment carried out on an IL-18 aircraft in the Tashkent region (Vinnichenko, Pinus, Shur, 1965) can serve as a good illustration of the dependence of the energy spectrum of turbulence on thermal stratification of the atmosphere. This example is typical for cloudless weather, the presence of unstable thermal stratification in the lower half of the troposphere and stable stratification at high altitudes, and weak vertical gradients of average wind speed.

During the flight experiment, carried out in September 1964, the weather was cloudless, the wind speed grew from 20 km/h at 1 km altitude to 70 km/h at an altitude of 9 km, and then diminished; up to an altitude of 1.5-2.0 km the atmosphere was unstably stratified. Curves of spectral density of pulsations of the horizontal wind-velocity component for altitudes of 1, 3, 6 and 9 km are shown on Fig. 4.13. The low-frequency segments (AB) of the curve $S_u(\Omega)$ were constructed according to Doppler meter data, while the high-frequency segments (CD) were constructed according to hot-wire anemometer data. The broken line indicates the insertion of segments obtained by other methods.

On Fig. 4.13 ($H = 1$ km) it is clear that saturation of $S_u(\Omega)$ in regions of small Ω is clearly evident on curve segment AB. Segment AB is continued with broken lines to the region of large frequencies according to the "minus 5/3" law. The experimental curve of spectral density, CD, lies above this line with a slope which is close to -5/3.

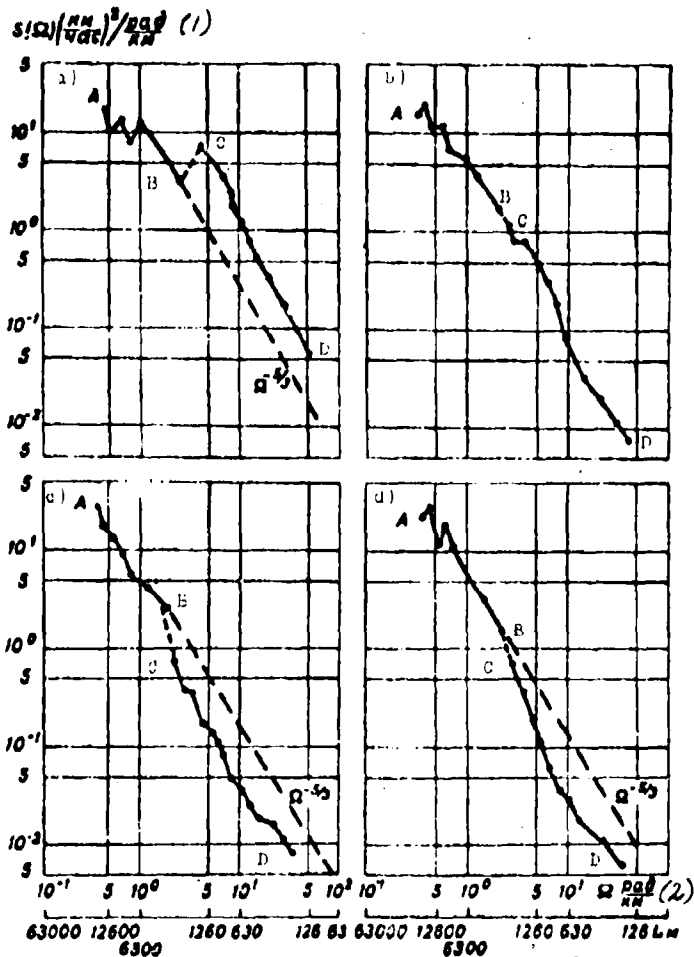


Fig. 4.13. Energy spectra of turbulence (horizontal components) at altitudes of 1, 3, 6 and 9 km. Temperature stratification at 1 km (a) is unstable; at 3 km (b), indifferent; at 6 km (c) and 9 km (d), stable.

KEY: (1) $S(\Omega)(\text{km/h})^2/(\text{rad/km})$; (2) rad/km .

Such a location of segment CD of the spectral density curve can be explained by the fact that in the region of scales from 1 to 3 km there was an influx of energy due to thermal instability of the atmosphere. This effect, which was well expressed at an altitude of 1 km, could be traced almost to 3 km altitude.

At an altitude of 3 km, i.e., where stratification was close to indifferent, the entire curve of spectral density ABCD corresponds (as is evident from the figure) to the "minus 5/3" law. For an altitude of 6 km, where stratification was stable, an increase in the slope of the curve $S_u(\Omega)$ on segment BC was clearly noticeable; this indicates a loss of turbulent energy expended on the resistance of turbulent perturbations to Archimedean forces. Finally, the spectral density of pulsations of the horizontal wind-velocity component at an altitude of 9 km has the same nature as $S_u(\Omega)$ for an altitude of 6 km, but the slope of the curve $S_u(\Omega)$ at this altitude is still great; this is connected with the greater thermal stability of the atmosphere which is observed at this level.

§ 4. TRANSFER OF ENERGY IN THE SPECTRUM AND GENERALIZED SPECTRUM OF TURBULENCE OF THE FREE ATMOSPHERE

In the inertial interval, spectra differ from one another only in the level of turbulent energy, which is determined by the quantity

$$\epsilon = c^{-1} S(\Omega)^{1/3} \Omega^{5/3}. \quad (4.19)$$

We will assume that even if no limitations of any type are imposed on the spatial structure of turbulent formations (i.e., even in the case of anisotropic and nonuniform turbulence), in a turbulent atmosphere transfer of energy from perturbations of large scales to small-scale perturbations takes place. In spectral terms this means that the flow of energy is directed toward the large wave numbers. This entails the possibility of determining the rate of energy transfer in the spectrum ϵ_Ω as a function of the wave number Ω . For the inertial interval

$$\epsilon_\Omega = \text{const} = \epsilon.$$

Here energy neither arrives nor is consumed within the inertial interval, but is only transferred from one set of motions (large scales) to another set (small scales).

The lines $\varepsilon = \text{const}$, where $\varepsilon_1 < \varepsilon_2 < \dots < \varepsilon_n$ are depicted on Fig. 4.14a in the coordinates $S(\Omega)$ and Ω . If the function of spectral density $S(\Omega)$ is parallel to these lines, the rate of energy transfer in the spectrum is constant. Segment BC of the spectrum proceeds parallel to isolines ε . In other words, in the wave-number interval $\Omega_B - \Omega_C$ sources and drains of turbulent energy are absent. On the segment AB, with an increase in wave number the spectral curve intersects isolines ε , transferring to levels of ever greater and greater energies. In this interval of wave numbers energy arrives in the spectrum - i.e., in the $\Omega_A - \Omega_B$ region a source of turbulent energy is operative. On the segment CD the spectral curve intersects isolines ε in the direction from large ε to small. This means that in the wave-number interval $\Omega_C - \Omega_D$ kinetic energy of turbulent pulsations does not transfer from scale to scale completely, but with losses - i.e., in the $\Omega_C - \Omega_D$ region a consumer of turbulent energy is operative.

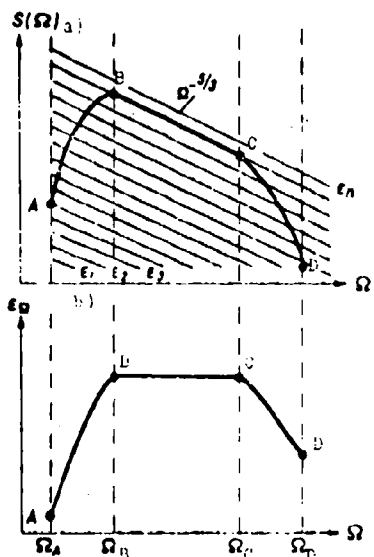


Fig. 4.14. Construction of the function $\varepsilon_\Omega = f(\Omega)$ according to the graph of $S(\Omega) = f(\Omega)$.

The curve of the function $\epsilon_{\Omega} = f(\Omega)$ is a very convenient form of presentation of experimental data in those cases when we wish to trace the transfer of energy within the spectrum of turbulence; this curve is shown on Fig. 4.14b. On such a curve both the regions where energy arrives in the spectrum and regions where energy is "pumped out" from the spectrum can be clearly singled out.

The difference between the rate of arrival of energy in the spectrum, ϵ_r , and the rate of dissipation of energy ϵ can be quite significant, with the sign of this difference depending on the type of stratification. Figure 4.15 presents curves of ϵ_r and ϵ calculated from the spectra presented on Fig. 4.13. Since the spectra show good subordination to the "minus 5/3" law on segments AB in Fig. 4.13, although it is difficult to expect isotropy and local homogeneity on these scales, the quantity ϵ_r was calculated from the spectra on the AB segments according to formula (4.19). The dissipation rate ϵ was calculated from the spectrum on the segments CD with the same formula.

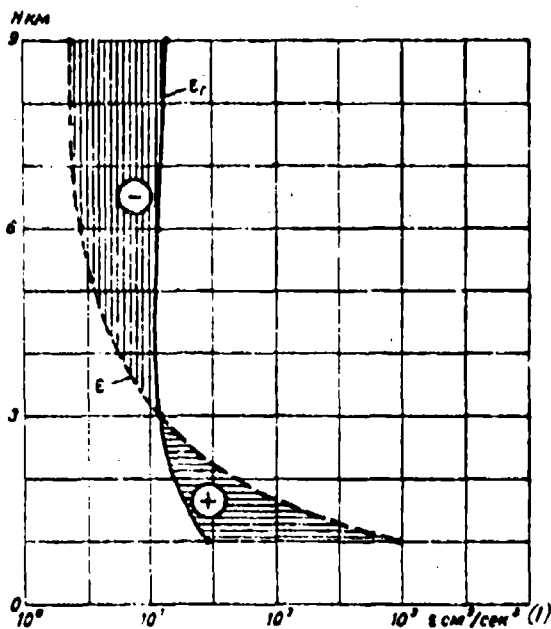


Fig. 4.15. Generation rate ϵ_r and dissipation rate ϵ of turbulent energy as functions of altitude (from the spectra presented on Fig. 4.13).
KEY: (1) cm^2/s^3 .

As is evident from Fig. 4.15, ϵ drops sharply with altitude, while ϵ_r remains practically constant beginning with an altitude of 3 km. In the zone up to 3 km ($\epsilon_r - \epsilon$) > 0, indicated on the figure by the "+" sign, while at high altitudes ($\epsilon_r - \epsilon$) < 0; this is indicated by the "-" sign.

The experimental data on the magnitude of ϵ obtained by A. G. Gorelik (1965) and by Yu. V. Mel'nicuk (1964) by the radar method, by V. N. Ivanov (1964) from measurements on a tower, etc., relate mainly to the lower 500-meter layer of the atmosphere. For comparison with the data presented on Fig. 4.15, we will introduce data obtained by F. K. Ball (1961) concerning the dependence of the rate of dissipation of turbulent energy ϵ on altitude. Figure 4.16 shows the curve $\epsilon = f(H)$ per Ball, with our data with respect to ϵ plotted in the form of blackened diamonds. As is evident from the figure, the various data do not, in general, contradict one another, if we consider that there was developed convection at low altitudes in the experiment (see the legend of Fig. 4.13).

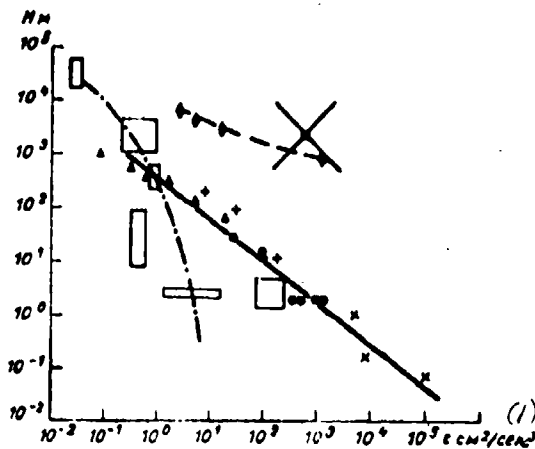


Fig. 4.16. Dissipation rate ϵ as a function of altitude, per Ball (1961). The large cross corresponds to dissipation during developed convection. Our data are indicated by the black diamonds (see Fig. 4.15).

KEY: (1) cm^2/s^3 .

The reduction in ϵ with altitude does not, however, mean that the intensity of turbulence drops sharply with altitude. As is clear from Figs. 4.13 and 4.15, the intensity of turbulence for small wave numbers (large scales) is reduced extremely slowly with altitude. As was indicated above, the intensity of turbulence can be characterized by the quantity ϵ_Ω ; since this quantity is related to a certain wave number, it can also be used for the characteristic of turbulence intensity outside the inertial interval.

Figure 4.17 shows curves of $\epsilon_\Omega = f(\Omega)$ obtained from the results of aircraft experiments in clear air with stable stratification of the atmosphere (Shur, 1967). Curves 1 and 2 were constructed for the horizontal component and curve 3, for the vertical. Curve 3 lies somewhat above curves 1 and 2, since it corresponds to the presence of intensive buffeting of the aircraft - i.e., significantly high energy of turbulence. All curves clearly show a region of reduction in ϵ_Ω (buoyancy subrange). It is interesting to note that for high intensities of turbulence the buoyancy subrange is displaced toward the side of large wave numbers.

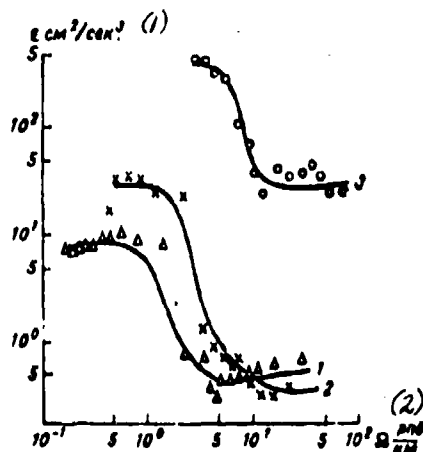


Fig. 4.17. Experimental functions $\epsilon_\Omega = f(\Omega)$ for clear-air turbulence. 1 and 2 - horizontal components; 3 - vertical component.

KEY: (1) cm^2/s^3 ; (2) rad/km .

These experimental data on the spectral structure of free-atmosphere turbulence were obtained by very different methods. Each method makes it possible to obtain the spectrum of turbulence in a certain interval of scales. However, it is possible to construct the diagram of a certain generalized spectrum of turbulence in the free atmosphere (as a rule, having stable thermal stratification) in a broad range of scales. The concept formulated above on the rate of energy transfer within the spectrum is used to construct such a spectrum.

Figure 4.18 shows a graph of the function $\epsilon_{\Omega} = f(\Omega)$. Region I on the graph is the region of wave numbers where generation of turbulent energy occurs due to the instability of the average flow. In this case a portion of the energy of the main flow goes into the formation of fluctuations. Region I is characterized by a growth in ϵ_{Ω} . This does not mean that in this region there is only arrival of the energy of turbulence. The increase in ϵ_{Ω} makes it possible to conclude only that the arrival of energy into the spectrum proceeds more rapidly than the outflow (consumption) of this energy.

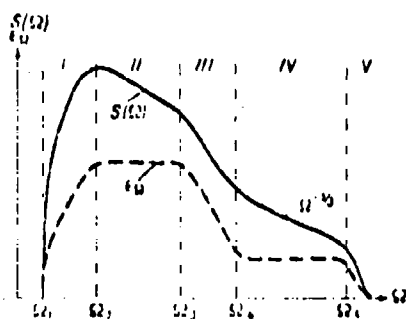


Fig. 4.18. Generalized energy spectrum of developed turbulence in the free atmosphere and the corresponding function $\epsilon_{\Omega} = f(\Omega)$.

Region II is characterized by a certain quasi-equilibrium between the arrival of energy in the spectrum and losses of this energy. Under losses one should not understand the transfer of energy over the spectrum. The nature of these energy losses requires study. The presence of a region of quasi-equilibrium is confirmed by numerous experimental data. The rate of energy transfer in this region remains virtually constant, although the condition of local isotropy is not deliberately fulfilled here.

Region III is a region of wave numbers in which a powerful consumer of turbulent energy is operative in a stably stratified atmosphere - i.e., Archimedean forces of stable stratification. The energy of turbulence converts to potential energy of stratification, while at the same time there is virtually no arrival of energy in the spectrum in the region of wave numbers $\Omega_3 - \Omega_4$. Owing to losses of energy expended in counteracting the forces of negative buoyancy, the rate of energy transfer ϵ_Ω drops with an increase in Ω .

Region IV is the classical inertial interval. Here the spectrum in the inertial interval is constant and equals the rate at which the energy of turbulence converts into thermal energy on the right boundary Ω_5 - the dissipation rate ϵ .

Region V is the viscous interval, where the energy of turbulence converts into heat due to viscosity. In this region ϵ_Ω drops from ϵ to zero.

The shape of the spectral curve changes in accordance with the changes in the rate of energy transfer in different segments of the spectrum. A generalized spectrum for a stably stratified atmosphere is presented on the same Figure 4.18. In the inertial interval the spectrum is described by the "minus 5/3" law. The inertial interval is bounded on the right by the wave number Ω corresponding to the so-called Kolmogorov microscale. As experiments have shown, its left boundary Ω_4 corresponds to scales of about 1000 m in a free atmosphere.

While by definition there are neither sources nor consumers of turbulent energy in the inertial interval, and there is only inertial transfer of energy over the spectrum from large scales to small ones, in the interval of quasi-equilibrium both sources and outflows of energy are operative. However, since $\epsilon_\Omega \approx \text{const}$ in this interval, the spectrum can be described by the expression

$$S(\Omega) \propto \Omega^{-\frac{5}{3}}. \quad (4.20)$$

The expression for the spectrum in the viscous interval can be obtained theoretically from the known equation of Helmholtz (see Chapter 1) and has the form

$$S(\Omega) \approx \Omega^{-7}. \quad (4.21)$$

Experiments carried out in wind tunnels do not confirm such a relationship. However, as an approximation the spectrum in the viscous interval drops more steeply than in the inertial interval. Since ϵ_{Ω} is reduced with a growth in Ω , in the buoyancy subrange the spectrum should also drop more steeply than in the inertial interval.

Experimental spectra obtained for pulsations of the vertical wind-velocity component can be approximated by the power relationship $S(\Omega) \sim \Omega^{-n}$, where n varies within the limits 2.2 to 3.1. It should be pointed out that G. N. Shar (1962) and J. Lumley (1964) consider the slope of the spectral curve in the buoyancy subrange to be variable, since it is a function of the wave number.

The shape of the spectrum in the region of turbulent energy generation depicted on Fig. 4.18 ensues from the general physical presentations and is a direct consequence of the growth in ϵ_{Ω} . Any amount of reliable experimental data relating to the spectral region for a free atmosphere will be insufficient to construct an empirical formula describing the spectrum in this region. The turbulence spectrum depicted on Fig. 4.12 is a certain general scheme for developed turbulence in the free atmosphere. Motions of all scales exist in such developed turbulence. The spectrum includes also the buoyancy subrange. In certain cases - for example, when the temperature stratification is close to indifferent - the buoyancy subrange may be absent from the spectrum of turbulence. Cases are also possible when energy arrives in the spectrum not only because of instability of the average flow, but also because additional local sources of turbulent energy exist.

As E. Reiter and A. Burns (1965, 1966) indicated, gravitational waves which are breaking down can serve as such a source of turbulent

energy in a stably stratified atmosphere. In this case secondary maxima will appear in the turbulent spectrum in the region of wave numbers corresponding to the length of disintegrating gravitational waves.

Disintegrating mountain waves can be another local source of turbulent energy. The mechanism of formation of such waves and the conditions under which they lose stability will be discussed in detail in Chapter 6.

The first work on the experimental investigation of the turbulence spectrum in the stratosphere (Vinnichenko, Pinus, Shur, 1967) was carried out in a mountainous region precisely because the probability of detecting zones of developed turbulence is high in such a region.

Figure 4.19 presents two spectra of the vertical wind-velocity component obtained during experiments in the regions of the Caucasian ridge. Curve 1 relates to a zone of turbulence in clear air at an altitude of 15 km. The increment of aircraft overload reached ± 1.0 g. Curve 2 represents the spectrum of the vertical component of wind speed in clear air above mountains at an altitude of 9.3 km in the presence of the jet stream; the axis of the stream was located at an altitude of 13 km. The overload increment in this flight reached ± 1.2 g.

For comparison spectra obtained above level terrain in clear air are presented on this figure. Curve 3 corresponds to turbulence in the jet-stream zone at an altitude of 8 km with an overload increment up to 0.5 g, while curve 4 represents weak turbulence along the axis of the stream (10 km) with an overload increment on the order of 0.1 g.

As is evident from Fig. 4.19, the spectral curves above mountains have characteristic breaks, in contrast to the more monotonic spectra above level terrain.

During experimental studies of turbulence in different regions and with extremely different conditions it was far from always

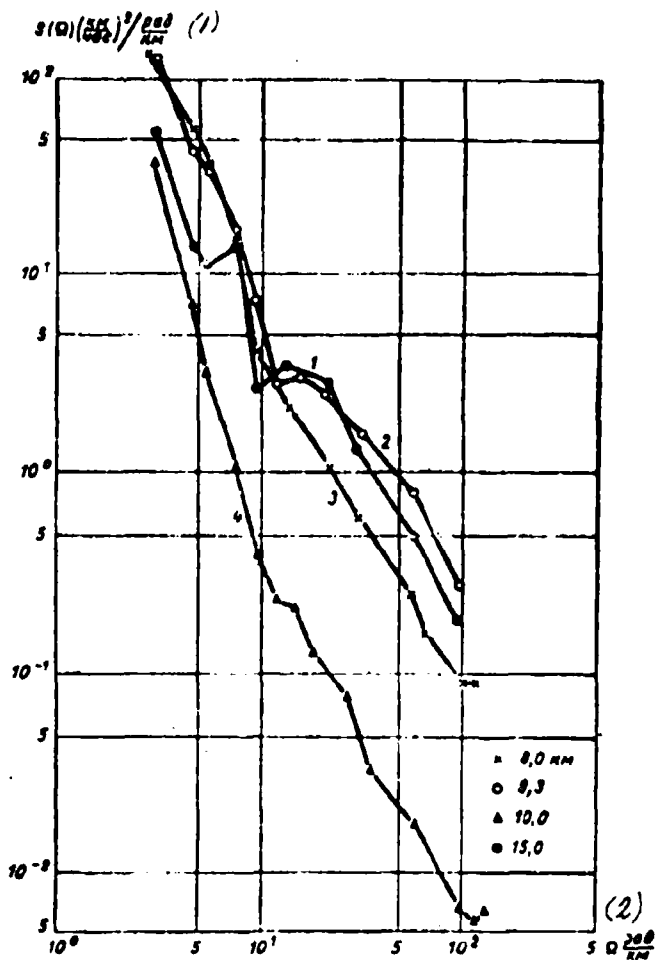


Fig. 4.19. Spectra of pulsations of the vertical wind-speed component.
 KEY: (1) $S(\Omega)(\text{km/h})^2/\text{rad/km}$; (2) rad/km .

possible to detect turbulent formations on wave numbers ordinarily included in the inertial interval. This means that the velocity pulsations corresponding to these wave numbers either lie below the sensitivity threshold of the equipment or are altogether absent.

Such spectra (with a limited band of wave numbers) are of definite interest and will be examined separately.

§ 5. SOME PARTICULAR FEATURES OF EXPERIMENTAL SPECTRA OF TURBULENCE IN CLEAR AIR

Experimental results and theoretical considerations touching upon the shape of the generalized spectrum of turbulence in the free atmosphere are, generally speaking, related to cases of developed turbulence with a continuous spectrum, containing measurable fluctuations of all scales, including the inertial interval. As a particular case the spectrum for strong stability of the atmosphere is superimposed on the proposed schemes; in this spectrum virtually all of the energy arriving in the spectrum in the generation region converts to potential energy of stratification in the buoyancy subrange. We will examine just how the shape of the generalized spectrum of turbulence in a stably stratified atmosphere can change as a function of the degree of thermal stability and power of the sources which are generating the turbulence. We will note that thermal stratification is only one of the "causes" of distortion of the shape of the spectral curve.

During strong thermal stability of the atmosphere, which as a rule always occurs in the stratosphere, turbulization of the flow requires large gradients of wind velocity. The very fact of the appearance and development of turbulence in such a medium attests to the fact that this condition is fulfilled.

However, although the reserve of thermal stability turns out to be inadequate to prohibit the birth of turbulence, forces of buoyancy intensively counteract the cascade transfer of energy over the spectrum. Here three cases corresponding to the three curves on Fig. 4.20 are possible.

1. With very strong thermal stability of the medium the spectrum of turbulent perturbations can be localized in a narrow band of wave numbers (curve 3). In this case the spectrum obtained during treatment of a realization of finite length will differ virtually not at all from the spectrum of purely harmonic oscillation if existing methods of machine statistical processing are used (see Chapter 3).

Such quasi-wave perturbations differ from purely wave perturbations in the fact that transfer of energy in them occurs from large scales to small scales and then all energy is expended on counteracting buoyancy forces.

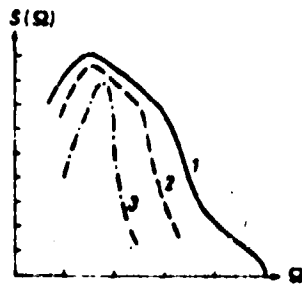


Fig. 4.20. Three particular cases of the shape of the energy spectrum of a stably stratified atmosphere.

2. With somewhat less thermal stability of the atmosphere or, which is the same thing, with greater dynamic instability, and also in those cases when the source of turbulent energy is located in a region of wave numbers remote from the buoyancy subrange, the spectrum of turbulence is found to be significantly wider and differs substantially from the spectrum of purely harmonic oscillations (curve 2). However, in this case also buoyancy forces absorb all kinetic energy of turbulent pulsations.

3. The most frequently encountered case is that when a continuous spectrum of turbulence exists in which kinetic energy is transferred from large scales to small ones. A portion of the energy is converted into potential energy and then at scales where the buoyancy forces do not play a significant role inertial transport occurs in accordance with the "minus 5/3" law. In the end the kinetic energy remaining in the spectrum converts to heat in the viscous interval (curve 1).

The different variants of spectra which are given on Fig. 4.20 represent particular cases of the general scheme shown on Fig. 4.13; they characterize the distribution of energy in the spectrum of developed turbulence.

It is of interest to evaluate the degree of isotropicity of turbulence in clear air in different wave-number intervals.

The ratio between different components of the vector of velocity pulsations was studied experimentally by E. R. Reiter and A. Burns (1965). They utilized a "Canberra" aircraft equipped with an anemoclinometer for these studies. Flights were carried out at altitudes of 8-11 km over Australia. The degree of isotropy of turbulence up to scales $L = 300$ m can be evaluated from the fulfillment of the known relationships (Batchelor, 1958)

$$\begin{aligned} S_u(\Omega) : S_v(\Omega) &= \frac{4}{3}, \\ S_v(\Omega) : S_w(\Omega) &= \frac{4}{3}. \end{aligned} \quad (4.23)$$

Table 4.7 gives data obtained by Reiter and Burns for a turbulent scale equal to 60 m. As we see, at high wind velocities relationship (4.23) is satisfactorily fulfilled for the vertical component and poorly fulfilled for the transverse horizontal component. At wind velocities of about 80 km/h relationship (4.23) is not fulfilled.

Table 4.7. Ratio between $S_u(\Omega)$, $S_v(\Omega)$ and $S_w(\Omega)$.

(1) Номер полета	(2) Высота, м	(3) Курс полета, град.	(4) Направление ветра, град.	(5) Скорость ветра, км/час	$\frac{S_u(\Omega)}{S_v(\Omega)}$	$\frac{S_v(\Omega)}{S_w(\Omega)}$
18B	8595	155	270	167	1.88	1.80
18Д	8870	260	261	167	1.34	1.35
27E	8530	280	228	174	0.92	1.42
33E	9770	255	260	167	1.09	1.30
45E	8670	095	258	80	0.67	0.85
46E	8920	218	278	83	0.93	0.88

KEY: (1) Flight number; (2) Altitude, m; (3) Flight course, deg.; (4) Wind direction, deg.; (5) Wind velocity, km/h.

§ 6. SOME EXPERIMENTAL DATA ON THE INTENSITY OF TURBULENCE AT HIGH ALTITUDES

Experimental investigations of pulsations of the longitudinal and vertical components of wind speed carried out on captive

(Devyatova, et al., 1958) and free balloons (Pinus, 1949, 1952; Litvinova and Silayeva, 1960), aircraft (Pinus, 1962, 1963a, 1964) and with radar equipment (Gorelik, 1965; Yu. V. Mel'nichuk, 1964, 1966) made it possible, to some degree, to study the dependence of turbulence intensity on different atmospheric parameters, altitude above the ground, etc.

First of all we should note the presence of a dependence between the relative intensity of turbulence ψ and the average wind velocity. Data from radar measurements of horizontal wind-velocity component pulsations in the scale range of 100 m to 2-3 km show that with an increase in wind velocity the relative intensity of turbulence is reduced; beginning with a velocity on the order of 5-6 m/s it is independent of changes in the average wind velocity and, on the average, comprises 0.02.

A similar relationship is the function $\psi = f(\bar{u})$, obtained from data of aircraft measurements made with the Doppler navigation system and related to scales ranging from a few kilometers up to 50-60 km; the largest value of ψ is observed at wind speeds of less than 50-60 km/h. At wind velocities greater than 60-70 km/h, on the average $\psi = 0.1$.

The connection between the quantity ψ and the average wind velocity can be used in practice to evaluate the magnitude of wind-velocity pulsations from data obtained by measuring average wind velocity.

Radar and balloon observations also made it possible to clarify the dependence of ψ on altitude. Although in each individual case the vertical profile of ψ has a complex laminar character connected with the nature of the vertical profiles of air temperature and average wind velocity, overall a reduction in ψ is observed with altitude. Table 4.3 gives a presentation of these data; it includes data from balloon observations.

Table 4.8. Turbulence intensity as a function of altitude

(2)	Высота, м (1)							
	100-200	300-400	500-700	800-1000	1200-1500	1800-2500	3000-4000	5000-6000
σ_u см/сек.	99	53	76	55	53	47	43	54
ψ %	9,6	5,9	9,2	4,5	5,5	3,2	2,8	2,6

KEY: (1) Altitude, m; (2) cm/s.

For ranges of motion scales which are close to the scales of the radar measurements, the change in ψ with altitude can be approximated with sufficient accuracy by the expression

$$\psi(H) = kH^{-0.5} \quad (4.24)$$

where H is altitude in km and k is a constant which depends on local conditions; for level terrain its value falls in the limits 5-15.

Similar results were obtained by Gorelik and Mel'nichuk from radar measurement data (Fig. 4.21). The value of ψ diminishes more sharply with altitude in the lower 500-meter layer of the atmosphere; in the middle troposphere ψ equals, on the average, 2%; in the upper troposphere an increase in ψ with altitude is noted. The growth in ψ with altitude in the upper troposphere is noted also from data of aircraft Doppler measurements (Pinus, 1963):

Altitude, km	7 ± 0.5	8 ± 0.5	9 ± 0.5	10 ± 0.5	11 ± 0.5
σ_u km/h	11.0	13.5	10.8	14.4	8.2
ψ	0.127	0.190	0.165	0.195	0.11

Monographs by P. A. Vorontsov (1960, 1966) give detailed data on the intensity of turbulence and of pulsations of wind-velocity components in the atmospheric layer up to a height of 300 m. Some of these data were presented in § 1 of this chapter.

We will now examine the intensity of turbulence according to data on fluctuations of the vertical component of wind velocity. At the Central Aerological Observatory numerous measurements were

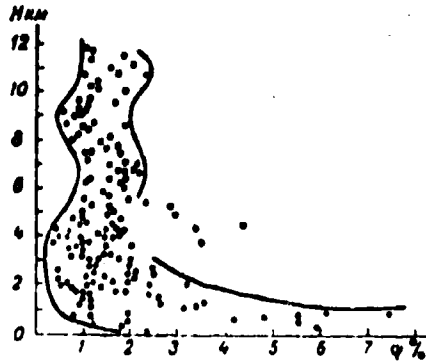


Fig. 4.21. The quantity ψ as a function of altitude according to radar data.

made of vertical motions of air during flights on free balloons (Pinus, 1949, 1952). Velocity averaged for 6-10 s was taken conditionally as a single measurement. The studies, conducted in cloudless weather or away from clouds, showed that the distribution of w with altitude had, as a rule, a laminar character. Besides this, the average speed of ascending motions (\bar{w}_+) did not always equal the average velocities of descending motions (\bar{w}_-). As an example, Table 4.9 presents the results of measurements carried out during two flights of free balloons conducted on 12 and 31 May 1949.

Table 4.9. Characteristics of the components w_+ and w_- of vertical motions of air.

(1) Высота, км	\bar{w}_+	\bar{w}_-	(1) Высота, км	\bar{w}_+	\bar{w}_-
(3) 12 мая 1949 г.			(3) 31 мая 1949 г.		
0,0	—	—	0,0	—	—
0,4	0,84	110	0,26	-1,96	3
1,0	1,24	103	0,57	0,71	11
1,8	0,68	46	1,0	0,78	25
2,0	0,70	46	1,5	0,70	21
2,15	0,13	—	2,0	0,64	23

KEY: (1) Altitude, km; (2) cm/s; (3) May.

The first flight was conducted in the presence of cumulus cloudiness. Ascending motions predominated in the layer up to 1000 m. On the average they exceeded 1 m/s, with the maximum rates reaching 2 m/s. In the layer of the atmosphere above 1000 m the average speeds

of ascending and descending motions were virtually identical, but here the maximum values reached 1-2 m/s. The second flight was carried out in cloudless weather in the presence of thick haze up to an altitude of 2.0-2.5 km. On the upper boundary of the temperature inversion layer the average speeds of ascending and descending motions were less than 10 cm/s; even their maxima did not exceed 18 cm/s. At high altitudes the maximum speeds reached 50-80 cm/s.

It should be noted that in these flights, as in many others, intensification or weakening of vertical motions had a "flare" character. At certain moments of time the speeds of ascending and descending motions achieved great values. On the other hand, over a prolonged period of time (especially on 31 May) speeds were below the initial sensitivity of the instrumentation (1 cm/s).

In many flights of free balloons the speeds of vertical motions of the air reached 2.5-3.0 m/s, but on the average they comprised 30-50 cm/s in the daylight hours and 2-15 cm/s at night. Changes in the sign (direction) of speeds had an unordered nature; however, they were sometimes periodic, with a broad range of period values. In 80% of the cases they did not exceed 120 s. It was noted also that high speeds preserved their sign (direction) longer.

Figure 4.22 shows the recurrence of speeds of vertical motions for zones with developed turbulence at altitudes of 1000-3000 m, measured during the flight of two free balloons on 25-26 July 1949. From this figure it is evident that the distribution curves for w_+ and w_- have, in general, a symmetrical character. Similar distributions were obtained in other flights, although asymmetrical distributions of w_+ and w_- were observed quite frequently. As investigations showed, the degree of asymmetry is determined by the magnitude and frequency of maximum values of speeds of ascending or descending gusts of air. In the overwhelming majority of cases the magnitude and sign (direction) of the maximum gusts also determine the ratio between the average values \bar{w}_+ and \bar{w}_- .

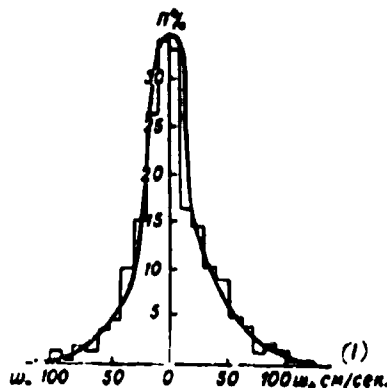


Fig. 4.22. Frequency of w_+ and w_- according to balloon data.

KEY: (1) cm/s.

Table 4.10 gives data on the average velocities of ascending and descending vertical motions obtained from a large series (38) of flights of free balloons and substratosphere balloons; the mean square values of velocity σ_w at altitudes are also included.

Table 4.10. Distribution of velocity of vertical air motions in altitude.

(1) Descents, m	\bar{w}_+	\bar{w}_-	$\frac{\bar{w}_+}{\bar{w}_-}$	(2) σ_w cm/sec.
	(2) cm/sec.			
200-600	49.3	22.2	2.22	45.0
600-1200	25.4	22.0	1.15	29.6
1200-1800	24.0	24.0	1.00	31.0
1800-2000	36.3	36.0	1.00	45.1
2000-2500	27.5	35.5	0.78	40.0
2500-3000	26.0	27.0	0.96	33.1
3000-4000	—	—	—	30.5
4000-5000	—	—	—	34.5
5000-6000	—	—	—	29.5
6000-7000	—	—	—	37.0
7000-8000	—	—	—	36.0
8000-9000	—	—	—	27.0

KEY: (1) Altitude, m; (2) cm/s.

From Table 4.10 it is evident that in the lower layer of the atmosphere in cloudless weather $\bar{w}_+ > \bar{w}_-$ on the average, and that this inequality is most sharply expressed in the atmospheric layer up to 600 m, while in the 1200-2000 m layer $\bar{w}_+ \approx \bar{w}_-$.

From comparison of the data in Tables 4.4 and 4.10 it is evident that on the average $\sigma_u > \sigma_w$ in the lower troposphere, especially at low altitudes.

Analysis of experimental data showed that σ_w grows with an increase in vertical temperature gradients and in average wind velocities and correlates well with the Ri number. According to the data of Ye. K. Verle, the correlation coefficient between σ_w and Ri equals 0.8.

In a flight on a substratosphere balloon carried out on 18 August 1950 measurements of vertical motions of air at an altitude of 10,450 meters in an isothermic-type layer directly under the tropopause were successfully carried out over a period of 6630 s. Oscillograms of these measurements were published in the article by N. Z. Pinus and V. D. Litvinova (1962). If the value of velocity averaged over approximately 20 s is taken as a single measurement, the highest recurrence is found in ascending and descending motions with a speed of 10-15 m/s, while the maximum values reached 130-150 cm/s and more. In general, in this flight the velocities of vertical motions were greater than 50 cm/s in 50% of the cases.

CHAPTER 5

ATMOSPHERIC CONVECTION AND THERMAL TURBULENCE

One of the broadest classes of turbulent motions is the so-called thermal turbulence, which represents pulsations of the vertical speed of air caused by buoyancy forces (Archimedean forces) which arise in individual segments of the atmosphere. Thus, thermal turbulence is a consequence of the development of atmospheric convection - i.e., the displacement of individual portions of air caused by differences in their density from the density of the surrounding air. Below the condensation level the greater portion of the energy of convection is derived from the thermal energy of the heated underlying surface. Convective currents with which clouds are associated obtain a significant and frequently predominate portion of their energy due to the realization of the latent heat of phase transitions of water.

A distinction is made between ordered and disordered convection. The first includes various forms of cellular circulation, during which the flow is broken down into regular circulation cells which have approximately identical dimensions and structure. Sometimes these cells are closed (for example, Bénard cells) and sometimes they are observed in the form of parallel bands of ascending and descending flows oriented along the wind vector or at a certain angle to it.

During disordered convection the spatial arrangement of individual convective flows (elements) has a more or less chaotic character.

Outside of clouds the elements of convection have linear dimensions ranging from several centimeters to hundreds of meters, while the most intensive convective flows inside cumulus and especially cumulonimbus clouds sometimes have thicknesses of several kilometers. It should be emphasized that during convection accompanied by phase transitions of water the parameters of the ascending and descending flows depend strongly on these transitions. Condensation leads to a growth in the speed of the ascending flow and the height to which it rises. The evaporation of drops, on the other hand, inhibits ascending motions but at the same time intensifies descending flows.

§ 1. DISORDERED ATMOSPHERIC CONVECTION

a. Structure of Convection Elements

Two concepts concerning the geometric shape of elements of disordered convection - thermals - are most widespread. According to the first of these, thermals represent individual, isolated masses of air - so-called bubbles. According to the other concept, thermals have the form of approximately vertical air jets. At present it can be considered to have been established that thermals can be formed and exist both in the form of bubbles and as jets, depending upon the thermal and dynamic conditions in the atmosphere and the nature of the underlying surface.

The hypothesis that the primary elements of convection are isolated volumes of air was first put forward by P. A. Molchanov and Ye. S. Selezneva, who identified thermals with large eddies arising during the day in the upper portion of the bottom layer of the atmosphere. Later a very similar hypothesis was proposed by F. Ludlam and R. Scorer (1953) and developed by Scorer (1957), B. Woodward (1959), J. Malkus and G. Witt (1959), and others. They considered that the leading portion of the bubble has the form of a hemisphere, while the trailing portion represents a long train of relatively cold air (Fig. 5.1a). Such a presentation of the elements of convection is the generalized method of particles, but in contrast to it here the interaction of the rising volume of air with the surrounding

medium, disrupting the adiabaticity of the process, is taken into account. This interaction is manifested in the presence of turbulent exchange of momentum and of other characteristics between the bubble and the surrounding air. Such a process is most active in the leading portion of the bubble. Such an exchange "erodes" the bubble and during its rise its boundary layer is continually washed away by the flow into the wake zone behind the thermal.

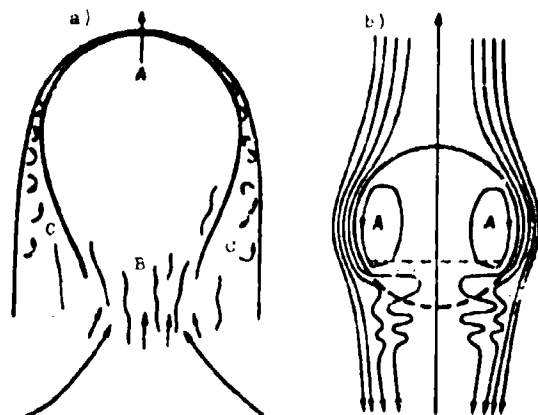


Fig. 5.1. Structure of a "bubble."
 a) diagram of bubble: A - heated mass of air; B - wake zone; C - erosion layer. b) current line in a rising bubble (per Levine): A - circular eddy.

According to the laboratory and theoretical studies by R. Scorer and S. Ronne (1956), B. Woodward (1959), J. Levine (1959) and others, an extremely important property of the bubble is the presence within the leading portion of the thermal of a quasi-stationary circulation of air similar to a Hill circular eddy (see Fig. 5.1b). This circulation plays a stabilizing role, preventing rapid complete mixing of the bubble with the surrounding air.

Most frequently bubbles have dimensions ranging from several meters to tens of meters. The largest are formed when several small bubbles flow together. This is facilitated by the fact that the pressure is somewhat reduced in the wake of the bubble and thermals are drawn into the track of the so-called mother bubble, rising

earlier than the followers; the track has an area many times greater than the area of the bubble cross section.

The acceleration of bubble rise can be described in the first approximation by the equation

$$\frac{dw}{dt} = g \frac{\theta^* - \theta_0^*}{\theta_0^*} - \frac{3}{8} \left(\frac{3}{2} K^* + c_d \right) \frac{w^2}{R}, \quad (5.1)$$

where θ^* and θ_0^* are the virtual potential temperature of the thermal and of the ambient medium; K^* is the portion of the thermal mass which participates in exchange with the surrounding atmosphere in the course of a half cycle ($K^* \leq 1$); c_d is the drag coefficient; R is the bubble radius.

A detailed investigation of the process of ascent of a thermal in the atmosphere was undertaken by C. Priestley (1954, 1955). He showed that if $\frac{\partial T_e}{\partial z} = \text{const}$ (the subscript e designates the values of meteorological elements outside the thermals) and if $w_e = 0$, by ignoring the square term, which is very small, one can obtain the following equation for w :

$$\frac{d^2w}{dt^2} + (K_1 + K_2) \frac{dw}{dt} + \left[\frac{g}{T_e} \left(\frac{\partial T_e}{\partial z} + \tau_e \right) + K_1 K_2 \right] w = 0, \quad (5.2)$$

where K_1 and K_2 are the rates of mixing for momentum and heat; K_1 and K_2 are inversely proportional to the dimensions of the thermal.

Analysis of the equation (5.2) shows that small thermals rise to small altitude, where they approach the level of equilibrium with the ambient medium asymptotically. The total distance passed (characteristic scale of buoyancy) L_{bu} equals

$$L_{\text{bu}} = \frac{\left| \frac{g}{T_e} \tau_e + K_1 w_0 \right|}{\frac{g}{T_e} \left(\frac{\partial T_e}{\partial z} + \tau_e \right) + K_1 K_2}, \quad (5.3)$$

where T_e' and w_0 are the initial heating and initial rate of ascent for the thermal.

Equation (5.2) is valid for large thermals only if $\left| \frac{\partial T_e}{\partial z} \right| < \gamma_e$.

In this case a moving thermal first jumps through the equilibrium level and then near it accomplishes damped oscillations with the period

$$\tau = 2\pi \left[-\frac{g}{\gamma_e} \left(\frac{\partial T_e}{\partial z} + \gamma_e \right) - \frac{(K_1 - K_2)^2}{4} \right]^{-\frac{1}{2}}. \quad (5.4)$$

If $\left| \frac{\partial T_e}{\partial z} \right| > \gamma_e$, motion is unstable and w increases exponentially.

Thus, while a thermal is located inside an unstably stratified layer its altitude should, theoretically, grow exponentially. When the thermal rises to a stable layer its vertical velocity is gradually reduced and harmonic oscillations appear near the equilibrium level.

Convective bubbles can be put in the category of freely floating thermals, since their displacement in the atmosphere is not directly connected with the terrain above which they are formed. In many cases the level of origin of the bubbles is located not at the very surface, but somewhere inside the unstably stratified portion of the lowest layer of the atmosphere; below this layer stratification can even be stable.

Along with the type of convective elements described above, the atmosphere can also contain convective jets whose vertical dimension is 5-10 times greater than their horizontal dimensions. Although such jets are typical mainly for the internal portion of cumulus-type clouds (see Chapter 8), they can also be formed below the condensation level. C. Priestley (1964), for example, arrived at a similar conclusion on the basis of data from synchronous measurements of the vertical velocities of the air w at different altitudes on meteorological towers. He found that pulsations in w in a broad range of altitudes correlated with one another; this proves the jet nature of the convective elements.

The theory of convective jets was examined in the works by Ya. B. Zel'dovich (1937), J. Batchelor (1954), C. Priestley (1954, 1955), A. S. Monin and A. M. Obukhov (1954), I. V. Vasil'chenko (1958), and others. Both laminar and turbulent jets were studied.

The base of the jet can be "tied" to a certain segment of the underlying surface and, thus, can be fixed or can be displaced together with the wind. The first type of jet is usually formed above strongly heated segments of the underlying surface, only if the wind speed at the ground level is small. The base of such a jet (convective tube) is, as it were, tied to the source of heat. Such tubes, sometimes clearly visible, are observed particularly frequently in the summer above rocky mountain peaks, above forest fires, over volcanoes, etc. The vertical dimensions of jets which are tied to the ground can reach hundreds or even thousands of meters. If the instability in the convection layer is great, convective jets frequently undergo rotation around the vertical axis in the clockwise or counterclockwise direction. The dust or sand devils frequently observed in the summer in desert and steppe regions are examples of rotating jets.

If the wind close to the ground intensifies, convective jets first bend in the direction of the wind and then are torn away from the earth, thus being converted into free-floating thermals. After breakaway of a thermal the rising heated air is replaced by cooler air, entering from above and from the sides. After a certain interval of time this "new" air is again heated and the process of evolution of a thermal starts over from the beginning. The outlined scheme shows that if calm conditions are ignored, the convective elements in the lowest layer of the atmosphere will, probably, sooner or later take on the form of bubbles, even if they had the form of jets beforehand.

Diagrams of the formation and evolution of thermals are shown on Figs. 5.2 and 5.3.

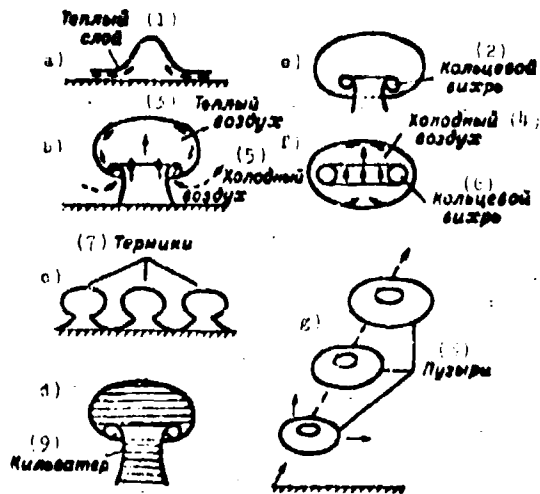


Fig. 5.2. Evolution of a "bubble" (per Cone).

KEY: (1) Warm layer; (2) Annular eddy; (3) Warm air; (4) Cold air; (5) Cold air; (6) Annular eddy; (7) Thermals; (8) Bubbles; (9) Wake.

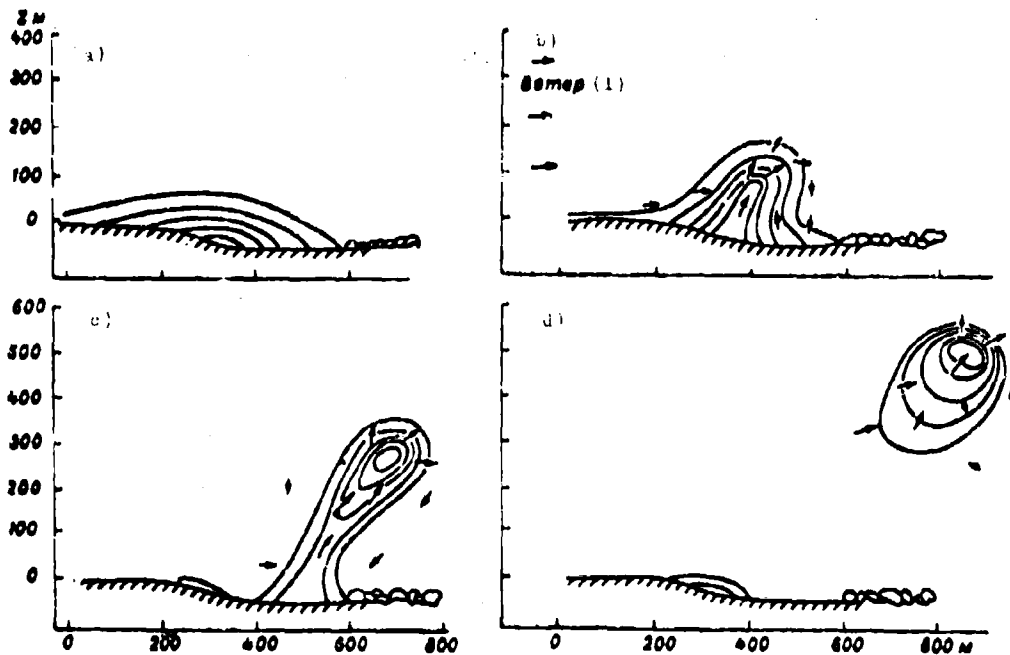


Fig. 5.3. Ascent of a thermal with a weak wind (per Woodward).

KEY: (1) Wind

b. Experimental Data on Disordered Atmospheric Convection

Observation data indicated that thermal turbulence - which means also disordered convection - will have a clearly expressed diurnal variation. Above land it is characterized by a maximum around midday and by a minimum at night. Above seas and large lakes and swamps the diurnal variation is reversed. This is connected with the fact that here stratification in the lower portion of the boundary layer is less stable in the dark hours. Below we will not touch upon the characteristics of thermal turbulence above water surfaces.

In summer during a cloudless sky after sunrise the development of convection begins first of all at the very ground surface. Only at 0800-0900 is convection extended over the entire lowest layer of the atmosphere and begin to penetrate to greater altitude. In the midday hours thermals are detected up to altitudes of 2-2.5 km, while above tropic deserts the height may even reach 3-5 km. After 1600-1700 convection begins to weaken, with this weakening proceeding at different rates at different altitudes. This is explained by the fact that according to pilot observations several thin layers with buffeting are usually observed in the boundary layer in the evening hours.

Experimental data show that depending on just where the instability begins, the lower boundary of the convective layer can be located either at the surface of the earth or at a certain height above it.

Tables 5.1 and 5.2 give empirical data on the degree of stability of the atmosphere during the day with active development of convection; the latter is indicated by the presence of Cu clouds (Table 5.1) or even Cb clouds (Table 5.2) during the sounding period.

These tables show that quite frequently (according to Table 5.2, in 55% of the cases) the thermal stratification of the atmosphere is stable in the period of development of convection in the lower portion of the boundary layer. In this case analysis of individual

Table 5.1. Average vertical temperature gradient during the day in the presence of cumulus clouds (per M. P. Churinova, 1950).

(1) Время, часы	(2) Границы слоев, км			
	0,2-0,4	0,5-1,0	1,0-1,5	1,5-2,0
6	0,17	0,62	0,78	0,60
8	0,93	0,66	0,72	0,55
10	0,87	0,78	0,84	0,50
12	1,00	0,66	0,72	0,62
14	1,16	0,66	0,58	0,64
16	0,80	0,58	0,60	0,80
18	0,93	0,55	0,76	0,72

KEY: (1) Time, h; (2) Boundaries of layers, km.

Table 5.2. Frequency (per cent) of sign of energy instability

$E = R \int_{p_1}^{p_2} (T - T_0) d \ln p$ in different layers in the presence of cumulonimbus clouds.

	(1) Границы слоев, км			
	(2) Земля - 0,4	0,4-1,0	1,0-1,5	1,5-2,0
$E > 0$	27	34	49	57
$E = 0$	18	15	12	5
$E < 0$	55	41	39	38

Remarks. 1. R - gas constant; p_1 and p_2 - pressure on the boundaries of the layer. 2. Calculations were made for cases of temperature sounding above different points in the European territory of the USSR.

KEY: (1) Boundaries of layers, km;
(2) ground.

soundings shows that isothermal or even inversion distribution of temperatures occurs on occasion in the lower 100 m. Such a situation is frequently observed in the morning but is also sometimes encountered around noon.

This indicates that it is not mandatory that convection begin from the surface of the earth, but that it can arise somewhere within the boundary layer. Naturally, in this case the elements of convection should most frequently have the form not of jets, but of bubbles from the very beginning. The cause of the beginning of convection here may be the presence of a raised thermally unstable layer or the appearance of local zones of increased humidity - i.e., segments of the atmosphere with relatively lower density. Spatial fluctuations of moisture may be connected with dynamic turbulence developing at those altitudes where vertical shears are great. The role of humidity in the appearance of convection was considered by N. I. Vulfson (1963), who indicated, in particular, that it is greatest over reservoirs.

On the basis of his experimental studies, A. A. Skvortsov (1947) proposed the so-called stratum diagram of the development of convection. First of all (usually in the morning) small-scale turbulence transfers water vapor and heat from the earth to an altitude of 50-100 m. Later eddies (thermals) of larger scales are formed at this altitude; they carry heat and moisture to greater altitudes.

Vertical wind shears ($\beta = \frac{\partial w}{\partial z}$) play a double role in the convection process. On the one hand, with a growth in β the intensity of turbulence and, in particular, the probability of the appearance of large "turbulent bodies" capable of causing the beginning of convection is increased. On the other hand, as shown, for example, by the theoretical studies of B. N. Trubnikov (1960, 1964), a growth in β suppresses the development of convection. In each specific case the actual development of convection is determined by the ratio of the indicated effects of vertical wind shear.

The spatial structure of thermals was studied by W. Georgii, C. Priestley, H. aufm Kampe and H. Weickmann, Yu. V. Chernov, and others. Figure 5.4 gives data on the structure of thermals under the lower edge of cumulus clouds per aufm Kampe and Weickmann. The thermals have the form of "sausages," with the vertical speed of the air being maximum in their axial portion. The fact that within the

period of 20 min two thermals with a length of about 2.5 km and width ranging from 500 to 1000 m rise through one and the same "channel" at an average speed of about 2 m/s is clear on the figure.

Figure 5.5 shows the distribution of vertical velocities under Cu with weak winds at ground level; this distribution was obtained by W. Georgii. The complex structure of the w field, characteristic for disordered convection, is clearly visible.

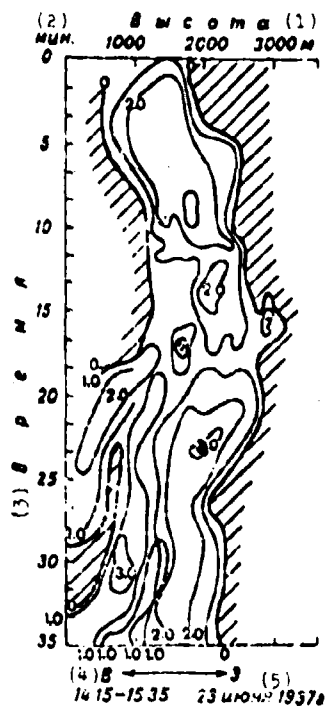


Fig. 5.4. Structure of ascending flows in a thermal (per aufm Kampe and Weickmann). The zone of descending motions is shaded.

KEY: (1) Altitude; (2) minutes; (3) Time; (4) E on the left and W on the right; (5) 23 June 1937.

According to data by A. Yates (1953), who studied thermals by means of gliders, above segments of heated soil about 2 km^2 in area a single thermal is formed every 5-15 min; these appear most often in the form of bubbles. The frequency of thermal appearance depends on the terrain relief, wind speed, the thermophysical characteristics of the soil, etc. We will note that the studies by Yates, P. A. Vorontsov (1940), and others showed that thermals are formed particularly frequently above segments where the characteristics of the underlying surface change sharply.

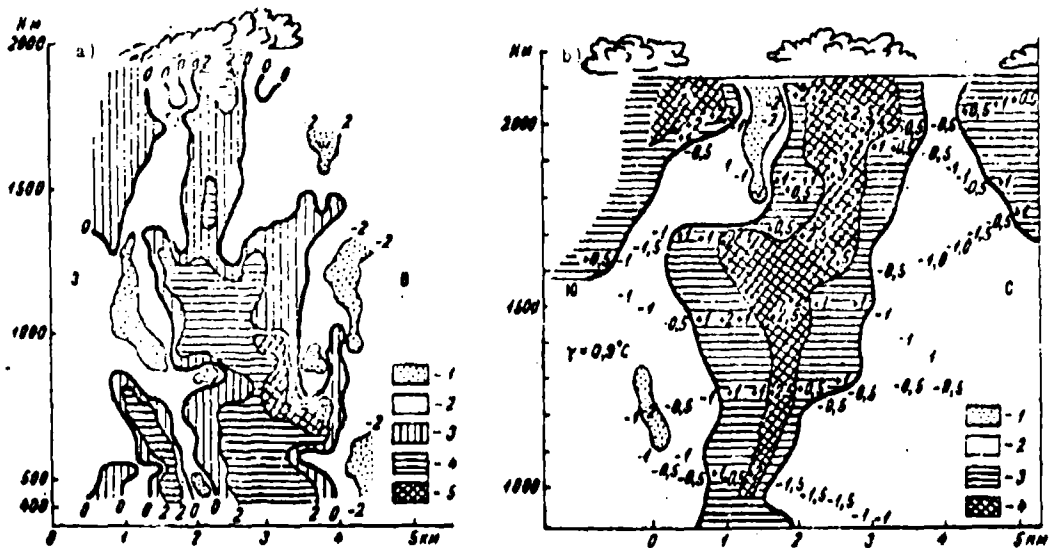


Fig. 5.5. Distribution of vertical flows above a 5-km-long segment. 23 June 1937 (per Georgii). a) section from west to east; b) section from south to north. 1 - descending flow with speed greater than 2 m/s; 2 - $-2 \text{ m/s} \leq w \leq 0$; 3 - $0 \leq w \leq 2 \text{ m/s}$; 4 - $2 \text{ m/s} \leq w \leq 3 \text{ m/s}$; 5 - $w > 3 \text{ m/s}$.

The number of parameters which determine the structure of elements of atmospheric convection include their dimensions, the distribution of temperatures and vertical speeds of air inside the thermals, etc. Instrument investigations which permit, with one or another degree of completeness, the determination of values of such parameters for thermals located above the lowest layer of the atmosphere but below the condensation level have been carried out, for example, by D. James (1953), A. Yates (1953), and N. I. Vul'fson (1961a). Interesting materials on the dimensions of thermals and vertical speeds of air within them were obtained by Yu. V. Chernov (1965). Some data on the structure of the field of the turbulence coefficient in the upper portion of the boundary layer under convection conditions were obtained by N. Z. Pinus (1965).

The studies by James and Yates were carried out directly under the base of cumulus clouds. Much broader studies were carried out by Vul'fson, who made measurements both in thermals located above the condensation level and inside cumulus clouds. The measurements

were made during horizontal flight on a laboratory aircraft equipped with a low-inertia high-sensitivity thermometer, a piezoelectric accelerograph, and other instruments.

Figure 5.6 shows the densities of the distribution of probabilities of horizontal dimensions of thermals. Since it was impossible to determine the shape of thermals during flights on a single aircraft, the calculation was carried out in two variants - for bubbles (ellipsoids of revolution) and for jets. As is evident from Fig. 5.6, the horizontal dimensions of thermals vary in wide limits. The most probable lengths of their diameters lie in the range from 30-40 to 70-80 m, but in individual cases can exceed these values by 10-15 times.

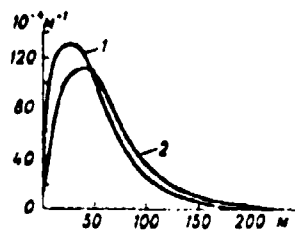


Fig. 5.6. Distribution of convective flows with respect to dimensions. 1 - "bubbles," 2 - jets.

The relative area or relative volume of ascending flows equals approximately 0.21; therefore if we assume that the descending compensating flows are realized outside the zone of ascending flows uniformly throughout the entire space, their speed should be, on the average, 4-5 times less than the speed of the ascending flows.

Table 5.3 shows how the parameters of thermals vary with altitude.

From Table 5.3 it is clear that thermals grow quite rapidly with altitude in the layer from 10 to 50 m, while above this they remain virtually unchanged. The concentration of thermals is reduced comparatively rapidly with altitude. As compared with the 10-meter level, the concentration of jets is reduced by 10 times at the 1000-meter level and that of bubble, by more than 30 times. The relative area occupied by the thermals changes appropriately.

Table 5.3. Change in average dimensions, concentration, and relative area (volume) of thermals with altitude (per N. I. Vul'fson, 1961).

(1) Высота, м	(2) Число измерений	(3) Средние размеры термиков, м		(4) Концентрация термиков		(5) Площадь или объем термиков
		(6) струи	(7) пузырей	(8) струй/км ²	(9) 1/м пузырей/км ³	
10	701	42	31	306	11 200	0,50
30	2480	49	37	217	6 180	0,50
50	7611	55	43	138	3 180	0,50
100	8728	61	46	87	1 910	0,44
300	4748	68	58	52	809	0,32
500	4007	70	61	40	620	0,27
1000	2658	72	64	29	334	0,21
2000	1409	74	65	29	298	0,20
3000	523	81	74	20	203	0,19

Remarks. 1. Under "dimensions of thermals" understand lengths of the diameters of jets or the horizontal axes of ellipsoids. 2. m is the ratio of the length of horizontal axes of ellipsoids to the vertical axes.

KEY: (1) Altitude, m ; (2) Number of measurements; (3) Average thermal sizes, m ; (4) Concentration of thermals; (5) Relative area or volume of thermals; (6) jets; (7) bubbles; (8) jets/ km^2 ; (9) $1/m$ bubbles/ km^3 .

Table 5.4 gives data on the amount by which temperatures in the center of the thermal exceed those outside it.

Table 5.4. Average excess of temperature (ΔT°) in the center of thermals at different altitudes (per N. I. Vul'fson, 1961).

(1) Форма термиков	(2) Высота, м								
	10	50	50	100	100	100	1000	2000	3000
(3) Струи	0,64	0,23	0,23	0,23	0,15	0,12	0,12	0,10	0,19
(4) Пузыри	0,54	0,18	0,19	0,18	0,11	0,11	0,10	0,09	0,17

KEY: (1) Type of thermal; (2) Altitude, m ; (3) Jet; (4) Bubble.

The data in the table were calculated from the results of both midday and morning and evening measurements; at the latter times the height of rise of thermals and their "overheating" are least. Therefore data on ΔT at $z \geq 500$ m are understated. It should be noted

that the dimensions of thermals, their overheating, and also the height and speed of rise have a maximum in the daylight hours.

It is interesting that the Vul'fson data indicate that ascending flows are not only warmer but also more humid than the surrounding air. This is apparently explained by the fact that the dimensions of zones of nonuniformity of the atmospheric refraction coefficient and zones of temperature excess vary approximately parallel with altitude (see, for example, Pakhomov, Pinus, Shmeter, 1960).

Measurement results made it possible to establish the shape of the curve representing ΔT° and w in a jet with radius R as functions of altitude above ground level, z , and of distance from the axis of the thermal, r . If z is measured in meters, then

$$\Delta T \approx 1.1z^{-\frac{1}{3}} \left(1 - \frac{r^2}{R^2}\right)^{\frac{1}{3}}. \quad (5.5)$$

$$w \approx 0.2z^{\frac{1}{3}} \left(1 - \frac{r^2}{R^2}\right)^{\frac{1}{3}}. \quad (5.6)$$

We will note that the form of formulas (5.5) and (5.6) agrees well with the laws $w(z, r)$ and $\Delta T(z, r)$ proposed earlier by A. S. Monin and A. M. Obukhov (1954), J. Batchelor (1954), and C. Priestley (1959), who considered a theoretical model of spontaneous (i.e., arbitrarily appearing) turbulent jets.

A comparatively great number of studies of convective flows have been carried out on gliders. Unfortunately, as a rule these studies are limited to qualitative evaluations of the width and, more rarely, the vertical velocity of those thermals within which glider ascents were accomplished. The few instrument investigations include the work carried out in 1962-1963 under the leadership of Yu. V. Chernov (1966).

More than 200 passes through thermals were carried out on the L-13 "Blanik" glider, equipped with measuring apparatus which made it possible to determine the speed and temperature of vertical flows.

These through-flights were accomplished with the control elements fixed in one of the planes of symmetry of the thermal (the working hypothesis used was that of the axisymmetrical nature of ascending flows). The laboratory-glider was guided to the center of the thermal by means of another glider of the same type. To determine the center of the flow, thermometers were installed on the wingtips and the difference between their temperatures, ΔT^* , was recorded. Obviously, during passage of the glider to the center of the flow $\Delta T^* = 0$.

Study of the connection between the maximum vertical velocity w_{\max} and thermal diameter D showed that w_{\max} generally grows with a growth in D .

Analysis of individual through-flights confirmed the axisymmetrical nature of thermals: the maximum speeds of flow are observed in the center of the flow, while a loop of descending motions is usually observed along with the ascending flow. Characteristically, in 79% of the cases a zone with approximately constant vertical velocities was observed instead of a sharp maximum of w on the axis of the thermal. In narrow flows it occupied 10% of the diameter of the thermals, while in broad flows it took up 32%.

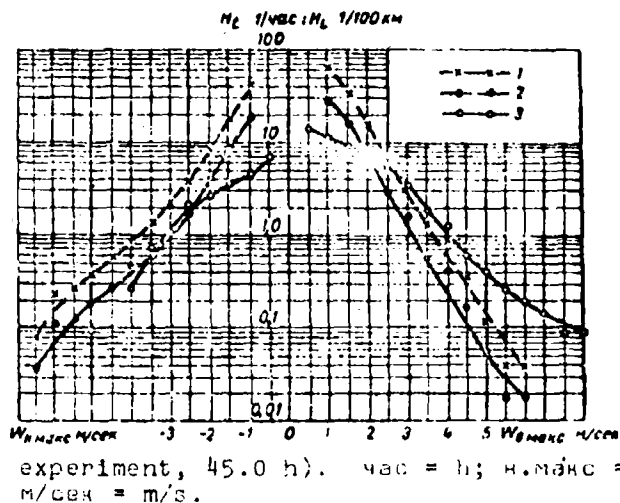


Fig. 5.7. Accumulated recurrences of ascending and descending air flows per 1 h of flight and per 100 km of route according to data from a 1963 experiment, in comparison with results of 1962 studies. 1 - recurrence of flows per 100 km of route H_t (data from 1963 experiment based on a planned route of 2546 km); 2 - recurrence of flows per 1 h of flight, H_t (data from 1963 experiment 54.5 h in volume); 3 - the same (data from 1962 experiment, 45.0 h). $\text{чис} = h$; $\text{н. макс} = d. \text{ макс}$; $\text{в. макс} = a. \text{ макс}$; $\text{м/сек} = \text{m/s}$.

Figure 5.7 shows the cumulative frequencies of maximum velocities of ascending ($w_{a,max}$) and descending ($w_{d,max}$) flows per 1 h of flight and per 100 km of route. The increased frequency of ascending flows noticeable in the 1962 materials is a consequence of the fact that in this year the flights were carried out by more highly qualified glider pilots, better able to pick out the zones in which $w > 0$ was observed.

§ 2. CELLULAR CONVECTION

Along with gravitational-shear waves (see Chapter 6), cellular convection is one of those forms of quasi-ordered mesoscalar atmospheric motions in which loss of stability is accompanied by intensive generation of turbulence. We will also note that while crossing of a zone of cellular convection aircraft experience variable cyclic overloads whose influence on controllability and strength of aircraft and helicopters frequently exceeds the influence of "ordinary" turbulence.

Although cellular convection is quite frequently encountered above the boundary layer of the atmosphere¹, as yet the accumulation of experimental data on this subject is inadequate. This is connected basically with the difficulty of finding convective zones only if clouds are absent from them. Besides this, frequently even in those cases when clouds are present it is virtually impossible to distinguish by external indications gravitational-shear waves and the so-called two-dimensional cells which are characterized by bands of ascending and descending flows which are extended in the direction of the wind shear vector. Therefore the basic data on the physical laws inherent to cellular convection have been obtained by means of laboratory experiments, which show the following.

¹At ground level ordered convection usually cannot develop due to the perturbing influence of nonuniformities of the underlying surface and the strong development of dynamic turbulence here.

1) the existence of cellular convection requires that the vertical gradient of temperature in its layer exceed a certain critical magnitude which depends basically on the thickness of the convective layer and the intensity of turbulent diffusion;

2) the shape of the forming cells, their dimensions, the direction of vertical motions in different parts of the cell, and other characteristics of circulation depend on the thickness of the convection layer and on the physical properties of the air. An essential role is also played by temperature and wind stratification of the atmosphere at the altitudes where convection is developing.

Convective cells are moved along with the wind, while their characteristics change quite rapidly with time. Observations of cloudiness arising in the cell zones have shown that the entire cycle from appearance of cells to complete dissipation usually occurs within 10-20 min. However, in certain cases the cells may be retained for hours without noticeable changes.

The theory of cellular convection was developed in works by a number of scientists, beginning with Rayleigh and H. Jeffries [Geoffries]. A detailed survey of the obtained results can, for example, be found in the article by B. N. Trubnikov (1967).

In the classical theory of cellular convection use is made of the system of equations of hydrothermodynamics of the atmosphere with consideration of the simplified theory of free convection; the essence of the latter lies in the assumption that air is incompressible and its density changes only due to changes in temperature. Considering, in addition, the speeds of convective motions to be small as compared with the basic unperturbed state, it is possible by using the complete system of equations of hydrothermodynamics of the atmosphere for a viscous medium to obtain an equation for determining vertical velocity:

$$\left(\frac{1}{Pr} \frac{\partial}{\partial t} - \nu \nabla^2\right) \left(\frac{\partial}{\partial t} - \nu \nabla^2\right) \cdot \nabla^2 w - Ra \nabla^2 w = 0. \quad (5.7)$$

where $Pr = \frac{\nu}{\kappa}$ is the Prandtl number (ν is turbulent viscosity of the air, κ is coefficient of temperature conductivity); $\nabla^2 = 1 \frac{\partial^2}{\partial x^2} + 1 \frac{\partial^2}{\partial y^2} + k \frac{\partial^2}{\partial z^2}$, $\nabla_1^2 = \nabla^2 - k \frac{\partial^2}{\partial z^2}$, $Ra = g \frac{(T_a - T)^0}{\nu T}$ is the Rayleigh number (γ_a and γ are the adiabatic and actual vertical temperature gradients).

Since (5.7) is a sixth order equation, six boundary conditions in altitude should be assigned for its solution. Considering that convection is developed in a layer with thickness h between two free surfaces, we assign these conditions in the form

$$\begin{aligned} w|_{z=0} = w|_{z=h} = \frac{\partial^2 w}{\partial z^2} \Big|_{z=0} = \frac{\partial^2 w}{\partial z^2} \Big|_{z=h} = \\ = \frac{\partial^4 w}{\partial z^4} \Big|_{z=0} = \frac{\partial^4 w}{\partial z^4} \Big|_{z=h} = 0. \end{aligned} \quad (5.8)$$

The relationships in (5.8), as is easily seen, follow from the fact that tangential viscous stresses are absent on the free surfaces.

With boundary conditions (5.8), equation (5.7) makes it possible to describe motion in cells of different shapes. As an example we will examine its solution for shells which have a rectilinear form in the plane. In this case

$$w = w_0 \sin\left(\frac{\pi x}{L_x}\right) \cos(\Omega_x x) \cos(\Omega_y y) \exp(nt), \quad (5.9)$$

where $\Omega_x = \frac{2\pi}{L_x}$, $\Omega_y = \frac{2\pi}{L_y}$ are the wave numbers along the axes ox and oy (L_x , L_y are the distances between cell centers) and w_0 is the speed at the center of the cell. Substituting (5.9) into (5.7), we obtain a quadratic equation for the eigenvalues of n :

$$n^2 + (Pr + 1)(a^2 + \pi^2)n + Pr \left[(a^2 + \pi^2)^2 - \frac{a^2 Ra}{a^2 + \pi^2} \right] = 0, \quad (5.10)$$

where

$$a^2 = \Omega_x^2 + \Omega_y^2.$$

It is known from the theory of hydrodynamic stability that the solution of (5.9) will be stable with respect to small oscillations if all eigenvalues have negative real parts. According to equation (5.10), the so-called boundary motion which corresponds to $n = 0$ and which separates regions of stable and unstable perturbations from one another is possible when

$$(a^2 + \pi^2)^2 = a^2 Ra. \quad (5.11)$$

When h , κ , ν and \bar{T} are fixed, equation (5.11) can be used for unique determination of the distance between the centers of cells and that minimum critical temperature gradient γ_{HP} whose achievement marks the breaking down of the flow into cells.

To find γ_{HP} from (5.11) we will use the fact that the boundary regime corresponds to the minimum value of Ra , i.e., to the condition $\frac{d(Ra)}{d(a^2)} = 0$, from which $Ra_{\text{HP}} = \frac{27}{4} \pi^4 \approx 657$. From this

$$(\gamma - \gamma_a)_{\text{HP}} = \frac{27}{4} \pi^4 \frac{\nu \bar{T}}{g h^4} \approx 657 \frac{\nu \bar{T}}{g h^4} \quad (5.12)$$

and, consequently, for cellular circulation to exist it is necessary that the following inequality be fulfilled:

$$\gamma - \gamma_a > 657 \frac{\nu \bar{T}}{g h^4}. \quad (5.12a)$$

If, for example, $\bar{T} = 250^\circ\text{K}$, $h = 100 \text{ m}$, $\nu = \kappa = 10^4 \text{ cm}^2/\text{s}$, then $\gamma - \gamma_a = 0.02 \text{ deg}/100 \text{ m}$.

Formulas (5.12) and (5.12a) were obtained on the assumption that Coriolis force does not influence the convection process. As indicated by L. S. Gandin (1947), Coriolis force increases stability; as a result the development of cellular circulation on the rotating earth requires a certain large vertical temperature gradient, which follows from equation (5.12a). Also, in this case horizontal dimensions of the cells are reduced.

When $Ra_{\mu p}$ is maintained stationary, each cell represents an isolated region with independent closed air circulation. However, as a result of linearization of the initial system of equations and the indeterminate nature of the connection between Ω_x and Ω_y , the classical theory of cellular convection does not permit unique determination of the form of the appearing cells or on the magnitude and sign of the vertical speed at their centers. Therefore these characteristics were determined by means of laboratory experiments. It was found that where the average speed of flow in the convection layer does not change with altitude or, which is the same thing in principle, is equal to zero in it, two types of cells are formed most frequently - hexagonal (top view) and round.

The horizontal distribution of w within cells of different forms was studied in detail by A. Pellew and R. Southwell (1940). It was found that in the framework of classical theory (without consideration of the effect of Coriolis force) hexagonal cells (the so-called Bénard) are characterized by the wavelength $\lambda = 3.77 h$, while for round cells $\lambda = 2.16 h$; here λ in the first case is the doubled length of the side of a regular hexagon, while in the second case it equals the diameter of a circle.

In Bénard cells

$$w = \frac{w_0}{3} \sin\left(\frac{\pi z}{h}\right) \left[2 \cos\left(\frac{2\pi}{\lambda\sqrt{3}} x\right) \cos\left(\frac{2\pi}{3\lambda} y\right) + \cos\left(\frac{4\pi}{3\lambda} y\right) \right], \quad (5.13)^1$$

while in circular (cylindrical) cells,

$$w = w_0 \sin\left(\frac{\pi z}{h}\right) J_0\left(\frac{\alpha\lambda}{2h}\right), \quad (5.14)$$

¹In formula (5.13) $n = 1$; this corresponds to the basic vibration tone which is excited at minimum $Ra_{\mu p}$. In this case a single convective layer arises; on its boundaries $w = 0$.

where J_0 is a zero-order Bessel function. We will note that if w is known, by expressing u and v through w in the initial system of equations it is possible to determine also the distribution of horizontal components of air velocity inside the cells.

Judging by data from observations of clouds forming in zones of cellular convection, horizontal dimensions of atmospheric cells usually comprise several kilometers¹, while the ratio λ/h comprises about three. Unique cellular clouds (Cu mammatus) can be observed on the lower surface of cumulonimbus clouds. They have an eroded [translation not verified - translator] form with a descending flow in the center of the cell.

Above we examined the characteristics of convection for the case when there is no wind in the convective layer or when its velocity and direction do not vary with altitude. Such a situation is rarely encountered in the atmospheric layers from $h \geq 500-1000$ m. The question of the influence of vertical shear on the development of convection has not as yet been finally resolved. Thus, L. S. Gandin (1947) showed² that if the direction of the wind and the convective layer remains unchanged (or changes little) but its velocity depends on altitude, two-dimensional cells will be formed (Fig. 5.8); these represent longitudinal bands of ascending and descending motions stretched out in the direction of the wind. They also indicate that if both the speed and direction of the wind change sharply in the convective layer, cellular circulation clearly cannot arise.

Ye. F. Vorob'yeva and B. N. Trubnikov (1967) studied the structure of cellular convection for the case when the wind vector can be broken down into two components in such a way that one of them does not change with altitude, while the vertical profile of the second has non-zero curvature ($u'' \neq 0$). Calculations show that in

¹Here we are not concerned with large-scale cellular convection whose elements (as is evident from photographs of the cloud cover from artificial earth satellites) have horizontal dimensions of several tens of kilometers.

²Gandin does not introduce strict proof of his conclusions, limiting himself to qualitative considerations.

this case two-dimensional cells extended along that wind component whose curvature differs from zero will be formed.

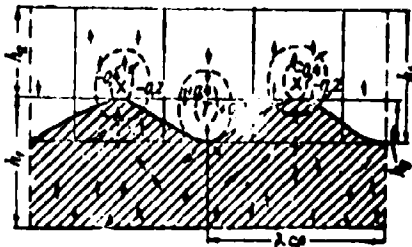


Fig. 5.8. Diagram of cellular circulation near the upper boundary of laminar clouds (per V. A. Zaytsev and A. A. Ledokhovich). h_1 - thickness of clouds; h_2 - thickness of the above-cloud layer in which cellular circulation is noticed (100-200 m); h_3 - thickness of cloud layer in which cellular circulation is noticed (50-100 m); h_4 - layer of air in which periodic oscillations of temperature along the horizontal are distinguished (150-300 m); T - heat; X - cold; wavelength $\lambda = 890$ m.

In conclusion we will pause briefly on the connection of cellular convection with turbulence. We can assume that during loss of stability by cells the energy of cellular circulation should serve as a source of turbulent energy. Since cellular circulation can be regarded as the result of the interference of several standing gravitational waves (Haman, 1962), in all probability the stability criteria developed for these waves (see Chapter 6) will be valid for such circulation in the first approximation. This means, in particular, that the shorter the waves, the less stable they will be.

From equation (5.11) it follows that during boundary motion the size of cells (a^2) is uniquely determined by Ra_{kp} . A different picture should be observed if $Ra > Ra_{kp}$ - i.e., $\gamma > \gamma_{kp}$. In this case the so-called supercritical regime appears; in this case two systems of cells correspond to each value of Ra . One of these has smaller λ than that found in the boundary regime (Zierep, 1959). It is evident that in this case transition from cellular circulation to small-scale turbulent pulsations is favored. This assumption requires experimental checking.

CHAPTER 6

WAVES AND ATMOSPHERIC TURBULENCE

Periodic motions, including in particular waves and cellular convection, are one of the most widespread forms of mesoscalar atmospheric motions. They are of considerable interest both in themselves and also in connection with the fact that their loss of stability leads to the appearance of turbulent eddy formations of all scales. Thus, frontal cyclones and anticyclones are connected with degradation of waves hundreds or even thousands of kilometers in length, while comparatively small eddies which cause, in particular, buffeting of aircraft, apparently arise due to the degradation of so-called short waves, whose length usually does not exceed a few kilometers and whose dynamics are not affected by the deflecting force of the earth's rotation.

If we ignore acoustic waves arising due to the compressibility of air, atmospheric short waves can be broken down into gravitational waves and gravitational-shear waves. The first arise under the action of gravity and develop due to the potential energy of the position of particles of the air, if the latter, for one reason or another, are removed from the equilibrium state. Gravitational-shear waves (the so-called Helmholtz waves) are also formed under the action of gravity, but appear when a tangential break in wind velocity is observed near the boundary surface, along with a sharp change (jumpwise at the boundary) in the density of the air¹.

¹Generally speaking, waves can arise also in the presence of a discontinuity in wind velocity alone (the so-called shear waves). However, as we will show below, they are unstable - i.e., they cannot be observed in the stationary state.

The most widespread type of gravitational waves are waves formed during flow over mountains - the so-called mountain or obstacle waves. In the free atmosphere a discontinuity in density is observed most frequently in zones where there is a simultaneous sharp change in wind velocity; for example, this is typical for atmospheric fronts, the tropopause layer, above-cloud inversions, etc. Therefore it is not gravitational waves, but gravitational-shear waves which arise most frequently under these conditions; we will pause first of all on the description of gravitational-shear waves.

§ 1. GRAVITATIONAL-SHEAR WAVES

a. Principal Characteristics of Stationary Waves

We will pause first on the connection between the principal characteristics of stationary waves (their length λ , phase velocity c , and amplitude A) and discontinuities in the temperature or density of the atmosphere; we will also consider the discontinuity in wind velocity near the boundary surface. In this case we will limit ourselves to examination of internal waves, since waves on a free surface are not typical for the atmosphere.

The most substantial results of studies of gravitational-shear waves are found in the works by D. L. Laykhtman (1947), B. Haurwitz (1951), L. S. Gandin (1957, 1958) and K. Naito (1966). In all these works it is assumed that waves develop as a result of the imposition of small wave perturbations on a basic horizontal flow of an ideal fluid. Since only short waves were examined, the deflecting force of the earth's rotation was not considered during compilation of the equations of motion.¹ In addition, the process was considered to be adiabatic.

¹In particular, such an assumption means that the boundary should be horizontal in the unperturbed state.

If we assume that the basic motion is stationary and, in addition, its characteristics do not depend on the horizontal coordinates but vary only with altitude z , the equations of small oscillations can be written in the form

$$\begin{aligned}
 \frac{\partial u'}{\partial t} + \bar{u} \frac{\partial u'}{\partial x} + \bar{v} \frac{\partial u'}{\partial y} + \bar{w} \frac{\partial u'}{\partial z} &= -\frac{1}{\rho} \frac{\partial p'}{\partial x}, \\
 \frac{\partial v'}{\partial t} + \bar{u} \frac{\partial v'}{\partial x} + \bar{v} \frac{\partial v'}{\partial y} + \bar{w} \frac{\partial v'}{\partial z} &= -\frac{1}{\rho} \frac{\partial p'}{\partial y}, \\
 \frac{\partial w'}{\partial t} + \bar{u} \frac{\partial w'}{\partial x} + \bar{v} \frac{\partial w'}{\partial y} + \bar{w} \frac{\partial w'}{\partial z} &= -\frac{1}{\rho} \frac{\partial p'}{\partial z} - \frac{g}{\rho} \rho', \\
 \frac{\partial \rho'}{\partial t} + \bar{u} \frac{\partial \rho'}{\partial x} + \bar{v} \frac{\partial \rho'}{\partial y} + \bar{w} \frac{\partial \rho'}{\partial z} + \bar{\rho} \left(\frac{\partial u'}{\partial x} + \frac{\partial v'}{\partial y} + \frac{\partial w'}{\partial z} \right) &= 0, \\
 \frac{\partial p'}{\partial t} + \bar{u} \frac{\partial p'}{\partial x} + \bar{v} \frac{\partial p'}{\partial y} + \bar{w} \frac{\partial p'}{\partial z} &= -\kappa \frac{\partial p'}{\partial t} - \bar{p} \left(\frac{\partial u'}{\partial x} + \frac{\partial v'}{\partial y} + \frac{\partial w'}{\partial z} \right) = 0.
 \end{aligned} \tag{6.1}$$

The first three equations of system (6.1) were obtained from the equations of motion, while the fourth and fifth were derived from the equations of continuity and the equations of the inflow of heat, respectively. Here u , v , and w are velocity components; t is time; ρ is air density; p is pressure; $\kappa = c_p/c_v$ is the ratio of heat capacities; and g is the acceleration of gravity. Lines above the symbols designate characteristics of the principal motion, while the prime signs indicate characteristics of small perturbations. System (6.1) consists of linear equations with respect to unknowns (u' , v' , w' , etc.).

The following boundary conditions are normally used during the solution of system (6.1). First of all it is assumed that the components of velocity along the normal to the boundary surface are identical on both sides of the latter - i.e., there is no mixing here. Secondly, on the boundary surface the pressure is assumed to be continuous. Besides this, all functions should be limited at infinity.

D. L. Laykhtman (1947) defined the characteristics of plane waves for the case when the basic flow on both sides of the boundary

surface is directed along the axis ox , while the potential temperature θ varies linearly with altitude. On the boundary surface $z = 0$ wind velocity, temperature, and the potential temperature gradient all undergo discontinuity.

The characteristics of the waves were sought in the form

$$\begin{aligned}
 u' &= u_1(z) \sin 2\pi \left(\frac{t}{\tau} - \frac{x}{\lambda} \right), \\
 w' &= w_1(z) \cos 2\pi \left(\frac{t}{\tau} - \frac{x}{\lambda} \right), \\
 p' &= p_1(z) \sin 2\pi \left(\frac{t}{\tau} - \frac{x}{\lambda} \right), \\
 \rho' &= \rho_1(z) \sin 2\pi \left(\frac{t}{\tau} - \frac{x}{\lambda} \right), \\
 f' &= A \sin 2\pi \left(\frac{t}{\tau} - \frac{x}{\lambda} \right).
 \end{aligned} \tag{6.2}$$

where τ is the period; λ is wavelength; A is oscillation amplitude.

By substituting (6.2) into the system (6.1) and by ignoring infinitesimal quantities of higher order, it is possible to obtain an ordinary differential equation for momentum $\tilde{w} = \bar{\rho} w_1$:

$$\frac{d^2 \tilde{w}}{dz^2} + \beta \frac{d\tilde{w}}{dz} + \tilde{w} \left[-\Omega^2 + \frac{\kappa^2}{(c-u)^2} \right] = 0, \tag{6.3}$$

where $\beta = \frac{d \lg \theta}{dz}$; $\Omega = \frac{2\pi}{\lambda}$ is the wave number; $c = \frac{\lambda}{\tau}$ is the phase velocity.

Using the boundary conditions, from (6.3) it can be found that

$$\begin{aligned}
 \tilde{w}_n(z) &= A \exp \left\{ \left[-\frac{\beta_n}{2} + \sqrt{\frac{\beta_n^2}{4} + \Omega^2 - \frac{\kappa_n^2}{(c-u_n)^2}} \right] z \right\} \times \\
 &\quad \times \Omega \bar{\rho}_n(0) (c - u_n), \\
 \tilde{w}_s(z) &= A \exp \left\{ \left[-\frac{\beta_s}{2} - \sqrt{\frac{\beta_s^2}{4} + \Omega^2 - \frac{\kappa_s^2}{(c-u_s)^2}} \right] z \right\} \times \\
 &\quad \times \Omega \bar{\rho}_s(0) (c - u_s),
 \end{aligned} \tag{6.4}$$

where the subscripts "n" and "s" relate to layers located below and above the boundary surface. The connection between c and Ω is

determined by the dispersion equation

$$\begin{aligned} & \bar{\rho}_n(0)(c-u_n)^2 \left[\frac{3}{2} + \sqrt{\frac{k_n^2}{4} + \Omega^2 - \frac{k_n^2 u_n}{(c-u_n)^2}} \right] - \\ & - \bar{\rho}_s(0)(c-u_s)^2 \left[\frac{3}{2} - \sqrt{\frac{k_n^2}{4} + \Omega^2 - \frac{k_n^2 u_s}{(c-u_s)^2}} \right] = \\ & = K [\bar{\rho}_n(0) - \bar{\rho}_s(0)]. \end{aligned} \quad (6.5)$$

From equations (6.4) and (6.5) it is clear that vertical velocities at the boundary surface, the phase velocity of wave propagation, and wavelength depend, other conditions being equal, on the velocity of the flow and the density of the air on both sides of the boundary surface and also on the stability of stratification of the atmosphere.

In the particular case¹ when $\beta_H = \beta_B = 0$, i.e., when the atmosphere is stratified indifferently on both sides of the boundary surface, from (6.5) it follows that

$$\bar{w}_p(z) = A \Omega \bar{\rho}_n(0) (c - u_n) e^{-\Omega z}, \quad (6.6)$$

$$\bar{w}_s(z) = -A \Omega \bar{\rho}_s(0) (c - u_s) e^{-\Omega z}, \quad (6.6)$$

and

$$\begin{aligned} c &= \frac{\bar{\rho}_n(0) u_n + \bar{\rho}_s(0) u_s}{\bar{\rho}_n(0) + \bar{\rho}_s(0)} \pm \\ &= \sqrt{\frac{K}{\Omega} \frac{\bar{\rho}_n(0) - \bar{\rho}_s(0)}{\bar{\rho}_n(0) + \bar{\rho}_s(0)} - \frac{\bar{\rho}_n(0) \bar{\rho}_s(0) (u_n - u_s)^2}{[\bar{\rho}_n(0) + \bar{\rho}_s(0)]^2}}. \end{aligned} \quad (6.7)$$

According to formula (6.6), the vertical velocities connected with waves diminish exponentially with distance from the boundary surface.

In formula (6.7), which determines the magnitude of phase velocity, the first term equals the weighted mean flow velocity as a whole, while the second describes the way in which the magnitudes of

¹In the more general case when $\beta_H = \beta_B = \beta \neq 0$, equation (6.5) can be solved with respect to c by making use of the fact that $3/\Omega \ll 1$.

air-density and wind-velocity discontinuities influence the value of c during transition through the boundary surface. It is clear that the phase velocity is increased with a decrease in Ω - i.e., with a growth in wavelength λ . It is not difficult to demonstrate that at λ not exceeding a few kilometers the phase velocity will not be more than a few meters per second.

It is obvious that at a certain ratio of Ω and the discontinuities in density and velocity ($\Delta\rho$ and Δu) the expression under the radical sign will become negative on the boundary surface; this means that c is a complex quantity. In this case motion becomes unstable and the waves will degenerate. Below we will pause to consider the stability of waves in greater detail.

If $c = 0$, i.e., if we examine standing waves, then as is evident from the formulas in (6.2) a succession of zones of ascending and descending flows is observed along the boundary surface; the arrangement of these zones does not change with time. If $\beta_H = \beta_G = \beta$, then the length of such waves will be

$$\lambda_{\text{cr}} = \frac{2\pi(\Delta u)^2}{g} \frac{T_0}{\sqrt{4(\Delta T)^2 + \frac{(\Delta u)^2 \Delta T_0^2}{g^2} \left[1 - \frac{1}{4} \beta (\Delta u)^2 \right]}} \quad (6.8)$$

Here $\Delta u = u_0 - u_n$, $\Delta T = T_n - T_0$, T_0 is the temperature on the boundary surface, while

$$\beta = \frac{d \ln \theta}{dz} = \frac{2T_0 - T_n}{T_0 + T_n}$$

From formula (6.8) it is clear that wavelength grows with an increase in wind discontinuity Δu and with a decrease in the temperature discontinuity ΔT . Besides this, since $\beta (\Delta u)^2 \ll g$ ($\beta \approx 1.3 \cdot 10^{-3} \text{ 1/m}$, $\Delta u \approx 1 \text{ m/s}$), an increase in thermal stability leads to a reduction in λ_{cr} . Under real conditions λ_{cr} can vary from hundreds of meters to several kilometers.

K. Naito (1966) calculated the phase velocity and amplitudes of plane gravitational-shear waves for two- and three-layer models of the atmosphere under the assumption that the density of the air and the wind velocity remained unchanged inside each of these layers. The assumption that the density of air in one or another layer is independent of altitude - i.e., the condition of quasi-incompressibility of the air - is a very rough one and, thus, the Naito models are less satisfactory than the Laykhtman setup examined above. However, if the layers are not very thick the quantitative results of calculations from the quasi-incompressible model will not contain substantial errors, while the simplicity of calculations represents a definite advantage. Figure 6.2 shows the results of calculation of phase velocities (c) and periods (τ) by a three-layer model (Fig. 6.1), while Fig. 6.3 shows the amplitudes of gravitational-shear waves for λ_1 equal to 100, 500, 1000 and 5000 m. The results of calculations of amplitude are given individually for the horizontal and vertical components of perturbations. Four profiles u' and w' are given for each of the values of λ_1 , in accordance with the four values of phase velocities (see Fig. 6.2). The amplitudes are given in conditional units. In the case $\lambda = 100$ m the scale is increased. The degree of increase is shown on the figures. The wavy arrows intersecting the vertical axis show the zones where the sign of the perturbations changed sharply.

From Fig. 6.3 it is clear that the amplitudes of perturbations are maximum at the boundary surface; the smaller λ , the more rapidly they diminish with distance from the surface. Despite the fact that the height of the lower boundary surface H_1 comprises a total of 170 m, at $\lambda = 100$ m perturbations do not reach the surface of the earth, while at $\lambda = 500$ m they do not reach it at all values of phase velocities. Thus, the results of the Naito calculations explain the fact (known from observations) that short gravitational-shear waves are rarely observed close to the ground surface.

At small λ in a narrow zone adjacent to the boundary surface the intersection of the latter is accompanied by a change in the sign of u' with an unchanging direction w' (Fig. 6.3). Analysis of

the equations describing gravitational-shear waves for the three-layer model show that generally speaking u_2^j is 90° ahead of w_2^j in phase, w_2^j and w_3^j have identical phases, and u_3^j lags 90° behind w_2^j .

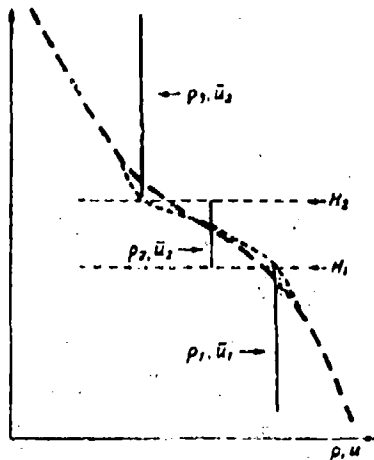


Fig. 6.1. Diagram of the three-layer model of the wave zone.

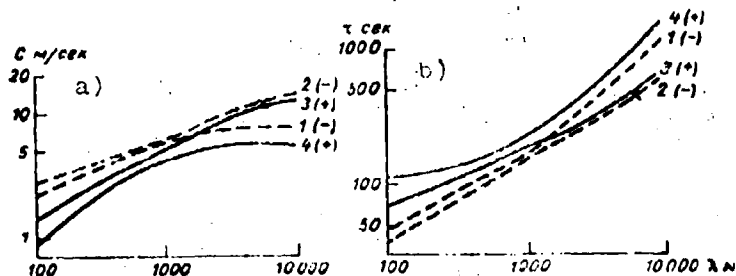


Fig. 6.2. Example of calculation (per Naito) of phase velocities (a) and periods (b) of internal gravitational waves. Experimental data from Gossard and Munk are indicated by a cross.

Designations: $m/sec = m/s$; $sec = s$.

The above shows that orderly circulation develops at the boundary surface, as depicted on Fig. 5.4. The close circulation cells should move in a horizontal direction together with the flow existing in the boundary surface zone.

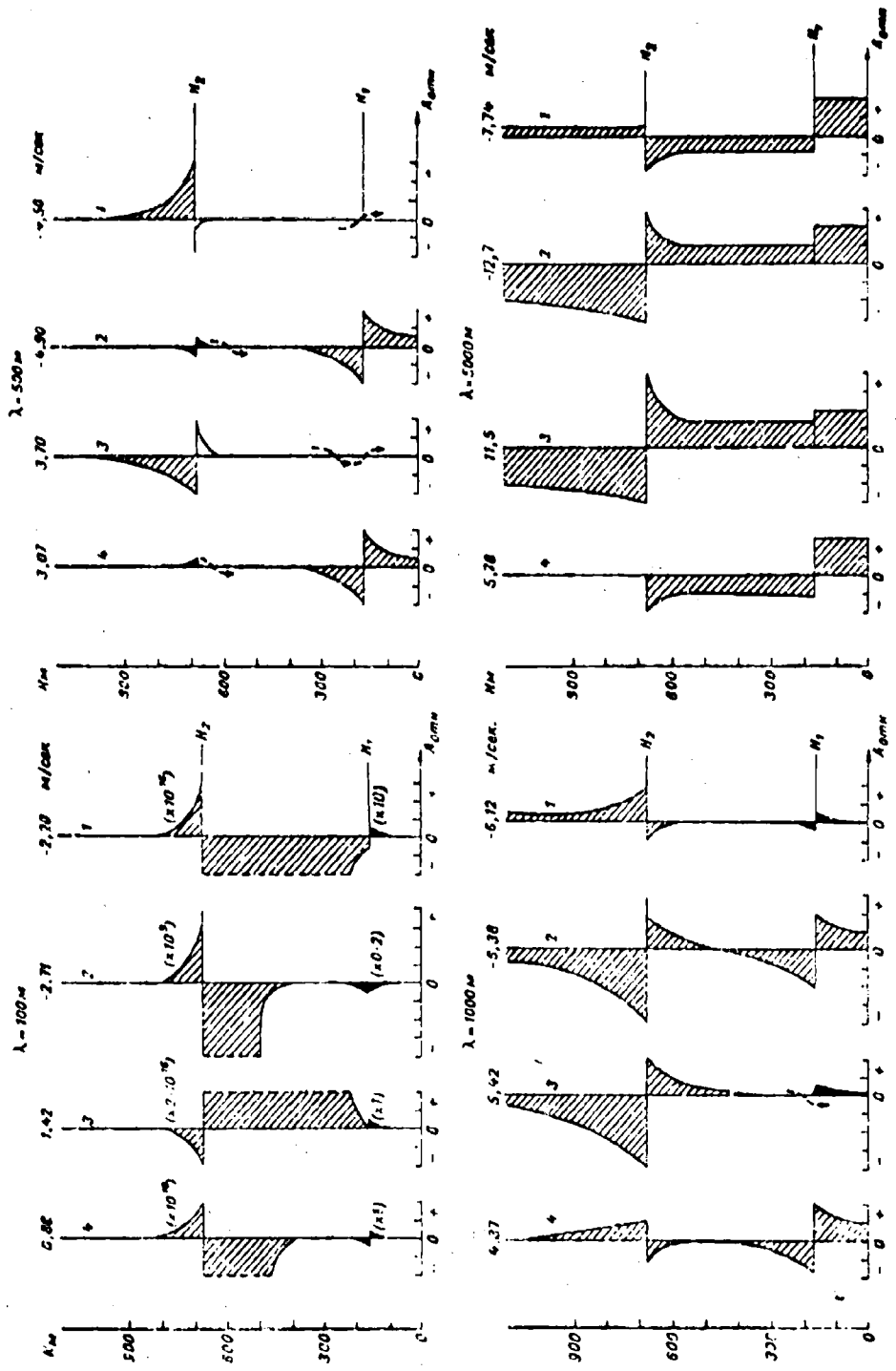


Fig. 6.3a. Vertical profiles of amplitudes of waves for the horizontal component of velocity (per Naut).

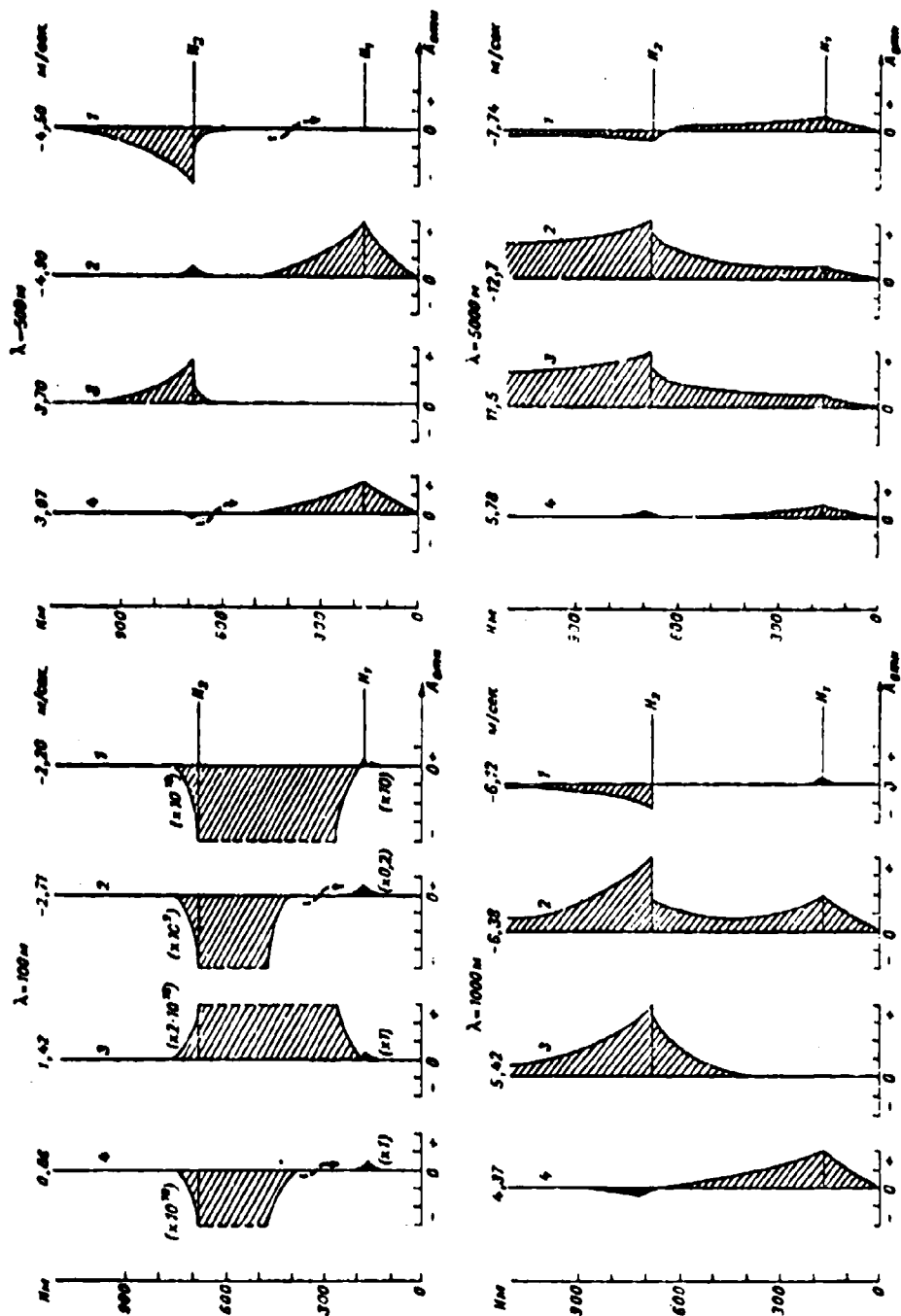


Fig. 6.3b. Vertical profiles of amplitudes for the vertical component of velocity (per Naito).

Designations: $m/sec = m/s$; $A_{0rel} = A_{rel}$.



Fig. 6.3. Diagram of air circulation in water at the boundary surface.

KEY: (1) Boundary surface.

Table 6.1 gives data on the amplitudes of oscillations of both boundary surfaces for this model with the following values of input parameters: $H_1 = 170$ m, $H_2 = 670$ m, $\bar{u}_1 = -1.2$ m/s, $\rho_1 = 3.30$, $\bar{u}_2 = -1.25$ m/s, $\rho_2 = 3.39$, $\bar{u}_3 = -1.30$ m/s, $\rho_3 = 3.28^1$.

Table 6.1. Amplitudes of oscillations of the boundary surface.

(1) Длина волны λ м	(2) Фазовая скорость c м/сек.	(3) Период T сек.	(4) Амплитуда		Отношение амплитуды (5) к длине волны	
			(6) поверхность			
			7 нижняя	8 верхняя	9 нижняя	10 верхняя
100	-1,71	59,5	31,1	27,3	0,31	0,27
500	-2,30	217	69,8	60,5	0,14	0,12
1000	-2,66	376	75,9	77,4	0,076	0,077
5000	-3,05	1610	90,5	69,4	0,018	0,014

Remark. The amplitude of the horizontal perturbation of wind velocity u' is assumed to equal 1 m/s in the calculation. When u' is doubled, the amplitude of oscillations of the boundary surface is also doubled.

KEY: (1) Wavelength λ , m; (2) Phase velocity c , m/s; (3) Period T , s; (4) Amplitude; (5) Ratio of amplitude to wavelength; (6) surface; (7) lower; (8) upper; (9) lower; (10) upper

From Table 6.1 it is clear that the shorter the wave the greater the magnitude of the ratio of wave amplitude to λ ; this ratio also grows with an increase in u' . At small λ the great steepness of the wave front is noticeable. Thus, when $\lambda = 100$ m and $u' = 1$ m/s the transition from the peak to the trough of the wave occurs at a distance of 50 m ($\lambda/2$) in approximately 30 s ($T/2$) and is accompanied

¹Density values are given in relative units.

by an altitude drop of 60 m (peak-to-peak). Naturally, at large u' the wave-front steepness will be still greater. Thanks to this, even in those cases when c is real and, thus, the waves are, as it were, stable, the wave peaks have a tendency to periodic reversal (like ocean waves) and to the formation of isolated upswelling with a horizontal axis, carried along by the common flow. When c is real the latter remains laminar. Naturally, the described process should be observed frequently in those atmospheric layers where the "background" turbulence is depressed.

In the models examined above plane waves were studied, while the authors ignored perturbations along the oy -axis. Therefore the peaks of waves are arranged perpendicular to the direction of the general transfer (transverse waves). However, observations showed that bands of clouds caused by ascending motions in the peaks of waves are most frequently oriented at a sharp angle to the wind or are even arranged parallel to it. Naturally, in order to explain the indicated empirical data an effort was made to solve the spatial and not the plane problem. In this case the perturbations in the wind field are given in the form

$$u_i = \bar{u}_i \exp i(\Omega_x x + \Omega_y y - m t), \quad (6.9)$$

where u_i' is the i -component of the perturbation of the flow velocities; Ω_x , Ω_y and m are constants, with $\Omega_x = \frac{2\pi}{L_x}$, $\Omega_y = \frac{2\pi}{L_y}$, where L_x and L_y are the scales of length in the direction of the axes ox and oy .

Studies of three-dimensional waves were made in the works of Z. Sekera (1948), K. Doi (1962), N. F. Vel'tishchev (1965), and others. According to Sekera, if a thin transition layer, within which the wind speed varies continuously, is studied instead of the boundary surface, from system (6.1) one can, by using (6.9), determine the necessary conditions for the existence of waves if only in each of the layers the vertical wind shear does not vary with altitude.

This requires that

$$2\bar{F}(U_2)^2 \left[R \left(1 + \frac{U_2^2}{U_1^2} \right) \right]^{-1} \leq 1 - \gamma_a. \quad (6.10)$$

where $U_1' = \frac{\partial U}{\partial z}$ is the vertical gradient (shear) of the wind. Thus, close to the level where wind velocity equals the speed of the wave¹ it is necessary that stratification of the atmosphere be at least different. This conclusion is in agreement with empirical data given by D. Brunt (1937) and S. Mal (1939); according to these data everytime bands of clouds parallel to the wind were observed - i.e., when there were waves in the atmosphere directly under an inversion layer - γ was greater than γ_a .

We will note also that according to formula (6.10) the spatial arrangement of the waves at given γ is determined by the quantity U_2' . It is clear that the formation of transverse waves requires the presence of small wind shears, while the formation of longitudinal waves requires large ones.

The upper limit of the value $\gamma_a - \gamma$ should give, in formula (6.10), the conditions under which orderliness of circulation disappears and spontaneous development of turbulence sets in. It should be noted that apparently the range of values of $\gamma_a - \gamma$ lying between the lower and upper limit is not great and therefore insignificant changes in the external parameters (e.g. U_2' or T) and lead to destruction of orderly circulation. This, in particular, probably explains the relative rarity of undulate clouds and their short lifetime.

Following Sekera, a theoretical evaluation of the influence of temperature and wind stratification of the atmosphere on the orientation of waves was carried out by K. Bel (1962), H. P. Vol'tishchev

¹Formula (6.10) was derived by Sekera on this assumption.

(1965), and others. According to Vel'tishchev, waves form the angle $\Delta\varphi = \varphi_1 - \varphi_2$ with the wind, where $\varphi_1 = -\arctg \frac{L_y}{L_x}$ is the angle between the direction of the isoline of equal phases in the wave (for example wave peaks) and the ox-axis, while φ_2 is the angle formed by wind direction with the ox-axis:

$$\varphi_2 = \arctg \left\{ \frac{-2C \frac{L_x}{L_y} - R^2 \left(\frac{L_x}{L_y} \right)^2}{2 \left[D^2 \left(1 + \frac{L_x^2}{L_y^2} \right) + R^2 \frac{L_x}{L_y} + C \left(\frac{L_x}{L_y} \right)^2 \right]} \pm \frac{\left[1 + \left(\frac{L_x}{L_y} \right)^2 \sqrt{R^2 - 4D^2(C + D^2)} \right]}{2 \left[D^2 \left(1 + \frac{L_x^2}{L_y^2} \right) + R^2 \frac{L_x}{L_y} + C \left(\frac{L_x}{L_y} \right)^2 \right]} \right\}, \quad (6.11)$$

where $D^2 = \frac{g}{T} \frac{y_0 - y}{U^2}$ is the Dorodnitsyn parameter (see § 3),

$$R^2 = \frac{2}{U} \frac{d\bar{u}}{dz} \frac{d\varphi}{dz} + \frac{d^2\varphi}{dz^2},$$

$$C = \left(\frac{d\varphi}{dz} \right)^2 - \frac{1}{U} \frac{d^2u}{dz^2} - \frac{1}{2T} \frac{dT}{dz^2} - \frac{4h^2}{(L_x L_y)^2} (L_x^2 + L_y^2) - \frac{h^2}{h^2}$$

(here h is the thickness of the layer within which waves are formed).

Thus, the mutual orientation of the wave and the wind depends on the temperature T , wind velocity u , the gradients of T and U , the curvature of their vertical profiles $\frac{d^2T}{dz^2}$, $\frac{d^2U}{dz^2}$, and the nature of the change in wind direction with altitude $\left(\frac{d\varphi}{dz}, \frac{d^2\varphi}{dz^2} \right)$.

Analysis of formula (6.11) showed that the direction of waves depends to the greatest degree on $\frac{dT}{dz}$, U , $\frac{d\varphi}{dz}$ and $\frac{d^2\varphi}{dz^2}$, while the role of wind velocity shear dU/dz is somewhat smaller. We will note that this conclusion of Vel'tishchev differs from the results of the works by Sekera and Doi, who ascribe a determining role in wave orientation to wind shear.

The most favorable conditions for the development of waves arise during stratification which is close to adiabatic. If, in addition,

$\frac{d\psi}{dz} = \frac{d^2\psi}{dz^2} = 0$, then $\Delta\phi \rightarrow 0$ - i.e., waves are oriented along the flow.

b. Empirical Data on Gravitational-Shear Waves in the Atmosphere

Owing to the fact that the study of waves in clear air, when there are no visible signs of their existence, is extremely difficult, the amount of such materials is, as yet, very small.

E. Gossard and W. Munk (1954) carried out instrument investigations of parameters of gravitational-shear waves in clear air on the California coast for seven cases of their existence. For this purpose they utilized synchronous recordings of high-sensitivity ground microbarographs, barovariographs, and anemographographs, installed along the shoreline. During analysis of the data materials from vertical temperature wind soundings were also used. Fig. 6.5 shows an example of recording of wind and atmospheric pressure fluctuations connected with the presence of waves.

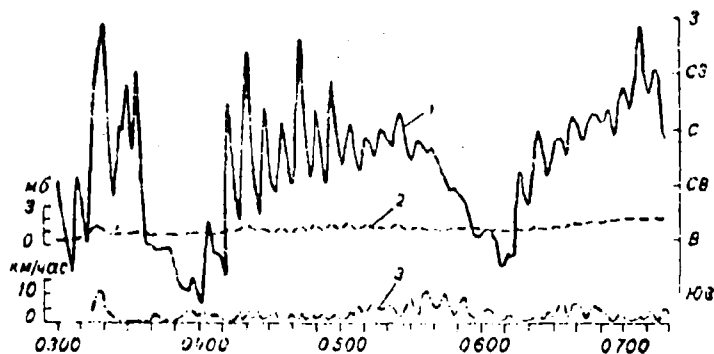


Fig. 6.5. Changes in atmospheric pressure and in wind direction and speed in the presence of gravitational waves on 14 October 1952 (per Gossard and Munk). 1 - wind direction; 2 - pressure; 3 - wind speed.

Designations: 00 = mb; km/h = km/h; J = W; 03 = NW; 0 = N; 03 = NE; 0 = E; 00 = SE.

In a period when waves were observed an inversion layer was located above the observation region and the wind speed was comparatively small. Data on parameters of waves and also on the characteristics of the inversion layer are given in Table 6.2. The azimuth of the point from which the waves moved was taken as the direction of wave displacement.

Table 6.2. Parameters of waves observed in the period April 1952 to May 1963 above the California coast.

	4 IV	27 VII	4 VIII	4 IX	2 X	16 X	16 X	12 V
Погода (1)	(2) Туман	(3) Ясно	(2) Туман	(3) Ясно	(2) Туман	(2) Туман	(2) Туман	(3) Ясно
Скорость ветра, м/сек. (4)	1,4	0,0	2,9	2,2	1,2	0,8	0,9	0,7
Направление ветра (5)	ССЗ	СВ	З	С	ЗЮЗ	ССВ	СЗ	ВСВ
Амплитуда пульсаций (6)								
(7) ветра, м/сек. (град.)	1,0 (200°)	1,3 (78°)	1,2 (175°)	0,5 (318°)	3,2 (240°)	1,4 (268°)	0,9 (282°)	1,6 (280°)
(8) давления, мб	0,14	0,18	0,18	0,07	0,43	0,20	0,13	0,13
Период колебаний, мин. (9)	14,0	7,5	6,5	5,5	8,8	7,5	7,5	11,0
Частота, 1/сек. (10)	0,0075	0,014	0,016	0,019	0,012	0,014	0,014	0,0096
Высота инверсии, м (11)								
нижняя граница (12)	170	170	300	260	210	180	180	100
верхняя граница (13)	600	670	1190	740	1000	670	670	400
Изменение потенциальной температуры в инверсии, °C (14)	15,0	14,0	20,0	10,5	11,5	17,5	17,5	6,0

Remark. On 16 October 1952 waves were recorded twice.

KEY: (1) Weather; (2) Fog; (3) Clear; (4) Wind speed, m/s; (5) Wind direction; (6) Amplitude of pulsations; (7) of wind, m/s (deg.); (8) pressure, mb; (9) Period of oscillations, min; (10) Frequency, 1/s; (11) Height of inversion, m; (12) lower boundary; (13) upper boundary; (14) Change in potential temperature in inversion, °C.

Designations: CCЗ = NNW; СВ = NE; З = W; С = N; ЗЮЗ = WSW; ССВ = NNE; СЗ = NW; ВСВ = ENE.

Analysis of the experimental data showed that the phase velocities of waves were close to 10 m/s - i.e., they significantly exceeded the wind speed. It is characteristic that the magnitude of wind pulsations caused by the waves was also very substantial, especially on 27 July, 2 and 16 October, and 12 May. Wavelengths varied from

4 to 10 km, with the wave peaks being oriented approximately perpendicular to the wind shear vector.

We will note that the quantities c_1 and λ_1 obtained in the studies by Gossard and Munk are in good agreement with the data calculated by Naito for the three-layer model at input parameter values taken from Table 6.2.

W. Georgii (1959) used balloons to study vertical motions in gravitational-shear waves forming close to inversion layers in the lower half of the troposphere. According to his data, ordinarily $\lambda = 500$ m, $w_{\max} = \pm 1-2$ m/s in such waves. I. V. Vasil'chenko and A. A. Ledekhovich (1962) detected periodic pulsations of temperature with $\lambda = 1.0-1.2$ km and with temperature oscillations up to 1.2° from data on the horizontal distribution of air temperature above an inversion layer at an altitude of 500 m.

Studies of waves in clear air have also been carried out by tracking the transfer and deformation of streams of smoke emitted into the atmosphere by pocket tracers or by other means. Such experiments were carried out by H. Lottler and B. Davidson (1957), T. H. Cooke (1962), K. Hahn (1963), and by others. We will present the data obtained by T. Cooke as an example. In his experiment it was found that although the vertical stream of smoke was displaced as a whole at the average wind speed, individual portions of it moved more rapidly or more slowly than the wind (Fig. 6.6). The picture shown on Fig. 6.6 may be considered with the presence of large turbulent eddies in the examined layer of the atmosphere; however, analysis of the obtained experimental data showed that it was far more probable that it was conditioned by quasi-stationary short waves.

The largest quantity of empirical data was obtained for those cases when clouds were observed in the peaks of the waves. Especially large quantities of such materials have been accumulated by observations from aircraft (Malkin and Nichl, 1964; Fashov, 1964; Borovikov and Nazin, 1967; Pakhomov, 1967, and others), and also from photographs

taken from artificial meteorological earth satellites. It should, however, be mentioned that due to inadequate resolution (see, for example, Kondrat'yev et al., 1966) satellite photographs provide data mainly on comparatively long waves with λ of several kilometers.

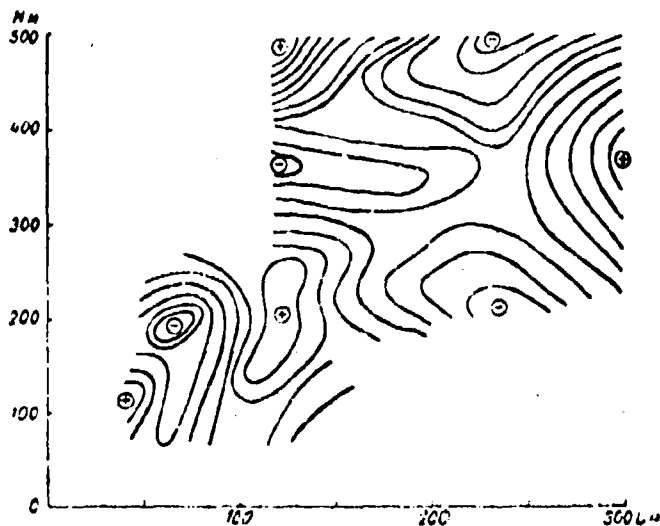


Fig. 6.6. Isolines of wind velocity deviations $\Delta u = u - u_{\infty}$ in a zone of waves (per Cooke).

Statistical processing of the photographs of cloudy skies from the "Tiros" satellites and analysis of the obtained data carried out by Vel'tishchev showed that geometrically correct structural cloud formations are observed in approximately 15% of the cases, while cloud strips (waves) are observed in 13% of the cases. As a rule, cumulus-type clouds have a band structure. The direction of the bands most frequently coincides with the wind direction in the lowest layer, but with an increase in altitude the wind rotates to the right with respect to the strips. In the 1-2 km layer the wind usually is deflected from the direction of the strips by $\pm 10^{\circ}$. Generally, empirical data agree with the theoretical predictions. Thus, with longitudinal strips of cloud the most frequent observation is of temperature gradients on the order of 0.7-0.8 deg/100 m - i.e., virtually adiabatic - while wind speed is greater than that with a chaotic distribution of clouds. Besides this, in the majority of cases the direction of the wind does not change with altitude.

Data closely resembling those presented above are given in the works of other authors. Thus, on the basis of analysis of radar data on precipitations from Cb clouds above Japan, K. Doi (1962) arrived at the conclusion that bands of precipitation - which means also clouds - are clearly distinguishable in 84% of the cases with vertical wind shears $U''_z > 3$ m/s at 1 km and in 55% of the cases when $U''_z \geq 7$ m/s at 1 km. On the other hand, the majority of cases of absence of bands were recorded during days when $U''_z \leq 3$ m/s at 1 km in the zone of clouds. In this case bands of precipitation are usually extended parallel to the wind when the wind rotates weakly with altitude. Experimental data also showed that if the vertical wind velocity shear is small the bands of clouds are arranged perpendicular to the wind.

§ 2. CRITERIA OF THE STABILITY OF INTERNAL GRAVITATIONAL-SHEAR WAVES AND THE CONNECTION OF TURBULENCE WITH DEGENERATING WAVES

As is evident, for example, from formulas (6.7) and (6.8), at certain values of ΔT , ΔB and β the expression under the radical sign becomes negative - i.e., σ is a complex quantity. Then the size of perturbations grows without limit in time - stable motion disappears. For example, in the particular case when $\beta''_z = \beta'_z = \beta \neq 0$, all waves for which the length $\lambda < \lambda_{\text{crit}}$ are unstable, where

$$\lambda_{\text{crit}} = \frac{2\pi (\Delta T)^2 \bar{T}}{g \Delta T + \sqrt{(g \Delta T)^2 + \frac{c^2 \bar{T}^2 (\Delta T)^2}{8}}} \quad (6.12)$$

From formula (6.12) it is clear that the region of instability is the broader (i.e., λ_{crit} is the greater), the greater ΔB and the smaller ΔT .

A detailed investigation of the stability of waves was carried out by L. S. Gandin (1957, 1958). For the evaluation of wave stability he proposed the dimensionless parameter σ , determined by the formula

$$\Gamma = \frac{\gamma^2}{g} \bar{\beta} \left(\frac{\Delta T}{\Delta T} \right)^2. \quad (6.13)$$

This parameter describes the influence of static stability of the atmosphere on the dynamic stability of flows at the boundary surface. The critical wavelength λ_{00} is expressed through Γ as follows:

$$\lambda_{0p} = \frac{\lambda_0}{\sqrt{1+\Gamma}}. \quad (6.14)$$

where

$$\lambda_0 = \frac{\pi T}{g} \left(\frac{\Delta T}{\Delta T} \right)^2. \quad (6.15)$$

As is evident from formula (6.12), λ_0 is the critical wavelength for the case of indifferent stratification ($\bar{\beta} = 0$).

From equality (6.14) it follows that with a growth in Γ the critical wavelength is reduced - i.e., the zone of instability is compressed. Since $\Gamma > 0$ corresponds to $\bar{\beta} > 0$, with an increase in static stability the dynamic stability will also grow. When $\Gamma \leq -1$ absolute dynamic instability occurs - i.e., instability of perturbations of all wavelengths. The same thing is observed when $\Delta T \leq 0$.

L. S. Gandin also studied the dependence of wave stability on the direction of propagation. For approximate evaluation of such a relationship, he examined a two-layer model in which air density ρ_u and ρ_n and the horizontal velocity components u_u, v_u and u_n, v_n are constant in each of the layers.

We will set $u_u = \omega_u \cos \varphi_u$, $u_n = \omega_n \cos \varphi_n$, $v_u = \omega_u \sin \varphi_u$, $v_n = \omega_n \sin \varphi_n$, where φ_u and φ_n are the angles between the wind and the ox-axis in each of the layers.

In the considered case the phase velocity is

$$c_{ph} = \frac{\rho_u \omega_u \cos(\varphi_u - \alpha) + \rho_n \omega_n \cos(\varphi_n - \alpha)}{\rho_u + \rho_n} \pm \sqrt{\frac{g \lambda}{2\pi} \frac{\rho_u - \rho_n}{\rho_u + \rho_n} - \frac{F_1 F_n}{(\rho_u + \rho_n)^2} - [\omega_u \cos(\varphi_u - \alpha) - \omega_n \cos(\varphi_n - \alpha)]^2}. \quad (6.16)$$

where α is the angle between the ox-axis and the direction of wave propagation.

From formula (6.16) it is clear that

$$\lambda_{np} = -\frac{2\omega_n \omega_p}{\omega_n^2 - \omega_p^2} [\omega_n \cos(\varphi_n - \alpha) - \omega_p \cos(\varphi_p - \alpha)]^2, \quad (6.17)$$

i.e., the stability of a wave of given length depends on the direction of its propagation. If ξ is the angle of deflection of direction of flows from the average direction and φ^* is the angle between this average direction and the direction of wave propagation, then

$$\lambda_{np} = -\frac{2\omega_n \omega_p}{\omega_n^2 - \omega_p^2} [\omega_n \cos(\varphi^* - \xi) - \omega_p \cos(\varphi^* + \xi)]^2. \quad (6.18)$$

Formula (6.18) shows that if the basic flows are collinear - i.e., $\xi = 0$ - then waves propagating along these flows are the most unstable, while waves propagating perpendicular to them are always stable ($\lambda_{np} = 0$). If the velocities of the basic flows coincide and $\xi \neq 0$, then waves propagating in the direction of the bisector of the angle between the directions of the main flows are always stable, while those propagating in a direction perpendicular to it are the most unstable.

Fronts and the tropopause are among the most typical boundary surfaces for the atmosphere. Although formulas (6.14), (6.18), etc., given above were obtained by Sandin for strictly horizontal boundary surfaces, they can also be used for analysis of the stability of waves on fronts and on the tropopause. This is connected with the fact that the slope of these boundary surfaces is not great and does not have a substantial influence on the dynamics of short waves. When considering the stability of the latter on fronts, Γ and λ_0 can be expressed through the slope of the front α_f and the Coriolis parameter f :

$$\begin{aligned} \Gamma &= \frac{2g}{f} - \text{tg}^2 \alpha_f, \\ \lambda_0 &= \frac{2g}{f} - \frac{2g}{f} \text{tg}^2 \alpha_f. \end{aligned} \quad (6.19)$$

The wind velocity component perpendicular to the front experiences comparatively minor discontinuity; as a result the direction of the vector of the wind velocity difference on both sides of the front is close to its direction. Therefore the appearance of instability is greater in waves propagating along the front. This means that the greatest amplitude should be found for gusts of wind in this direction.

In the preceding chapters we pointed out repeatedly that loss of stability by atmospheric waves is apparently accompanied by the generation of small-scale turbulence. A similar assumption has been expressed, in particular, by O. Phillips (1967), E. Reiter and A. Burns (1965), and by others.

Of interest in this connection is the example given in the article by N. K. Vinnichenko (1966), who used a high-sensitivity hot-wire anemometer (see Chapter 2) installed on an IL-18 laboratory aircraft for his studies.

The flight was carried out at 5400 m in a zone of a slow-moving secondary front with waves under the axis of the jet stream, which was oriented from the SW to the NE. The average wind speed at the flight altitude comprised about 28 m/s. Close to the flight level $\frac{dV}{dz} = 0.61$ m/s per 100 m; the change in wind direction with altitude was $\frac{d\gamma}{dz} = 3.4$ deg/100 m, and $\gamma = 0.63$ deg/100 m. At places the flight was accompanied by weak buffeting $|\Delta n| \leq 0.2 g$.

Figure 6.7 shows individual spectra of horizontal wind-velocity component pulsations for the quiet segment of the flight and the segment on which buffeting was observed. Figure 6.8 shows a bit of a recording of the hot-wire anemometer encompassing the end of the quiet flight segment and the beginning of the turbulent section. It is clear that, beginning from a certain instant of time, waves disappear and pulsations of wind velocity acquire a turbulent character. Figure 6.7 shows that at scales close to 2 km there is a sharp local maximum on the curve of spectral densities; this is apparently connected in its origin to the disruption of atmospheric waves.

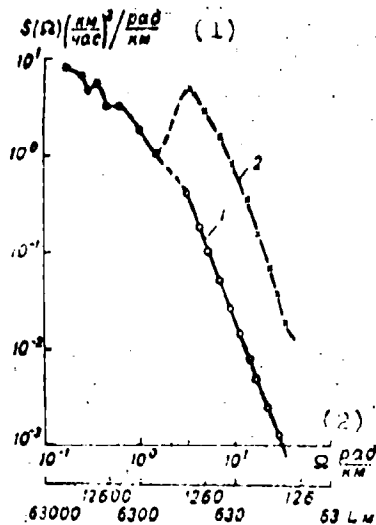


Fig. 6.7. Spectra of horizontal wind-velocity component pulsations (per N. K. Vinnichenko). $H = 5400$ m, $\bar{U} = 99$ km/h. 1 - 1645.00 hours to 1701.30 hours of quiet flight; 2 - 1701.30 hours-1711.00 hours of weak buffeting, presence of wave motion.

KEY: (1) $S(\Omega)(\text{km/h})^2/\text{rad}/\text{km}$; (2) rad/km .



Fig. 6.8. Segment of recording of an airborne hot-wire anemometer showing wave perturbations (per N. K. Vinnichenko).

KEY: (1) 3 m/s; (2) 17 h 01 min 30 s; (3) 10 s.

§ 3. MOUNTAIN WAVES

During flow over mountains the structure of the air flow is changed sharply; these changes may have either an ordered or a random character. The first type of motions include the so-called mountain waves and mountain-valley circulation, representing one form of mesoscalar convective motions; the second type includes turbulence arising both during loss of stability by mesoscalar motions and as a consequence of dynamic deformation of the flow during interaction with the underlying surface. Naturally, the presence of all types of perturbations in the wind field and, especially, their intensity will also depend to one or another degree on the thermal stratification of the atmosphere, the altitude and form of the range, its

orientation with respect to the wind, etc. A change in even one of these factors can have a noticeable influence on the general character of the flow over the mountains. It should be noted that usually both ordered and turbulent perturbations are observed simultaneously in a flow above mountains. An especially close connection is observed between them in a free atmosphere, where loss of stability by waves is apparently the major source of turbulence.

a. Characteristics of Mountain Waves and Their Connection With Atmospheric Conditions

Mountain waves represent a particular form of gravitational waves which form above mountains and behind them (Fig. 6.9) if the wind blows across the obstacle or at an angle close to a right angle. The length of these waves is most often close to 10 km, although in individual cases it can vary from 2-3 to 25-30 km. Oscillations occur near the level of equilibrium of the unperturbed portion of the flow, with the source of perturbations being the mountain and the static stability of the atmosphere playing the role of a restoring force.

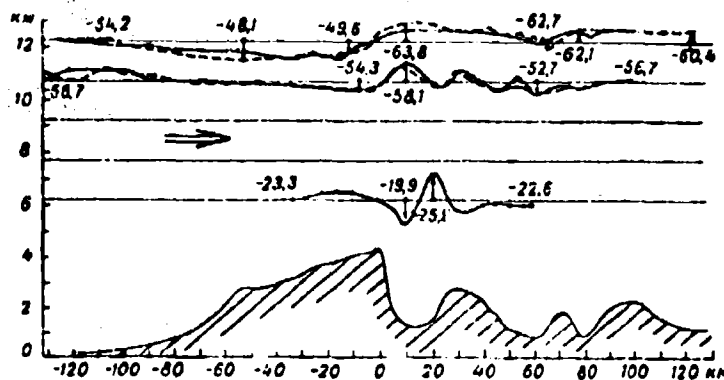


Fig. 6.9. Flow lines above the Sierra Nevada (USA) on 1 April 1955 (per Holmboe and Klieforth).

The presence of wind leads to a situation in which an air particle which is displaced upward by the mountain simultaneously

participates in oscillatory (with stable stratification) and translational motions and in successive moments of time is located above different points of the earth's surface. In this way an air wave is formed; its length is determined by the speed of the flow (distance of horizontal drift per unit time) and by the stability of the atmosphere (period of oscillations).

Thanks to the lenticular and undulatus clouds which form in the middle (and sometimes lower and upper) layers in mountain waves when the air is sufficiently humid, it is possible that mountain waves can be detected visually.

The amplitude A of mountain waves is significantly greater than the amplitudes of internal gravitational-shear waves. Thus, according to the data of V. Panchevskiy (1957), above the Carpathians the quantity A reaches several hundreds of meters; L. Gaz (1961) recorded an amplitude of 1500 m above the Czechoslovak Tatras; while V. A. Patsuyev (1964) used balanced pilot balloons to study waves with $A = 2400$ m in the upper troposphere in the Tashkent region. Approximately similar amplitudes were recorded during flights on gliders over the Rocky Mountain (USA) (see the article by J. Roimbe and H. Klieforth, 1957) and over the Alps (France).

Vertical speeds at the peaks and troughs of mountain waves can be very great. Thus, according to Patsuyeva's data, vertical speeds in mountain waves above the Tashkent region reached 10 m/s, while the data of American investigators indicate that they reached 25 m/s above the Cordilleras (USA). The values of A and w are usually maximum in the middle troposphere.

The first theoretical studies of mountain waves were carried out by N. Ye. Kochin (1938), who solved the problem of the flow of an ideal incompressible fluid around irregularities in relief. The change in air density with altitude was calculated by presenting the atmosphere in the form of a two-layer medium in which the lower and upper layers had different densities. Although this method did not make it possible to take into account the influence of the

baroclinicity of the atmosphere and therefore represented a very rough idealization of the problem, the merit of Kochin's approach lies in the fact that he was the first to use the assumption that the irregularity of the earth's surface is not small.

The compressibility of air was first taken into account in the problem of flow above mountains by A. A. Dorodnitsyn (1938, 1940, 1950). Works very similar in statement and in obtained results were carried out by P. Kine [spelling not verified - Translator] (1936, 1941), by G. Lira (1940), and by others. In the enumerated works the subject was stationary flow of a compressible (baroclinic) ideal fluid over a crest. Equations of motion, the continuity equation, and the equation of heat influx were taken as the initial equations. The system of these equations was linearized on the assumption of the smallness of perturbations introduced by terrain irregularities relative to the incoming flow. Solution was accomplished by the method of short waves¹; Coriolis force was not taken into account. It should be noted that, as Dorodnitsyn pointed out (1950), the linear theory is suitable only in the case when the height of the mountains is less than the characteristic length $L_{\text{exp}} = \frac{U}{g} \sqrt{\frac{T}{\gamma_0 - \gamma}}$, which corresponds to the "natural frequency" of the flow. In real conditions L_{exp} usually does not exceed 2 km. However, as will be shown below, experimental data confirm the correctness of the qualitative conclusions from linear theory for higher obstacles as well.

A. A. Dorodnitsyn clarified the influence of baroclinicity of the atmosphere on characteristics of mountain waves and found that λ depends on the parameter D^2 :

$$D^2 = \frac{R}{gH} (\gamma_0 - \gamma). \quad (6.20)$$

¹I. A. Kibel' (1944) studied the properties of air flows above mountains by the long-wave method, which made it possible for him to reduce the problem to an ordinary (and even a linear) differential equation.

which below will be referred to as the Lorenz parameter¹.

The dependence of λ on D^2 is given by the relationship

$$\lambda_1 = \frac{2\pi}{\sqrt{D^2 - \frac{n_1^2 H^2}{H^2}}}, \quad (6.21)$$

where H is the thickness of the flow and n_1 is the quantity of wave systems formed behind the ridge. The value of n_1 depends on the speed of the wind and the stability of stratification. In real conditions $n_1 = 1, 2, 3$ - i.e., a system of three waves of different lengths is formed behind a ridge.

The amplitude of the waves is increased with a reduction in γ , i.e., with a growth in D^2 . Besides this, for various wave systems λ_1 and A_1 grow rapidly with an increase in the number of waves n_1 . Therefore qualitatively speaking the flow picture is determined almost completely by a single wave system, while the remaining waves influence only the quantitative characteristics. We will note that from formula (6.21) it follows that waves may exist only in the case when $D^2 > 0$, i.e., $\gamma < \gamma_1$; this means that stratification of the atmosphere is stable. Below we will show that such a conclusion is correct only when the wind velocity or its gradient does not change with altitude.

The works by A. A. Lorenz and other investigators also pointed toward two extremely important properties of flows above mountains which were later confirmed by experimental data - rotation of stream lines and the presence of unique resonance.

The first of these properties consists in the fact that stream lines are not parallel to one another at all altitudes. Above and

¹In foreign works D^2 is called the Scorer parameter.

²Rotation of stream lines takes place both in the wave zone and in the averaged flow corresponding to the basic picture of flow around an obstacle.

below certain levels, called junction [nodal?] surfaces or levels of rotation, the shapes of the current lines are mirror images of one another; as a result of this zones of descending motion are located above regions of ascending flows, and vice versa (Fig. 6.10). A natural consequence of rotation of current* lines is the fact that the geometric location of the troughs and peaks of waves is not vertical, but is slanted along the flow or against it; this can be seen in the presence of multilayer lenticular clouds. A simple method for determining the altitude of junction surfaces z_0 within the troposphere is described in the book by Sh. A. Musayelyan (1962).

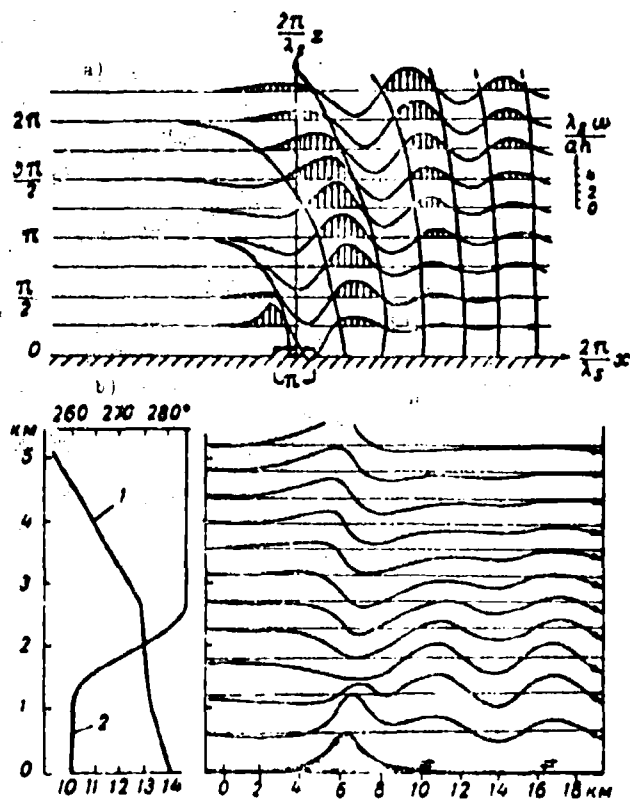


Fig. 6.10. Diagram of current lines in mountain waves. a) per Lira; b) per Scorer. 1 - change in temperature with altitude; 2 - change in wind speed with altitude.

*[Translator's Note. Here and below, read "stream lines" for "current lines"].

The vertical speed of air above mountains is described by the formula

$$w(z) = \bar{U} \left(1 - \frac{T}{T_0}\right)^{\frac{R(1-\gamma) + g}{2R\gamma}} \frac{\sin D(H-z)}{\sin DH} \frac{dc}{dx} \quad (6.22)$$

where \bar{U} is average wind speed; $z = z(x)$ is the equation of the surface of the obstacle in the flow; $\gamma = \frac{c_p}{c_v} \approx 1.4$ is the ratio of heat capacities at constant pressure (c_p) and constant volume (c_v); H is the height of the tropopause, at which w is set equal to zero; R is the gas constant.

From formula (6.22) it is clear that where $\sin D(H-z) > 0$, the sign of vertical velocity $w(z)$ is the same as the sign of dc/dx , i.e., the current lines repeat the shape of the mountain profile. Above the level where $\sin D(H-z) = 0$, i.e., above the junction surface, $\sin D(H-z) < 0$; this means that rotation of flow lines occurs, with the lines taking on a configuration which is the reverse of that which they had under the surface $w = 0$. Since within the limits of the troposphere $\sin d(H-z)$ can have several zeroes, several junction surfaces can be observed here; these are defined by the equation

$$z_{0n} = H - \frac{n_1 \pi}{D} \quad (6.23)$$

where $n_1 = 0, 1, 2, \dots$

It is obvious that in each case there can exist only a finite number of junction surfaces, whose altitude depends on the Dorodnitsyn parameter D^2 . The thickness of the zones of forward and reverse vertical flows is determined clearly by the relationship

$$\delta = \pi U \sqrt{\frac{T}{g(\gamma-1)}} \quad (6.24)$$

We will note that for typical conditions in the troposphere $\delta = 2-4$ km.

Vertical flows generated by mountains cause corresponding changes in air temperature (Fig. 6.11). If the process of ascent and descent of air is considered to be adiabatic, the oscillations in temperature ΔT are approximately determined as

$$\Delta T = T - T_0 = -\gamma_0 \zeta(x, z), \quad (6.25)$$

where ζ is the vertical displacement of the current lines. It is obvious that the signs of temperature perturbations and of w will be opposite, but the altitude of the junction surface in fields of T and w coincide.

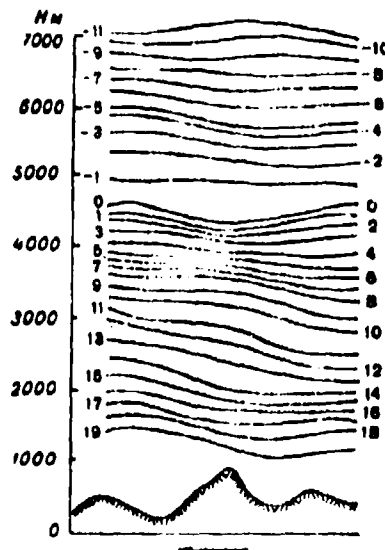


Fig. 6.11. Field of isotherms above the Suramskiy range, 21 August 1955 (per S. M. Shmeter). The arrow shows wind direction.

The phenomenon of resonance consists in the fact that if λ is close to the width of the mountain, the amplitude of the wave (other conditions being equal) will be maximum and may even exceed the height of the obstacle. Thus, waves with large amplitudes may be observed over mountains which are not particularly high - for example, the Carpathians, Tatars, etc.

One of the basic simplifications used by Dorodnitsyn during solution of the problem of mountain waves was the assumption that wind speed in the atmosphere did not change with altitude. The role of vertical wind shear was clarified in the works by K. S. Scorer (1949, 1953, 1956). Although some investigators resolved the problem of air flow above mountains in a much more complete form later, we will phrase on the results obtained by Scorer in more detail, since they indicate very clearly the connection of waves with the thermodynamic conditions in the atmosphere.

Scorer examined flow around an obstacle described by the formula

$$\zeta = \frac{hb^2}{b^2 + x^2}, \quad (6.26)$$

where h is the height of the ridge; $2b$ is its width; x is the distance from the ridge to a given point. The flow was assumed to be laminar and isentropic; the influence of the earth's rotation was not considered.

After a number of simplifications the following formula was found for the stream function ψ :

$$\frac{\partial^2 \psi}{\partial z^2} - \left(\frac{g}{c_s} + \beta \right) \frac{\partial \psi}{\partial z} + \left(\frac{g^2}{U^2} - \Omega^2 - \frac{1}{U} \frac{\partial^2 U}{\partial z^2} \right) \psi = 0, \quad (6.27)$$

where c_s is the speed of sound; $\beta = \frac{1}{T}(\gamma_a - \gamma)$; $\Omega = \frac{2\pi}{\lambda}$ is the wave number in expansion of function (6.26) in Fourier series. The quantity

$$F = \frac{g^2}{U^2} - \frac{1}{U} \frac{\partial^2 U}{\partial z^2} \quad (6.28)$$

was subsequently called the Scorer parameter. Since in a free atmosphere¹ $\frac{1}{U} \frac{\partial^2 U}{\partial z^2} \ll \frac{g\beta}{U^2}$, ordinarily $F \approx D^2$.

¹ According to the data of A. A. Vasil'yev (1965), in the boundary layer the magnitudes of the two terms in (6.28) are sometimes close in value. Similar data are given by H. Felts (1967) for the zone of jet streams.

In (6.27) by ignoring the term with $\frac{d\psi}{dz}$, which reflects the influence of compressibility of the air on the amplitude of a perturbation and which becomes essential only at large altitudes, we obtain

$$\frac{\partial^2 \psi}{\partial z^2} + (\beta^2 - \Omega^2)\psi = 0. \quad (6.27a)$$

To determine just how the change in U with z influences the characteristics of waves, Scorer examined a ridge in a flow consisting of two layers in each of which $U_1^2 = \text{const}$, but $\beta_1 \neq \beta_2$ (the subscripts 1 and 2 relate to the lower and upper layers, respectively).

The solution showed that the existence of waves required that the parameter U^2 be positive and be reduced with altitude. From formula (6.28) it is clear that the latter is caused most often by a growth in U , since the range of change in β with atmosphere is much narrower than the range of U . It should be noted that from formula (6.28) it follows that in a flow where $\frac{\partial U}{\partial z} \neq 0$, waves are possible in principle even during unstable stratification, if only

$$\frac{\partial U}{\partial z} < 0, \text{ and} \\ \frac{1}{U} \left| \frac{\partial^2 U}{\partial z^2} \right| > \beta \left| \frac{1 - \gamma}{\gamma U^2} \right|.$$

Empirical data confirmed the correctness of the theoretical conclusions on the role of thermal stratification in the formation of waves. Thus it was found that waves are observed most frequently during stable stratification, especially if there is a layer with isothermic or inversion distribution of temperatures above the mountain. However, waves have sometimes been observed during unstable stratification in the lower portion of the troposphere. The amplitudes of such waves were, as a rule, very small, while the length was comparatively great.

According to Scorer, wavelength λ is included between a maximum and a minimum from the $2\pi/l$ values in layers in which waves are formed.

As is evident from formula (6.28), this means that λ is directly proportional to wind velocity and is inversely proportional to the stability of stratification.

G. Corby and C. Wallington (1956) generalized the results of the Scorer studies in order to determine the amplitudes of mountain waves. They showed that the deflection of the current lines ζ_z at altitude z from their equilibrium position in the unperturbed portion of the flow is determined by the formula

$$\zeta_z = -2\pi h b c^{-2a} \left(\frac{U_1}{U_2} \right) \psi_{z,z} \left(-\frac{\partial \psi_{z,u}}{\partial z} \right) \sin \Omega x, \quad (6.29)$$

where U_1, U_2 are the speed of the wind at the ground and at level z ; $\psi_{z,u}, \psi_{z,v}$ are the stream functions for the corresponding level, satisfying equation (6.27a). The maximum vertical velocity in the wave, w_{\max} , corresponds to the deflection point $\zeta_{z,2}$:

$$w_{\max} = \left[U_2 \frac{\partial \zeta_z}{\partial x} \right]_{\max} = -2\pi h b c^{-2a} U_1 a_n \Omega, \quad (6.30)$$

[since $\zeta_z = \max$]

where

$$a_n = \psi_{z,v} \left(-\frac{\partial \psi_{z,v}}{\partial z} \right)^{-1}.$$

Since Ω and ψ are functions of U^2 , the amplitudes of the waves depend also on the vertical profile of the wind in the atmosphere. With an identical profile U^2 , the greatest amplitudes will occur in those cases when U_1 is greatest - i.e., waves are more intensive with strong winds at ground level. We will note that empirical data show that the appearance of waves is normally observed if the wind speed at the level of the ridge exceeds a certain critical magnitude $U_{1 \text{ cr}}$. Above lower mountains (mountains in England, the Crimean mountains, the French Alps, etc.) $U_{1 \text{ cr}} = 8-10$ m/s. Above higher ranges, such as the Cordillera, $U_{1 \text{ cr}} \geq 12$ m/s.

The factor $hbe^{-\Omega b}$ describes the influence of the height and width of the range on the amplitude of displacements of current lines. The higher the mountain (i.e., the larger h), the greater the amplitude. Besides this, the quantity $be^{-\Omega b}$ is maximum if $b = \Omega^{-1}$.

When flow occurs over a range around its upwind slope a region of increased pressure arises, while during flow on the lee side there is a region of reduced pressure. As a result counterflows arise at ground level behind the range; these are accompanied by the formation of eddies with a horizontal axis - rotors. According to observation data the dimensions of such rotors may reach 0.5-1.0 km. Rotors are periodically "stripped away" from the slope and float away with the flow, while new rotors arise in their place.

According to J. Förchtgott (1949), a lee rotor located directly behind a ridge is subjected to the basic flow in the same manner as a solid obstacle would be. Naturally, in this case the "effective" width of the mountain is increased.

The characteristics of mountain waves given above were obtained for the case when the motion can be considered plane; this condition is satisfactorily fulfilled only if waves develop near long ranges whose altitude changes little from point to point. The theory of three-dimensional mountain waves was developed by K. Scorer (1953, 1954, 1956), I. A. Kibel' (1955), Sh. A. Musayevyan (1960), M. Würtele (1957), Ye. M. Pekelis (1965, 1966), and others. These studies showed that near short ranges and especially near monoliths, wave perturbations arise not only in the vertical plane but also in the field of the horizontal component of wind, propagating away from the mountain and down along the flow. Junction surfaces are also formed in the field of horizontal waves; the magnitude of wind perturbations on these equals zero. Along with this, the characteristics of waves in the vertical plane are also somewhat different than during plane flow around an obstacle (especially in direct proximity to the mountain). In particular, waves are formed not only along the flow but also across it.

The characteristic of the process of spatial flow around an obstacle is a consequence of the fact that in this case the oncoming flow passes partly over the obstacle and partly along its sides. As the numerical calculations of Pekelis showed, thanks to this splitting of the flow the perturbations behind the mountain interfere, with waves intensifying each other at places and attenuating each other at other places. Partial flow around a mountain from the sides - i.e., a reduction in the mass of air streaming beyond it - leads to a reduction in the amplitude of waves and to their comparatively rapid damping downward along the flow. This process is intensified with a growth in L^2 . The greatest amplitudes should be observed above the lee slopes. They grow with a growth in height of the obstacle, although the growth is more rapid than that of the obstacle height.

Empirical data showed that the frequency and amplitude of mountain waves around relatively low mountains undergo a diurnal and annual variation, basically determined by the corresponding changes in the Deardorff-Sorensen parameter and its vertical gradient. Ordinarily the maximum amplitudes are observed in the morning and evening. Their daily minimum is connected mainly with the fact that at this time the stability of stratification close to the mountain surface drops very strongly and, despite the intensification of wind which occurs simultaneously, L^2 is sharply reduced. Occasionally L^2 even begins to grow with altitude and waves generally cannot exist. The nocturnal minimum in frequency of waves is connected with a sharp weakening of the wind on the ground surface at this time; this sometimes causes its velocity to drop below the critical value.

Waves which form above high mountains normally do not have a clear-cut daily variation. The change in their intensity is connected mainly with processes on a synoptic scale. These also determine the annual variation in recurrence of mountain waves.

Theoretical investigations carried out by G. N. Zhabnikov (1954) showed that the diurnal variation in mountain waves should be

influenced substantially by the diurnal variation in the difference between the temperatures of the mountain surface and the surrounding air. If the mountain is warmer than the air, which is typical for rocky peaks during the day, the amplitude of the waves is reduced. Above rocky peaks at night and above snow during the day the waves, on the other hand, are intensified because the mountain is colder than the surrounding air. Trubnikov showed that the above-indicated pattern is confirmed by the daily variation in occurrence of lenticularis clouds located in the peaks of the waves.

We will pause briefly on the spatial extent of zones of mountain waves. Behind a ridge downward along the flow the amplitude of waves diminishes rapidly; both theoretical and experimental data indicate that by the third-fifth wave the amplitude becomes negligibly small.

The height of propagation of waves even above comparatively low mountains is apparently very great. Thus, in the Northern Alps a number of flights were made in mountain waves on gliders up to altitudes of 9-10 km; flights were made above the Sierra Nevada (USA) up to 13-14 km, and so on. These altitudes are not maximum. According to K. Stömer (1948) even over Scandinavia, where the height of mountains does not exceed 2.5 km, waves are observed up to an altitude of 22 km and even more. I. Kotass (1958) [spelling not verified - Translator] reported observing mother-of-pearl clouds similar in shape to the mountains in 1950 over Alaska at altitudes of 18-24 km.

Unfortunately at present theoretical evaluation of the vertical dimensions of the wave zone is still impossible. This is connected with the fact that the altitude at which the calculations indicate the waves attenuate varies strongly as a function of the particular boundary conditions relating to the z-axis, method of calculating the presence of the stratosphere, etc., which are used in the various works.

An interesting method of taking into account the influence of the tropopause on penetration of waves into the stratosphere was proposed by E. Palm (1958), B. N. Trubnikov (1966), and others. They showed that propagation of gravitational waves within the zone of atmospheric boundary surfaces is subject to laws similar to the laws of geometric optics. In particular, under certain conditions determined by the values of the Doroditsyn-Sorerer parameter on both sides of the boundary surface (e.g., the tropopause), waves may be partially reflected from the surface.

The coefficient of "transparency" for the tropopause equals

$$p = \frac{2 \cos \theta}{\cos \theta + \sqrt{\left(\frac{l_2}{l_1}\right)^2 - \sin^2 \theta}}, \quad (6.31)$$

where θ is the angle of incidence of the wave on the tropopause, while the subscripts 1 and 2 relate to the troposphere and stratosphere, respectively. The quantity $\left(\frac{l_2}{l_1}\right)^2$ is the "refractive index" of the tropopause. According to (6.31), the vertical speed of air of the tropopause is determined by the relationship

$$w_p = A \exp\{kx l_1 \sin \theta + kz \sqrt{\frac{l_2}{l_1} - l_1 \sin^2 \theta}\}, \quad (6.32)$$

where z is counted off from the tropopause. Calculations by the above formulas indicate that with typical values of l_1 and l_2 ($l_1 = 0.82$ 1/km, $l_2 = 1.35$ 1/km) 75% of gravitational waves normally incident on the tropopause pass through it. Thus, although mountain waves weaken with transfer into the stratosphere, nevertheless the tropopause is not, as a rule, absolutely opaque to them.

b. Turbulence in a Zone of Mountain Waves

A zone of mountain waves can be broken down into two parts - a lower, ranging approximately from the base of the obstacle to the level of its upper edge, and an upper part ranging from the upper edge of the ridge to the altitude at which the waves disappear. The

lower portion of the wave zone is characterized by the presence of rotors (see section "a" of this chapter), with which extremely strong turbulence is normally connected.

Experimental investigations carried out in France and in the USA showed that within the rotors w goes to 10 m/s; the velocities of horizontal gusts are also very great. Characteristically "additional" large (but smaller than the rotors) eddies are formed close to the rotors; rotation within these eddies does not necessarily proceed around the horizontal axis (see the article by M. Berenger and N. Gerbier, 1956).

Above the rotor zone turbulence weakens, but vertical and horizontal turbulent gusts are observed here quite frequently. Thus, turbulence was recorded in 20 out of 66 flights in the wave zone carried out by S. Pilsbury (1955) over England. We can assume that it is generated here by wind shears caused by wave motions in the horizontal plane; these are imposed on the unperturbed wind profile. Berenger and Gerbier established that if the wave zone at a certain altitude above mountains contains a thin layer in which wind speed is sharply weakened, waves will decay into large eddies within it; this layer then becomes the upper boundary of wave propagation. Turbulence also arises in layers where wind speed grows sharply¹. Figure 6.12 shows diagrams of lee waves with different forms of the vertical wind profile.

As pointed out by M. Berenger and N. Gerbier (1956) and by J. Keuttner (1958), the transition from wave motion to turbulent motion frequently occurs very rapidly. They connect such a transition with loss of stability by waves; in particular, this is indicated by the fact that it frequently is observed in cases when the waves are very short (usually $\lambda < 2$ km) - i.e., when they are least stable.

¹When speaking of intensification or weakening of the wind, we have in mind (as in § 3) the wind component normal to the ridge.

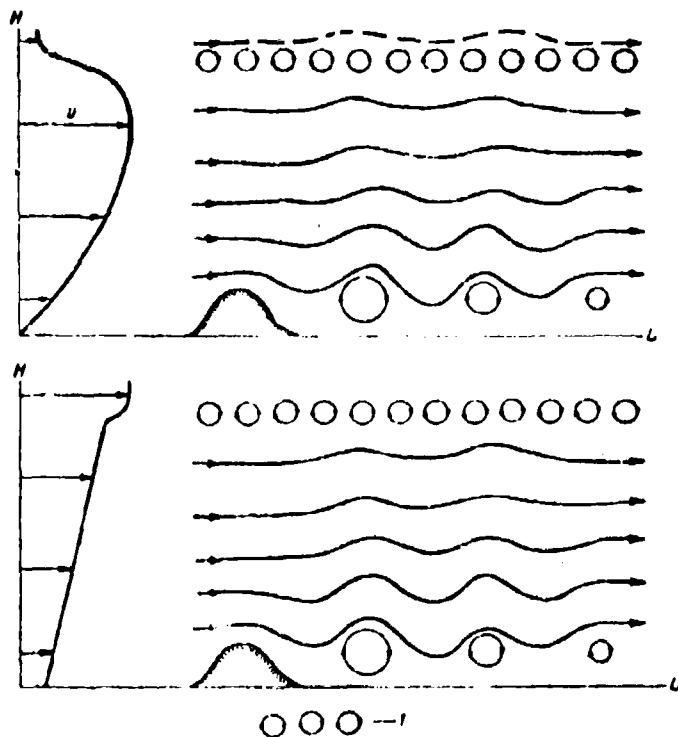


Fig. 6.12. Lee waves and turbulence (per Berenger and Gerber). 1 - turbulent zone. The vertical wind profile is given on the left.

According to Keuttner (1958) and H. Poitz (1967), normally an increase in clear-air turbulence in the zone of jet streams above the Rocky Mountains (USA) is connected with mountain waves; in this area w values of 20 m/s have been recorded, with the horizontal extent of gusts comprising about 2 km. Increased turbulence is sometimes observed in the zone of waves above inversion layers. It is possible that the intensification of turbulence close to the tropopause is connected with the effect described above of partial reflection of mountain waves from the tropopause. During interference between forward and reverse waves a sharp increase in oscillation amplitude is possible, while in individual cases there may be loss of "total wave" stability.

c. Turbulence on the Lee Side of Mountains

Above we examined turbulence arising in the zone of mountain waves because of loss of stability by the waves. However, turbulence above mountain regions arises more frequently from other causes. Of these the main cause is the formation of eddies on the lee slope as the result of dynamic interaction of the flow with the relief. The intensity of turbulence is increased with an increase in wind strength and with a growth in steepness of the slopes. This is connected with the fact that both of these factors facilitate convergence of the wind above the ridge, thus increasing turbulization of the flow running onto the ridge. Even above such a comparatively smooth range as the Sulamskiy, vertical wind shears arising in the convergence layer can exceed 5 m/s per 100 m (as shown by A. Kh. Khrgian (1958)). It is obvious that such large wind shears should facilitate loss of stability of the flow in the convergence zone.

Especially strong perturbations arise if the flow is incident not on an individual height, but on an obstacle consisting of a large quantity of them. In this case, according to D. L. Laykhtman and E. K. Byutner (1965), mountains form a unique turbulizing grid. Energy of turbulence is generated in a layer ranging from a certain level \bar{h} up to the peak, while above this turbulence is conditioned basically by downward diffusion of eddies. With stable stratification the energy of turbulence diminishes with upward diffusion owing to expenditure of energy on counteracting buoyancy forces and also due to dissipation into heat.

Proceeding from dimensionality considerations, Laykhtman and Byutner found that at height z above low mountains the mean square gustiness of the flow \bar{U}'^2 is determined by the formula

$$\bar{U}'^2 = U^2 \Phi\left(\frac{z}{L}, \frac{L}{\lambda^*}\right), \quad (6.33)$$

where $\Phi\left(\frac{z}{L}, \frac{L}{\lambda^*}\right)$ is a certain function determined experimentally; L is the characteristic scale of eddies and is dependent on the class of

the mountains, while λ^* is a parameter having the dimensionality of length and equalling

$$\lambda^* = \frac{U^3}{R \frac{R}{\rho c_p T}}, \quad (6.34)$$

where R is the radiation balance.

From formula (6.34) it is clear that at a given height the intensity of turbulence depends on wind speed, eddy scale, and the radiation balance. The dependence on the latter is a consequence of the fact that stratification of the atmosphere is connected with it; this means that the intensity of thermal turbulence, whose contribution is especially great with weak winds, is also connected to the radiation balance.

Thermal stratification has the greatest influence on turbulence above mountains. The lower the stability the greater the altitude to which eddies diffusing upward can be lifted.

The dimensions of the zone of orographic turbulence are very great. According to data from S. M. Shmeter (1958, 1960a), the vertical extent of such zones can exceed the height of the obstacle by 3-4 times. The horizontal dimensions of turbulent regions are especially great. Even above mountains 1-2 km in height they reach values of several tens of kilometers. This is connected with the fact that the transfer of eddies arising close to the ridge by the wind can be accompanied by disruption of flow stability at a significant distance from the mountain massif. If the flow is located on the boundary of unstable equilibrium, such eddies begin to play the role of "initial turbulence," generating the subsequent development of turbulent motions which cannot at this point be considered completely orographic.

Some ideas of the distance at which the perturbing action of high mountains influences air flows can be obtained from data on aircraft buffeting above Yerevan. These data show that during strong

southwest winds at altitudes up to 4-5 km observation of bumping is the rule. Its intensity is especially great in summer, when stratification of the atmosphere in this layer is close to indifferent. Increased turbulence above Yerevan is obviously connected with the fact that the high mountains Greater Ararat (5156 m) and Little Ararat (3914 m) are located 40-50 km to the SSW of the city. The deformation of southwest flows above them causes an increase in the turbulence of the atmosphere below the level of the upper edge of the mountains.

Figure 6.13 shows an example of typical structure of a turbulent zone above mountains. Above the lee slope a region of very intensive turbulence with $w \geq 5$ m/s is clearly visible. Above and aside from it the value of w gradually decreases. The "calm" layers observed in turbulent zones above level terrain are absent above mountains.

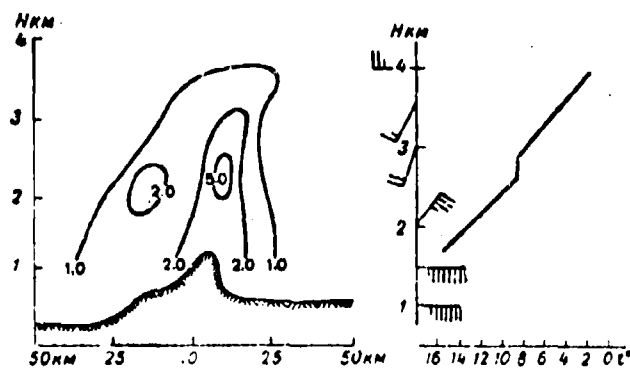


Fig. 6.13. Turbulent zone above Suram-skiy Pass on 3 September 1955 (per S. M. Shmeter). Isolines w_T are counted in m/s. Vertical profiles of temperature and wind are shown on the right.

Regions of orographic turbulence are extended in the direction of the wind, being arranged basically above the lee side of the mountain. Thus, a unique "turbulent banner" similar to the widely known "banner clouds" is formed behind the range.

The described structure of turbulent sections is characteristic for isolated mountains or for sections of a range on which its altitude and shape varies very little. If the structure of the mountain system is more complex, it is necessary to consider the possibility of mutual superposition of perturbations generated by individual elevations. In this case the thickness of the turbulent zone and the intensity of turbulence are most usually increased.

Characteristic data on the structure of turbulence above the shore of the Black Sea on the lee side of the Caucasian range during the Novrossiyskaya bora of 31 October-2 November 1963 were presented by A. A. Reshchikova (1965). In the depth of the bora the entire layer from the surface of the ocean up to an altitude of 1500 m was enveloped by turbulence. Comparison of characteristics of turbulent zones with the profile of the Caucasian range in the region of flights (on the route Gelendzhik-Betta) showed that the turbulent zone extended higher than the range only over a small segment; on the greatest part of its extent the upper boundary of the zone was on the level of the peaks of the range or below it.

Table 6.3 gives data on turbulence determined during flights of 31 October and 1 November. As is evident from the table, the turbulence coefficient K has little spatial variability. The quantity K changed little either with altitude or along the horizontal. Thus, the maximum values of K for the entire segment of the flight did not differ from its mean value. Only once (on 31 October 1963) at an altitude of 400 m was a higher value noted: the maximum coefficient of turbulence was double the average value.

A. A. Reshchikova explains the constant level of K by the fact that the linear dimensions of gusts grew to the same degree as the reduction in the increment of overloads Δn .

We will pause now on experimental data concerning the dependence of the intensity of orographic turbulence on the general thermodynamic conditions in the atmosphere. Up to the present such studies have been carried out basically near mountain ranges whose heights do not

Table 6.3. Data on turbulence during the Novorossiyskaya bora on the Gelendzhik-Betta route.

(1) Высота над уровнем моря, м	(2) Относительная протяженность спокойных участков, %		(3) Средний коэффициент турбулентности, м ² /сек.		(4) Максимальный коэффициент турбулентности, м ² /сек.		(5) Максимальная перегрузка в доли g		(6) Плотность перегрузки с интенсивностью			
	31 X	1 XI	31 X	1 XI	31 X	1 XI	31 X	1 XI	>0.2g		>0.5g	
									31 X	1 XI	31 X	1 XI
400	31	—	61	—	128	—	—	—	—	—	—	—
750—800	10	7	51	51	87	67	0.48 —0.60	—	400	582	5	1
900	—	25	—	36	—	56	0.61 —0.62	—	—	380	—	—
1000	35	—	49	—	69	—	0.38 —0.35	—	211	—	—	—
1200	—	38	—	30	—	41	—	0.31 —0.34	—	70	—	—
1500	100	52	—	28	—	36	—	0.24 —0.25	—	30	—	—

Remark. The overload increment $\Delta n = 0.1$ g corresponds to $w = 1$ m/s.

KEY: (1) Height above sea level, m; (2) Relative extent of calm segments, %; (3) Average turbulence coefficient, m²/s; (4) Maximum turbulence coefficient, m²/s; (5) Maximum overloads in fractions of a g; (6) Density of overloads with intensity of:

Reproduced from
best available copy.

exceed 2-3 km (Carpathians, Crimea, Transcaucasia, Eastern Siberia, etc.). The results have been published in articles by J. Förcztgott (1949), N. Z. Pinus and S. M. Shmeter (1958), S. M. Shmeter (1958, 1960a), A. A. Vasilyev (1965), P. A. Vorontsov (1966), and others.

Despite certain specific peculiarities of the development of turbulence of different mountain systems, it was possible to clarify a number of situations which are common and characteristic for all geographic regions. It was found that the nature of motions above a range and especially over its lee side are determined by certain characteristics of the wind and temperature fields in the unperturbed (upwind) portion of the flow. These characteristics include the magnitude of the wind speed component perpendicular to the ridge on the level of the peak U_H and the vertical gradients of temperature γ_H and wind β_H in the layer from the peak to a level exceeding the height of the mountain by several hundred meters.

During stable stratification of temperature ($\gamma_H < \gamma_a$) and a light wind (for the majority of regions studied, when $U_H \leq 5$ m/s) turbulence was little developed; the current lines above the mountain were approximately parallel to the profile of the obstacle, and the amplitude of their deflection decreased rapidly with altitude.

During moderate and strong wind (usually when $U_H > 10$ m/s) the nature of the flow depends strongly on γ_H and β_H .

If $\gamma_H < \gamma_a$ and $\beta_H \geq 0$, lee waves are formed above the ridge and behind it, while under them below the height of the ridge there is a system of rotors, in which zone very strong turbulence is observed.

When $\beta_H < 0$ the flow loses stability and turbulence develops, intensifying approximately in parallel with the growth in U_H . The thickness of the turbulent layer can significantly exceed the height of the ridge, especially if $\gamma_H \geq \gamma_a$ above the ridge. However, during strong winds orographic turbulence develops only during stable thermal stratification and even when isothermal and inversion layers are present above the mountains.

Occasionally the shape of flows typical for the case $\beta_{II} < 0$ is called "rotor," after Förchtgott. This term is not a happy choice, since it may lead to mixing of two completely different types of flows: rotor flow under mountain waves, characterized by the presence of large eddies with a horizontal axis, and turbulized flow observed from the ground up to a level located somewhat higher than the ridge and characterized by the presence of comparatively small eddies with axes which are arbitrarily oriented in space.

In conclusion we will note that turbulence of orographic origin can be intensified by thermal turbulence. The latter may even predominate in summer above rocky and forested mountains at small wind speeds. Thermal turbulence develops in the morning hours and, continuing to develop up to midday, it continually embraces an ever thicker layer of the atmosphere. In this case its development begins earliest of all above rocky mountains facing the sun, and develops only somewhat later above level terrain areas.

The upper boundary of the layer of thermal turbulence is elevated above mountains and is lower above valleys. Under the influence of the wind zones of thermal turbulence arising above mountains are shifted somewhat in the direction of flow. Evening damping of turbulence begins from the ground, but is accompanied by the appearance at high altitudes of layers in which turbulence weakens sharply. Usually such layers are located where the temperature gradients are small.

CHAPTER 7

TURBULENCE WHICH INFLUENCES AIRCRAFT FLIGHT

As was pointed out above, the flight of an aircraft in a turbulent zone is accompanied by pulsations in its velocity, angle of attack, bank, and other characteristic motions. This leads to the appearance of additional alternating overloads manifested in so-called buffeting of the aircraft.

During studies of the effect of turbulence on flight vehicles (aircraft, rockets, etc.) two turbulence models are usually used:

a) turbulence is represented in the form of the totality of individual (discrete), mutually independent gusts of air;

b) turbulence is considered to be the statistical totality of random gusts.

§ 1. METHODS OF EVALUATING THE INTENSITY OF TURBULENCE WHICH INFLUENCES THE FLIGHT OF AN AIRCRAFT

As was shown in Chapter 2, an aircraft reacts not to any and all turbulent gusts, but only to a comparatively narrow segment of the turbulent spectrum. Upon entry into long-period perturbations the aircraft adapts to the motions of the air and is carried up or down along with it, without experiencing additional overloads. On the

other hand, high-frequency perturbations lead to such small overloads that they are virtually unnoticeable. As flight speed increases it is possible for longer-period gusts of air to cause noticeable overloads on the aircraft. Thus, for example, while perturbations with a length ranging from 10-20 m up to 3-4 km (up to 6-7 km for heavy aircraft) can influence the motion of an aircraft at subsonic speeds, motion of supersonic aircraft flying at altitudes of 20 km and above is affected by waves with a length up to 15-20 km.

From this it is clear that when we speak of the intensity of turbulence sufficient to cause buffeting we must bear in mind not the intensity of turbulence in general, but the intensity of that portion of its spectrum which is operative under given flight conditions. In other words, in this case the intensity of buffeting of the aircraft can serve as a measure of turbulence intensity. We will note that such an approach is characteristic for the first of the turbulence models listed above.

a. Evaluation of the Intensity of Buffeting

The intensity of buffeting, which is normally defined as the magnitude of aircraft overload increment, depends not only on the magnitude of turbulent pulsations in wind velocity and gust scales but also on the aerodynamic characteristics of the airplane. For example, this is clear from the following formula, which permits approximate evaluation of the magnitude of overload increment for an inelastic aircraft in horizontal flight encountering an isolated vertical gust characterized by an effective velocity w_{eff} :

$$\Delta n = n - 1 = \pm \frac{\rho v^2 c_n^{\alpha}}{20/S} \quad (7.1)$$

[at = off]

Here ρ is the air density; v is flight speed; c_n^{α} is a derivative of the lift coefficient with respect to angle of attack; G is the aircraft weight in flight; S is wing lift surface; n is aircraft overload, equal to the ratio of its lift to its weight. During a gust

horizontal flight $n = 1$. We have already discussed the relationships between w_{eff} and the true speed of a gust in Chapter 2.

Evaluation of the intensity of buffeting (given in Table 7.1) both from instrument measurement data and by the "perception" of the crew on a four-mark scale, is accepted practice.

1. Energy Spectrum of Atmospheric Turbulence Causing Buffeting of an Aircraft

For a number of practical problems it is necessary to consider the influence on flight not only of the velocities of gusts, but also of their frequency characteristics. In this case it is necessary to resort to a statistical presentation of turbulence (second model) and to use the spectral density of turbulent gusts as a measure of turbulence intensity.

If we regard an aircraft as an indicator of atmospheric turbulence, we can consider that the components of the pulsation velocity $u'(x)$ are small in comparison with its flight speed and therefore we can assume that the pulsation velocity at any point of the flight trajectory is essentially unchanging while the aircraft flies through the neighborhood of a point where the correlation connection between fluctuations of wind velocity is great. In this case the field of pulsation velocities of the vector can be regarded as a stationary uniform random field. For such a field a single-valued connection $x = vt$ exists between the horizontal coordinate x and time t . We can further presume that the pulsation velocity of the wind is identical for all points on the aircraft - i.e., within the limits of the dimensions of the aircraft it is possible to ignore the dependence of fluctuations of the wind vector component on the coordinates. This assumption is apparently the more valid the smaller the size of the aircraft. In this case the pulsation velocity of the wind is a function only of the coordinate x or time t .

Table 7.1. Scale for evaluating effect of turbulence on aircraft.



(1) Название	(2) Интенсивность боковых, баллы		(6) Диапазон перегрузок в зоне г-прерываний в зоне g	(7) Характеристика поведения самолета в баллах	(8) Рекомендации по пилотированию	(9) Характеристика поведения пассажиров
	(3) обозначение	(5) ИКАО				
(10) Слабая болтанка	(4) отсутствующие	(5) НИКАО	$0,8 \leq n \leq 1,2$ Дл $\approx \pm 0,2$	(11) Отдельные легкие вздрагивания самолета	(12) Полет выполняется на автопилоте	(13) При длительном длительном вылете неприятные ощущения у отдельных пассажиров
(14) Умеренная болтанка	(4) δ(1)		$0,5 \leq n \leq 1,5$ Дл $\approx \pm 0,5$	(15) Частые толчки, связанные с поочередным самолетом и изменением высоты, но не вызывающие затруднений в пилотировании самолетом. Наблюдаются заметные колебания стрелок индикаторов в пилотажных приборах; вариометра и указателя скорости. Установившийся режим полета самолета сохраняется	(16) Пилотирование допускается на автопилоте	(17) Вызывает неприятные ощущения у значительной части пассажиров и затрудняет ходьбу в самолете
(16) Сильная болтанка	(4) δ(2)		$0 \leq n \leq 2,0$ Дл $\approx \pm 1,0$	(19) Разные вздрагивания и отдельные броски самолета, сопровождающиеся большими частыми кренами и рысканьем. Изменение высоты, частые и резкие перегрузки затрудняют использование автопилота. Отмечается неустойчивая работа вариометра и указателя скорости. Установившийся режим полета нарушается по высоте и курсу. При больших отряпательных перегрузках ощущается нехватка, а при положительных, наоборот, сильное прижатие к креслу	(20) Пилотирование выполняется в соответствии с рекомендациями по летной эксплуатации в условиях болатанки для каждого типа самолета	(21) Незакрепленные предметы начинают смещаться. Ходящие по самолету могут вызвать ударом пассажиров. Необходимо пристегивание пассажиров ремнями. Иногда переломится большинство элементов экипажа и пассажиров и утомляет экипаж

Table 7.1 (Cont'd).

(3) Название	(4) Идентификатор по плану, базе		(6) Диапазон перегрузок в г примененный в зоне g	(7) Характеристика положения самолета в баллистике	(8) Рекомендации по пилотированию	(9) Характеристика комфорта пассажирам
	(2) общее	(5) ИКАО				
(12) Шторковая или общая система бортанки	(4) общее	(5) ИКАО	(6) $-0.1 < n < 2.1$ $\Delta n \pm 1.1$	(7) (23) Исключительно резкие броски самолета, сопровождающиеся большими перегрузками, сильно пружинающиеся или отрывающиеся от кресла. Подлет происходит с большими отклонениями по высоте и курсу, нарушается установившийся режим полета. Показания вариометра и указателя скорости сильно искажаются. Положение самолета в пространстве определяется средним положением планки лампозонита. Ухудшается управляемость самолета, и воздушным действиям пилота может быть создан режим по скорости, опасный для прочности самолета	(8) (24) Пилотирование самолета стро-го в соответствии с руково-дством по летной эксплуатации в условиях бо-латанки	(9) (25) Вызывает ощущение от-красел и заклинивание кресла, а при воз-можных перегруз-ках затянное прижа-тие к креслу. В слу-чае же прерывистых рывков пассажиры могут получить сли-шком сильные травмы. Резкие и большие перегрузки вызывают у пасса-жиров болевые явления

Remark. Maintaining flight speed regimes and monitoring instrument readings is carried out in accordance with manuals on flight operation for each type of aircraft.

KEY: (1) Intensity, marks; (2) designations; (3) nomenclature; (4) Soviet; (5) ICAO; (6) Range of overloads and increments in fractions of g; (7) Characteristics of behavior of aircraft in turbulence; (8) Piloting recommendations; (9) Effect on passengers; (10) Weak turbulence; (11) Individual events of mild shaking of aircraft; (12) Flight on autopilot; (13) If prolonged causes discomfort for some passengers; (14) Moderate turbulence; (15) Frequent jerks, connected with rocking of the aircraft and a change in altitude, but not causing difficulties in pilot- ing. Noticeable vibrations of instrument indicators are observed on the pilot panel: vari- ometer and speed indicator in particular. Steady-state flight regime is maintained; (16) Flight on autopilot is permitted; (17) Causes discomfort in a significant portion of the passengers and hampers movement about the airplane; (18) Strong turbulence; (19) Sharp shaking and individual jerks of airplane, accompanied by frequent rolling and yawing movements. Change in altitude, frequent and sharp overloads hamper the use of autopilot. Unstable operation of variometer and speedometer is noted. Steady-state flight regime is disrupted with respect to

KEY to Table 7.1 (Cont'd):

altitude and heading. During large negative overloads weightlessness may be perceived, while during positive overloads personnel are pressed against their seats; (20) Piloting is carried out in accordance with the manual on flight operations in turbulent conditions for each type of aircraft; (21) Loose objects begin to spill about. Moving about within the cabin can lead to passenger injury. Passenger seat belts must be fastened. Found highly unpleasant by majority of passengers; causes symptoms of airsickness and fatigues the crew; (22) Violent or extreme turbulence; (23) Extremely sharp surges of aircraft, accompanied by severe g-forces throwing people out of seats or pressing them strongly to them. Flight is accompanied by major deviations in altitude and heading; the steady-state flight regime is disrupted. Variometer and speed indicator readings are strongly distorted. Position of aircraft in space is determined by average position of artificial horizon strip. Aircraft controllability is poor and incorrect action by the pilot may create conditions leading to speeds which threaten the structure of the aircraft; (24) Piloting in strict accordance with the manual on flight operation under turbulent conditions; (25) Passengers may be pulled from the seat and suspended on the belts, while during positive g-forces they will be pressed tightly to the seats. If the seat belts are not fastened passengers may receive serious head injuries and traumas. Sharp large-scale g-forces cause airsickness in the majority of passengers.

If the turbulence of the atmosphere is statistically uniform and isotropic, it is sufficient for its description to know the two correlation functions $R_u(\Delta x)$ and $R_w(\Delta x)$, where the first is the correlation function of pulsations of the longitudinal wind-velocity component, while the second is the correlation function of pulsations in the transverse component. In aerodynamic calculations it is assumed that

$$R_u(\Delta x) = \sigma_u^2 e^{-\frac{\Delta x}{L}} \quad (7.2)$$

where L is a certain average size of turbulent perturbations, determined as the distance at which reduction of the correlation function by a certain number of times occurs, most frequently down to a magnitude half the value at $\Delta x = 0$. From the continuity equation it follows that for a three-dimensional vector field the connection between the correlation functions for the longitudinal and transverse components of wind velocity pulsations has the form (see, for example, Landau and Lifshitz, 1953)

$$R_w(\Delta x) = R_u(\Delta x) + \frac{\Delta x}{2} R'_u(\Delta x), \quad (7.3)$$

therefore

$$R_w(\Delta x) = \sigma_w^2 \left[1 - \frac{\Delta x}{2L} \right] e^{-\frac{\Delta x}{L}}. \quad (7.4)$$

The following spectral densities correspond to correlation functions (7.2) and (7.4):

$$S_u(\Omega) = \sigma_u^2 \frac{L}{\pi(1 + \Omega^2 L^2)}, \quad (7.5)$$

$$S_w(\Omega) = \sigma_w^2 \frac{L(1 + 3\Omega^2 L^2)}{\pi(1 + \Omega^2 L^2)^2}, \quad (7.6)$$

where Ω is the wave number.

If we assume that turbulence is isotropic, strictly speaking the longitudinal correlation function is described by the expression

$$R_u(\Delta x) = \sigma_u^2 \left[1 - \frac{A}{2} (\Delta x)^2 \right],$$

and not by expression (7.2). Here $A = \frac{c\epsilon^{1/2}}{\sigma_u^2}$, where ϵ is the rate of turbulent energy dissipation and c is a universal dimensionless constant having the order of unity. However, the assumption made above that the longitudinal correlation function is exponential satisfactorily approximates, from the practical point of view, the experimental correlation functions obtained from the aircraft.

When formula (7.6) is used to describe the energy spectrum of pulsations of the vertical wind velocity component in various types of aviation calculations the scale of turbulence L is determined as

$$L_w = \int_0^{\infty} R_w(\Delta x) d(\Delta x) \quad (7.7)$$

or, with consideration of (7.3), as

$$L_u = 2 \int_0^{\infty} R_u(\Delta x) d(\Delta x) = 2L_w; \quad (7.8)$$

L_u and L_w characterize the linear dimensions of the region within which a high correlation of pulsations of flow velocity exists; they are called the longitudinal and transverse integral scales of this turbulence region.

Along with a simple relationship of the (7.2) type, for practical utilization of data on atmospheric turbulence during solution of certain aviation problems it is necessary to know the functional form of the autocorrelation function. N. I. Bulla (see J. Taylor, 1965) proposed the following functional form for a family of normalized autocorrelation functions:

$$R_u(\Delta x) = \left[\left(\frac{\Delta x}{a} \right)^2 / 2^{n-1} (n-1)! \right] K_n \left(\frac{\Delta x}{a} \right), \quad (7.9)$$

where a and n are parameters which determine the form and scale; K_n is the Bessel function of an imaginary argument of the second kind; $(n-1)!$ is a gamma function when n is not a whole positive number.

By substituting expression (7.9) into (7.7) and (7.3), we obtain the following expressions for the integral scale of turbulence:

$$L = \frac{\sqrt{\pi} \left(n - \frac{1}{2} \right)!}{(n-1)!} a \quad (7.10)$$

and the transverse autocorrelation function

$$R_w(\Delta x) = \frac{\left(\frac{\Delta x}{a} \right)^n}{2^n (n-1)!} \left[2K_n \left(\frac{\Delta x}{a} \right) - \frac{\Delta x}{a} K_{n-1} \left(\frac{\Delta x}{a} \right) \right]. \quad (7.11)$$

If $R_u(\Delta x)$ and $R_w(\Delta x)$ are known, by using the Fourier transform it is possible to find the expressions for the function of spectral density:

$$S_u(\Omega) = \frac{4\pi^2 L}{(1 + 4\pi^2 \Omega^2)^{n+\frac{1}{2}}}, \quad (7.12)$$

$$S_w(\Omega) = \frac{2\pi^2 L [1 + 8\pi^2 \Omega^2 (n+1)]}{(1 + 4\pi^2 \Omega^2)^{n+\frac{3}{2}}}.$$

where

$$a = \frac{L(n+1)!}{1 \pi \left(n - \frac{1}{2}\right)!} \quad (7.13)$$

Thus the turbulence spectrum is determined by only two quantities - scale L and the parameter n.

In aerodynamics, in particular, two models of families of autocorrelation functions and the functions of spectral density are considered: the Dryden model, for which $n = 1/2$, and the Kármán, for which $n = 1/3$.

For the first model,

$$L = a, \quad (7.14)$$

$$S_w(\Omega) = \frac{4a^2 L}{1 + (2\pi a \Omega)^2}, \quad (7.15)$$

$$S_w(\Omega) = \frac{2a^2 L [1 + 3(2\pi a \Omega)^2]}{[1 + (2\pi a \Omega)^2]^2}, \quad (7.16)$$

while for the second model

$$a = L \frac{\left(-\frac{2}{3}\right)!}{1 \pi \left(-\frac{1}{3}\right)!} = 1,339L, \quad (7.17)$$

$$S_w(\Omega) = \frac{4a^2 L}{[1 + (2\pi (1,339L) \Omega)^2]^{5/6}}, \quad (7.18)$$

$$S_w(\Omega) = \frac{2a^2 L \left[1 + \frac{8}{3} (2\pi (1,339L) \Omega)^2\right]}{[1 + (2\pi (1,339L) \Omega)^2]^{11/6}}. \quad (7.19)$$

It should be noted that autocorrelation functions described by formulas (7.2) and (7.4) correspond to the Dryden model. The Kármán model, for which $n = 1/3$, coincides with the model for which the "minus 5/3" law is valid. Therefore formulas (7.18)-(7.19) satisfactorily describe turbulent motions for conditions of indifferent thermal stratification of the atmosphere.

Formulas (7.14)-(7.19) are widely used in aerodynamic calculations. It should, however, be emphasized that in the end they are approximate and cannot completely replace the actual spectra of atmospheric turbulence.

In order to use expression (7.19), which describes the spectral density of pulsations of the vertical wind-velocity component, in various practical problems it is necessary to know the characteristic magnitude L of the scale of turbulence. This quantity has been determined by many investigators by approximation of the empirical functions of spectral density through expression (7.19) and by selection of the corresponding value of L in this case for each curve $S_w(\Omega)$.

As studies have shown, scale L for pulsations of the vertical wind-velocity component generally grows with altitude in the atmospheric layer up to a height of 300-500 m. Above a smooth surface and in conditions of indifferent or unstable thermal stratification the scale L approximately equals the altitude above the surface, while above a broken surface it is approximately double the altitude; in both cases the mean square deviation comprises about 25-30% of the average value of L . The indicated dependence of L on altitude above the surface of the earth, as indicated by experimental data, cannot be extrapolated to altitudes exceeding 300-500 m. At high altitudes the scale of L varies in wide limits and demonstrates a complex dependence on the thermal and wind stratification of the atmosphere.

Experimental studies of turbulence on TU-104 and IL-18 aircraft made it possible to establish tentative intervals of the magnitude of spectral density corresponding to buffeting of aircraft with different intensities. These intervals $S(\Omega)$ were established for that high-frequency portion of the spectrum in which, apparently, the "minus 5/3" law is always realized - i.e., for the region of wave numbers $\Omega \geq 10^1$ rad/km. In this case in order to evaluate the intensity of aircraft turbulence it is sufficient to indicate the intervals of values of spectral density for any one wave number - in particular, for $\Omega = 10^1$ rad/km, presented in Table 7.2.

Table 7.2. Dependence of intensity of aircraft turbulence on $S(\Omega)$ for $\Omega = 10^1$ rad/km.

(1) Интенсивность волнения самолета	(2) σ	(3) $S(\Omega) \left(\frac{\text{km}}{\text{h}} \right)^2 / \frac{\text{m}^2}{\text{km}}$
Слабая (2)	$\sigma^{(1)}$	$\sim 4 \cdot 10^{-1} - 2 \cdot 10^0$
Умеренная (3)	$\sigma^{(2)}$	$2 \cdot 10^0 - 4 \cdot 10^0$
Сильная (4)	$\sigma^{(3)}$	$4 \cdot 10^0 - 10^1$
Очень сильная (5)	$\sigma^{(4)}$	$> 10^1$

KEY: (1) intensity of aircraft turbulence; (2) Weak; (3) Moderate; (4) Strong; (5) Extreme; (6) $S(\Omega)(\text{km/h})^2/(\text{rad/km})$.

§ 2. CHARACTERISTICS OF TURBULENCE IN THE TROPOSPHERE AND IN THE LOWER STRATOSPHERE

In recent years in many countries (USSR, USA, England, Canada, and others) a great deal of attention has been focused on the study of turbulence as it influences aircraft flight. These studies are of practical significance, especially as regards flight safety. In turn, by using aircraft as turbulence indicators it has been possible (as was shown in the preceding chapters) to study in more detail disorderly motions of air in the atmosphere.

In addition to materials gathered with special flights on aircraft equipped with measuring instruments, turbulence data has been collected from crews of scheduled airliners.

Certainly, instrument materials have the greatest value - especially in the case of continuous recording of measurement results. A major drawback in visual observations is the subjectivity in evaluation of turbulence intensity, since the evaluation depends on the physiological peculiarities and flight experience of the aircraft crew. This is clear from Table 7.3, which shows the g-forces measured by accelerograms and the agreement (in %) of visual evaluations of turbulence intensity made by the crew (N. S. Pinus, 1955).

Table 7.3. Connection between the intensity of turbulence as evaluated by pilots and g-forces acting on the airplane.

(1) Приращение перегрузки в долях g	(2) Интенсивность турбулентности по оценке пилотов		
	слабая (1)	умеренная (2)	сильная (3)
0,1-0,2	71	24	5
0,2-0,3	53	40	7
0,3-0,5	—	78	22
0,5	—	—	100

KEY: (1) g-force increments in fractions of g; (2) Turbulence intensity as evaluated by pilot; (3) weak; (4) moderate; (5) strong.

With aircraft overloads not exceeding 0.2g, i.e., during weak buffeting (see Table 7.1), pilots frequently evaluate turbulence as moderate (24% of cases) or even as strong. In 22% of the cases pilots evaluate atmospheric turbulence with g-forces of 0.2-0.5g - i.e., moderate - as strong turbulence. Thus visual observations, as a rule, lead to overstated frequency of moderate and strong turbulence.

In order to obtain reliable data on turbulence in the upper troposphere, N. Z. Pinus and S. N. Shmeter (1962) utilized the results of special research flights on TU-104, IL-18, and IL-28 aircraft, along with accelerograms from numerous scheduled flights on aircraft of these types. During processing those segments of the recordings which were distorted by maneuvering of the aircraft were eliminated.

We will examine the particular features of the vertical distribution of turbulence and certain parameters of turbulent zones.

1. Frequency of Occurrence of Turbulence at High Altitudes

With respect to the nature of turbulence, the frequency of its occurrence, etc., the troposphere can be divided into the following layers: lower (0-2 km), middle (2-6 km), and upper (6-10 km). It is also possible to examine the troposphere and stratosphere separately.

From Fig. 7.1, constructed from data of aircraft observations, it is clear that the frequency of turbulence is maximum in the lower layer of the troposphere and minimum in the middle troposphere. Subsequently it grows with approach to the tropopause or to the level with maximum wind velocity. The maximum frequency of buffeting is found at altitudes of 8-12 km, where the frequency comprises 5-20%.

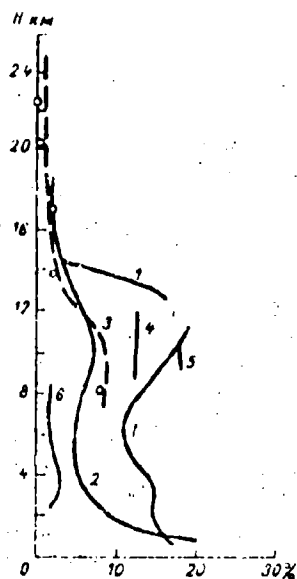


Fig. 7.1. Frequency of turbulence at different altitudes. 1 - USSR, southern latitudes; 2 - USA; 3 - USA (U-2 data); 4 - USSR, middle latitudes; 5 - on London - Far East and London - North Africa routes; 6 - over the North Atlantic.

It should be noted that the results of determining the frequency of turbulence affecting aircraft depends on the nature of the flights. Thus, for example, piston aircraft which are normally used on short routes and which fly at comparatively low altitudes find themselves in turbulence more frequently than aircraft flying on long routes and at high altitudes. This is evident from Fig. 7.2, which shows the quantity of overloads encountered by piston aircraft on local, short and long-range airlines in the USA on flights totalling $16 \cdot 10^6$ km. Table 7.4 gives the average duration of a single flight and the altitude of the flight.

As is evident from the table, at an altitude of 5 km at average flight duration equaling 3 h a transport aircraft experiences an increment of g-forces exceeding 0.5, 50% times less frequently than aircraft on local lines flying at 1000-1200 m.

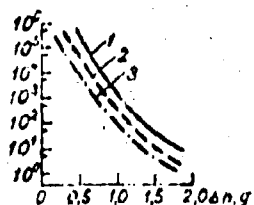


Fig. 7.3. Quantity of overloads encountered by aircraft during $16 \cdot 10^6$ km of flights: on local lines (1), short lines (2) and long distances (3).

Table 7.4. Characteristic duration and altitude of piston aircraft flights.

(1) Название	(2) Продолжительность полета, часы	(3) Высота полета, м
Местная (4)	0,5	1200
Короткая (5)	1,0	2100
Дальняя (6)	3,0	3000

KEY: (1) Air route; (2) Flight duration, h; (3) Flight altitude, m; (4) Local; (5) Short; (6) Long.

Turbulent zones in the atmosphere are characterized by the fact that their horizontal extent is many times greater than their thickness. Therefore it is less likely that an aircraft will penetrate a turbulent zone during horizontal flight than during vertical probing of the atmosphere (including climb of scheduled aircraft or during descent for landing). Besides this, one should consider that during a climb and descent the dynamic stability of the aircraft is somewhat lower than that during horizontal flight.

According to data compiled by V. N. Buvshkin (1966), turbulence was encountered 2-3 times more frequently by scheduled TU-104 aircraft during climb and (especially) descent than on the horizontal segments of flight.

We will turn now to consideration of Fig. 7.1. Curve 1 characterizes the frequency of turbulence according to data of vertical sounding of the atmosphere in the southern latitudes of the USSR, while curve 2 represents this figure above the USA according to data obtained from U-2 flights. This same figure shows data developed by

E. A. Hyde (1954) for the London - Far East and London - North Africa routes, and also data for the North Atlantic compiled by A. F. Crossly (1961).

Over the middle latitudes of the USSR the frequency of turbulence at altitudes of 8-12 km comprises an average of 11.7%. It is lower than the frequency of turbulence at the same altitudes in the northern regions of the USSR, where the average value is 15-16%. This estimate is close to Hyde's data for the London - North Africa and the London - Far East routes, passing through Rome, Cairo, Karachi, or Delhi. Of particular interest is the low frequency of turbulence suffered by aircraft at altitudes of 2-8 km over the North Atlantic, obtained by Crossly from data of more than 15,000 reports by transport aircraft crews. At altitudes of 3-4 km in January it averaged 4.7%; in July the average was 2.1%, while at altitudes of 7-8 km the corresponding values were 3.1 and 1.0%.

Curves 1 and 4 indicate the frequency of turbulence causing aircraft buffeting in the stratosphere. As we see, in this case the frequency of turbulence drops quite rapidly with altitude: from aircraft ascent data it does not exceed 3-4% at altitudes of 14-15 km above the southern USSR, while from U-2 flight data gathered over the USA it comprises about 2.5%, diminishing to 0.5-0.1% at altitudes of 18-23 km. Table 7.5 presents the results of observations carried out in the USA (Steiner, 1965) on the U-2 aircraft; these were used to construct curve 4 on Fig. 7.1.

Table 7.5. Frequency of turbulence according to data collected on U-2 flights.

(1) Высота, км	(2) Общая дальность, тыс. км	(3) Полет в турбулентных зонах	
		(4) тыс. км	%
6-9	30,86	2,41	7,9
9-12	12,62	3,03	9,4
12-15	19,91	2,60	2,5
15-18	229,09	4,53	1,9
18-21	928,86	5,22	0,5
21-23	11,32	0,014	0,1

KEY: (1) Altitude, m; (2)
Total distance flown, 1000 km;
(3) Flight in turbulent zones;
(4) 1000 km.

It should be noted that curve 1 on Fig. 7.1 was constructed mainly from flight observations. The distribution of turbulence frequency with altitude for winter may differ from this curve due to seasonal differences in the temperature and wind-velocity profiles in the troposphere and lower stratosphere.

In this connection the data collected by V. N. Barakhtin (1966) on the seasonal variation in aircraft turbulence frequency on the Moscow - Khabarovsk route are of great interest; these were obtained from accelerograms of more than 10,000 flights by TU-104 aircraft. The calculations include only measurements on horizontal segments of the flights.

From Table 7.6 it is clear that over the entire route the frequency maximum occurs in the summer and the minimum occurs in the winter, with the exception of the Moscow - Omsk segment, for which the minimum occurs in the spring. In the upper troposphere, where the major portion of the flights were carried out, the frequency of turbulence affecting the aircraft was 2.4-3.6 times greater in summer than in winter.

Table 7.6. Frequency (in %) of turbulence as a function of season on the Moscow - Khabarovsk route.

(1) Участок трассы	(2) Зима	(3) Весна	(4) Лето	(5) Осень	(6) В среднем
Москва-Омск (7)	3,2	2,1	7,6	4,1	4,2
Омск-Иркутск (8)	2,4	3,8	8,5	1,0	4,7
Иркутск-Хабаровск (2)	5,2	8,1	12,4	7,6	8,3

KEY: (1) Section of route; (2) Winter; (3) Spring; (4) Summer; (5) Fall; (6) Average; (7) Moscow - Omsk; (8) Omsk - Irkutsk; (2) Irkutsk - Khabarovsk.

Studies of turbulence up to an altitude of 20 km above Moscow, carried out by V. P. Bolyayev, et al. (1965) by means of g-measuring radiosondes (see Chapter 7), showed that during the winter the frequency of moderate and strong turbulence in the middle and upper troposphere is small, while in summer it is comparatively great. The reverse picture is observed in the stratosphere.

Aircraft measurements carried out above the USA (Colson, 1963) also showed that turbulence is most probable in the stratosphere in the period January-March.

b. Intensity of Turbulence

As was already stated, the intensity of turbulence is evaluated approximately from the magnitude of g-forces experienced by the aircraft (i.e., in terms of the effective velocity of vertical air gusts). Outside of storm clouds aircraft overloads rarely exceed 0.9 g. However, in one of [several] flights on a "Comet" aircraft carried out in a clear turbulent zone, C. S. Hislop (1951) observed overload increments (Δn) reaching ± 1.5 g. H. H. Bindon (1951) described the case of an experimental flight in a clear turbulent zone of Canada at an altitude of 7.3 km in which $\Delta n \approx 3$ g. During this flight many measuring instruments were rendered inoperative. In the USA a case was recorded in which the rudder fin and elevator of a "Boeing B-52H" aircraft were damaged when the plane entered a turbulent zone in a clear sky above a mountainous region.

At altitudes of 8-12 km in the middle latitudes over the USSR no cases were noted in which the magnitude of Δn was greater than ± 1.0 g during flights on a TU-104 aircraft in a clear atmosphere. The results of these investigations (Pinus and Shmeter, 1962) are given in Table 7.7. Even the g-force increments reaching ± 1.0 g were observed only in individual cases.

Table 7.7. Frequency of turbulence intensity (in %) in clear air at altitudes of 8-12 km in the middle latitudes.

$\sigma^{(1)} + \sigma^{(2)} + \sigma^{(3)}$	$\sigma^{(1)}$	$\sigma^{(2)}$	$\sigma^{(3)}$
11.7	5.7	5.6	0.4

Some idea of the dependence of turbulence intensity on altitude and weather conditions for US territory can be obtained from Fig. 7.3. This figure makes it possible to evaluate the probability of exceeding a given magnitude of σ_w . Considering turbulence to be very weak if

$\sigma_w \leq 0.5$ m/s and to be strong when $\sigma_w \geq 2.5$ m/s, we can draw the following conclusions on the basis of Fig. 7.3.

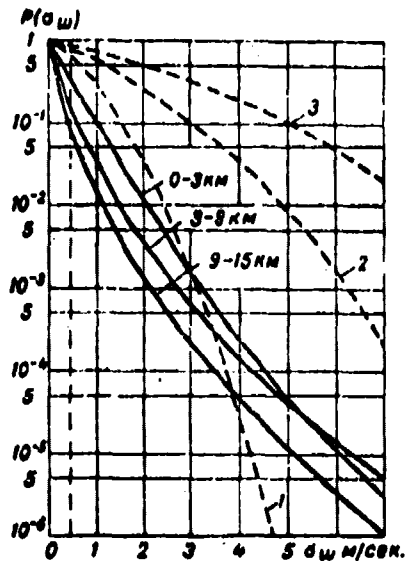


Fig. 7.3. Distribution of dispersion of pulsations of vertical wind movement velocity. 1 - clear weather; 2 - woolpack clouds; 3 - thunderstorm clouds.

Designation: m/сек = m/s.

With an increase in altitude the probability of values of $\sigma_w \leq 0.5$ m/s grows. Where the probability of such values of σ_w is about 70% in the atmospheric layer 0-3 km, for the layer 9-15 km it grows to 93%. Extremely strong turbulence ($\sigma_w > 4$ m/s) has virtually identical probabilities in the 0-3 and 3-9 km layers, but it is substantially less for the 9-15 km layer.

In clear weather the probability of flights with $\sigma_w < 0.5$ m/s is greater (50%), while under thunderstorm conditions it is, on the other hand, least ($\approx 20\%$). With the same value of the probability distribution function the quantity σ_w is double the clear weather value for woolpack clouds and approximately triple that value for thunderstorm conditions.

Similar results were obtained (Kulik and Sakach, 1967) for the territory of the Soviet Union (Fig. 7.4). From this figure it is clear that for $\sigma_w \geq 3$ m/s the probability distribution function in a zone of thunderstorm activity is approximately six times greater than that in turbulent zones above mountains and is $3 \cdot 10^3$ times greater than that in a cloudless sky in turbulent zones of jet streams.

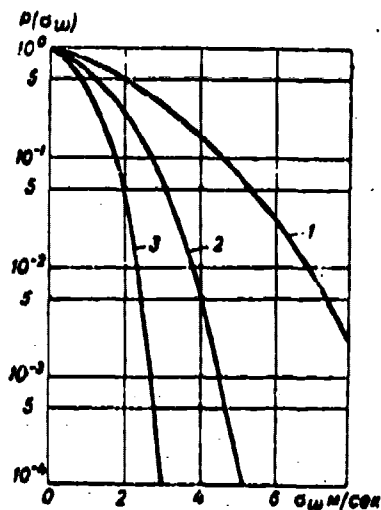


Fig. 7.4. Distribution of dispersion of vertical air movement velocities. 1 - thunderstorm clouds; 2 - above mountains; 3 - in the jet-stream region.

Designation: σ_w m/sec =
= m/s.

Data on the intensity of turbulence in the stratosphere are of special interest. From Table 7.8 it is clear that in the 12-21 km layer strong turbulence is observed most frequently at altitudes of 15-18 km. Judging from the number of turbulent zones, this is where the greatest frequency of turbulence is observed.

c. [Vertical] Thickness of Turbulent Zones

Numerous observations have shown that turbulent layers in which effects of turbulence are noted on aircraft have comparatively sharp

boundaries. This can apparently be explained by the fact that turbulent conductivity is small on the boundary of perturbed layers (Gandin et al., 1955); this is characteristic for completely or nearly completely unperturbed regions surrounding a turbulent zone in which aircraft experience buffeting.

Table 7.8. Frequency and Intensity of turbulence in the stratosphere above the USA (Colson, 1963).

(1) Высота, км	(2) Количество полетов	Количество полетов в турбу- лентных зонах	Встречено турбулент- ных зон (4)	Количество зон в одном полете (5)	(6) Повторяемость интенсивности, %		
					$\delta^{(1)}$	$\delta^{(2)}$	$\delta^{(3)}$
12-15	35	21	27	1,39	25,4	28,8	4,8
15-18	139	71	135	1,90	20,9	21,9	8,2
18-21	228	78	142	1,82	18,7	12,9	2,4

KEY: (1) Altitude, km; (2) No. of flights; (3) No. of flights in turbulent zones; (4) Turbulent zones encountered; (5) No. of zones in one flight; (6) Intensity frequency, %.

The data on the thicknesses of turbulent zones presented by different authors are quite close. Figure 7.5 shows curves of the integral frequency of thicknesses of turbulized layers for different latitudes over the territory of the Soviet Union. The same figure shows the curve of frequency of thicknesses of layers at altitudes of 5.5-13.5 km over Canada (Clodman, 1953). It is clear that with a drop in latitude the frequency of relatively large thicknesses of turbulent layers increases. Where a thickness less than 1000 m is observed in approximately 70% of cases in the southern latitudes of the Soviet Union, in the middle and high latitudes this value is seen in 85-90% of the cases.

We will note that data from American investigators indicate that the thickness of turbulent layers during flight in clear air at altitudes from 3 to 15 km is, as a rule, less than 300 m. More recent studies carried out on the U-2 aircraft showed that the thickness of turbulent layers in the stratosphere above the USA comprises, on the average, 500-1000 m. Certain authors (Press, Schindler, and Tompson, 1953; Clodman, 1953) consider that moderate and strong turbulence is, as a rule, observed in layers of greater thickness than

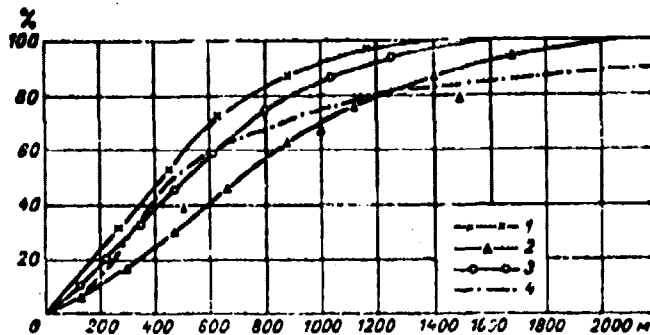


Fig. 7.5. Integral frequency of different thicknesses of turbulent layers. 1 - northern latitudes; 2 - middle latitudes; 3 - southern latitudes; 4 - Canada.

weak turbulence. Others (Shmeter, 1958), on the other hand, arrive at the conclusion that the more intensive the turbulence, the less the thickness of the turbulent layer. This question requires further investigation. Apparently, these connections depend substantially on specific conditions of the formation of turbulence in a free atmosphere.

d. Horizontal Dimensions of Turbulent Zones. Structure of Turbulent Zones

The determination of the horizontal extent of turbulent zones is connected with well-known difficulties, since the aircraft may cross them in different directions and at arbitrary distances from the center of the horizontal section of such zones. Besides this, up to now the precise shape of the horizontal section of turbulent zones is not known. Certain authors indicate that in jet streams the turbulent zones are extended in the direction of air flows: their length is greater than their width.

Analysis of accelerograms made it possible to determine, along with the intensity of turbulence in each flight, the horizontal extent of the turbulent zones and the nature of turbulence on their boundaries. It was found that at altitudes of 8-12 km turbulent zones of two types are encountered: solid (type I) and interrupted (type II).

Interrupted zones consist of several local solid turbulent segments between which aircraft flight is calm. The number of local turbulent segments in turbulent zones of type II varied from two to seven, but in 79.5% of the cases it did not exceed three.

The frequency of continuous turbulent zones in the middle latitudes (31.8%) is approximately half that of solid zones (68.2%).

As is evident on Fig. 7.6, in the middle latitudes the horizontal extent of turbulent zones of type I ($\Delta_1 L$) is less than 60 km in 83.3% of the cases and is greater than 100 km in only 7.5%. The distribution of horizontal dimensions of local turbulent zones in turbulent zones of type II (ΔL) is virtually the same. Specifically, in 86.6% of the cases these zones are less than 60 km in extent, and they exceed 100 km in only 6.6% of the cases.

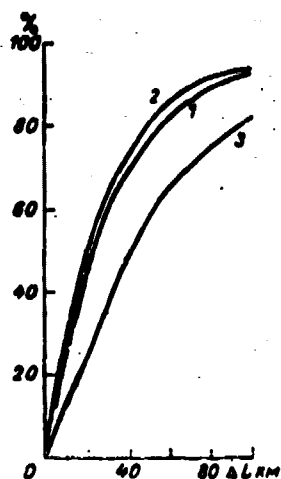


Fig. 7.6. Integral frequency of horizontal dimensions of continuous turbulent zones (1) local turbulent zones (2), and unperturbed zones (3) in interrupted turbulent zones.

Curve 3 on Fig. 7.6 characterizes the total frequency of horizontal dimensions of calm segments ($\Delta_1 L$) located between turbulent zones (ΔL). Comparison of this curve with curve 2 on the same figure shows that the quiet segments most frequently have greater dimensions than the turbulent sections.

The conditions for the appearance of interrupted turbulent zones are as yet not clear. It is possible that they are connected with loss of stability of atmospheric waves or that they reflect particular

features of the intermittence or degeneration of turbulence in turbulent zones. One way or another, the turbulent zones of large horizontal extent are most frequently of the interrupted type.

Analysis of accelerograms made it possible also to reveal two forms of rise of intensity of turbulent buffeting on the boundaries of turbulent zones:

a) when the intensity of buffeting on the boundary of the zone is no less than moderate;

b) when the intensity of buffeting from the boundary and into the depth of the zone grows more or less smoothly from very weak to weak or to moderate.

In the first case the entry of the aircraft into the zone of atmospheric turbulence in clear air is not only unexpected, but is also sudden; the crew must make rapid decisions concerning measures to guarantee flight safety. In the second case the crew has more time for preparation to meet the moderate or strong turbulence ahead.

In the middle latitudes the frequency of sudden entry into a turbulent zone with moderate or strong turbulence on the boundary equals 3.6%.

We will return now to the horizontal dimensions of turbulent zones. As is clear on Fig. 7.7, the length of turbulent zones varies from several kilometers up to 400-500 km and more, although they usually do not exceed 60-80 km. In the middle latitudes of the USSR the dimensions of turbulent zones were less than 100 km in approximately 72% of the cases and were greater than 400 km in only 4%; in the southern latitudes the corresponding values were 68% and 10%. Thus, the horizontal extent of turbulent zones, like their thickness, grows with a decrease in latitude.

The horizontal extent of turbulent zones encountered during U-2 flights in the stratosphere above the USA was less than 30 km in 70%

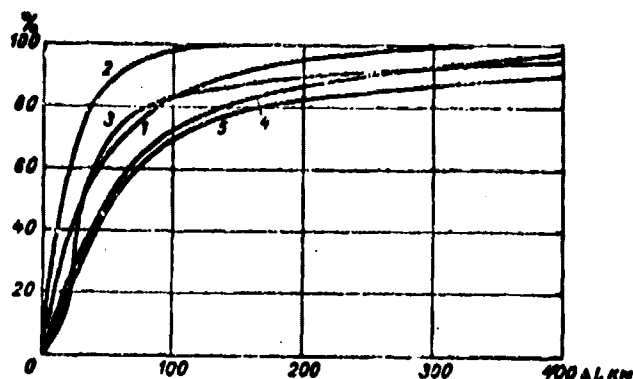


Fig. 7.7. Integral frequency of the magnitude of horizontal extent of turbulent zones. 1 - USA (upper troposphere); 2 - USA (stratosphere); 3 - USSR, middle latitudes; 4 - Canada; 5 - USSR, southern latitudes.

of the cases and greater than 100 km in only 0.5%. No clear dependence of horizontal dimensions of turbulent zones on altitude in the stratosphere was established. In general turbulent zones in the stratosphere (altitudes of 15-21 km) above the USA are apparently shorter than those in the troposphere. Thus, a value of 70% integral frequency in the upper troposphere corresponds to turbulent zone dimensions equalling 60 km, while in the stratosphere the value is 30 km for the 70% level. If we assume that this relationship is stable and reliable, it can be used to evaluate the horizontal dimensions of turbulent zones in the stratosphere above other geographic regions if we have data on their dimensions in the upper troposphere.

e. Life Expectancy of Turbulent Zones

An important characteristic of turbulent zones is the duration of their existence. Experimental studies of the "lifetimes" of these zones require continuous tracing of the evolution of turbulence within them. Such tracing is hampered by the fact that under cloudless conditions turbulent zones cannot be distinguished visually and, in addition, they move along with the flow.

To determine the duration of existence of turbulent zones it is usually necessary to carry out multiple flights between geographic

control points. This permits determining the survival time of turbulence in a flow of air between these points; this factor apparently depends both on the variability of the turbulence and on the dimensions of the turbulent segments. These data are extremely useful for evaluating the applicability of forecasts of turbulence duration from data on preliminary weather reconnaissance.

Figure 7.8 shows the results of observations of turbulent atmosphere carried out by N. Z. Pinus and S. M. Shmeter (1962) on May 14, 1960 between Nizhne-Tambovskoye and Yelabuga in the Far East. The wind was almost perpendicular to the line joining these points. Observations at 7200 m were carried out in the course of 1 h 40 min. Since wind speed at this altitude was 85 km/h, a flow with a "length" of 145 km proceeded between these points during the observation period. During this time, as is evident from Fig. 7.8, the nature of turbulence and its distribution between the control points were virtually unchanged. Observations at 8200 m were carried out with a break in time equalling 2 h 46 min. The average wind velocity at this altitude was 120 km/h and a flow 366 km long ran between the control points; as we see, the nature of turbulence was strongly variable.

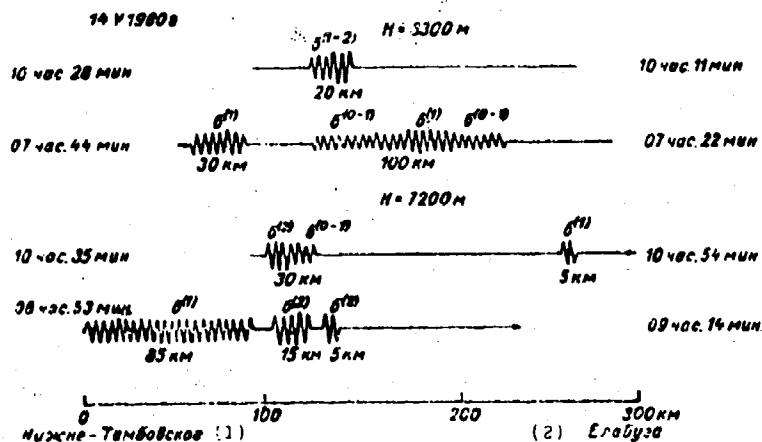


Fig. 7.8. Nature of turbulence during repeated flights of an aircraft between points.

KEY: (1) Nizhne-Tambovskoye; (2) Yelabuga.

Designations: час. = h; мин = min.

According to experimental data presented by V. N. Barakhtin (1963), at altitudes of 8-10 km the turbulent regime can sometimes remain unchanged for 24 h or more.

Observations made with radiosondes equipped with overload attachments can give some idea of the "lifetime" of turbulence over specific points. V. P. Belyayev et al. (1964) carried out several series of launches of such radiosondes at launch intervals of 1 to 3 h. It was found that the probability of invariability of the turbulent state of the atmosphere in the course of an hour in the 8-12 km layer is on the order of 80-90%. In the course of 1.5, 3, 6 h in the middle and upper troposphere the probability that the "turbulence situation" will remain unchanged equals 60-75%; at high altitudes (12-20 km) this value does not exceed 50%. For time intervals greater than 6 h this probability does not exceed 50% at virtually all altitudes.

Close to the tropopause and the level of the tropospheric maximum of wind speed the probability that the state of the atmosphere will remain unchanged turned out to be equal to 70%.

§ 3. TURBULENCE IN JET STREAMS AND IN THE TROPOPAUSE ZONE

If we exclude from consideration flight in clouds in the upper troposphere, the highest frequency of buffeting and the maximum overloads are observed in jet streams and close to the tropopause. It is here that observations of the so-called clear-air turbulence occur most frequently; encounter with CAT is the most dangerous for the pilot, owing to its unexpected nature.

We will pause first on buffeting in jet streams. Since buffeting differs in different sectors of these streams, we will present a brief outline of the aerological structure of the jet stream.

a. Frontal Structure of Jet Streams

The results of investigations of the aerological structure of jet streams carried out on the basis of materials from standard

aerological observations have been generalized by V. I. Vorob'yev (1960), E. Reiter (1961), V. A. Dzherdzhio and N. V. Petrenko (1964).

In a number of countries special flight studies of jet streams have also been carried out. Principal results from these are outlined in the works by R. M. Endlich and C. S. McLean (1957, 1965), K. C. Brundidge and J. L. Clodman (1962), N. Z. Pinus and S. M. Shmeter (1962), and J. Briggs and W. Roach (1963). In particular, in the USA experimental studies were carried out in the project "Jet Streams" (Endlich and McLean, 1957, 1965) on two aircraft (B-29 and B-47) equipped with instruments recording the temperature and pressure of the air, aircraft g-forces, and also Doppler installations for measurement of wind speed and direction.

The experimental data showed that in the lower latitudes the jet streams have a frontal structure. In the upper troposphere the front, called the jet-stream front, separates warm air from colder. It is outlined well dropping downward from the tropopause to an altitude of 5-3 km. The axis of the jet stream is located in warm air, in the sector between the frontal surface and the tropical tropopause.

The horizontal and vertical wind-speed gradients on the cold (cyclonic) side of the jet stream are greater than those from the warm side. In particular, the horizontal gradients of wind velocity are approximately 1.5 times greater than on the warm (anticyclonic) side. They are reduced along the horizontal on both sides from the core of the jet stream.

A broad complex of experimental studies of jet streams was carried out in the USSR (see Pinus, Shmeter, 1962). The studies were carried out on TU-104 and IL-18 aircraft equipped with instruments for recording wind speed and direction (by the Doppler method), the temperature and pressure of the air, aircraft g-forces, and angles of pitch and bank.

The flights were carried out over the European territory of the Soviet Union, the Far East, and in Middle Asia. They were made most

frequently across the jet stream, with each experiment accomplishing 4-6 horizontal passes through the jet stream, each having an extent of 300 to 500 km. The data obtained on temperature and wind measurements, along with radiosond materials from observations at aerological points located along the route of the experimental flights, were used to construct vertical sections of the atmosphere.

The studies showed that even in the middle latitudes the jet streams have a frontal structure, where it is possible to examine two models of jet streams. The first describes a jet stream which is connected with frontal activity encompassing the entire thickness of the troposphere - i.e., from the tropopause down to the surface of the earth. The second model differs from the first in that the jet stream in it is connected with frontal activity which is distinctly expressed only in the upper half of the troposphere. In particular, the experimental studies showed that in the upper troposphere in the Far East the transition zone between warm and cold air masses acts as a front which is clearly expressed due to the great horizontal and small vertical temperature gradients. The upper portion of this front is adjacent to the tropopause in a zone of discontinuity or of a sharp slope of the latter, while the lower part is usually traced down to a level of 400-500 mb. A front connected with a jet stream which corresponds to the second model may have different slopes to the horizontal. In the Far East jet-stream fronts have a slope to the horizontal ranging from $1/225$ to $1/150$. It is interesting that when the slopes are small the front is extended so that its lower portion forms an almost horizontal layer with a temperature inversion.

From Fig. 7.9, which presents an averaged vertical cross section of a jet stream, it is clear that even in the middle the horizontal contrasts of temperature in the frontal zone connected with the jet stream reached 2.5° per 100 km. The isolines of relative velocity are also most compressed in the zone of the front, as can be seen from Fig. 7.9. Wind speed diminishes by approximately 50% in the layer 3-4 km above the axis of the jet stream. The horizontal contrasts in wind speed on the cold side of the jet stream are larger than those on the warm side, where in general they are not particularly great.

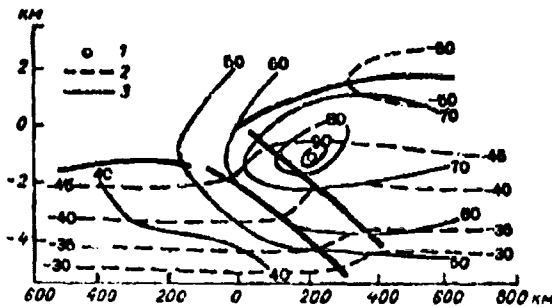


Fig. 7.9. Vertical cross section of a jet stream. 1 - stream axis; 2 - isotherms (in degrees); 3 - relative isotacs (in %).

Empirical data (Pinus, 1961) showed that the change in wind velocity with altitude under the level of maximum wind speed and also above it can be described by the exponential function

$$u_z = u_0 e^{-\alpha |z - z_0|}, \quad (7.20)$$

where z_0 is the height of the level with maximum wind velocity u_0 . The change in wind velocity in the horizontal plane relative to the jet-stream axis can be described similarly (Pinus, Litvinova, 1965):

$$u_y = u_0 e^{-\beta |\Delta y|}. \quad (7.21)$$

We should note that in a number of cases, particularly on the anticyclone side of jet streams, wind speed diminishes linearly with distance from the axis or from the velocity maximum. However, this does not destroy the generality of the approximation, since expression (7.21) can be written approximately in the form

$$u_y = u_0 (1 - \beta |\Delta y|). \quad (7.22)$$

If we limit ourselves to the first two terms of the expansion of the quantity $\exp(-\beta |\Delta y|)$ in the series. Such an approximation introduces an error not exceeding, on the average, 10% when $|\Delta y|$ does not exceed 500 km. The quantities α and β are given in Table 7.9.

Table 7.9. Averaged values of α and β .

(1) Область течения	$\bar{\alpha}_{\text{км}^{-1}}$	$\bar{\beta}_{\text{км}^{-1}}$
Под осью струи (2)	0,1314	--
Над осью струи (3)	0,2388	--
С циклонической стороны струи (4)	--	0,00150
С антициклонической стороны струи (5)	--	0,00080

KEY: (1) Region of stream; (2) Below the jet axis; (3) Above the jet axis; (4) On the cyclone side of the jet; (5) On the anticyclone side of the jet.

We should point out that the quantity β depends on altitude, growing with approach to the axis of the stream from below and diminishing above the jet stream.

The jet streams observed in the Far East are close to the model constructed by Endlich and McLean (1957, 1965) from materials from the "Jet Stream" project.

Twin jet streams are often observed in the lower latitudes. In this case the axis of the second jet is located to the south and above that of the first. Fronts connected with these streams are well expressed in the temperature field. The complex of jet streams of this type, frequently observed over Middle Asia, was studied in detail by V. A. Dzhordzhio.

b. Experimental Data on Turbulence Causing Aircraft Buffeting in the Jet-Stream Region

Studies of the frequency and average intensity of turbulence affecting aircraft were carried out by N. Z. Pinus and S. M. Shmeter (1962) with consideration of models of the cross section of the jet stream. In these studies the frequency of turbulence was calculated as the ratio of route in turbulent zones to the total length of the route traveled by the aircraft with a horizontal section of the jet stream at the given level, while the average intensity of turbulence in the perturbed zones was calculated from the formula

$$\bar{\sigma} = \frac{\sum_{i=1}^n n_i \sigma^{(i)}}{\sum_{i=1}^n n_i} \quad (7.23)$$

where $\sigma^{(1)}$ is the intensity of aircraft buffeting in scale marks; n_i is the number of cases of buffeting of given intensities; $\sigma^{(1)}$ was taken as equal to unity, $\sigma^{(2)}$ equal to two, etc.

Figure 7.10 gives the frequency of turbulence in different parts of the jet stream. The isolines of frequency corresponding to 50% cover a zone in the cold portion of the jet stream between the front and the polar tropopause. Turbulence frequency diminishes most rapidly on the warm side of the jet stream, where at as little as 200-300 km from the front it does not exceed 15%. An increase in turbulence frequency (up to 30% and more) is observed above the front in the warm part of the stream.

The segment of most intensive turbulence is located below the axis of the jet stream close to the front, where $\bar{\sigma} = 1.6-1.8$.

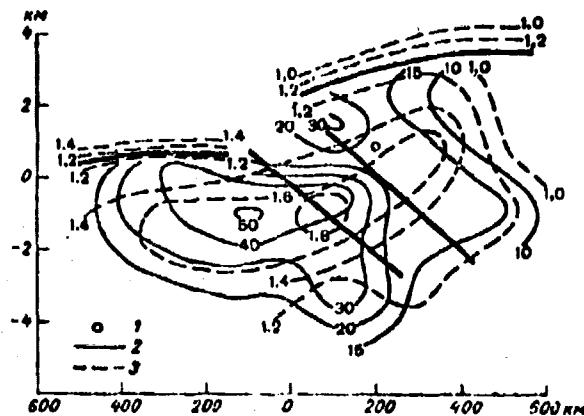


Fig. 7.10. Frequency (%) of turbulence and average intensity (in scale marks) of turbulence in a jet stream (cross section). 1 - stream axis; 2 - frequency; 3 - average intensity.

It should be noted that in the warm portion of the jet stream the drop in turbulence intensity along the horizontal occurs less

sharply than the drop in frequency. This means that in spite of the fact that frequency of turbulence as a whole in this portion of the jet stream is not great, turbulence of significant intensity can be observed here. The data on aircraft investigations by V. Briggs (1961) indicate that above England the greatest relative quantity of cases with strong buffeting of aircraft was observed below the axis in the cyclonic portion of the jet stream and above the axis in the anticyclonic portion (Table 7.10). Similar results were obtained by V. N. Barakhtin (1966) for Siberia and the Far East.

Table 7.10. Frequency of turbulence (No. of cases) in different parts of the jet stream.

	(1) Часть струйного течения	
	(2) Циклоническая	Антициклоническая (3) Чаская
Выше оси (4)	10	15
Ниже оси (5)	46	2

KEY: (1) Part of jet stream; (2) cyclonic; (3) anticyclonic; (4) Above the axis; (5) Below the axis.

According to studies by J. K. Bannon (1951, 1952), D. S. Jones (1954) and E. Chambers (1955) buffeting of aircraft was observed in 75% of the cases on the cold side of the jet stream.

N. I. Davydov (1959) showed that significant turbulence is encountered in regions of greatest vertical gradients of average wind velocity under the tropopause and above the front on the northern periphery of the stream.

The described distribution of frequency and average intensity of turbulence in different portions of the jet stream cross section can be disrupted by the influence of mountain relief. According to studies by N. S. Gel'mgol'ts (1963), the most turbulent portion in jet streams above Kazakhstan is that located above mountains. Analysis of the distribution of turbulence in jet streams when their warm part was located above mountains and the cold part above level

terrain shows the presence of increased turbulence in the warm portion of the jet stream; however, this is always less intensive than on its cold side.

It is clear that one should expect an opposite nature of turbulence distribution in the lower stratosphere on levels above the axis of the jet stream, where the anticyclonic portion of the stream is simultaneously the cold part.

The spatial structure of turbulent zones in jet streams above the USA as constructed by Endlich and McLean (1957) in general agrees well with data on turbulence obtained in jet streams over the USSR.

c. Turbulence in the Region of the Tropopause and Near the Level of Maximum Wind

We will begin by examining peculiar features of the distribution of frequency and average intensity of turbulence in the zone of the tropopause. The presence or absence of turbulence and also the intensity of turbulence were determined individually for layers located below and above the polar and tropical tropopauses on horizontal segments 25 km long in the layer 0-500, 500-1000, and 1000-1500 m below and above the tropopause. Figure 7.11 shows the distribution of frequency and average intensity of turbulence in the region of the polar and tropical tropopauses obtained by N. Z. Pinus and S. M. Shmeter (1962) from data obtained in experimental studies in the Far East. It is clear that the distribution curves for these types of tropopause are not identical. The frequency of turbulence in the 1500-1000 m layer under the polar tropopause equals 70%; in the 1000-500 m layer it is 67%, and in the 500-0 m layer it is 69%. Above the lower boundary of the polar tropopause in the 0-500 m layer the frequency diminishes to 57%; in the 500-1000 m layer it drops to 20%, and then a tendency to growth appears and frequency equals 50% in the 1000-1500 m layer. The average intensity of turbulence under the tropopause is maximum in the 500-0 m layer, where $\bar{\delta} = 1.45$; above the lower boundary of the polar tropopause turbulence intensity equals 1.0 in the 0-500 m layer, while in the 500-1000 m layer it grows to a

value of 1.5 with a subsequent drop to 1.0 in the 1000-1500 m layer. A. A. Reshchikova (1964) obtained approximately the same variation in turbulence distribution relative to the polar tropopause for the European territory of the USSR.

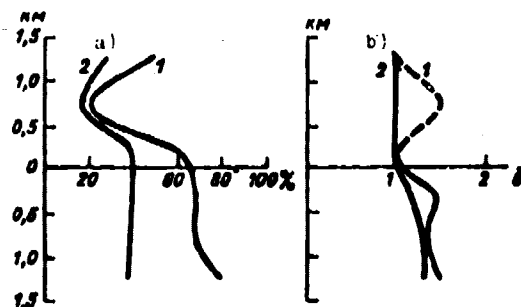


Fig. 7.11. Distribution of frequency (a) and average intensity (b) of turbulence in the zone of the polar (1) and tropical (2) tropopause.

We will now pause on the distinguishing features of the variation in frequency of turbulence in the region of the tropic tropopause. From Fig. 7.11 it is clear that in the 1500-m layer underneath the tropopause the frequency of turbulence does not change and equals 38%. Above the lower boundary of the tropopause it diminishes to 17% in the 500-1000 m layer, and then grows slightly. The average intensity of turbulence below the tropopause equals 1.2-1.3, while above its lower boundary $\bar{\sigma} = 1.0$. A similar distribution of turbulence in the zone of the tropopause was obtained by V. P. Belyayev et al. (1965) for the Moscow region; they used radiosondes equipped with an overload attachment.

The data obtained by N. F. Gel'mgol'ts (1963) indicates that above Kazakhstan in an inversion-free tropopause turbulence generally diminishes with altitude. In an inversion tropopause turbulence weakens sharply. On its lower boundary and approximately 500 m above and below it there are maxima of frequency and intensity of turbulence.

Such a difference in the distribution of frequency and average intensity of turbulence for the polar and tropic tropopause may, as we will see below, be connected with peculiarities in the vertical distribution of temperature and the average wind velocity and, in particular, with the difference in the ratios between the altitude of the tropopause and the altitude of the level of maximum wind velocity in the middle and tropical latitudes.

We will now examine the distribution of turbulence with respect to the level of maximum wind speed. This distribution is shown on Fig. 7.12 for the region of the Far East. Curve 1 on this figure characterizes the average intensity of turbulence $\bar{\sigma}$, while curve 2 represents the average intensity of turbulence with account taken of the frequency of calm flights and is calculated according to the formula

$$\bar{\sigma}_1 = \frac{\sum_{i=0}^4 n_i \sigma^{(i)}}{\sum_0^4 n_i} \quad (7.24)$$

Here $\sigma^{(0)}$ is a calm flight and n_0 is the number of such flights. Curve 3 on this figure characterizes the frequency of turbulence which is sufficient to affect the aircraft. As we see, two layers of the atmosphere in which turbulence has the maximum frequency and greatest average intensity can be noted: one is below the level of maximum wind speed and the other is above it. If we accept that only turbulence with an intensity $\bar{\sigma}_1 > 1.0$ noticeably influences flight conditions, it is possible to evaluate the average thickness of the turbulent layer; this can be called the effective thickness under the level of maximum wind and above it. From Fig. 7.12 it is clear that for the Far East Region the effective thickness below the level of maximum wind is approximately equal to 1.0 km.

Presently available experimental data have made it possible to study turbulence only in the layer located below the level of maximum wind velocity. As yet the accumulation of experimental data on turbulence above this level is inadequate.

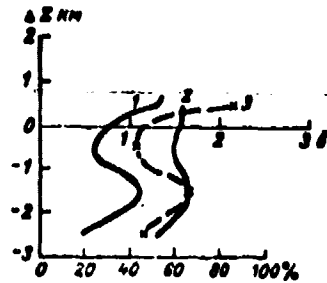


Fig. 7.12. Distribution of frequency (3) and average intensity (2 and 1) of turbulence in the zone of maximum wind.

On the basis of information on the distribution of frequency and average intensity of turbulence in the tropopause region and in the region of the level with maximum wind velocity, it is possible to construct three models of the distribution of turbulence with respect to the tropopause: a single-layer, two-layer, and a three-layer model (Fig. 7.13).

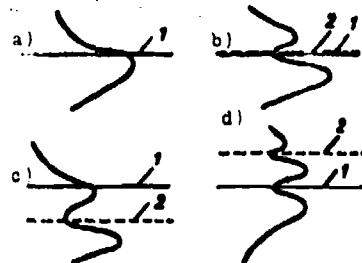


Fig. 7.13. Model of turbulence distribution in the zone of the tropopause and of the level of maximum wind.

The single-layer model of turbulence frequency distribution is typical for cases of weak winds in the tropopause region, with which the tropospheric maximum of wind velocity is barely expressed, if at all. In this case the layer with maximum frequency and intensity of turbulence is observed only under the tropopause (Fig. 7.13a).

The two-layer model characterizes a situation in which the altitude of the tropopause (1) and the level of maximum wind (2) (Fig. 7.13b) almost coincide or in which the tropopause is located above the level of maximum wind (Fig. 7.13c). In the first case a single turbulent layer can be observed under the tropopause, along with intensified influence of the jet stream; in the second case it is in the layer of the tropopause and is conditioned by the influence of the jet stream. In the second case (Fig. 7.13c) the turbulent

layer directly under the tropopause is intensified by the influence of the jet stream.

The three-layer model of turbulence frequency distribution in the tropopause zone is typical for cases when the level of maximum wind is located above the tropopause (Fig. 7.13d). In this case two turbulent layers are arranged above the tropopause and one beneath it. Both of the upper layers are caused by the influence of the jet stream.

Therefore statistical data on the difference Δz between the altitudes of the tropopause and of the level with maximum wind velocity are of considerable interest. Figure 7.14 shows curves of the integral frequency of the quantity Δz for the Moscow and Leningrad regions. From this figure it is clear that in the Moscow region in the spring, summer, and fall cases in which the tropopause is located above the level with maximum wind velocity predominate, while in the winter, on the other hand, cases below this level are dominant. Certain numerical characteristics are given in Table 7.11.

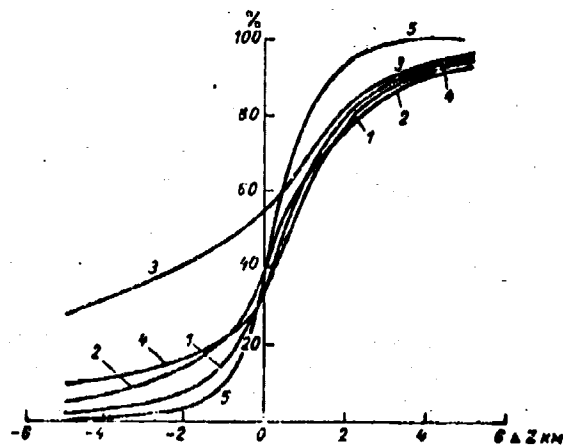


Fig. 7.14. Integral frequency of the difference in altitude between the tropopause and the level of maximum wind. 1 - summer, 2 - fall, 3 - winter, 4 - spring, 5 - annual average for Leningrad.

Table 7.11. Frequency (%) of the difference between the altitude of the tropopause and the altitude of the level with maximum wind velocity (Moscow).

(1) Season	Below	At	Above	Below	Above
Spring (2)	67	33	54	20	74
Summer (3)	66	34	53	29	82
Fall (4)	61	39	48	28	78
Winter (5)	48	54	36	18	54

KEY: (1) Season; (2) Spring; (3) Summer; (4) Fall; (5) Winter.

From Table 7.11 it is clear that over Moscow the tropopause is located below the level of maximum wind in 33-34% of the cases in spring and summer, in 39% in the fall, and in 54% of the cases in the winter; from this it follows that the three-layer model of distribution of turbulence in the tropopause zone should be observed quite frequently above Moscow in the fall and especially in the winter. This is solidly confirmed by data from radiosond observations with overload attachments (Belyayev et al., 1965).

We will note that data presented by V. I. Vorob'yev (1960) indicate that above Leningrad the level with maximum wind velocity over the course of the year on the average is located below the tropopause in 68% of the cases, coincides with the tropopause in 10% of the cases, and in 22% the tropopause is located below the level of maximum wind velocity. As we see, over Moscow the frequency of cases when the level with maximum wind velocity is below the tropopause is close to that given for Leningrad (with the exception of the winter period).

In those cases when the level with maximum wind velocity is located below the tropopause, the difference in their altitudes for the Moscow region in spring, summer and fall does not exceed 3 km in 48-54% of the cases; when this level is located above the tropopause this is true in only 20-29% of the cases. On the average the wind velocity maximum is located in the ± 3 -km layer with respect to tropopause altitude in 74-82% of cases in the summer and in the transition seasons, while for winter the figure is 54%. We will

note that Vorob'yev's data indicate that over Leningrad the level with maximum wind velocity is located in a layer ranging from 2 km below the tropopause to 1 km above it in 83% of the cases.

§ 4. CONNECTION OF TURBULENCE AFFECTING AIRCRAFT WITH THERMAL AND DYNAMIC CONDITIONS IN THE ATMOSPHERE

1. The Possibility of Using the Richardson Number As a Criterion of Turbulence Sufficient to Affect Aircraft

In recent years many works have appeared concerned with the study of the dependence of turbulence sufficient to buffet aircraft on various characteristics of the temperature and wind-velocity fields. In particular, it has been found that aircraft buffeting behaves as a function of vertical and horizontal gradients of average wind velocity, rotation of the wind vector with altitude, horizontal temperature gradients, Richardson number, etc. According to data presented by C. S. Hislop (1950, 1951), buffeting of aircraft was observed during vertical gradients of average wind velocity exceeding 2 m/s per 100 m altitude and with horizontal temperature gradients exceeding 5° per 100 km. Similar results were obtained by I. A. Klemin and N. Z. Pinus (1954), while Yu. V. Kurilov (1960) concluded that in the upper troposphere turbulence is most probable in the presence of vertical temperature gradients in the interval 0.6-1.0° per 100 m and with vertical wind-velocity gradients exceeding 0.5 m/s per 100 m of altitude. As regards horizontal wind-velocity vectors, according to Hislop's data turbulence was observed at 5 m/s and more per 100 km; D. Jones (1954) reported observation of turbulence at 8-12 m/s and more per 100 km. According to data provided by A. A. Reshchikova (1964), at gradients greater than 17 m/s per 100 km the frequency of aircraft turbulence reaches 75%, while at smaller gradients it drops sharply and comprises a total of only about 5%.

In many works the Richardson number is used for evaluating the turbulent state of the atmosphere as a condition causing buffeting of

aircraft. In the work by I. A. Klemin and N. Z. Pinus (1954) it was found that weak buffeting of aircraft is observed when $0.5 < Ri < 4$, while moderate and strong turbulence occur when $Ri \leq 0.5$. Many foreign researchers have arrived at approximately similar criteria. Thus, for example, J. Bannon (1951a, b; 1952) considers that aircraft turbulence is observed when $Ri < 4$; J. Sugimoto (1956) gives a figure $Ri < 3.5$; Sasaki (1958) gives $Ri < 2.65$, and M. Berenger and J. Heissat (1959) give $Ri < 5$.

W. Georgii (1960) evaluates the nature of the motion and intensity of turbulence by means of the Richardson number as follows: $Ri = 1$ is a quasilaminar flow; $0.5 < Ri < 1$ is weak or moderate dynamic turbulence; $0 < Ri < 0.5$ is moderate or strong dynamic turbulence, and $Ri < 0$ is thermoconvective turbulence.

B. Briggs (1961) studied 105 cases of strong turbulence in clear air in the upper troposphere over England and found that in 70% of the cases turbulence was recorded with $Ri < 0.5$. In 80% of the cases of strong turbulence, horizontal gradients of average wind velocity exceeding 8 m/s per 100 km were observed along with such extremely small Ri values. Investigations carried out by R. Endlich and R. L. Mancuso (1965) showed that the vertical gradient of average wind velocity and the Ri number are the best indicators of turbulence sufficient to affect aircraft. As turbulence indicators, both of these parameters give approximately identical results when compared with data from observations of aircraft buffeting. This may apparently explain the fact that in the absence of clouds in the upper troposphere the vertical temperature gradient changes within comparatively narrow limits and therefore changes in the Ri number are determined mainly by the contribution of vertical wind-velocity shear. D. Colson indicates a satisfactory connection between the probability of turbulence in clear air and the values of Ri numbers of vertical gradients of average wind velocity (1963).

The determination of the critical value of the Richardson number for evaluating turbulence causing buffeting of aircraft was also the subject of works by M. V. Zavarina (1959) and by M. V. Zavarina and

M. I. Yudin (1960). For this purpose they utilized data of simultaneous sounding of the atmosphere with radiosondes and LI-2 aircraft (up to altitudes of 5-6 km), carried out at a number of points of the aerological network of the USSR in cloudy weather.

The curve $Ri = 1$ is given on Fig. 7.15, constructed by Zavarina for a two-year series of aircraft and radiosond observations in Minsk (April). As is clear from the figure, with large values of the vertical temperature gradient γ the greater part of the cases with aircraft buffeting remain to the left of this curve. If we draw the curve $Ri = 4$ on the figure, nonetheless many cases with buffeting remain on the left. This is a result of the fact that during calculations of Ri number for evaluating turbulence in clouds it is necessary to use not the dry adiabatic, but the wet adiabatic temperature lapse rate [gradient]. The curve $Ri_w = 1$, constructed for the case when the moist adiabatic gradient is inserted into the formula for Ri instead of the dry adiabatic rate, satisfactorily separates the case with aircraft buffeting in clouds from the case of calm flight.

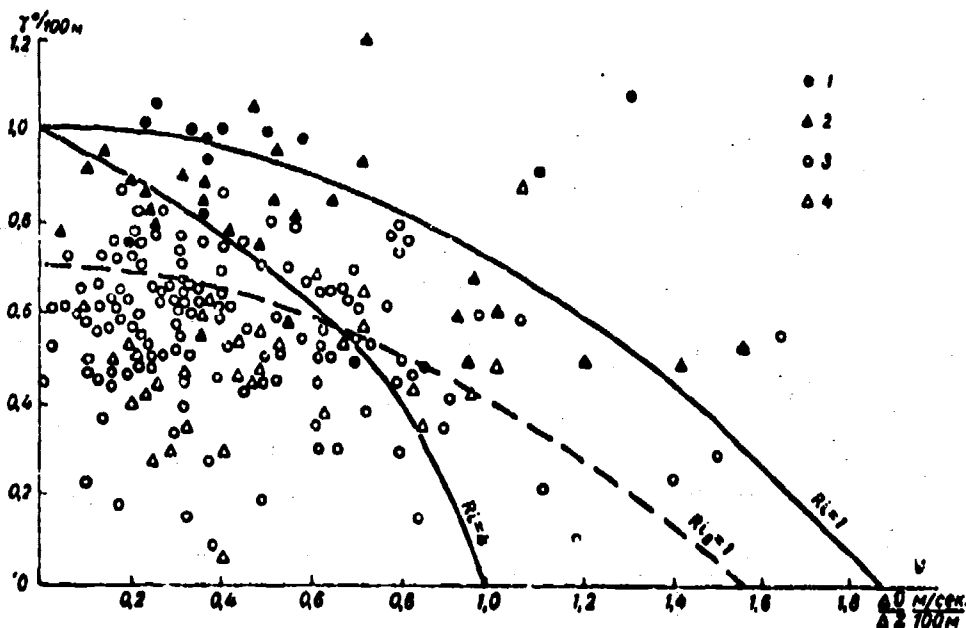


Fig. 7.15. Demarcation graph (Minsk, April 1953 and April 1954). Cloudless layer with turbulence (1) and without (3); cloudy layer with (2) and without (4) aircraft turbulence. [$m/сек = m/s$; $a = w$].

We will note that there is no great difference in the upper troposphere between the values of the dry (1°/100 m) and moist adiabatic temperature gradients (Table 7.12).

Table 7.12. Values of the moist adiabatic temperature lapse rate.

(1) Температура, °C	(2) Давление, мб			
	300	400	500	600
-30	0,890	—	—	—
-40	0,884	0,942	0,922	0,866
-50	0,944	0,979	0,971	0,936
-60	0,998	0,998	0,992	0,945

KEY: (1) Temperature, °C; (2) Pressure, mb.

To evaluate the success of application of the Ri number in diagnosing the presence of buffeting of aircraft, M. V. Zavarina used the coefficient of correctness of alternate forecasts proposed by A. M. Obukhov (1955):

$$Q = 1 - (\alpha + \beta), \quad (7.25)$$

where α is the relative number of unsuccessful forecasts (diagnoses) of the presence of buffeting, while β is the relative number of unsuccessful forecasts (diagnoses) of the absence of buffeting of aircraft. It was found that the correctness coefficient varies from 0.68 to 0.86.

On the other hand, some investigators did not find a satisfactory correlation between Ri number and turbulence affecting aircraft, especially for the upper troposphere in a cloudless sky. Thus, according to N. I. Davydov (1959), the probability of buffeting of aircraft in the upper troposphere and lower stratosphere is identical for large and small values of the Ri number. C. S. Hislop was also unable to establish a reliable dependence between aircraft turbulence and the value of the Richardson number. I. G. Pchelko (1962) and Yu. V. Kurilov (1960) reached similar conclusions, although they did indicate that there was a low probability of aircraft turbulence with

large Ri numbers. We will note that in a recent work (1966) carried out according to the program of the World Meteorological Organization, Pchelko gives data concerning the fact that moderate and strong aircraft turbulence exists at altitudes of 6-10 km above the USSR in 70-75% of the cases with Ri values in the limits 0.0-4.0 and in 35% of the cases when Ri < 1. Results obtained by several authors are given in Table 7.13.

Table 7.13. Frequency (%) of turbulence as a function of Richardson number.

(1) Автор	(2) Число Ричардсона			
	<0.3	0.1-4.0	<10	>10
(3)				
И. А. Клемин, Н. З. Пинус (1954)	80-90	50	—	—
Ю. В. Курилова (1960) (4)	—	—	79	—
М. Беранже и Эсса (1959) (5)	75-90	—	—	—
И. Г. Пчелко (1962) (6)	—	—	31	12
Е. К. Верле (1963) (7)	74	36	—	26
А. А. Решчикова (1964) (8)	78	58	—	13
М. В. Заварина (1958) (9)				
	Коэффициент оправданности (10) по Обухову 0,75			

KEY: (1) Author; (2) Richardson number; (3) I. A. Klemin, N. Z. Pinus (1954); (4) Yu. V. Kurilova (1960); (5) M. Berenger and Heissat (1959); (6) I. G. Pchelko (1962); (7) Ye. K. Verle (1963); (8) A. A. Reshchikova (1964); (9) M. V. Zavarina (1958); (10) Coefficient of correctness per Obukhov 0.75.

The main reason for the great scatter of data given in Table 7.13 is the fact that turbulence, as was indicated in Chapter 1, is not uniquely connected with the Ri number. Besides this, when the Ri number is calculated from network aerological data it is necessary to take into account the large errors inherent to measurements of wind speed and direction, especially in the upper troposphere and lower stratosphere. For this reason the errors in Ri calculations can reach 200-300% (Shmeter, 1957).

An extremely important circumstance which can lead to erroneous values of Ri is incorrect selection of the thickness of the layers during calculation of the values of vertical gradients of temperature and average wind velocity entering into the magnitude of Ri (Zavarina, 1959; Pinus, 1960). When analyzing available experimental data on the

dependence of frequency and intensity of turbulence on Ri it is also necessary to consider the fact that in a number of cases researchers had at their disposal materials which were characterized by inadequate synchronization of aerological observations and observations of aircraft turbulence. The separation of observations in time sometimes exceeded 3 h. Besides this, frequently the point of aerological observations was separated from the region of the flight by 100-200 km and more.

Along with this, the results of calculating Ri are very noticeably influenced by the variability of temperature and wind in space and in time. This influence is strong even in those "ideal" cases when turbulence, temperature, and wind are measured on one and the same aircraft. In the given case the measurements of T and u at different altitudes turn out to be asynchronous. It is known that the temperature in the region of the jet stream at any given altitude can change by $\Delta T = \pm 2^\circ$ in an hour, while wind speed can vary by $\Delta u = \pm (2-5)$ m/s. The Ri number is very sensitive to such time changes of temperature and wind speed. We shall demonstrate this on the following example.

Assume that at some moment of time the difference between temperatures on two levels located 1 km apart equals 7°C ; the difference in average wind speed is 8 m/s, and the average air temperature in the layer is 230°K . The Ri number for this layer equals 2.02. If we now take the variability of temperature and wind speed on the upper level as equal to the quantities given above, it is easy to compute values which can be obtained under the condition that the time of measurements on the two levels differs by 1 h. The results of such a calculation for $\Delta u = \pm 2$ m/s and $\Delta T = \pm 2^\circ$ are given in Table 7.14.

Table 7.14. Ri as a function of changes in wind (Δu) and temperature (ΔT) on the upper level in an hour.

u/s 30 m/sec.	ΔT°		
	0	-2	+2
0	2,02	0,67	3,36
+2	1,29	0,43	2,15
-2	3,60	1,30	6,00

Thus, with a true value $Ri = 2.02$ the values of this number obtained from measurement data can turn out to be completely different: from $Ri = 0.43$, when (according to Klemin and Pinus) we can expect moderate or even strong buffeting of the aircraft, to $Ri = 6.00$, when the flight should, in general, be calm.

N. Z. Pinus and S. M. Shmeter (1962) used materials from flight experiments carried out in the Far East to compare average data on aircraft buffeting in jet streams with average values of Ri number. The dry adiabatic temperature lapse rate was used in the calculations for cloud-free layers, while the moist adiabatic gradient was used for cloudy layers. In the majority of calculations the horizontal temperature gradient was used instead of the vertical gradient of average wind speed. The Ri number was not calculated for the region of the tropopause.

Figure 7.16 gives the distribution of average values of Ri number on a transverse vertical section of the jet stream. From this figure and from Fig. 7.10 it is clear that in the zone where $\bar{\sigma} \geq 1.8$ - i.e., where on the average aircraft buffeting was close to moderate - $Ri \ll 1$. In the cold portion of the jet stream, where $\bar{\sigma} < 1.8$, $1 < Ri < 5$. To the right of the jet-stream axis, where $\bar{\sigma} < 1.4$, values of Ri grow quite rapidly.

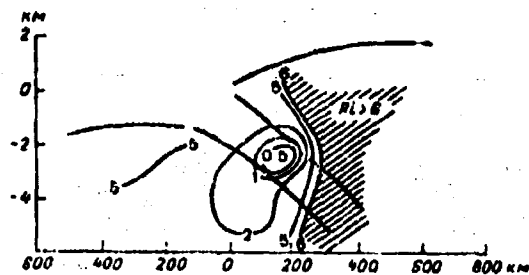


Fig. 7.16. Distribution of average values of Ri on a vertical section of the jet stream.

Figure 7.16 shows that by using the Ri number it is possible to obtain the background of turbulence distribution in the zone of a jet stream, but not the details of its distribution which are clearly visible on Fig. 7.10.

D. Colson and H. A. Panofsky (1965) undertook to evaluate clear-air turbulence by means of a special turbulence index. They considered the average magnitude of the energy of pulsations of the vertical wind-velocity component, $E' = \frac{w'^2}{2}$, to be the principal quantitative characteristic of turbulence intensity. The expression for E' is found from considerations of dimensionality under the assumption that E' is uniquely determined by the vertical scale of eddies λ and the rate of arrival of energy

$$\Phi_0 = K \left(\frac{du}{dz} \right)^2 + \alpha K_r \frac{K}{\lambda} \frac{d\Phi}{dz} \quad (7.26)$$

where α is a quantity somewhat greater than unity, characterizing the fact that hydrostatic forces directly influence pulsations of the vertical wind-velocity component, whereas wind shear gives rise to pulsations of the longitudinal wind-velocity component; the energy of these pulsations will then be redistributed among all the components.

It is further assumed that $K \approx K_r \approx \lambda \gamma E'$. As λ the thickness of the turbulent layer Δz is used, while $\frac{\partial u}{\partial z}$ is replaced by the ratio of finite differences. As a result the authors obtained the expression

$$J = (\Delta u)^2 \left(1 - \frac{Ri_{sp}}{Ri_{sp}} \right) \approx E' \quad (7.27)$$

On the basis of evaluation of empirical data it is assumed that

$$Ri_{sp} = \frac{1}{\frac{K}{K_r^2}} \approx 0.5.$$

The quantity $J \equiv E'$ is taken as the index of clear-air turbulence. Colson and Panofsky found the characteristic values of J for turbulence of various intensities over the territory of the USA; these values agree satisfactorily with experimental data on aircraft buffeting.

D. L. Laykhtman and Yu. Zh. Al'ter-Zalik (1966) proposed a method for using aerological data to evaluate turbulence causing buffeting of aircraft in the free atmosphere. They proposed that the turbulent flow is stationary and uniform along the horizontal. The average spatial scale of turbulence was evaluated in terms of the magnitude of the "mixing path" in the Prandtl-Kármán sense, while the role of thermal stratification of the atmosphere was assumed to be similar to the role of the vertical wind-velocity gradient. Then the known Kármán formula can be generalized for the scale of turbulence:

$$l \approx 2\kappa \left| \frac{\left(\frac{d\bar{u}}{dz} \right)^2}{\frac{d}{dz} \left(\frac{d\bar{u}}{dz} \right)^2} \right|, \quad (7.28)$$

(where $\kappa \approx 0.4$ is the Kármán constant) to the case of a thermally stratified atmosphere by replacing $\left(\frac{d\bar{u}}{dz} \right)^2$ in (7.28) by the function

$$\psi = \left(\frac{d\bar{u}}{dz} \right)^2 + \left(\frac{d\bar{v}}{dz} \right)^2 - \alpha \frac{g}{\bar{v}} \frac{d\bar{\theta}}{dz},$$

where α is a quantity equal to the ratio of the coefficients of turbulent mixing for heat and momentum.

If we ignore turbulence diffusion, the connection between the kinetic energy of turbulence, the average turbulence scale, and the vertical distribution of wind velocity and air temperature is described by the following equations:

$$K\Phi - \epsilon = 0, \quad (7.30)$$

$$K = l(E')^{\frac{1}{2}}, \quad (7.31)$$

$$\epsilon = c(E')^{\frac{3}{2}} l^{-1}, \quad (7.32)$$

$$l = \tilde{\kappa} \left[\frac{d}{dz} \ln \psi \right]^{-1}, \quad (7.33)$$

where K is the coefficient of turbulent mixing; E' is the kinetic energy of turbulence; ϵ is the rate of dissipation of turbulent energy into heat; c and $\tilde{\kappa}$ are dimensionless constants equal to 0.046 and 0.37,

respectively. The constant \bar{K} is connected to the Kármán constant by the relationship $\bar{K} = 2\kappa^2$.

If the vertical distribution of temperature and average wind velocity is known it is possible to obtain the principal characteristics of turbulence:

$$\begin{aligned} E' &= 0.75 \text{clg}^2 \varphi, \\ l &= 0.185 \text{clg} \varphi, \end{aligned} \quad (7.34)$$

where

$$\text{clg} \varphi = \left[\frac{d}{dz} \cdot \Phi^{1/2} \right]^{-1}. \quad (7.35)$$

Calculations by D. L. Laykhtman and Yu. Zh. Al'ter-Zalik with formula (7.34) are confirmed by data from experimental studies.

b. Connection Between Turbulence and the Divergence of Horizontal Wind Speed

During theoretical consideration of turbulence in the free atmosphere it is usually assumed that the flow is uniform along the horizontal. Actually, as we have seen, in a jet stream the horizontal gradients of wind velocity are substantial and very variable. The fact that many researchers ignore the role of horizontal wind-velocity gradients is based on the fact that the latter are at least an order of magnitude less than the vertical gradients of average wind velocity.

S. K. Kao and A. H. Sizoo (1966) used materials from flight experiments carried out above the USA during the "Jet Stream" project to study the dependence of the frequency of turbulence of different intensity on the sign and modulus of the divergence of horizontal wind velocity (the so-called plane divergence).

The following expression was used for calculations of plane divergence:

$$\nabla_z \cdot \mathbf{v} = \frac{\partial v_z}{\partial z} + \frac{\partial v_{\perp}}{\partial r} \quad (7.36)$$

where z is altitude; v_{\parallel} is wind speed parallel to the jet axis, and v_{\perp} is the speed of wind normal to the jet axis. The quantity Δv_{\perp} was obtained from data of the aircraft Doppler navigation system, since the flights were carried out across the axis of the jet stream; Δv_{\parallel} was calculated from data of network radio wind observations; Δz and Δr were taken as equal to 5.5 and 111 km, respectively.

It was found that turbulence frequency (P%) as a function of plane divergence of wind velocity can be described by the exponential function

$$P = a e^{-b \nabla_z \cdot \mathbf{v}} \quad (7.37)$$

The parameters a and b depend essentially on the intensity of turbulence (Table 7.15).

Table 7.15. Values of the parameters a and b and of the range of change in the magnitude of plane divergence $\nabla_z \cdot \mathbf{v}$ as a function of turbulence intensity.

(1) Интенсивность турбулентности	a	b в сек.	$\nabla_z \cdot \mathbf{v}$ 10^{-3} см
Слабая (2)	8,00	$2,16 \cdot 10^4$	-16 +28
Умеренная (3)	6,83	$7,70 \cdot 10^3$	-18 +8
Сильная (4)	2,05	$1,20 \cdot 10^4$	-30 +10
В среднем (5)	19,00	$4,33 \cdot 10^3$	-30 +28

KEY: (1) Intensity of turbulence; (2) Weak; (3) Moderate; (4) Strong; (5) Average.

With an increase in the intensity of turbulence the magnitude of the parameter a is reduced, while parameter b , on the other hand, grows. Besides this, with an increase in wind velocity convergence ($\nabla_z \cdot \mathbf{v} < 0$) the intensity of turbulence buffeting the aircraft grows.

c. Certain Synoptic Conditions
Which Favor the Development of
Turbulence Sufficient to Influence
the Flight of Aircraft

Charts of the baric topography of different levels are used by many investigators to clarify the particular features of the pressure field or the wind-velocity field at which the presence of conditions favorable for the development of turbulence sufficient to influence aircraft flight is most probable. In this case it is most essential to clarify those regions in the fields of pressure or of wind velocity where clear air turbulence can be observed.

I. G. Pchelko (1962) considers that favorable conditions for turbulence development in the upper troposphere are observed in the cyclonic portion of the jet stream and, mainly, to the left of its axis, where in his opinion the dominant role is played by horizontal wind shear across the flow; he also considers that favorable conditions can be observed also in the zone of divergence of current lines, accompanied by anticyclonic curvature of the current lines where the horizontal wind shears are directed along a flow. Moderate and strong turbulence is observed if the horizontal gradient of average wind velocity on short segments is greater than 50 km/h per 100 km.

I. G. Pchelko's article (1966) gives data which indicate that in the cyclonic part of jet streams moderate and strong turbulence is observed most frequently with comparatively small horizontal wind shears (less than 10 m/s per 100 km) but with comparatively large vertical shears (over 0.8 m/s per 100 m) and considerably less frequently with large horizontal shears (over 10 m/s per 100 km) and small vertical shears (less than 0.8 m/s per 100 m). According to this work, in the anticyclonic part of jet streams moderate and strong turbulence is observed with small horizontal and vertical wind shears (less than 10 m/s per 100 km and 0.8 m/s per 100 m). At the same time, according to A. A. Reshchikova (1964), who processed materials from the flight experiments conducted on an aircraft equipped with a Doppler navigation system, the frequency of turbulence with wind shears smaller than 60 km/h per 100 km does not exceed 9-13%, whereas at larger values of shear it reaches 75%.

We should note a contradiction in the data of many researchers concerning the dependence of the frequency of turbulence which interferes with aircraft flight on the curvature of isohypses and divergence of the lines of flow in jet streams and also about the characteristic magnitude of horizontal wind shear. To a considerable extent this is the result of differences in the procedure used by the different authors for analysis of charts of baric topography and comparison with the data on aircraft buffeting. Furthermore, some authors use data on wind obtained on the comparatively thin aerological network, thanks to which the averaging during the calculations of the horizontal wind shear is great, whereas other authors use the data of airborne measurements which allow calculation of wind shear for relatively short distances, comparable to the horizontal scales of turbulent zones. According to Reshchikova (1964), turbulent zones in most cases are observed directly in the zone of large wind shears. Cases are encountered in which turbulence is observed in zones with small horizontal shears (in a zone of strong winds) in immediate proximity to sections with the large shears. Naturally, the data from the aerological network are not always suitable for evaluation of the magnitude of horizontal wind shear in a zone in which turbulence causing buffeting of an aircraft was observed.

CHAPTER 8

TURBULENCE IN CLOUDS

Turbulence is usually more strongly developed in clouds of any type than in the surrounding atmosphere. This is connected principally with the fact that indifferent or even unstable temperature stratification is frequently observed in clouds, especially cumuliform. Turbulence in them could also be intensified by the great horizontal nonuniformity of the fields of air temperature and density which is characteristic for these clouds.

On the immediate upper edge of the clouds turbulence is intensified by a sharp local increase in vertical temperature gradients owing to the cooling of the air occurring here due to evaporation of cloud elements; at night cooling is also caused by radiation. Besides this, in this layer there is sometimes strong rotation of the wind, which facilitates an increase in dynamic instability of the flow.

Finally, one should consider that turbulence is one of the main cloud-forming factors; owing to turbulence clouds develop most often in the zones in which the general "turbulent background" is elevated.

§ 1. TURBULENCE IN STRATIFORM CLOUDS

Until recently the intensity of turbulence in stratiform clouds was determined basically in terms of the g-forces experienced by aircraft during flight - i.e., according to data on the intensity

of buffeting. Table 8.1, based on materials developed by N. Z. Pinus (1960), shows the frequency of buffeting of high-speed aircraft in various clouds.

Table 8.1. Frequency (in %) of aircraft buffeting in clouds of different types.

Str.: St; Sc	Ns.-As	Ac	Cl; Cs; Cc	⁽¹⁾ Без уточнения формы
34,0	30,0	29,0	34,0	40,0

KEY: (1) Without exact definition of form.

Very similar data were obtained for St and Sc clouds by Ye. G. Zak (1938) and for clouds of the upper layer by S. M. Shmeter (1960); by Shmeter's evaluation, in particular, the frequency of buffeting in Cl and Cs was about 10 times greater than in a clear sky at the same altitudes.

In the overwhelming majority of cases the speeds of vertical air gusts (w_T) in stratiform clouds do not exceed 2-3 m/s. For example, according to M. Watson (1967) inside Ac they do not exceed 2.2 m/s. According to his data the magnitudes of w_T depend on the vertical gradients of temperature and wind within the cloud layer. However, if a deep inversion is located above Ac clouds the turbulence at their upper edge is weakened.

Individual gusts with a velocity approaching 10-15 m/s can be observed in stratiform clouds above mountains and in intensive jet streams.

The most intensive turbulence is observed with the greatest frequency near the boundaries of the cloud layer, especially if these boundaries are uneven. Within the cloud layer turbulence intensity depends on the structure of the cloud. In clouds which are uniform in density it usually is not great. If the clouds are optically nonuniform - i.e., if more and less dense segments alternate within them - the intensity of turbulence can be substantial.

It should be noted that in very thin clouds turbulence is usually the same as in the surrounding cloudless air.

Up to now no systematically organized data have been published on the frequency of gusts of different magnitudes in low-level and high-level stratiform clouds. Table 8.2 presents data for high-level clouds obtained during flight studies carried out in 1959-1964 by S. M. Shmeter.

Table 8.2. Speed of vertical gusts w_T in turbulent zones within Ci and Cs.

(1)	<1	1-2	2.1-4	4.1-6	>6
w_T , м/сек.					
(2) Повторяемость, % . . .	42	38	16	3	1

KEY: (1) m/s; (2) Frequency, %.

The length of segments within which $w_T > 4$ m/s does not exceed 10 km. Segments with $w_T \leq 2$ m/s can have a length up to several tens of kilometers. Occasionally the size of perturbed zones is close to the size of the entire cloud field, but usually this is observed only near the upper edge of strongly heated Cs.

Table 8.3, taken from the article by Yu. V. Kurilova (1960), shows the relative extent of perturbed zones in clouds on the basis of buffeting data.

a. Coefficient of turbulent exchange in stratiform clouds

During studies of turbulence in low-level stratiform clouds substantial attention has been paid to determining the coefficient of turbulence K in them, since knowledge of this quantity is necessary for theoretical calculation of the cloud-formation process.

Table 8.3. Relative extent of segments with buffeting within clouds.

(1) Форма облаков	(2) Общая длина пути в облаках, км	(3) Длина участка с буфетин- гом, км/%	(4) Наиболь- шее перегруже- ние в долях g
(5) Ac, As сплошные	900	7,37	±0,26
(6) Ac, As слоими	700	9,3 21,0 30,0	±0,56
Cl, Cc	110	28,8 16,0	±0,22
Cu, Sc	860	395,6 46	±0,62

KEY: (1) Type of clouds; (2) Total length of path in clouds, km; (3) Length of segment with buffeting, km/%; (4) Greatest overload in fractions of g; (5) solid; (6) in layers.

M. P. Churinova (1955) calculated K from data of pilot-balloon observations, using the formula proposed by D. L. Laykhtman (1952):

$$K = \frac{2(\lg e)^2 l}{\frac{d}{dz} \lg [(U_g - u)^2 + v^2]} \quad (8.1)$$

where l is the Coriolis parameter, e is the natural log base, U_g is the speed of the geostrophic wind, and u and v are components of the velocity of the actual wind. Table 8.4 gives the results of the calculations.

As is evident from this table, the coefficient of turbulence within clouds is approximately 20% greater than that in a cloudless sky.

L. T. Matveyev (1958), M. A. German (1963, 1964) and V. Ye. Minervin (1966) calculated K in clouds in different types from data on g-force increments of aircraft. The calculations were carried out by the Lyapin'-Dubov formula:

$$K = \frac{\bar{b} \Delta n \bar{t} V}{\Delta} \quad (8.2)$$

where \bar{b} is a proportionality factor depending on the aerodynamic characteristics of the aircraft; \bar{t} is the averaged time of retention of the sign of the g-force increment (Δn); $\Delta = \frac{\rho_0}{\rho}$; V is the speed of the aircraft. Tables 8.5 and 8.6 show the results of the calculations.

Table 8.4. Average value of turbulence coefficient K in the friction layer.

(1) Форма облаков	(2) Сезон	(3) K м ² /сек.	(4) U м/сек.	(5) Число случаев
Sc	(6) Лето	28,2	10,0	25
St	Зима (7)	21,2	13,0	28
Sc	"	20,9	13,0	111
Ns	"	18,3	13,5	43
Безоблачно (8)	"	17,8	13,5	56

KEY: (1) Type of clouds; (2) Season; (3) m²/s; (4) m/s; (5) Number of cases; (6) Summer; (7) Winter; (8) Cloud-free.

Table 8.5. Frequency (in %) of different values of turbulence coefficients in clouds (per M. A. German).

(2) Форма облаков	(1) Коэффициент турбулентности, м ² /сек.								(3) Число случаев
	0-1	1-2	2-3	3-4	4-5	5-6	6-7	7-10	
Теплое полугодие (4)									
Ca	—	30,8	33,2	11,9	11,9	7,1	2,4	—	42
Ac	—	6,2	6,3	12,5	12,5	25,0	25,0	12,5	16
Ax	—	10,0	10,0	5,0	20,0	15,0	10,0	—	20
Ns	1,9	7,7	9,6	19,3	25,0	25,0	11,5	—	52
Sc	—	—	7,4	11,0	37,1	37,1	7,4	—	27
Холодное полугодие (5)									
Ac	—	15,8	5,3	15,8	15,8	42,0	5,3	—	19
As	—	—	—	61,7	27,2	9,1	—	—	11
Ns	—	22,7	13,7	31,8	22,7	9,1	—	—	22
Sc	—	13,4	10,0	20,0	33,3	20,0	3,3	—	30

KEY: (1) Turbulence coefficient, m²/s; (2) Type of clouds; (3) Number of cases; (4) Warm half of year; (5) Cold half of year.

Table 8.6. Average and maximum values of K in m²/s within and outside of clouds.

	В облаках (1)					За облаком на высоте, км (2)			(3) Автор
	Св	Ас	Ал	Нс	Сс	<2	2-8	8-12	
Теплое полугодие (4)									
(5) Средние . . .	31	68	58	46	51	24	22	18	М. А. Герман (7)
(6) Максимальные	101	109	89	92	88	35	42	34	М. А. Герман (7)
Холодное полугодие (8)									
(5) Средние . . .		46	43	31	40	22	20	6	М. А. Герман (7)
(6) Максимальные		79	62	66	35	38	35	14	М. А. Герман (7)
(5) Средние . . .		55	27	56	59	-	-	-	Л. Т. Матвеев (9)

KBY: (1) Inside clouds; (2) Outside clouds at an altitude of (km); (3) Author; (4) Warm half of year; (5) Average; (6) Maximum; (7) M. A. German; (8) Cold half of year; (9) L. T. Matveyev.

V. D. Litvinova and V. I. Silayeva (1960) calculated values of K from data obtained by measuring the pulsations of vertical air velocity on free balloons. The value of K was found according to the T. Hesselberg formula

$$K = \bar{\tau} \overline{w^2} \quad (8.3)$$

where $\bar{\tau}$ is the average time of retention of the sign of the pulsation velocity; $\overline{w^2}$ is the mean square speed of vertical gusts.

It was found that in St-Sc values of K lie within the limits 2-10 m²/s.

From the above it is clear that in low-level stratiform clouds the values of K derived by different authors do not agree with one another. The main reason for this is the multiplicity of scales of atmospheric turbulence, due to which eddies of different dimensions (L) participate in exchange, with their specific contribution in this process being different - i.e., $K = K(L)$. Since the use of

different methods of measuring w results in data relating to different segments of the turbulence spectrum, the values of K which are computed with their aid do not necessarily coincide. Differences in the measurement procedure should also be taken into account. Thus, when pilot balloons are used the measurements are conducted during ascent - i.e., approximately along the vertical. Measurements on free balloons are carried out for the entire period in one and the same volume of air, i.e., it is not spatial but temporal fluctuations in w which are determined, etc.

During analysis of K values calculated with respect to aircraft g-forces one should take into account the following special features of the method of measuring the g-forces. First of all, as was indicated in Chapter 2, an increment in overloads is caused only by comparatively large eddies, whose size is comparable with the size of the aircraft. Secondly, the low threshold sensitivity of ordinary accelerographs causes filtering out of gusts with $w_{\perp} \leq 0.3-0.5$ m/s. Finally, in the third place, because aircraft overloads arise only in zones with intensive turbulence, the values of K obtained with respect to these forces characterize not the level of turbulence on the average for an entire cloud, but its intensity in turbulent zones within the cloud. We have already indicated that the extent of such zones in stratiform clouds in the general case comprises less than half their length, which means that the turbulence coefficient averaged for the entire cloud should be much less than indicated in Tables 8.5-8.6.

We will now examine the variation in K within clouds along the vertical. Examples of K -distribution in low-level stratiform clouds are given on Figure 8.1. Inside the clouds the magnitude of K changes comparatively rapidly with altitude, where it is maximum at the edges of the cloud. Especially large K are encountered at the upper boundary of the clouds with a heaped upper edge. If stratified cloudiness is observed, K will be sharply reduced in the cloud-free intervals. As the studies carried out by T. A. Tsitovich (1959) and A. A. Reshchikova (1960) indicated, a picture of this type is typical not only for internal clouds, but also for $Ns-As$ frontal cloud systems.

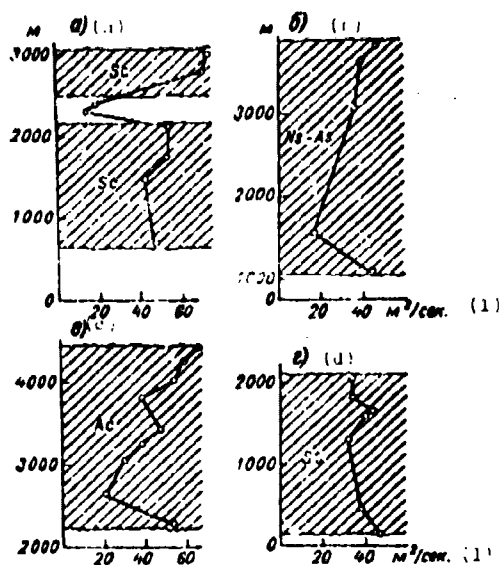


Fig. 8.1. Vertical profiles of the coefficient of turbulence (per M. A. German). a) Sc, 20 February 1961; b) Ns-As, 24 January 1958; c) Ac, 23 January 1958; d) St, 3 March 1961.

KEY: (1) m^2/s .

The vertical distribution of the intensity of the turbulent exchange in stratiform clouds can be illustrated also by the vertical profiles of spectral densities of turbulence. Figure 8.2 shows examples of such profiles taken from an article by A. S. Dubov and M. A. German (1965).

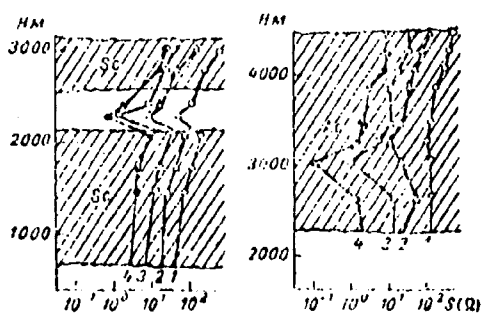


Fig. 8.2. Vertical profiles of spectral densities of turbulence (per A. S. Dubov and M. A. German) in Sc and Ac.

1) $L = 250$ m, 2) $L = 500$ m, 3) $L = 750$ m, 4) $L = 1000$ m.

Values of K also change rapidly in the horizontal direction; this is noticeable from the structure of buffeting zones, which are characterized by the fact that inside the clouds perturbed and unperturbed segments alternate with one another in time, with the transition from zones of buffeting to segments of calm flight occurring very sharply. Measurements showed, for example, that close to the cloud boundaries $\frac{\partial K}{\partial z}$ and $\frac{\partial K}{\partial s}$ (s - horizontal coordinate) can exceed 0.2-0.3 m/s.

§ 2. TURBULENCE IN CUMULIFORM CLOUDS

One of the characteristic features of cumuliform clouds is the presence within them and, sometimes, close to them of exceptionally strong vertical and horizontal turbulent gusts. The scale of the gusts can vary in extremely wide limits, so that inside the clouds turbulent eddies with a cross section in cumulus clouds ranging from several meters to several tens of meters, and in cumulonimbus clouds even hundreds of meters, can coexist. If we consider convective (mesoscalar) vertical flows to be also elements of turbulence, within Cb it is possible for elements of thermal turbulence to exist with transverse dimensions reaching several kilometers.

a. Turbulence in cumulus clouds

The turbulence in Cu hum.-Cu med. clouds is basically thermal; dynamic instability caused by large flow-velocity gradients begins to play a significant role in the formation of turbulence only at the boundaries of thermals, an area for which these gradients are characteristic.

The largest elements of turbulence in clouds are thermals. Their cross sections can sometimes approach 2-3 km in size, although N. I. Vul'fson (1961a, 1961b) indicates that the probability of appearance of such large thermals is small; this quite clear from Fig. 8.3 and Table 8.7.

Table 6.7. Change with altitude of convection parameters in Cu hum.-Cu med. clouds.

(1) Высота полета, м		(2) Размеры термиков (средние)		(3) Концентрация термиков		(4) Отношение площадей (объемов) восходящих потоков
над землей (5)	над облаками (6)	стор. (7)	высота (8)	стор. км ² (9)	1 м (10) / км ³	
2000	200	59	56	120	1890	0,51
2500	700	78	70	92	1370	0,66
3000	1200	97	74	59	835	0,72
3500	1700	104	82	16	616	0,80
4000	2200	111	94	11	403	0,76
4500	2700	113	104	26	266	0,77

Remarks: m is the ratio of the size of the horizontal axes of thermals to the vertical axes. It is assumed that a bubble will have the form of an ellipsoid of revolution.

KEY: (1) Flight altitude, m; (2) Dimensions of thermals (average); (3) Concentration of thermals; (4) Relative area (volume) of ascending flows; (5) above the earth; (6) above the base of the clouds; (7) jet; (8) bubbles; (9) jet, km²; (10) 1/m bubbles/km³.

The horizontal dimensions of thermals, R, vary with altitude according to a linear law. For example, for a jet

$$R \approx 27 + 0,015z, \quad (8.4)$$

where z is altitude in meters, counted upwards from the base of the cloud. The vertical velocity at any point of the jet up to an altitude comprising about 2/3 of the thickness of the clouds above the base is determined by the relationship

$$w \approx 0,02z^{\frac{2}{3}} \left(1 - \frac{r^2}{R^2}\right)^{\frac{1}{2}}, \quad (8.5)$$

where r is the distance from the axis of the jet to the given point. According to N. I. Vul'fson's data, around the peaks of the growing cumulus clouds there is a relatively broad zone of descending compensation flows whose speed is several times less than the speed of ascent of air in the thermals.

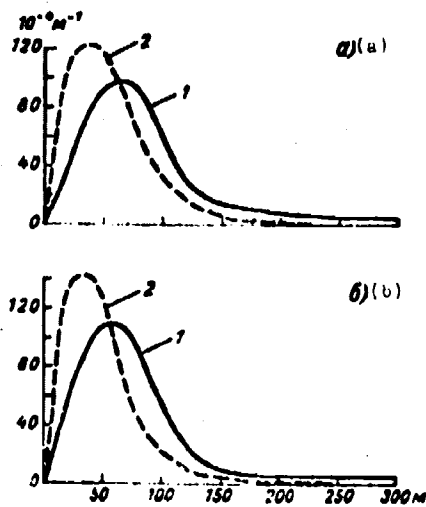
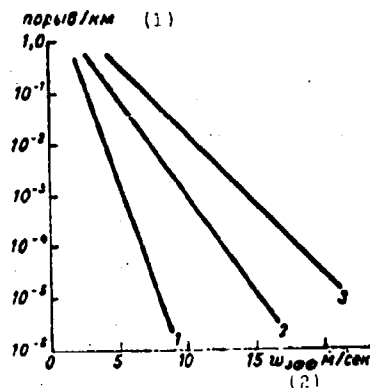


Fig. 8.3. Size distribution of convective flows in clouds (1) and outside the clouds (2). a - jets; b - "bubbles."

Studies carried out in the USA on the structure of vertical turbulent gusts inside cumulus clouds showed that on the average the slope of the spectrum $S(\Omega)$ inside them corresponds to the "minus five thirds" law; the mean square velocity of gusts was found to be 1.16 m/s. As is evident from Fig. 8.4, the probability of encountering vertical gusts of a given velocity inside cumulus clouds is 100-1000 times greater than in clear air. This difference grows with an increase in w .

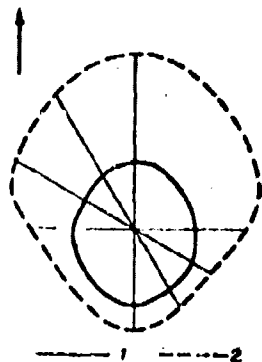
Fig. 8.4. Probability of encountering vertical gusts of a given magnitude (per Steiner and Rhyne). 1 - outside the clouds; 2 - in Cu; 3 - in Cb.
KEY: (1) gusts/km; (2) w_{eff} m/s.



The structure and distribution of turbulent zones around cumulus clouds have been studied only for trade-wind Cu (Ackerman, 1958).

According to these studies, the area of the turbulized zone around trade-wind Cu is 3.5 times greater than the area of the cloud at the same altitude. In this case the turbulent zone is most frequently asymmetrical and is extended along the vector of vertical wind shear (Fig. 8.5). Thus, during 379 crossings of 78 clouds Ackerman observed a symmetrical perturbed zone in only 27% of the cases.

Fig. 8.5. Distribution of turbulence in the zone of a cumulus cloud (per Ackerman). Arrow indicates the direction of the wind shear vector. 1 - boundary of cloud; 2 - boundary of turbulent zone.



According to Ackerman's data turbulence develops most strongly ahead of the cloud while J. Malkus (1949) indicated that it is more developed behind the cloud (relative to the direction of the wind shear vector). Such a divergence in opinion may possibly be explained by the fact that Malkus drew his conclusions for moderate and strong turbulence, while Ackerman considered turbulence without respect to its intensity.

The Ackerman studies also showed that as clouds "age" the dimensions of their turbulent zones continually increase (especially behind Cu). Even after the cloud has completely evaporated the segment of the atmosphere where it was located up to this point remains more perturbed than the surrounding air - i.e., turbulent zones live longer than the clouds with which they are associated. We will note that similar data were obtained by V. A. Zaytsev and A. A. Ledokhovitch (1961) for Cu cong.

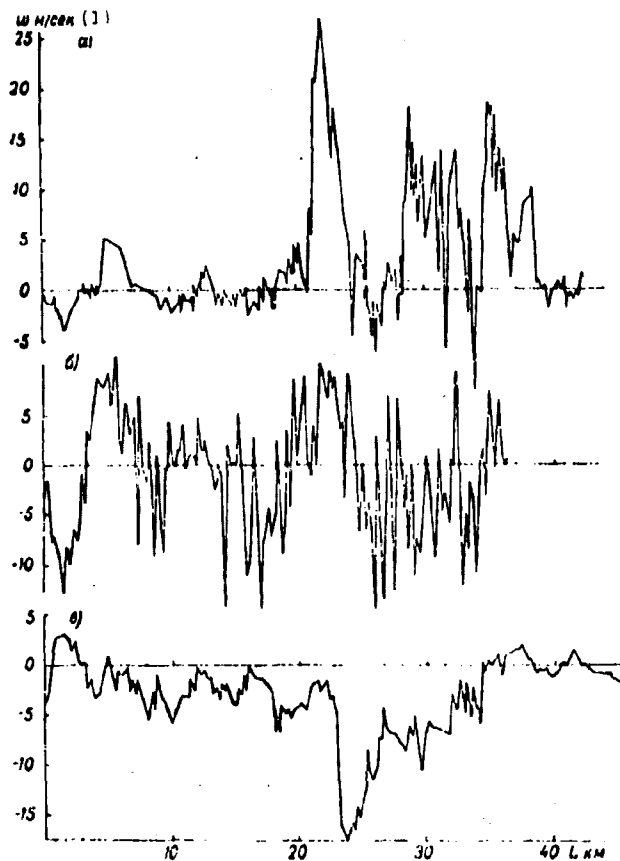


Fig. 8.6. Speeds of vertical motion of air within the peaks of cumulonimbus clouds (per S. M. Shmeter and V. I. Silayeva). a - growing cloud (24 July 1964, near Kiyev, flight altitude 8650 meters, height of upper edge of Cb 10-11 km); b - mature cloud (14 August 1961, near Voronezh, flight altitude 10,700 meters, height of upper edge of Cb approximately 12,000 m); c - beginning of stage of dissipation (8 August 1964, near Belou Lake, flight altitude 8,500 m, height of upper edge Cb approximately 12,000 m).
KEY: (1) w , m/s.

b. Turbulence in cumulonimbus clouds

Most frequently $L \leq 200$ m within cumulonimbus clouds, but mesoscalar flows with cross sections exceeding 5-7 km are also

encountered. Narrow flows with $L \leq 0.5-1.0$ km have the nature of short-cycle turbulent gusts for which magnitude and sign of velocity vary rapidly with time. The most characteristic feature of such gusts is the uniform probability of ascending and descending motions on all stages of cloud development.

The characteristics inherent to mesoscalar flows are different. Their horizontal dimensions vary from several hundreds of meters to 10-12 km, while velocity changes comparatively slowly with time, retaining its sign for several minutes. The predominant direction of such flows depends on the stage of cloud development (Fig. 8.6). Within growing clouds mainly ascending flows are observed. At the end of the mature stage of development ascending flows are retained mainly in the dome portion of the cloud, while air most frequently descends in its anvils. Finally, in the decay stage the ascending mesoscalar flows virtually disappear. The ascending and descending mesoscalar flows represent branches of convective circulation and, in the end, they determine all of the principal characteristics of the cloud - its dimensions, liquid-water content, intensity and nature of precipitation, etc. As is clear from Fig. 8.6, vertical flows inside clouds are usually the result of mutual imposition of short-period (turbulent) gusts on mesoscalar flows.

c. Mesoscalar flows inside CB

The presence within CB of a quasi-stationary heat source created by the intensive condensation of water vapor occurring inside the cloud leads to a situation in which elements of convection apparently have the form of jets. For example, H. Byers and R. Braham arrived at this conclusion on the basis of results of analyzing data from simultaneous intercession of Cu cong. and Cb at different levels with several aircraft.

b. Vonnegut et al. (see, for example, the article by Anderson, 1962) compiled data on the tension of the cable of a captive balloon placed inside a Cb, 500 m above its base, with the speed of growth of the apex of the cloud. Although the latter was located 3-7 km

higher than the base of the Cb, it was found that with growth of the cloud at $w \geq 2$ m/s the speed of ascent of the apex correlated closely with the tension on the cable. This is easily explained by assuming that both the balloon and the apex of the Cd were located inside one and the same ascending jet, penetrating through the entire cloud.

The most detailed information on mesoscalar vertical flows of air inside Cb was obtained by H. Byers and R. Braham (1948, 1949). Tables 8.8 and 8.9 present data obtained by these authors on the vertical velocities of mesoscalar flows of air inside Cb, compiled from materials from flights through 747 ascending and 339 descending flows.

Table 8.8. Frequency (in %) of velocities of ascending flows in Cb at different altitudes.

1) Градусы скорости, м/сек.	2) Высота, м									
	1830	3350	4870	6400	7920	1525	3050	4570	6100	7620
	3) Флориды					4) Огайо				
0,00—3,05	21,0	5,8	10,7	2,1	7,9	16,6	12,0	8,7	14,7	3,7
3,05—6,10	44,8	40,2	36,0	36,6	29,0	75,0	41,6	38,0	34,5	24,6
6,10—9,15	29,0	36,6	25,3	28,8	35,5	8,4	22,2	23,8	28,0	30,2
9,15—12,20	5,2	6,9	21,4	13,4	18,4	—	20,4	21,0	11,4	22,6
12,20—15,25	—	2,3	3,9	8,7	5,3	—	2,9	1,7	4,8	7,5
15,25—18,30	—	5,8	0,9	2,9	2,6	—	—	2,9	6,6	5,7
18,30—21,35	—	—	—	—	1,3	—	—	0,9	—	3,8
21,35—24,40	—	1,1	0,9	0,9	—	—	—	—	—	—
24,40—27,45	—	1,1	—	—	—	—	—	—	—	1,9
27,45—30,50	—	—	0,9	—	—	—	—	—	—	—
Число случаев (5)	38	87	103	101	76	12	108	105	61	538

KEY: (1) Velocity gradation, m/s; (2) Altitude, m;
(3) Florida; (4) Ohio; (5) Number of cases.

The average diameter of ascending flows turned out to be close to 1.5 km, where the figure for descending flows was 1.2 km. The maximum width of both was 12 km. The investigators did not succeed in detecting a definite relationship between the flight altitude and the width of mesoscalar vertical flows.

Table 8.9. Frequency (in %) of velocities of descending flows in Cb at different altitudes

(1) Градации скорости, м/сек.	(2) Высота, м									
	180	350	670	680	950	1325	3040	100	600	7620
	Флорида (3)					Огайо (4)				
0,00-3,05	18,2	14,3	7,5	21,2	10,4	50,0	25,6	20,9	19,2	9,1
3,05-6,10	50,0	47,6	55,9	51,5	41,8	41,6	30,6	45,6	42,4	36,4
6,10-9,15	22,7	23,8	22,7	21,2	26,5	8,4	32,6	16,2	31,6	22,8
9,15-12,20	4,5	11,9	11,3	3,0	7,9	-	8,2	9,4	3,8	13,6
12,20-15,25	-	-	3,8	3,1	7,9	-	2,0	1,6	-	9,1
15,25-18,30	-	-	-	-	2,6	-	-	2,3	-	1,5
18,30-21,35	4,6	2,4	1,8	-	-	-	-	-	-	1,5
Число случаев (5)	22	11	51	33	38	12	19	43	26	22

KEY: (1) Velocity gradation, m/s; (2) Altitude, m;
(3) Florida; (4) Ohio; (5) Number of cases.

In growing clouds ascending flows are observed throughout the entire thickness of the cloud. As the growth of Cb slows they weaken first in the lower half and then in the upper. In the lower portion of mature clouds descending flows predominate; in the opinion of the Byers and Brahm, they are caused by the entrainment of air by particles of falling precipitation and also by cooling of the air as the result of evaporation.

We will note that the most recent studies indicate that maximum values of w may be much larger than those shown in Tables 8.8-8.9. Thus, the measurements above the USA (Steiner, Rhyne, 1964) showed w_{\max} reaching up to 53 m/s. P. Ludlum (1963) showed¹ that in very thick cumulonimbus clouds w_{\max} reaches 100 m/s.

G. K. Sulakvelidze, M. Sh. Bibilashvili, and V. P. Lapcheva (1965) studied mesoscalar vertical flows inside Cu cong. and Cb, using balanced pilot balloons with corner reflectors as passive radar targets. The rate of rise (ascent) of such a pilot balloon

¹The value of w_{\max} was evaluated under the assumption that on the average the air in the cloud is 5° warmer than the surrounding air and stratification is "strongly unstable."

was accepted as the vertical speed of the air. In the opinion of the authors the relative error in measuring w did not exceed 30%. Twenty-four series of measurements were carried out. The observations showed that the speed of the ascending flow inside Cu cong. and Cb clouds from which precipitation had not begun to fall grows from the base of the cloud to its middle or the portion just below the top, after which it diminishes. In Cb from which rain was falling descending flows were observed along with the ascending flows; here the values of w_{\max} were similar in both flows. The largest values of w_{\max} comprised 20-25 m/s.

N. S. Shishkin (1964), G. Malkus and K. Scorer (1955), C. Anderson (1962), and others carried out approximate evaluation of the speeds of vertical motions close to the upper edge of Cb in terms of the rate of change of altitude of the latter (w_c). The most significant results were obtained by Anderson, who determined w_c by means of stereophotography of Cb tops. Considering the oscillations of w_c to be a random process, he applied methods of statistical analysis to the obtained data.

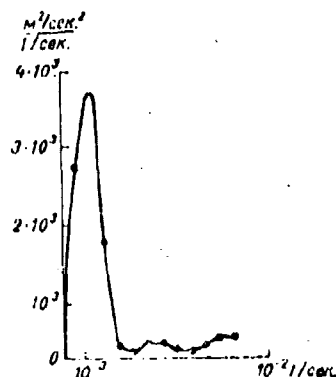
According to Anderson, the rate of Cb growth - which means also the vertical speed of air at the top of the cloud - fluctuates constantly. Besides high-frequency oscillations with a period of 1-2 minutes, w_c is subjected to low-frequency, almost sinusoidal, oscillations with a period of 10-12 minutes. As is clear from Fig. 8.7, the oscillations with a period close to 12 minutes have the maximum energy. Anderson considers that the high frequency oscillations have a turbulent origin, while the low-frequency oscillations are connected with the stability of stratification of the air surrounding the cloud.

According to R. Douglas and V. Hitchfield¹ (see, for example, the article by C. Newton, 1963), fluctuations of w_c are minimum in mature Cb and, besides this, the larger the cloud the smaller the fluctuations. On this basis Newton proposed that large pulsations

¹Spelling of names not verified - Translator.

in w_0 are observed only during free convection; in particular, this is confirmed by the observations of internal Cu. With the development of forced convection connected with the ascent of air ahead of the cloud, the ascending current becomes more stable. Naturally, the "steadying" effect of forced convection is maximum in mature Cb, when the dome of cold sub-cloud air - and thus forced convection ahead of the Cb - become greatest. A somewhat different opinion was expressed by F. Ludlam (1963), who considers fluctuations in the rate of growth of Cb to be caused by periodic penetration of new thermals into the cloud.

Fig. 8.7. Spectrum of vertical velocity of the Cb top (per Anderson).
 cex = seconds



d. Mesoscalar vertical flows in the neighborhoods of Cb

In 1959-1965, during flights on a Tu-104B laboratory aircraft, S. M. Shmets carried out detailed studies of the structure of the field of mesoscalar vertical motions in the neighborhoods of cumulonimbus clouds. Tables 8.10 and 8.11 give data on these flows at a distance of 0-1 km from the side surface of the upper half of mature Cb and in a layer 200 m thick above them.

From the tables it is clear that in the neighborhoods of Cb tops we most frequently find $|w| \leq 2$ m/s, while the horizontal dimensions of descending flows are greater than those of the ascending flows.

Measurements of w in precipitation below the base of Cb showed that here the average speed of mesoscalar vertical flows is close to 3 m/s for ascending flows and to 4 m/s for descending flows.

Table 8.10. Frequency (in %) of speeds of mesoscalar vertical motions around the upper half of Cb.

(1) УЧАСТОК	w м/сек.									
	0,0-2,0	2,1-3,0	4,1-5,0	6,1-8,0	8,1-10,0	0,0-2,0	2,1-3,0	4,1-6,0	6,1-8,0	8,1-10,0
	(2) Нисходящие потоки					(3) Восходящие потоки				
(4) Над Сб	81	30	5	2	2	81	17	2		
(5) Сбоку Сб	66	22	10	2	—	55	32	11	2	

KEY: (1) Segment; (2) Descending flows; (3) Ascending flows; (4) Above Cb; (5) Beside Cb.

Table 8.11. Frequency (in %) of horizontal dimensions of L of mesoscalar vertical flows around the upper half of Cb.

(1) УЧАСТОК	L км													
	<1,0	1,0-3,0	3,1-5,0	5,1-7,0	7,1-9,0	9,1-11,0	>11,0	<1,0	1,0-3,0	3,1-5,0	5,1-7,0	7,1-9,0	9,1-11,0	>11,0
	(2) Нисходящие потоки							(3) Восходящие потоки						
(4) Над Сб	6	19	25	15	10	6	19	19	29	29	15	—	2	6
(5) Сбоку Сб	6	28	26	6	—	16	18	34	21	27	4	4	10	—

KEY: (1) Segment; (2) Descending flows; (3) Ascending flows; (4) Above Cb; (5) Beside Cb.

Figure 8.8 shows the spatial structure of mesoscalar vertical flows in different portions of the zone of mature Cb. The diagrams were constructed without distortion of the relative linear scales of each of the segments. The length of the horizontal section of the Cb in the appropriate direction was selected as the unit of distance.

From Figure 8.8b it is clear that ahead of the upwind edge of mature Cb the ascending flows are localized. Their average velocity (\bar{w}) varies here from 0.5 to 1.5-2 m/s. Ascending motions with $|\bar{w}| \leq 1$ m/s are observed only in a narrow band adjacent to the side boundary of the cloud. In this case the segment with $w < 0$ behind the lee edge is twice as long as that in front of the windward edge. It is characteristic that the sign \bar{w} changes periodically behind the cloud, with the length of a wave being close to the "diameter" of the cloud.

A region of ascending flows is located inside the central portion of the Cb top; the average speed of these flows is close to 1 m/s.

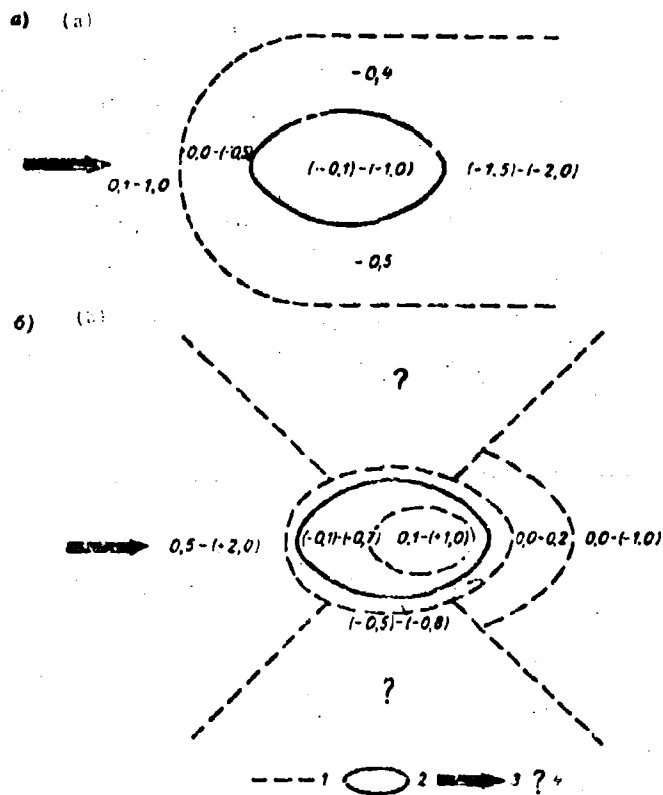


Fig. 8.8. Averaged vertical velocities in a zone of cumulonimbus clouds. Numbers indicate average speed in m/s. a - above Cb; b - inside the top and within it. 1 - demarcation lines separating segments with w of different signs; 2 - cloud; 3 - direction of cloud motion (vector of relative velocity of air); 4 - segment for which there are no reliable data on \bar{w} .

Descending motions predominate above Cb. Their speed is especially great above the center of the cloud and behind it on the lee edge. Here air settles, even on the average, at a speed exceeding 1 m/s.

A significant portion of the under-cloud zone is occupied by descending flows. Their highest speeds, with $\bar{w} = 1-2$ m/s, are localized in the central portion of the region of precipitation. The descending motions change to ascending motions in front of the lee edge of the Cb.

The overall structure of the \bar{w} field beside Cb-tops is reminiscent of the picture observed during flow over mountains with lifting of the air on the weather slope and the system of waves downstream. Descending motions on the side boundaries of the cloud are probably connected with the cooling of the air which occurs here during evaporation of cloud elements.

Beneath Cb the descending flows are connected with falling precipitation. This is confirmed by the coincidence of their areas and by the fact that the maximum velocity of descending flows is observed precisely where precipitation is strongest.

Ascending flows near the lower portion of Cb are probably caused in part by convective lifting of air from the underlying surface, and partly by dynamic lifting of air at the edge of the dome of cold under-cloud air as the cloud travels.

e. Short-period turbulent gusts inside Cb

The first systematic investigations of short-period vertical air gusts inside Cb were carried out by H. Byers and R. Braham (1949) in the USA. Since out of the various characteristics of perturbed motion of the aircraft they measured only g-forces, instead of true velocities of vertical gusts they determined only the effective velocities w_{eff} .

Table 8.12 shows the frequency of maximum values of $|w_{eff}|$ according to results of measurements during flights in Florida and Ohio. The intensity of turbulence was maximum in the middle (in altitude) portion of the Cb, i.e., where the velocities of mesoscalar ascending flows were also greatest.

The horizontal scales of gusts varied from 8 to 270 m. During the measurements the spectrum of gust sizes was automatically cut to 8 meters due to the inertia of the aircraft/accelerograph system. The limitation of sizes of turbulent gusts to a magnitude of 270 m has a conditional character, since gusts of larger sizes are related by the authors to the class of mesoscalar ascending flows.

Table 8.12. Frequency of maximum effective velocities $|w_{eff}|$ inside Cb.

(3) $ w_{eff} $ м/сек.	(1) Высота, км					(2) Общее количество порывов
	1,3-1,8	3,0-3,6	4,0-4,9	6,1-6,4	7,6-7,9	
0-1,2	40,0	36,0	38,5	40,2	45,1	8319
1,2-2,4	32,5	32,7	31,8	31,0	29,0	7053
2,4-3,6	18,2	18,4	17,1	17,1	15,1	3855
3,6-4,8	6,3	8,2	7,4	7,4	6,7	1057
4,8-6,1	1,9	3,1	3,3	2,7	2,8	632
6,1-7,3	0,6	1,1	1,3	1,1	0,7	228
7,3-8,5	0,5	0,3	0,3	0,3	0,5	70
8,5-9,8	—	0,1	0,2	0,2	0,1	31
9,8-11,0	—	0,1	0,1	0,1	—	10
>11,0	—	—	0,2	—	—	5
Общее количество порывов (2)	3315	5527	6003	4111	3083	22370

KEY: (1) Altitude, km; (2) Total quantity of gusts; (3) $|w_{eff}|$ m/s.

The results of later investigations of vertical turbulent gusts and measurement of their velocity during random encounters by aircraft equipped with accelerographs inside Cb show good agreement with the data of Byers and Braham. Thus, data collected by R. Steiner and R. Rhyne show that the mean square effective velocities measured during flights in Cb with jet aircraft at altitudes of 3-7 km over the USA fell within the limits 2-3 m/s. In June 1962 during flight

inside a Cb by a "Meteor" aircraft (USA) $|w_{eff}| = 11$ m/s was recorded, while on a "Northrop" aircraft a value of 14 m/s was registered. Apparently, larger w_{eff} are rarely observed¹.

Table 8.13 shows the frequency of maximum vertical gusts in the 0-500 m layer below the upper edge of Cb according to the data of V. S. Aleksandrov, V. I. Silayeva, and S. M. Shmeter (1967).

Table 8.13. Frequency (in %) of maximum velocities of turbulent gusts inside the near-apex portion of Cb.

(2) Стадия развития Cb	Вертикальная скорость, м/сек.		
	<2	2-5	>5
(3) Растущие и зрелые:			
(4) в куполах	26	54	20
(5) в анках пальцы	12	87	1
Распадающиеся (6)	73	26	1

KEY: (1) Vertical velocity, m/s; (2) Stage of Cb development; (3) Growing and mature; (4) in domes; (5) in anvils; (6) Decaying.

From Table 8.13 it is clear that even directly under the upper edge of growing and mature Cb the vertical velocities of turbulent gusts exceed, in the overwhelming majority of cases, 2 m/s. We will note that in clear air the frequency of such velocities is 10-20 times less.

During six crossing of Cb at a distance from the upper edge greater than 2 km, carried out during the Shmeter studies, it was found that here gusts with $|w_{eff}| > 5$ m/s always exist, while in growing and mature clouds the value can reach even $|w_{eff}| > 10$ m/s. The maximum speed of a vertical gust, equal to 12 m/s, was recorded on

¹Indications encountered in the literature concerning the presence of vertical velocities exceeding 30 m/s inside Cb relate not to turbulent, but to mesoscalar vertical flows.

24 July 1964 while crossing a thundercloud in the Kiyev region at a level of 8 km - 2-2.5 km below the upper edge of the Cb.

The measurements showed that inside Cb vertical gusts of one intensity or another are almost always observed, on an extent of more than $3/4$ of the diameter of the cloud in the flight area. Those cases in which none were observed related exclusively to approach to the peripheral portion of the anvils of dissipating clouds, but at a depth not exceeding 20-30 m.

A characteristic feature of turbulent zones inside Cb is the fact that the velocities of vertical gusts vary not only along the vertical, but also the horizontal. In clouds consisting of a single convective cell the gusts are maximum close to the cloud axis. If the Cb contains several cells the horizontal distribution of w_T is more complex. Although in general the velocities of gusts most frequently diminish from the center of the cloud to its lateral boundaries, several partial maxima of $|w_T|$ are observed within Cb; these are located inside the mesoscalar vertical flows or on their boundaries. The main maximum is usually connected with the cell inside which the mesoscalar vertical velocities are greatest. Thus there is apparently a connection between mesoscalar and turbulent motion inside Cb. According to American data, the coefficient of correlation between maximum velocities of turbulent gusts $|w_{T, M}|$ and the vertical velocity of mesoscalar flows $|w_H|$ equals 0.42 ± 0.02 for the entire range of $|w_H|$. According to materials gathered by S. M. Shmeter, when $|w_H| > 5$ m/s the mutual correlation between $|w_{T, M}|$ and $|w_H|$ weakens.

In the opinion of Byers and Braham (1949), the dependence of $|w_T|$ on $|w_H|$ is a consequence of the fact that turbulent eddies are generated close to the boundary of mesoscalar jets, where the horizontal gradients of vertical air speed are great. Subsequently, thanks to the "natural" horizontal speeds, the eddies can be displaced into other portions of the Cb.

It should be noted that the described dependence of $|w_{T, M}|$ on $|w_H|$ is characteristic only for growing and mature Cb. Within decomposing Cb the quantity $|w_H|$ frequently diminishes much more rapidly than $|w_{T, M}|$.

The characteristics of vertical turbulent gusts inside Cb were examined above. At present there have been virtually no measurements made of horizontal gusts. An exception is the work done by R. Steiner and R. Rhyne (1962), who used a special airborne inclinograph to measure horizontal turbulent gusts along with vertical gusts. According to their data, the mean square velocities of horizontal and vertical gusts inside Cb differ from one another by no more than a few percent. The spectral composition of the two types of gusts is also similar. Thus, turbulence is practically isotropic inside Cb.

f. Turbulence in the vicinity of Cb

Table 8.14 presents the characteristics of vertical turbulent gusts above Cb based on materials of 263 series of measurements. With elevation above the cloud the speed of gusts diminishes quite rapidly, so that with an altitude greater than 200 m above the clouds the probability of $|w_T| > 2$ m/s comprises less than 4%, while $|w_T| > 5$ m/s is about 1%. A certain growth in the intensity of turbulence at heights more than 400 m above the clouds is apparently not directly connected with the influence of the clouds, but is a consequence of intensification of turbulence under the tropopause.

The speed of gusts is greatest above growing clouds. In the mature stage above the dome portion of Cb the characteristics of turbulence are virtually unchanged as compared with those in the stage of cloud growth, while above the ridges of the anvil turbulence is noticeably weakened. A unique picture is observed above dissipating clouds. Ordinarily $|w_T| < 2$ m/s above them, but nonetheless the thickness of the turbulent zone remains the same as above mature Cb or may even be somewhat increased.

Table 8.14. Speed of vertical turbulent gusts $|w_T|$ m/s above Cb (per Aleksandrov, Silayeva, and Shmeter, 1967).

(2) $ w_T $ м сек.	Преципитация над Сб, м (1)					
	0-10	11-100	101-200	201-300	301-400	>400
<0.5	34	55	66	83	100	46
0.5-2.0	44	27	34	13	0	10
2.1-5.0	21	18	0	0	0	4
>5.0	1	0	0	4	0	0

KEY: (1) Height above Cb, m; (2) $|w_T|$ m/s.

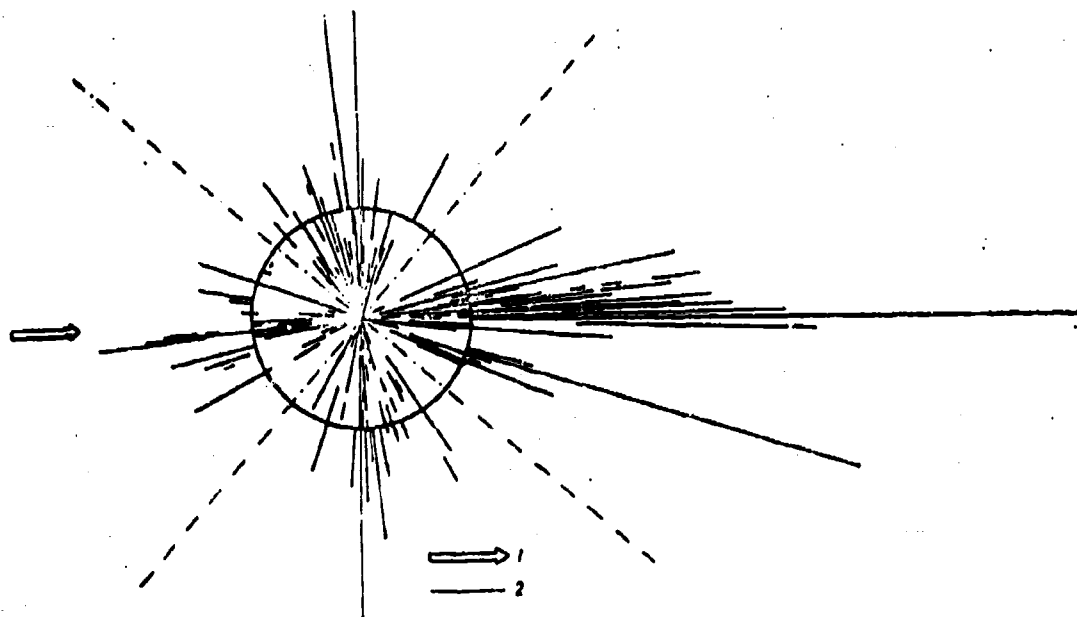


Fig. 8.9. Location of turbulent zones around the apex of Cb with respect to wind (per V. S. Aleksandrov, V. I. Silayeva, and S. M. Shmeter). 1 - direction of outer wind; 2 - turbulent sections.

The arrangement and length of turbulent segments in the 0-200 m layer above Cb are shown in Fig. 8.9. A segment was considered to be turbulent if the mean square vertical speed on it (σ_w) exceeded 1 m/s. The contour of the cloud is depicted in the form of a circle.

When the individual data were united the linear dimensions of specific clouds and their turbulent zones were reduced to a common scale. The orientation of turbulent segments is given with respect to the direction of the wind vector at the level of the cloud peak. For the sake of clarity, turbulent zones which coincided during different passes were plotted at a small angle to one another. Broken lines are used to separate the "weather" and "lee" sides and the regions located parallel to the wind vector. It is clear that the arrangement of turbulent zones with respect to wind is asymmetrical and, in particular, the frequency of turbulence and the length of turbulence zones is greatest behind the "lee" side of the Cb. Intensification of turbulence behind the "lee" half of the Cb is caused, most likely, by the effect of wind flowing around the cloud, a subject which we have already discussed above.

Table 8.15 gives S. M. Shmeter's data on the frequency of velocities of turbulent gusts at a distance of no more than 1 km from the side boundaries.

Table 8.15. Frequency (in %) of absolute values of maximum velocities of turbulent gusts (m/s) to the side of Cb.

	(1) Градации скорости, м/сек.							
	≤ 0.5	0.5-2.0	2.1-5.0	≥ 5.0	≤ 0.5	0.5-2.0	2.1-5.0	≥ 5.0
	Нижняя половина Cb (2)				Верхняя половина Cb (3)			
(4) Наветренная сторона	77	14	6	3	60	31	9	—
(5) Подветренная сторона	88	9	3	—	53	35	10	2
(6) Стороны, параллельные ветру	89	6	4	1	67	26	6	1

KEY: (1) Velocity gradations, m/s; (2) Lower half of Cb; (3) Upper half of Cb; (4) Weather side; (5) Lee side; (6) Sides parallel to the wind.

The total probability of turbulence¹ along side Cb was found to be less than that above the cloud; this is due to the fact that

¹The case $|w_r| < 0.5$ m/s can tentatively be considered to correspond to calm (nonturbulent) conditions.

measurements in the 0-500 m layer above the upper edge of the cloud were used above Cb (Table 8.14), while the measurements of w_T beside Cb (Table 8.15) were made at distances from the clouds reaching 500-1000 m.

g. Coefficient of turbulence in Cb

The high level of intensity of turbulence inside Cb leads to the development here of active vertical and horizontal turbulent exchange. At present, however, data are available only on the coefficient of vertical turbulent exchange K in Cb.

N. Z. Pinus (1963), Pinus and V. D. Litvinova (1962), and S. M. Shmeter and V. I. Silayeva (1966) calculated values of K from data on aircraft g-forces, using formula (8.2).

Table 8.16 gives the average values of K and various portions of the upper half of Cb according to the data of Shmeter and Silayeva (1966). To ensure statistical reliability the calculations were carried out only for cases when the length of the aircraft path inside the cloud (i.e., the length of the turbulent zone) exceeded 10 km. In the majority of cases it equaled 20-30 km, with gusts whose horizontal dimension does not exceed 600 m being considered as turbulent.

Table 8.16. Average coefficient of turbulence \bar{K} in different portion of Cb.

	Внутри вершины 1)	На верхней кромке 2)	На боковой кромке 3)
(4) \bar{K} м ² /сек.	215	146	95
Число случаев (5)	13	13	4

KEY: (1) Inside the peak; (2) On the upper edge; (3) On the side edge; (4) \bar{K} , m²/s; (5) Number of cases.

Analysis of materials from measurements made during individual passes showed that the quantity K is maximum in mature Cb, inside which it may exceed $500 \text{ m}^2/\text{s}$, while it is minimum in the end of the stage of Cb decay, when \bar{K} is usually $\leq 150 \text{ m}^2/\text{s}$.

N. P. Tverskaya (1964) evaluated the quantity \bar{K} inside Cb from data on temperature and wind sounding in the Leningrad regions; \bar{K} was calculated by the L. T. Matveyev formula:

$$\bar{K} = \frac{U^2}{\beta} [2.3 \lg p - 1.6 \lg (\gamma_a - \gamma) - 0.072], \quad (8.6)$$

where U is the velocity of the wind; β is the vertical wind velocity gradient; γ and γ_a are the real and adiabatic vertical temperature gradients. It was proposed that if the quantity of Cb exceeded 8 scale marks and if their altitude exceeded 8 km, the radiosonde would be located inside Cb during the course of its entire ascent in the troposphere. It was found that \bar{K} grows rapidly with approach to the upper edge of the Cb. Maximum values of \bar{K} , as a rule, exceeded $100 \text{ m}^2/\text{s}$ and sometimes reached $300 \text{ m}^2/\text{s}$. Thus, the general laws of change in \bar{K} with altitude and the order of magnitude of the obtained quantities turned out to be close to those given in Table 8.16.

In large Cb containing several convective cells there is no monotonic diminishing of K with approach to the edges of the cloud. The field of K in them has a complex spatial structure formed as the result of mutual imposition of "individual" K fields in the zone of individual cells. A substantial role is played by the fact that turbulence in different cells inside one and the same cloud will have different intensities; besides this, the dimensions of the cells are not identical. Since new cells can grow around the periphery of the Cb, the maximum values of K are sometimes observed close to one of the side edges of the cloud.

h. Statistical characteristics of atmospheric turbulence in the zone of Cb

Spectral analysis of the atmospheric turbulence inside Cb has been undertaken only in the last three-five years. In the period

1960-1961 laboratory aircraft in the USA carried out several crossings of Cb at altitudes ranging from 5 to 13 km. Measurements were carried out at subsonic and supersonic speeds, which made it possible to construct spectra of atmospheric turbulence in a wavelength range of 30 m to 4-5 km. About 70 spectra of turbulent gusts for segments inside Cb and their vicinity were calculated by S. M. Shmeter and V. I. Silayeva.

The use of data on $S(\Omega)$ to describe turbulence is advisable only in those cases when the process can be considered quasi-stationary. First of all this is necessary in order to ensure that the individual spectrum has physical meaning; secondly, the quasi-stationary state of turbulence over the extent of each stage of evolution of the cloud is required in order to obtain evaluations which are not random but which characterize the level of turbulent energy typical for the given period in the life of the Cb. Studies have shown that although the total life cycle of development of Cb occurs within a time on the order of one-two hours - i.e., quite rapidly - it is only in the initial stage of growth that the cloud characteristics (in particular, turbulence) change rapidly. During the remaining lifetime of Cb such changes are sharply retarded. For example, the mean clear rate of turbulent pulsations, the average velocity of mesoscalar vertical flows, and their dimensions ordinarily change by no more than 10-15% in 3-5 minutes; this makes it possible to consider the process to be quasi-stationary. This is even more valid for an interval of minutes, typical for the segments of time for which individual spectra are calculated.

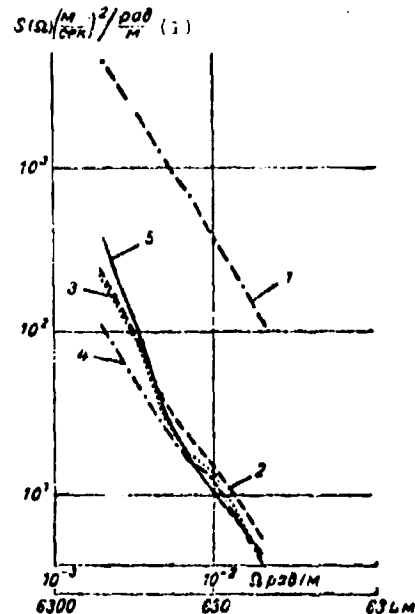
Figure 8.10 gives averaged spectra of the vertical velocities of air, $\bar{S}(\Omega)$, for different segments of the Cb zone, while Table 8.17 presents average and extremal values of $S(\Omega)$ for different linear scales of L.

The first group includes data on the magnitudes of $S(\Omega)$ in clouds below the lowest edge of the Cb, while the second case includes data for the side edges of the cloud. The third group includes data for the 0-200 m layer above the cloud, while the fourth relates to the

level inside the axial portion of the Cb located at a distance of a few hundred meters under the upper edge. Finally, the fifth group unites data for the levels inside the Cb located more than 2 km below the upper edge of the cloud.

Fig. 8.10. Averaged spectra of velocities of vertical motions in a Cb zone (per S. M. Shmeter and V. I. Silayeva). 1 - inside the central portion of Cb (four cases); 2 - inside the near-peak portion of the Cb (17 cases); 3 - above Cb (18 cases); 4 - to one side of Cb (18 cases); 5 - under Cb (10 cases).

KEY: (1) $S(\Omega)$ (m/s)²/(rad/m);
(2) Ω , rad/m.



Comparison of spectral densities averaged in terms of all cases of flight in the given portion of a Cb zone for which individual spectra were calculated shows that both the absolute values of $S(\Omega)$ and their change with a change in L in different segments of the Cb zone are different. The spectral density of vertical gusts inside the central portion of the Cb is 10 and more times greater than that on the circumference of the clouds and even than that within the near peak portion of the Cb. The difference between the quantities $S(\Omega)$ in all the portions of the Cb zone is comparatively small. Characteristically, it increases with a growth in L .

As is evident from Fig. 8.10, with a change in L the slope of the curves of spectral density is also changed. Thus, on the segments $600 \text{ m} < L < 1000 \text{ m}$ in every place except the subcloud portion of

the atmosphere and the internal portion of the Cb there is a sharp reduction in $|\operatorname{tg} \varphi|$ (φ - is the angle formed by the curve of spectral density with the abscissa). Inside near-peak region of the Cb and to one side of Cb on the segment $L < 600$ m and 1000 m $< L < 3000$ m $\operatorname{tg} \varphi \approx -5/3$. We will note that this is evident also on the majority of individual spectra. Within the central portion of Cb, $|\operatorname{tg} \varphi| \leq 5/3$ for all the considered values of L.

Table 8.17. Values of $S(\Omega)$ (m/s)²/(rad/m) in different portions of Cb zone.

		L м			
		300	1000	2000	3000
1. Под Сб (1)					
ξ		4	21	122	370
$S_{\text{мин}}$		3	14	53	90
$S_{\text{макс}}$		7	30	215	800
2. Сбоку Сб (2)					
ξ		4	19	53	105
$S_{\text{мин}}$		1	7	27	34
$S_{\text{макс}}$		20	40	100	195
3. Над Сб (3)					
ξ		4	21	105	215
$S_{\text{мин}}$		1	5	12	13
$S_{\text{макс}}$		21	77	360	850
4. В предвершинной части Сб (4)					
ξ		6	26	100	220
$S_{\text{мин}}$		1	7	16	44
$S_{\text{макс}}$		10	44	230	730
5. Внутри центральной части Сб (5)					
ξ		119	800	2300	4300
$S_{\text{мин}}$		4	40	110	275
$S_{\text{макс}}$		290	1580	4150	7400

KEY: (1) Under Cb; (2) beside Cb; (3) Above Cb; (4) In the near-peak portion of Cb; (5) Inside the central portion of Cb.

мин = min макс = max

The spectral density of vertical gusts above Cb and below them with $L < 600$ m changes with a change in L in approximate obedience to the "minus 5/3" law. At gust scales greater than 1000 m the slope of the curve $S(\Omega)$ grows sharply.

As was pointed out in Chapter 1, a change in the slope of the $S(\Omega)$ curve may be connected with a change in the rate of energy transfer along the spectrum in accordance with the range of scales - i.e., either with the accumulation of turbulent energy here or with acceleration of its consumption. The fact that $|\text{tg } \varphi| \leq 5/3$ inside Cb may be due to the instability of atmospheric stratification, while the growth in curvature of the spectrum at $L > 1$ km in the above-cloud segment is, on the other hand, connected with an increase in stability. This type of atmosphere stratification in a Cb zone is evident from Table 8.18.

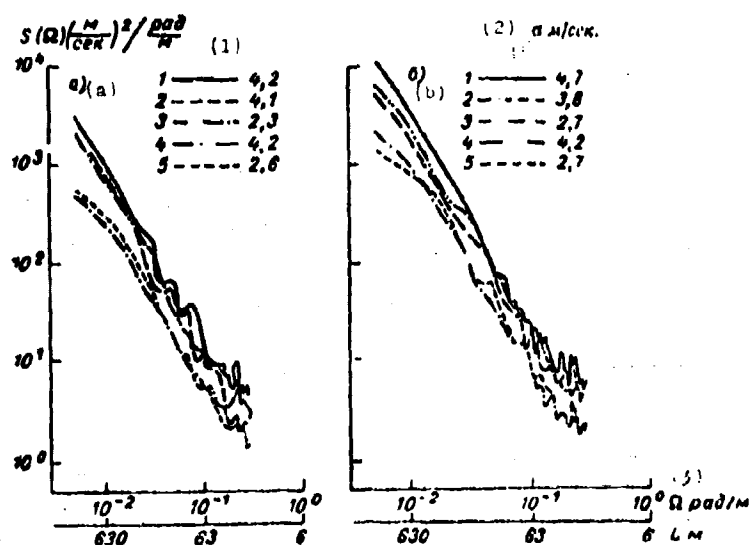


Fig. 8.11. Change in spectral density with time of vertical (a) and horizontal (b) turbulent gusts inside Cb (per Steiner and Rhyne). 1, 2, 3, 4, 5 - number of successive passes; σ - mean square velocity. KEY: (1) $S(\Omega)(\text{m/s})^2/(\text{rad/m})$; (2) σ , m/s; (3) Ω rad/m.

Along with $\bar{\gamma}$, Table 8.18 presents the mean square deviations from it. There were no data on the magnitude of $\bar{\gamma}$ inside Cb, since no vertical sounding of the atmosphere inside the cloud was carried out. We can assume that here $\gamma_{Ba} \leq \bar{\gamma} < \gamma_a$ (γ_a and γ_{Ba} are adiabatic gradients in dry and saturated air).

Table 8.18. Average vertical temperature gradients $\bar{\gamma}$ deg/100 m in a Cb zone.

Not Cb (1)	(2) Beside Cb	(3) Above Cb
0,65±0,01	0,80±0,13	0,69±0,03

KEY: (1) Under Cb; (2) Beside Cb; (3) Above Cb.

Clarification of the curve $S(\Omega)$ in the subcloud region segment is more complex, since in this case stratification is weakly stable and also the curve $S(\Omega)$ is the same as with strong stability.

Among the possible factors causing a deviation in the shape of the $S(\Omega)$ under Cb from the "minus 5/3" law, we should cite in the first place the influence of the underlying surface on the characteristic of turbulence in this layer. This conclusion follows from the fact that the altitude of the base of the Cb usually comprises 1-1.5 km above the ground - i.e., a quantity close to the dimensions of turbulent formations when $\Omega < 10^{-2}$ rad/m. It is clear that the degree of influence of the underlying surface on turbulence depends on the roughness of the surface, wind velocity, stratification of the lowest atmospheric layer, etc.

Data on $S(\Omega)$ in those cases when the "minus 5/3" law is fulfilled permit us to evaluate the rate ϵ of dissipation of turbulence energy. Inside Cb $\bar{\epsilon} \approx 2000 \text{ cm}^2/\text{s}^3$, while along the side edges of these clouds $\bar{\epsilon} = 10 \text{ cm}^2/\text{s}^3$. It is impossible to calculate ϵ for the above-cloud and subcloud segments because of the fact that when $L > 1000 \text{ m}$ in them the "minus 5/3" law is not fulfilled.

We will move now to consider the changes in spectral density of gusts in different segments of a Cb zone with time.

Figure 8.11 shows spectra of velocities of vertical and horizontal air gusts inside a mature Cb; these data were obtained during five successive crossings of the cloud in a period of 34 minutes. Data are also given on the mean square speeds of gusts for each crossing. A noticeable feature is the comparatively small time variability of the spectral characteristics of turbulence inside the Cb. This should be particularly emphasized, since in this case the measured variability of $S_w(\Omega)$ and $S_u(\Omega)$ should have been substantially greater than the actual values because of the impossibility of guiding the aircraft over the precisely identical route on successive passes.

CHAPTER 9

LOCAL STRUCTURE OF THE WIND VELOCITY FIELD

§ 1. LOCAL HETEROGENEITY OF THE WIND VELOCITY FIELD

The vertical cross section of a jet stream constructed from radiosonde data gives an idea of the distribution of average wind velocity in this stream. A more detailed picture can be obtained by using data from more frequent measurements of the velocity and direction of the wind made by means of Doppler equipment installed on an aircraft. Such studies of the wind are of great interest since the spatial mesoscalar variability of wind velocity and direction will naturally lead to a high degree of variability in vertical and horizontal wind-velocity gradients - i.e., precisely those parameters which render the greatest influence on the development of turbulence, especially at the altitudes where the atmosphere is, in general, stably stratified.

Experimental studies of the local structure of the wind field (Pinus, Shmeter, 1962) have shown that local maxima of wind velocity are observed in an airflow against a background of general transfer of air at a certain average velocity. These local zones represent flattened streams of various sizes. In a number of cases large local zones bounded by a common isotach in the horizontal plane or on a vertical section of the atmosphere consist of a series of much smaller zones with maxima or minima of wind velocity. Figure 9.1 shows clearly that within zones bounded by the 130 km/h isotach three

extrema with velocities of 140-150 km/h are observed. In this particular case the horizontal dimensions of local heterogeneities equal 10-50 km.

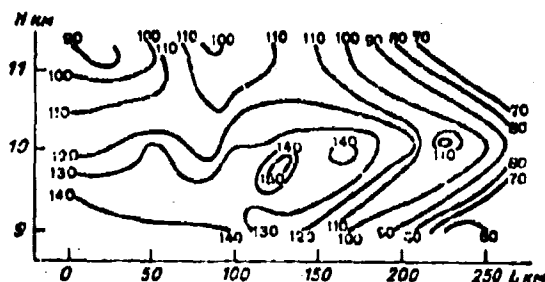


Fig. 9.1. Isotachs constructed from data obtained by measurements every 15 s of a flight.

It should be noted that local spatial changes in wind velocity do not always correlate with the spatial changes in air temperature and also that as a consequence the explanation of the appearance of perturbations in the wind field with scales of several tens of kilometers cannot always be found from the concepts on thermal wind. It should also be noted that during crossing of these heterogeneities turbulence sufficient to cause buffeting of the aircraft is, as a rule, observed.

Flight experiments showed that such heterogeneities in the wind field are observed most frequently in the region of divergence of airflows and in the small-gradient pressure fields, but are not observed in convergence zones.

As we know from aerodynamics, even an insignificant compression of the flow has a stabilizing influence on laminar flow, and with other conditions being equal the critical Reynolds number Re_{cr} turns out to be greater than for a noncompressed flow. With weakly expanding walls, on the other hand, turbulent flow arises with small Re_{cr} . With an increase in the angle of wall flare of a wind tunnel a reverse flow arises and breakaway from the walls occurs; breakaway does not occur simultaneously from both walls, but only from one.

Theoretical consideration of stationary motion of a fluid between two plane walls sloped toward one another at angle α was carried out by G. Hamel (1916).

The equations of motion for a flow of this type in cylindrical coordinates (r, z, ϕ) , where ϕ is the angle between the axis of symmetry and the radius-vector r) have the following form:

$$v \frac{dv}{dr} = -\frac{1}{r} \frac{\partial p}{\partial r} + v \left(\frac{\partial^2 v}{\partial r^2} + \frac{1}{r^2} \frac{\partial^2 v}{\partial \phi^2} + \frac{1}{r} \frac{\partial v}{\partial r} - \frac{v^2}{r^2} \right), \quad (9.1)$$

$$-\frac{1}{r} \frac{\partial p}{\partial r} + \frac{2v}{r^2} \frac{\partial v}{\partial \phi} = 0, \quad (9.2)$$

$$\frac{\partial(rv)}{\partial r} = 0. \quad (9.3)$$

During the derivation of these equations it is assumed that motion is uniform along the z -axis and that $v_\phi = v_r = 0$, while $v_r = v(r, \phi)$.

By introducing the function

$$u(\varphi) = \frac{1}{6v} rv, \quad (9.4)$$

on the basis of (9.2) it is possible to find that

$$\frac{1}{r} \frac{\partial p}{\partial r} = \frac{12v^2}{r^2} \frac{du}{d\varphi}, \quad (9.5)$$

and from this

$$\frac{p}{r} = \frac{12v^2}{r^2} u(\varphi) + f(r). \quad (9.6)$$

Now, substituting (9.6) into (9.1), we obtain the equation

$$\frac{d^2u}{d\varphi^2} + 4u + 6u^2 = \frac{1}{6v^2} r^2 f'(r). \quad (9.7)$$

As we see, the left side of equation (9.7) depends only on ϕ , while the right side depends only on r - i.e., each of them is a constant quantity which for convenience we will designate as $2c_1$. From this it follows that

$$f'(r) = -\frac{12v^2c_1}{r^3}, \quad (9.8)$$

$$f(r) = -\frac{6v^2c_1}{r^2} + \text{const.} \quad (9.9)$$

From (9.6) and (9.9), we find that

$$\frac{p}{\rho} = -\frac{6v^2}{r^2} \cdot (2u - c_1) + \text{const.} \quad (9.10)$$

Further, multiplying the left side of equation (9.7) by u' , after integration we find that

$$\frac{u'^2}{2} + 2u^2 + 2u^3 - 2c_1u - 2c_2 = 0, \quad (9.11)$$

and from this, that

$$2\varphi = \pm \int \frac{du}{\sqrt{-u^3 - u^2 + c_1u + c_2}} + c_3. \quad (9.12)$$

The constants c_1 , c_2 , and c_3 are determined from the boundary conditions on the walls:

$$u\left(\pm \frac{\alpha}{2}\right) = 0 \quad (9.13)$$

and from the condition that an identical quantity of fluid (gas) Q passes through any section $r = \text{const}$ per unit time:

$$Q = \rho \int_{-\alpha/2}^{+\alpha/2} vr d\varphi = 6\rho v \int_{-\alpha/2}^{+\alpha/2} u d\varphi. \quad (9.14)$$

If $Q > 0$, the fluid flows from the apex of the angle, i.e., there is a diverging (diffusor) flow; if $Q < 0$ there is a converging (confusor) flow.

Solution of the system (9.12)-(9.14) for $Q < 0$ shows that at large Reynolds numbers the flow in the confusor differs little from the potential, while the influence of viscosity is manifested only in a very thin near-wall layer, where there is a fairly rapid drop in velocity from the value corresponding to the potential flow down to 0 immediately on the wall itself.

In the case of a diffuser with ($Q > 0$) a diverging flow symmetrical with respect to the plane $\phi = 0$ is possible for a given angle α only at Reynolds numbers which do not exceed a certain maximum value Re_{max} . If $Re = Re_1 > Re_{max}$, the speed in the diverging flow has a single maximum and a single minimum and motion is asymmetrical with respect to the plane $\phi = 0$. With a further increase in Re number, when $Re > Re_1 > Re_{max}$, the flow contains a single minimum and two maxima of velocity, symmetrically arranged with respect to the plane $\phi = 0$. If $Re \rightarrow \infty$, the number of successive minima and maxima grows without limit. It should be noted that even when $Re = Re_{max}$ the motion is unstable and turbulent conditions arise.

With application to atmospheric conditions, the Re number (as shown in Chapter 1) is not the determining factor and therefore the described mechanism is inadequate to explain loss of stability in diverging atmospheric flows. For atmospheric conditions it is necessary to construct a different theoretical model, bearing in mind such facts as the characteristics of the transverse profile of the flow, vertical motions, and the baroclinicity of the atmosphere. The creation of such a model is for us a matter for the future.

Laboratory studies have shown that instability of a diffuser flow is the greater, the smaller the roughness of the diffuser wall surfaces. With application to the free atmosphere this means that segments with diverging flow may have several successive maxima and minima of velocity in both the vertical and horizontal profiles of the wind. The presence of breaks (inflections) in the wind-velocity profile is an important factor in the disturbance of stability of the flow and its turbulization.

§ 2. ENERGY SPECTRA OF MESOSCALAR TURBULENCE

Measurements of wind velocity and direction at high altitudes in the free atmosphere with Doppler navigation systems have made it possible to detect local heterogeneities in velocity fields of wind having a turbulent character, and also to obtain data on the statistical

characteristics of mesoscalar turbulence (Pinus, 1962, 1963). Such studies so far have been successfully carried out only in the upper troposphere and the lower stratosphere.

In the work by N. Z. Pinus (1962) empirical structural functions of wind-velocity pulsations were calculated from wind-velocity measurement data on horizontal segments 200-300 km long. Selection of segments of such length was conditioned by the need to ensure a sufficient quantity of wind-velocity measurements for statistical calculations with a minimum time requirement for the flight experiment, for which it is possible with a known approximation to consider the field of velocities to be stationary.

Curves of the structural function show that with an increase in Δx there is an increase in $\sigma_{\Delta u}^2$. Values of the structural function exponent obtained in this case (with approximation of empirical data by the expression $\sigma_{\Delta u}^2 = A(\Delta x)^n$) had a scatter ranging from 0.2 to 1.5. Figure 9.2 shows curves of the integral frequency of values of the exponent n with respect to materials from observations over regions of the European territory of the USSR and over the Far East. As we see, cases when n was close to $2/3$ were observed most frequently. In approximately 25% of the cases n was less than 0.4, i.e., the growth in $\sigma_{\Delta u}^2$ with an increase in Δx was comparatively slow; in 30-20% of the cases n was greater than 0.8. However, as is evident from Table 9.1 (which gives the average values \bar{n} at high altitudes), on the average the dependence of $\sigma_{\Delta u}^2$ on Δx was close to the "2/3" law.

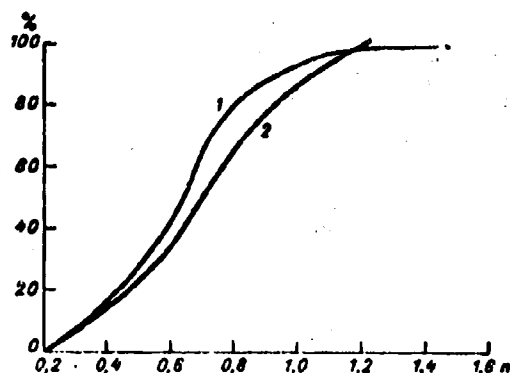


Fig. 9.2. Integral frequency of the exponent of the structural function. 1 - 1960; 2 - 1962.

Table 9.1. Parameters of the structural functions of fluctuations in the horizontal wind-velocity component.

	(1) Высота, км				
	7,0±0,5	8,0±0,5	9,0±0,5	10,0±0,5	11,0±0,5
\bar{n}	0,685	0,646	0,616	0,611	0,611
$(\Delta_1 x)_{\text{exp}}$ км	16,9	17,4	18,3	19,2	18,6

KEY: (1) Altitude, km.

Analysis of experimental data showed that a growth in $\sigma_{\Delta u}^2$ with an increase in Δx proceeds as a rule only with respect to a definite characteristic value $(\Delta x)_{\text{exp}}$. When $\Delta x > (\Delta x)_{\text{exp}}$ the quantity $\sigma_{\Delta u}^2$ either does not grow or its growth is retarded and it varies around the average value $\sigma_{\Delta u}^2$. Figure 9.3 shows the curve of integral frequency $(\Delta_1 x)_{\text{exp}}$, while the average value $(\bar{\Delta_1 x})_{\text{exp}}$ at high altitudes is given in Table 9.1. From Fig. 9.3 it is clear that in approximately 70% of the cases the characteristic distance was less than 20 km; in 47% of the cases it was less than 15 km, while in the remaining cases $(\Delta_1 x)_{\text{exp}}$ reached 45-50 km.

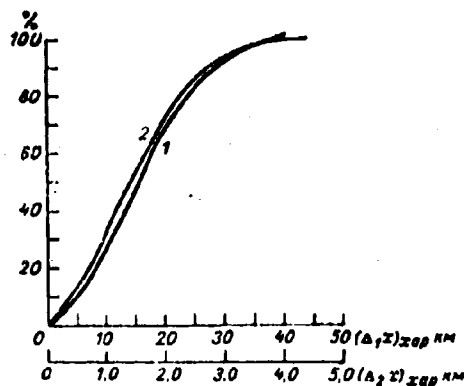


Fig. 9.3. Integral frequency $(\Delta x)_{\text{exp}}$. 1 - for the horizontal component; 2 - for the vertical component of wind velocity (per Yurgensen).

It is interesting to compare the characteristic scale of pulsations in the horizontal wind-velocity component with the characteristic

scale of $\Delta_2 x$ for the vertical component. The latter can be obtained from data on aircraft overloads during flights in a turbulent atmosphere. Figure 9.3 shows a plot of the curve of integral frequency $(\Delta_2 x)_{\text{exp}}$ obtained by A. P. Yurgenson from aircraft g-forces during flights in a turbulent atmosphere. From comparison of the curves of integral frequency $(\Delta_1 x)_{\text{exp}}$ and $(\Delta_2 x)_{\text{exp}}$ it is clear that they are identical, but $(\Delta_2 x)_{\text{exp}}$ for the vertical component is an order of magnitude less than $(\Delta_1 x)_{\text{exp}}$ for the horizontal component of wind velocity.

The circumstance that the exponent of the empirical structural function corresponds on the average to the "2/3" law serves as evidence that on the average the spectral density is described by the "minus 5/3" law. As studies have shown (Pinus, 1964), deviations from this law are connected with the nature of the thermal and wind stratification of the atmosphere. A theoretical consideration of the dependence of the characteristics of the local structure of the wind field on thermal stratification is the subject of the work by St. Panchev (1963).

Studies by S. K. Kao and H. D. Woods (1964), carried out with materials from the American scientific research project "Jet Stream," showed that the energy spectra for the longitudinal and transverse components of wind velocity are close to one another in shape and that $S(\Omega) \approx \Omega^{-2.0}$. The magnitude of dispersions of wind-velocity pulsations turned out to depend on the angle between the ruling direction of airflow and the direction of flight along which the measurements were conducted. These differences are evident from Table 9.2. The dispersion of pulsation velocity was greater during flights across the flow than during flights along it, and it was larger for the transverse component as compared with the longitudinal component during flights parallel to the flow.

Thus, experimental studies show that quasihorizontal heterogeneities ranging in length from several km to several tens of kilometers are observed in the free atmosphere. Their appearance is apparently connected with heterogeneity of the field of average wind velocity. As was indicated in Chapter 4, the presence of these

Table 9.2. Characteristics of wind pulsations.

(3) Направление полета	Средняя скорость ветра, (1) м/сек.		Дисперсия пульсационной (2) скорости, (м/сек.) ²	
	продольная компонента (4)	поперечная компонента (5)	продольная компонента (4)	поперечная компонента (5)
Вдоль потока (6)	59,0	6,1	1,0	1,61
Поперек потока (7)	62,3	6,9	2,6	2,03

KEY: (1) Average wind speed, m/s; (2) Dispersion of pulsation velocity, (m/s)²; (3) Direction of flight; (4) longitudinal component; (5) transverse component; (6) Along the flow; (7) Across the flow.

heterogeneities is not always accompanied by high-frequency fluctuations in the velocity of wind with significant intensity. H. Mantis (1963) also established the presence of significant fluctuations in windspeed in the region of mesoscales, according to data of studies of the motion of balanced automatic balloons. In the majority of flights either high-frequency fluctuations were weakly expressed or a specific minimum was observed in the turbulence spectrum on the segment of the spectrum between large and small "eddies."

§ 3. VERTICAL DISTRIBUTIONS OF WIND GUSTS AND THEIR SPECTRA

Above we examined the statistical characteristics of wind-velocity pulsations and their change in the horizontal plane. The vertical distribution of wind-velocity pulsations is of no less interest. If sufficiently detailed data on the vertical distribution of such pulsations are available, it is possible to use them to obtain correlation and spectral functions, as is done for the horizontal and timed distributions. Although such a vertical distribution of wind-velocity pulsations can only tentatively be considered to be the realization of a random process, nonetheless the spectral decomposition can have a completely determined physical meaning, permitting clarification of vertical scales of pulsations in wind velocity and of the spectral distribution of energy in these pulsations.

Below we will call such spectra energy spectra by analogy with the spectra of real random processes, implying in this name the physical meaning indicated above.

Energy spectra for small-scale pulsations (from a few meters to a hundred meters) were calculated by V. N. Kozlov, N. Z. Pinus, and L. V. Shcherbakova (1965) according to data from measurements of wind-velocity pulsations during ascents of automatic balloons equipped with special apparatus. They calculated autocorrelation functions for the atmosphere from ground level to an altitude of 10-12 km in layers 1 km thick. Analysis showed that the following expression is the best approximation for these empirical autocorrelation functions:

$$R(\Delta z) = e^{-\alpha \Delta z} \cos \varphi \Delta z, \quad (9.15)$$

to which the following spectral density corresponds:

$$S(\omega) = \frac{\alpha}{\pi} \frac{\omega^2 + \alpha^2 + \varphi^2}{(\omega^2 - \varphi^2 - \alpha^2)^2 + 4\alpha^2\omega^2}. \quad (9.16)$$

Vertical scales of perturbations $\Delta_0 z$, defined by the radius of correlation corresponding to $R(\Delta z) = 0$, vary from 10 to 350 m. In 62% of the cases they were less than 100 m, and in 16% of the cases they were greater than 200 m. The quantity α also varies in wide limits - from 0.005 to 0.15 m^{-1} . However, in 89% of the cases its value ranges from 0.005 to 0.05 m^{-1} . It was also found that the intensity of turbulence u'^2 and the scales of perturbations $\Delta_0 z$ grow with a reduction in Ri number. The drop in relative intensity of turbulence ψ with altitude is, on the average, inversely proportional to the square root of altitude.

At present no data are available on the vertical distribution of large-scale pulsations. S. K. Kao and E. E. Sands (1966) present data on the spectra of mesoscalar pulsations of wind velocity for the atmosphere from ground level up to a height of 50 km. They utilized the results of 210 rocket experiments which were accompanied by measurements of wind velocity. They calculated spectra for scales ranging from 1.5 to 50 km for each vertical profile of wind velocity,

using the procedure described in § 2 of Chapter 3. The calculations were carried out separately for the zonal and meridional components of wind velocity. The individual spectra were then averaged with respect to seasons.

Table 9.3 gives the values of normalized spectral data for different wave numbers ω , while Table 9.4 gives the magnitude of dispersions of zonal and meridional components of wind velocity in the different seasons.

Table 9.3. Seasonal values of spectral density of wind-velocity pulsations.

ω sec	L km	(1) Зима		(2) Весна		(3) Лето		(4) Осень		(5) Год	
		$S_u(\omega)$	$S_v(\omega)$	$S_u(\omega)$	$S_v(\omega)$	$S_u(\omega)$	$S_v(\omega)$	$S_u(\omega)$	$S_v(\omega)$	$S_u(\omega)$	$S_v(\omega)$
0,02	50	145,36	75,44	82,80	31,60	24,88	36,00	21,72	46,84	68,09	47,47
0,025	40	132,60	69,40	94,52	33,32	29,88	32,84	42,36	41,80	74,84	44,34
0,030	33,3	110,80	59,64	98,04	35,36	35,04	28,56	62,12	36,52	76,65	40,02
0,035	28,5	86,84	49,56	96,88	37,88	39,80	24,72	77,84	33,00	75,34	36,29
0,040	25,0	65,16	41,16	89,96	40,76	43,52	22,48	86,92	32,44	71,39	34,21
0,050	20,0	38,48	32,96	64,32	46,16	40,36	25,26	79,68	40,92	57,21	36,40
0,060	16,6	35,04	33,60	36,52	47,48	42,72	38,12	47,32	53,16	40,40	39,09
0,070	14,3	35,06	32,20	24,36	40,84	36,44	49,72	21,60	51,24	29,59	43,50
0,080	12,5	24,84	24,68	25,48	28,02	31,76	47,80	21,52	33,24	25,00	33,66
0,090	11,1	11,00	18,96	21,16	19,12	28,12	33,80	26,80	18,72	21,77	22,65
0,10	10,0	7,08	18,00	8,60	14,64	23,56	19,28	17,84	17,08	14,27	17,25
0,12	8,3	0,88	10,00	3,80	11,76	13,56	10,28	2,00	11,44	6,56	10,67
0,14	7,1	3,64	10,04	3,64	6,08	3,36	11,68	6,88	5,36	5,13	8,29
0,16	6,3	4,32	8,32	3,12	7,16	8,72	9,16	1,32	11,44	4,37	9,02
0,20	5,0	3,52	7,64	1,68	4,01	4,24	6,92	1,52	7,13	2,74	6,52
0,25	4,0	0,72	2,52	2,08	4,84	2,44	3,24	2,12	2,72	1,84	3,33
0,30	3,3	0,92	3,00	0,64	4,52	3,68	3,24	2,48	1,64	1,93	3,10
0,35	2,8	1,24	3,36	0,16	2,60	1,20	0,64	0,62	1,24	0,78	1,96
0,40	2,5	1,40	2,56	0,96	1,60	1,28	0,60	0,40	1,48	1,01	1,56

KEY: (1) Winter; (2) Spring; (3) Summer; (4) Fall; (5) Full year.

The curves of spectral density of pulsations of the zonal and meridional components of wind velocity have approximately identical form and can be described by the power law $S(\omega) \approx \omega^{-n}$. In the opinion of Kao and Sands, the spectral density is inversely proportional to the square of the wave number ω , but from Fig. 9.4 it is clear that the curves of $S(\omega)$ can be approximated, with equal justification, by the expression $S(\omega) \approx \omega^{-2}$, and by the expression $S(\omega) \approx \omega^{-2.0}$.

Table 9.4. Seasonal values of $\overline{u'^2}$ and $\overline{v'^2}$ in m^2/s^2 .

(1) Время года	$\overline{u'^2}$	$\overline{v'^2}$	$\overline{v'^2}/\overline{u'^2}$
Зима (2)	73,62	29,57	0,39
Весна (3)	56,61	20,93	0,37
Лето (4)	23,06	18,67	0,81
Осень (5)	48,68	24,09	0,49
Год (6)	50,49	23,32	0,46

KEY: (1) Time of year; (2) Winter; (3) Spring; (4) Summer; (5) Fall; (6) Annual.

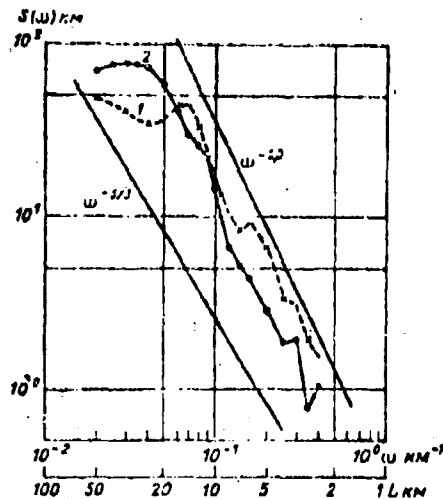


Fig. 9.4. Normalized spectral density of pulsations of zonal (1) and meridional (2) components of wind velocity.

In conclusion we should note that Table 9.3 presents data on normalized spectral density for scales up to 50 km, but the magnitudes of spectral density are sufficiently reliable only up to scales on the order of 20 km. Therefore we should not impute particular significance to the maximum in the region of low frequencies on the curves of spectral density.

§ 4. ON THE LOCAL METEOROLOGICAL MINIMUM OF ENERGY IN THE TURBULENCE SPECTRUM

It was shown in Chapter 1 that the magnitude of spectral density grows with a reduction in frequency. In the inertial interval this dependence is described by the "minus 5/3" law. The region of the spectrum adjacent to the inertial interval on the low-frequency side contains the basic portion of the kinetic energy of turbulent motions. This portion of the spectrum contains the energy maximum corresponding to a certain interval of scales of turbulent motions - the so-called energy-carrying range of the spectrum of atmospheric turbulence. At present there is as yet no theoretical description of the shape of the function of spectral density for this region of the spectrum. The low-frequency region adjacent to the maximum of the energy spectrum on the side of lower frequencies has been studied to a still lesser degree; it depends essentially on the conditions of appearance of turbulent conditions in the flow.

a. Energy Spectrum of Wind-Velocity Pulsations at Low Altitudes

An effort was made to calculate the spectrum for low altitudes above the surface in a wide range of frequencies in the works by J. Van der Hoven (1957) and V. K. Kolesnikova and A. S. Monin (1965).

Figure 9.5 shows the energy spectrum (in the coordinates $fS(f)$, $\log f$) for pulsations of the horizontal wind-velocity component in the interval of frequencies from 10^3 to 10^{-3} 1/h, obtained by Van der Hoven (1957) according to data from measurements on the 125-m meteorological tower in Brookhaven (USA). This spectrum was calculated for eight overlapping intervals, whose characteristics are given in Table 9.5.

From Fig. 9.5 it is clear that this spectrum has two maxima: a main maxima belonging to the frequency $f \approx 10^{-2}$ 1/h and a second maxima at $f \approx 6 \cdot 10^1$ 1/h. There is a partial maximum at approximately $f \approx 10^{-1}$ 1/h. The maximum in the so-called synoptic region ($f \approx 10^{-2}$ 1/h) is conditioned by the passage of large-scale baric systems,

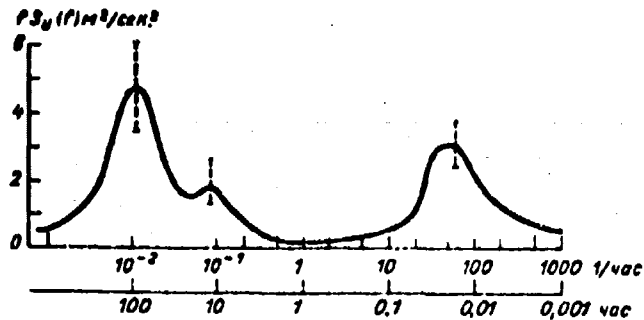


Fig. 9.5. Energy spectrum of pulsations of the horizontal wind-velocity component (per Van der Hoven).

Designations: смк = в; час = h.

Table 9.5. Intervals of the spectrum of pulsations of the horizontal wind-velocity component.

(1) Высота, м	(2) Период измерения	(3) Период осреднения	(4) Область частот, 1/час
108	(5) 10,0 месяца	(6) 5 дней(6)	$7 \cdot 10^{-1} - 1,2 \cdot 10^{-1}$
108	6,2	1 день(7)	$3,5 \cdot 10^{-2} - 2,1 \cdot 10^{-2}$
108	42 дня(8)	5 час.(9)	$10^{-2} - 10^{-1}$
108	26 час.(9)	30 мин.(10)	$10^{-1} - 10^0$
108	50	10	$5 \cdot 10^{-1} - 3 \cdot 10^0$
125	32	75 смк.(11)	$8 \cdot 10^{-1} - 2,4 \cdot 10^1$
91	1	30	$1,5 \cdot 10^1 - 9 \cdot 10^1$
91	1	2	$3 \cdot 10^1 - 9 \cdot 10^2$

KEY: (1) Altitude, m; (2) Measurement period; (3) Averaging period; (4) Frequency region, 1/h; (5) month; (6) days; (7) day; (8) days; (9) hours; (10) minutes; (11) seconds.

while the maximum in the micrometeorological region ($f \approx 6 \cdot 10^{-1}$ 1/h) is caused by small-scale turbulence of dynamic and convective origin. The most significant feature of this spectrum is the deep minimum (trough) in the mesometeorological [local] region ($f = 2 \cdot 10^{-1} - 10^1$ 1/h). According to Van der Hoven's data (1957), this feature is typical for many series of measurements. At low altitudes this trough is smooth in the presence of convection. L. R. Tsvang (1962) established that the spectra of air-temperature pulsations have a similar character at low altitudes.

At present there is as yet no theoretical explanation of the appearance of the mesometeorological minimum in the spectrum. We will pause on a qualitative explanation of this phenomenon. Studies of the statistical characteristics of atmospheric turbulence are based on considerations of the fact that the atmosphere is a dynamically unstable system and that periodic wave motions exist in it constantly. If these motions, in turn, become unstable, motions of a turbulent nature arise. Thus, turbulent motions are the result of the so-called secondary instability of the atmosphere. The synoptic maximum is caused by the secondary instability of large-scale dynamic processes in the atmosphere, connected with the difference in solar heating of the polar and tropical zones and also with the difference in the nature of the underlying surface (continents, oceans). In the process of "crumbling" of eddies, transfer of turbulent energy occurs from this maximum along the spectrum from large scales to small ones until the energy of turbulent motions dissipates into heat. In the small-scale segment of the spectrum of turbulence there can be generation of turbulence energy due to hydrodynamic instability in the wind field, especially in the planetary boundary layer of the atmosphere, and also thanks to the thermal instability of the atmosphere and the degeneration of short gravitational waves in the case when they lose stability. These local influxes of turbulent energy can form a second maximum in the energy spectrum.

The scales of turbulence to which the second maximum of turbulent energy applies depend not only on the nature of the vertical profiles of wind velocity and air temperature, but also on the distance from the surface. In particular, since the vertical scale of turbulent perturbations caused by thermal instability of the atmosphere grows with altitude, with a gain in altitude there should be a shift of the maximum of turbulent energy into the region of lower frequencies. On the other hand, since thermal stability of the air increases with altitude, on the average in the troposphere the role of thermal factors causing the appearance of the second maximum is weakened. In the middle and upper troposphere, except for the zones of the tropopause and cases of the presence of jet streams and atmospheric fronts, there are no dynamic conditions for direct generation of

turbulence in the microscale region. Therefore we can assume that in the free atmosphere there is no mandatory presence of a maximum of turbulent energy on microscales or the connected phenomenon of a mesometeorological minimum of energy in the energy spectrum of atmospheric turbulence.

b. Energy Spectra of Wind-Velocity Pulsations in the Troposphere and the Stratosphere

The greatest amount of published works contain the results of experimental studies of turbulence in the boundary layer of the atmosphere, while data on turbulence in the free atmosphere are substantially fewer. Besides this, these data touch only on individual segments of the spectrum of atmospheric turbulence. For example, Wan Chang-chin (1960) studied the time energy spectra of pulsations of the horizontal wind-velocity components on levels from 700 down to 50 mb for two points on the territory of the USA. For this purpose he used radio wind observations carried out in the course of a year and made once a day. The synoptic maximum of energy in the spectrum of wind-velocity pulsations is well defined by these investigations.

Spectra of pulsations of the horizontal component of pulsations [sic] of wind velocity obtained by S. K. Kao and H. D. Woods (1964) for the jet-stream region give, as we have seen, an idea of the particular features of energy spectra only in the region of mesoscales.

N. Z. Pinus (1966) in recent years carried out studies of spectra ranging from synoptic scales down to scales of several tens of meters. For this purpose he used radio wind observations and also aircraft measurements of wind made with a Doppler navigation system and with a hot-wire anemometer. The aircraft measurements made it possible to obtain unidimensional spatial spectra of pulsations of the horizontal wind-velocity component, while the radio wind measurements provided time spectra. The hypothesis of "frozen" turbulence was used during comparison of these spectra.

The work by Pinus (1966) gives spectra of $S(\Omega)$ of pulsations of the horizontal wind-velocity component for the 500, 300, and 200 mb levels. The low-frequency portion a of the spectra was obtained from materials of sounding carried out four times a day (1964-1965) and by special two-week (1960-1961) series of radio wind observations carried out every 2 hours; both were accomplished in Moscow. The middle portion b was obtained from aircraft measurements using a Doppler navigation system, while the high-frequency portion c was obtained from data of aircraft hot-wire anemometer measurements (Fig. 9.6).

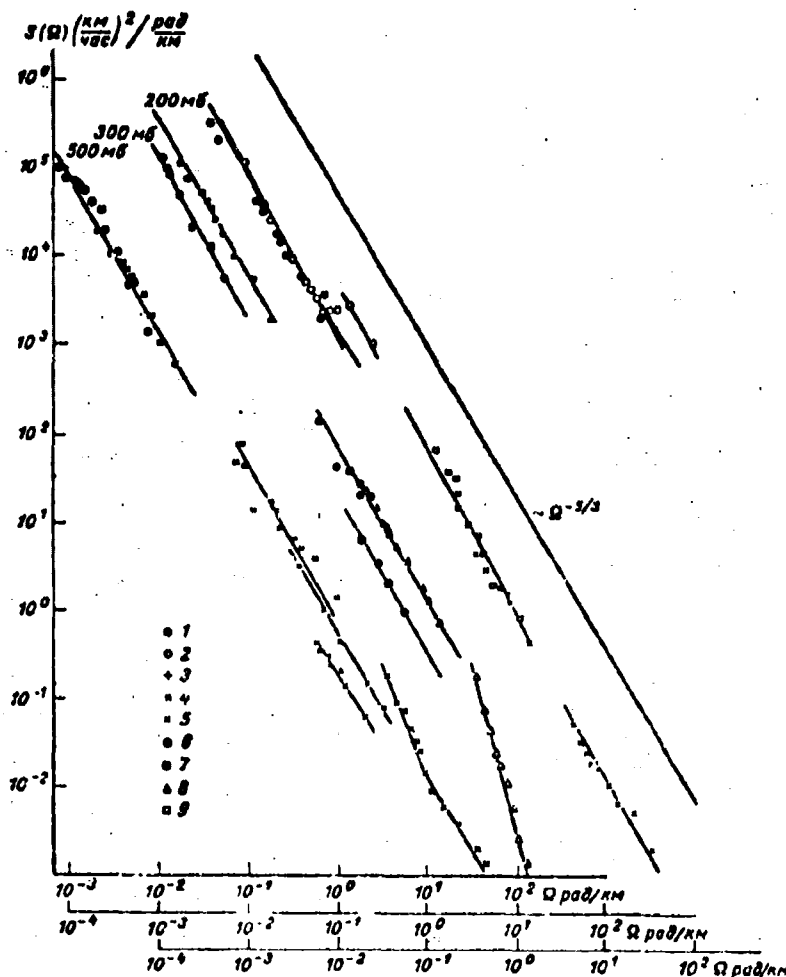


Fig. 9.6. Spectral density of pulsations of the horizontal wind-velocity component at various altitudes. 1 - Jan. 1965; 2 - Jan. 1961; 3 - 28 Dec. 1964; 4 - 21 Feb. 1962; 5 - 8 Feb. 1965; 6 - 19 Feb. 1962; 7 - 29 Dec. 1964; 8 - 13 Feb. 1965; 9 - 9 Feb. 1962. [км/час = km/h; рад/км = rad/km].

Segments a, b and c of spectra of atmospheric turbulence should, apparently, continuously transfer from macroscales to middle scales and then to microscales. The junctions of these segments of the spectra can be only tentatively assigned by the author, since the spectra a, b, and c were obtained in different regions and not simultaneously. Even in one and the same experiment the indicated breakdowns of the spectra (as regards aircraft measurements) had no overlaps in the area of adjacent frequencies. The impossibility of overlapping in the wave-number interval 1-3 rad/km is connected with particular features of methods of airborne Doppler and hot-wire anemometer measurements of wind velocity (see Chapter 2).

Investigations showed that at all altitudes the spectral density $S(\Omega)$ is increased with a reduction in Ω and that the dependence of $S(\Omega)$ on Ω may be described by a power law. On the average the exponent for segments a and b turned out to equal $-5/3$. From this it follows that the spectrum in the wave-number band from 10^{-3} to 10^0 rad/km at the 500, 300 and 200 mb altitudes obeys the "minus 5/3" law; this means that in it the rate of energy transfer along the spectrum is constant. The level of turbulent energy in this interval of frequency naturally depends in each case on the intensity of the source of turbulence energy.

Spectrum segment c in the wave-number interval 1-10 rad/km had a slope at the 500-mb level which was greater than that according to the "minus 5/3" law and, most importantly, it was located in a region of lower energies than would be indicated by simple extrapolation of segments a and b of the spectrum into the region of larger wave numbers. It is possible to assume that at the 500-mb level in the region of these wave numbers some sort of additional energy source existed. This was, possibly, gravitational waves undergoing destruction because of loss of stability.

Since the thermal stratification of the atmosphere is stable at the 500, 300 and 200 mb levels, generally speaking one would expect the presence of a "drain" of turbulent energy at these frequencies. Actually, judging by the nature of the spectrum, at the 500-mb level

this drain was more than adequately covered by the influx of energy, while at the 200-mb level balance apparently occurred between the influx of turbulent energy from some external source and the drain of energy caused by the stable thermal stratification of the atmosphere.

Analysis of these energy spectra shows that the maximum of turbulent energy at the 500-mb level is related to a wave number of about $3 \cdot 10^0$ rad/km - i.e., to scales on the order of 2000 m. No micrometeorological maximum was detected in spectra for high altitudes.

There is one more extremely important circumstance which should be noted: at the 500-mb level the energy in the region of the micrometeorological maximum is tens of times less than in the region of the so-called synoptic maximum, where it comprises tens of m^2/s^2 . At the same time, the data compiled by Van der Hoven (1957) indicate that at an altitude of about 100 m (Fig. 9.4) the energy in the regions of the micrometeorological and synoptic maxima is virtually identical and equals a few m^2/s^2 .

While at present the troposphere is represented by a considerable quantity of experimental data on the fine structure of turbulence - data covering different meteorological situations and relating to different regions of the earth - the quantity of such data available for the stratosphere is as yet small. Therefore a major problem at present is the accumulation of experimental results, which must then subsequently be systematized.

We can, certainly, attempt to obtain certain evaluations of the energy situation in turbulence in the stratosphere by indirect methods, as by extrapolating sufficiently reliable experimental data obtained in the upper troposphere.

Two series of experiments (summer and winter) were carried out in 1966-1967 at the Central Aerological Observatory in the Khar'kov region (Vinnichenko, Pinus, Shur, 1967). Each series was continued for one month (July and January). In the course of the month repeated launchings of radiosondes were made at intervals of 2 hours (360

launches per month). In the same area and at the same time flights were made on a laboratory IL-18 aircraft equipped with a Doppler navigation system, hot-wire anemometer, and other scientific apparatus. Eight to ten flights (2-3 flights per week) were made in the course of the month. The flights were carried out over horizontal areas 200-250 km in extent at altitudes of 1 to 10 km.

The raw experimental data were subjected to statistical processing on electronic computers in order to obtain the spatial energy spectra of the measured parameters. The hypothesis of the "frozen" nature of turbulence was used to obtain the spatial spectra of wind velocity. While the use of this hypothesis is widely accepted in aircraft investigations, during the processing of radiosonde data its application is a formal operation. Furthermore, while radiosonde measurements were carried out continuously throughout the entire month, the aircraft flights were made only every 2-3 days; therefore the airborne measurements cannot, in principle, cover all situations existing in the course of the month.

Up to an altitude of 10 km the turbulence spectra obtained by the method encompassed virtually all scales from several thousands of km down to hundreds of meters. Above 10 km, where no synchronous aircraft flights were carried out, only macroscale spectra from radiosonde data were obtained.

Figure 9.7 shows experimental spectra of pulsations of the horizontal wind-velocity component for July 1966 and January 1967. The macroscale spectra are given for altitudes of 5, 7, 9, 12, 15, and 18 km, while mesoscale and microscale spectra are given for altitudes of 5, 7, and 9 km.

The macroscale spectra for the troposphere and the stratosphere on Fig. 9.7 lie so close to one another (differing by no more than a single order) that it is not really possible to make any distinction between them. Obviously, one should expect that the mesoscalar and microscale spectra for the stratosphere also would not differ substantially from one another. Despite the use of a comparatively

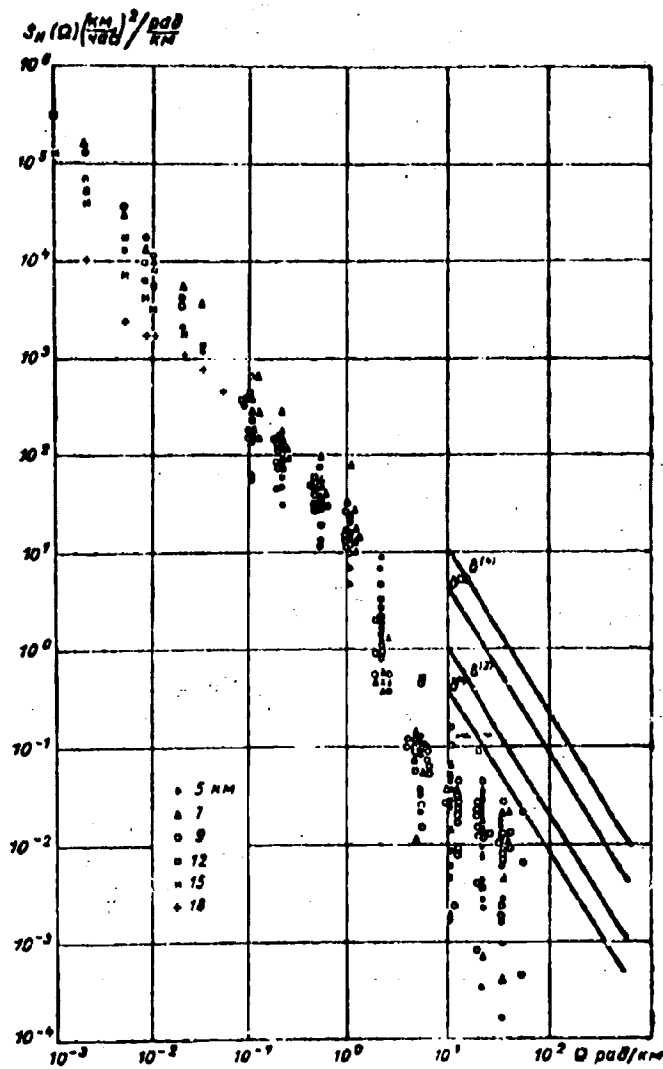


Fig. 9.7a. Spectra of pulsations of the horizontal wind-velocity component. July 1966. $\sigma^{(1)}$ - weak; $\sigma^{(2)}$ - moderate; $\sigma^{(3)}$ - strong; $\sigma^{(4)}$ - very strong buffeting of the aircraft.

Designations: км/час = km/h; рад/км = rad/km.

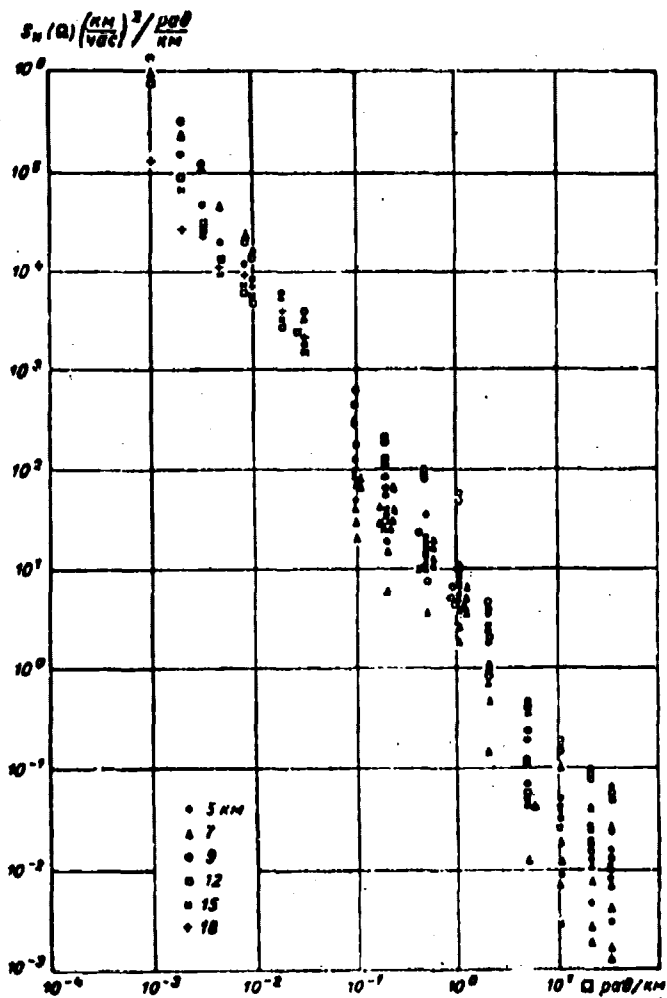


Fig. 9.7b. Spectra of pulsations of the horizontal wind-velocity component. January 1967.

Designations: км/час = km/h; рад/км = rad/km.

large mass of statistical material, at altitudes from 5-9 km no clearly expressed minima in the spectra, similar to those obtained on a tower by Van der Hoven, are observed.

The spectra shown on Fig. 9.7 can, on the average, be depicted as a uniformly diminishing curve. In the wave-number interval from 10^0 to 10^1 rad/km the average slope of the curve of spectral density

is greater than that at smaller wave numbers, exceeding it in absolute value by 5/3. This is especially clearly noticeable for July. If we proceed from the idea of cascade transfer of energy from smaller wave numbers to larger ones, it should be noted that in the upper troposphere and, apparently, in the stratosphere there is intensive draining of turbulence energy toward the work of counteracting forces of negative buoyancy. On wave numbers greater than 10^1 rad/km the scatter of experimental points reaches 3 orders of magnitude for July and 2 orders of magnitude for January. Such a large scatter of microscale spectra (as compared with mesoscalar) is apparently explained by peculiarities of the local structure of fine-scale turbulence and the fine structure of the temperature and wind profiles. Frequently cases can be observed in which fine-scale turbulence, if it exists, has an intensity below the threshold of sensitivity of the hot-wire anemometer (25 cm/s).

Tentative intervals of the magnitude of spectral density corresponding to buffeting of an aircraft at different intensities are tentatively plotted on Fig. 9.7. As is evident from the figure, only a few values of spectral density on the microscales fall within the zone close to the boundary of weak and moderate buffeting; this coincides with readings of the aircraft accelerograph installed on the IL-18.

The considered experimental data confirm that turbulence energy may not only be transferred along the spectrum due to a cascade mechanism from smaller wave numbers, but may also arrive in the spectrum due to local (with respect to wave numbers) sources of instability (decaying gravitational waves, orography). Since they are operative at comparatively large wave numbers, it is natural that in the presence of such sources we can expect an increase in intensity of turbulence in the appropriate region of wave numbers.

In these cases the energy spectrum of turbulence in the troposphere and that in the stratosphere may have a secondary maximum of spectral density and only then will this spectrum have the so-called mesometeorological minimum.

However, most frequently in the upper troposphere and, apparently, in the stratosphere the effect of drainage of energy expended on counteracting negative buoyancy forces should be manifested and the slope of the curve of spectral density in this region of scales of turbulence should exceed $5/3$ in absolute magnitude.

Certain concepts on the possible frequency of spectra with a secondary energy maximum in the spectrum are provided by data on the frequency of turbulence causing buffeting of aircraft (see Fig. 7.1). In particular, for the upper troposphere in the middle latitudes above the USSR it comprises about 12%, including that with moderate and strong turbulence (see Tables 7.2 and 7.7) - about 6%.

BIBLIOGRAPHY

- Александров В. С., Силасва В. И., Шметер С. М. 1967. Атмосферная турбулентность в зоне кучево-дождевых облаков. Труды ЦАО, вып. 78.
- Атлас Д. 1967. Успехи радарной метеорологии. Гидрометеонадат, Л.
- Барахтин В. И. 1963. Некоторые особенности зон болтанки самолетов на высотах 8—10 км. Метеорология и гидрология, 5.
- Барахтин В. И. 1966. Аэросиноптические условия болтанки самолетов в верхней тропосфере и нижней стратосфере над Азиатской территорией СССР. Труды ЦИП, вып. 157.
- Беляев В. П. [и др.] 1964. Некоторые результаты экспериментальных исследований турбулентности атмосферы с помощью радиозондов. Труды ЦАО, вып. 54.
- Беляев В. П. [и др.] 1965. Некоторые результаты сравнений радиозондовых и самолетных измерений турбулентности в свободной атмосфере. Тр. ЦАО, вып. 54.
- Беляев В. П. и Шур Г. И. 1960; 1961. Устройство для измерения и регистрации атмосферной турбулентности. Авт. свидетельства № 135265 и 152107.
- Бовшверов В. М., Гурнич А. С., Цванг Л. Р. 1959. Прямые измерения турбулентного потока тепла в приземном слое атмосферы. ДАН СССР, 125, № 6.
- Боровиков А. М. и Мазин И. П. 1967. Об ориентации облачных гряд. Труды ЦАО, вып. 79.
- Браславский Д. А., Лагунов С. С. 1954. Расчет и конструкция авиационных приборов. Оборонгиз, М.
- Бутчелор Дж. 1935. Теория однородной турбулентности. Изд-во иностр. лит., М.
- Васильев А. А. 1965. Распределение ветра над Крымскими горами и особенности болтанки вертолетов при различных синоптических положениях. Труды ГГО, вып. 171.
- Васильченко И. В. 1958. Расчет характеристик облачной конденсационной струи. Труды ГГО, вып. 82.
- Васильченко И. В., Ледухович А. А. 1962. Некоторые результаты самолетного зондирования в Голодной степи. Труды ГГО, вып. 135.
- Вельтищев Н. Ф. 1965. К вопросу об интерпретации мезоструктуры поля облачности. Труды ММН, вып. 8.
- Верле Е. К. 1963. Некоторые данные об атмосферной турбулентности в верхней тропосфере и нижней стратосфере. Труды ДВ НИГМИ, вып. 15.
- Винниченко Н. К. 1964. Опыт применения термоанемометра на самолете. Труды ЦАО, вып. 53.
- Винниченко Н. К. 1966. Турбулентность в ясном небе на высотах 6—12 км. Изв. АН СССР, серия физики атмосферы и океана, т. 2, № 11.
- Винниченко Н. К., Пинус Н. З., Шур Г. И. 1965. Некоторые результаты экспериментальных исследований турбулентности в тропосфере. Международный коллоквиум по тонкой структуре атмосферы, М.
- Винниченко Н. К., Пинус Н. З., Шур Г. И. 1967. Спектры пульсаций скорости ветра и температуры в стратосфере. Симпозиум «Метеорологические проблемы сверхзвуковой авиации XIV Генеральной ассамблеи Международного союза геодезии и геофизики. Цюрих.
- Винниченко Н. К. и Шур Г. И. 1959. Получение энергетического спектра стационарного случайного процесса, записанного графически. Труды ЦАО, вып. 31.

- Винниченко Н. К. и Шур Г. И. 1962. Система магнитной записи медленно меняющихся метеорологических параметров. Труды ЦАО, вып. 42.
- Винниченко Н. К. и Шур Г. И. 1965. Многоканальный бортовой кодирующий преобразователь. Труды ЦАО, вып. 63.
- Воробьев В. И. 1960. Струйные течения в умеренных и высоких широтах. Гидрометеондат, Л.
- Воробьев В. Ф., Трубицкий Б. И. 1967. Ячейковая конвекция при анизотропной турбулентности и наличии поля относительного вихря. Труды ЦАО, вып. 75.
- Воронцов П. А. 1960. Аэрологические исследования пограничного слоя атмосферы. Гидрометеондат, Л.
- Воронцов П. А. 1966. Турбулентность и вертикальные токи в пограничном слое атмосферы. Гидрометеондат, Л.
- Воронцов П. А., Васильев А. А. 1965. Вопросы метеорологического обеспечения полетов на вертолетных трассах в горных районах. Труды ГГО, вып. 171.
- Воронцов П. А., Герман М. А. 1964. К методике исследования турбулентного режима пограничного слоя по данным записей акселерографа на самолете ГО-2. Труды ГГО, вып. 154.
- Вульфсон Н. И. 1961а. Некоторые результаты исследования конвективных движений в свободной атмосфере. Сб. «Исследования облаков, осадков и грозового электричества». Изд. АН СССР, М.
- Вульфсон Н. И. 1961б. Исследование конвективных движений в кучевых облаках. Сб. «Исследование облаков, осадков и грозового электричества». Изд. АН СССР.
- Вульфсон Н. И. 1961в. Исследование конвективных движений в свободной атмосфере. Изд. АН СССР.
- Вульфсон Н. И. 1963. Влияние влажности воздуха на развитие конвективных движений в безоблачной атмосфере. ДАН СССР, т. 151, № 5.
- Гандли Л. С. 1947. Упорядоченная свободная конвекция в атмосфере. Труды ГГО, вып. 6.
- Гандли Л. С. 1957. Об устойчивости волны у поверхности раздела потоков, направленных под углом друг к другу. Изв. АН СССР, сер. геофиз., № 3.
- Гандли Л. С. 1958. Об образовании турбулентных движений на фронтах. Труды ГГО, вып. 76.
- Гандли Л. С. 1959. О колебаниях самолета, снабженного автопилотом, в турбулентной атмосфере. Труды ГГО, вып. 98.
- Гандли Л. С. [и др.] 1955. Основы динамической метеорологии. Гидрометеондат, Л.
- Гельмгольц Н. Ф. 1963. Атмосферная турбулентность и спокойствие полетов в зоне тропопаузы и струйных течений. Труды Каз. НИГМИ, вып. 19.
- Герман М. А. 1963. О турбулентном обмене в облаках. Метеорология и гидрология, № 10.
- Герман М. А. 1964. Некоторые результаты экспериментального исследования структурно-энергетических характеристик турбулентности в облаках. Труды ГГО, вып. 154.
- Гиссина Ф. А. 1966. О влиянии градиентов средней скорости и температуры на спектральные характеристики турбулентности. Изв. АН СССР, серия физики атмосферы и океана, том 2, № 8.
- Горелик А. Г. 1965. Одновременные измерения лагранжера и эйлерова масштабов турбулентности в осадках и в виде снега. Изв. АН СССР, серия физики атмосферы и океана, т. 1, № 9.
- Горелик А. Г., Костарев В. В., Черников А. А. 1958. Радиолокационные измерения турбулентности в облаках. Метеорология и гидрология, № 5.
- Горелик А. Г., Костарев В. В., Черников А. А. 1965. Координатно-доплеровский метод ветровых наблюдений и некоторые результаты исследования неоднородностей поля ветра в атмосфере. Метеорология и гидрология, № 10.
- Горелик А. Г., Черников А. А. 1964. Некоторые результаты радиолокационного исследования структуры поля ветра на высоте 50-700 метров. Тр. ЦАО, вып. 57.
- Гуранч А. С. 1962. Спектры пульсаций вертикальной компоненты скорости ветра и их связь с микрометеорологическими условиями. Труды ИФА АН СССР, № 4.
- Гуранч А. С. [и др.] 1967. Эмпирические данные о мелкомасштабной структуре атмосферной турбулентности. Сб. «Атмосферная турбулентность и распространение радиоволн». Изд. «Наука».
- Давыдов Н. И. 1959. Аэрохимические условия развития турбулентности в верхней тропосфере и нижней стратосфере. Воиниздат, М.
- Девятова В. А. [и др.] 1958. Исследования пульсаций горизонтальной составляющей скорости ветра до высоты 5 км. Труды ЦАО, вып. 21.

- Джорджано В. А., Петренко Н. В. 1964. Струйные течения в атмосфере. Гл. 4. Руководство по краткосрочным прогнозам погоды. ч. 1. Гидрометеонздат, Л.
- Дородницын А. А. 1938. Возмущения воздушного потока, вызванные неровностями на поверхности земли. Труды ГГО, вып. 23.
- Дородницын А. А. 1940. Некоторые задачи обтекания неровностей поверхности земли воздушным потоком. Труды ГГО, вып. 31.
- Дородницын А. А. 1950. Влияние рельефа земной поверхности на воздушные течения. Труды ЦИИП, вып. 21 (48).
- Дубов А. С. 1949. Определение скорости вертикальных порывов ветра при самолетных зондированиях с помощью акселерографа. Труды ГГО, вып. 16 (78).
- Дубов А. С. 1959а. К вопросу об определении вертикальных скоростей ветра по данным самолетного акселерографа. Труды ГГО, вып. 81.
- Дубов А. С. 1959б. Боковые колебания самолета, обусловленные влиянием порывов ветра. Труды ГГО, вып. 98.
- Дубов А. С. 1959в. Определение коэффициента турбулентного обмена по ускорению самолета. Труды ГГО, вып. 98.
- Дубов А. С. 1961. Определение вертикальных порывов ветра по колебаниям самолета в полете с учетом влияния летчика на рычаги управления. Труды ГГО, вып. 121.
- Дубов А. С., Геикин А. Л. 1959. Определение вертикальных порывов ветра по записям акселерографа на управляемом самолете. Труды ГГО, вып. 98.
- Дубов А. С., Герман М. А. 1965. О спектральной плотности вертикальных порывов ветра в облаках. Изв. АН СССР, сер. физики атмосферы и океана, т. 1, № 7.
- Дулко Г. К. и Резников Г. Б. 1964. Доплеровские измерители скорости и угла сноса самолета. Изд. «Советское радио».
- Дюбок А. Ф., Бибилова Т. Н. 1965. Условия образования облачности в зависимости от орографии. Труды ГГО, вып. 171.
- Дюбок А. Ф., Кожевников В. П. 1964. О роли азимутных членов ускорения движения в асимметрии характера обтекания симметричной горы. Вестник МГУ, № 6.
- Дюбок А. Ф., Трубников Б. Н. 1963. Некоторые вопросы теории локальных атмосферных процессов. Труды ВИАМС, т. 2.
- Заварина М. В. 1959. Определение критических значений числа Ричардсона как критерия повышенной турбулентности атмосферы. Труды ГГО, вып. 81.
- Заварина М. В., Юдин М. И. 1960. Уточнение и использование числа Ричардсона для выявления зоны болтанки самолетов. Метеорология и гидрология, № 2.
- Зайцев В. А., Ледохович А. А. 1959. Температура вблизи верхней границы внутримассовых туманов и слоистых облаков. Труды ААНИИ, т. 228, вып. 1.
- Зайцев В. А., Ледохович А. А. 1961. Условия полетов самолетов вблизи мощных кучевых и грозовых облаков. Сб. «Исследование облаков и осадков и грозового электричества». Изд. АН СССР, М.
- Зейтунян Х. Н. 1964. Гидродинамический расчет подветренных волн. Изв. АН СССР, сер. геофиз., № 9.
- Зейтунян Х. Н. 1965. Об учете поворота ветра с высотой при обтекании препятствий воздушным потоком. Труды ММЦ, вып. 6.
- Зельдович Я. Б. 1937. Предельные законы свободно восходящих конвективных потоков. ЖЭТФ, т. 7, вып. 12.
- Зубковский С. Л. 1962. Частотные спектры пульсаций горизонтальной компоненты скорости ветра в приземном слое воздуха. Изв. АН СССР, сер. геофиз., № 10.
- Зубковский С. Л. 1963. Экспериментальные исследования спектров пульсаций вертикальной компоненты скорости ветра в свободной атмосфере. Изв. АН СССР, серия геофиз., № 8.
- Иванов В. Н. 1964. Турбулентная энергия и ее диссипация. Изв. АН СССР, сер. геофиз., № 9.
- Казакон В. А. 1965. Вычислительные устройства машины непрерывного действия. Изд. «Машиностроение», М.
- Кибель И. А. 1944. Применение метода длинных волн в сжимаемой жидкости. Прикладная математика и механика, т. 8, вып. 5.
- Кибель И. А. 1955. Пространственная задача обтекания неровностей поверхности земли воздушным потоком. ДАН СССР, т. 100, № 2.
- Кибель И. А. 1957. Введение в гидродинамические методы краткосрочного прогноза погоды. Гостехиздат, М.
- Кибель И. А. 1965. Некоторые виды волновых движений в свободной атмосфере. Труды ММЦ, вып. 6.
- Клемми Н. А., Пинус Н. Э. 1954. Методические указания к диагнозу и прогнозу атмосферной турбулентности, выпавшей болтанке скоростных самолетов. Гидрометеонздат, М.

- Кобринский Н. Е. 1942. Методы и приборы для измерения ускорений. Изд. АН СССР.
- Козлов В. Н., Пилус Н. З., Щербатова Л. В. 1965. Некоторые статистические характеристики флуктуаций скорости ветра в тропосфере. Труды ЦАО, вып. 63.
- Колесникова В. К., Монин А. С. 1965. О спектрах колебаний метеорологических полей. Изв. АН СССР, серия физики атмосферы и океана, т. 1, № 7.
- Колмогоров А. Н. 1941. Локальная структура турбулентности в псевжидкой жидкости при очень больших числах Рейнольдса. ДАН СССР, т. 30, № 4.
- Кондратьев К. Я., Борисенков Е. П., Морозкин А. А. 1966. Практическое использование данных метеорологических спутников. Гидрометеонадат, Л.
- Копров Б. М. 1965. Спектры турбулентных пульсаций вертикальной компоненты скорости ветра в пограничном слое в условиях развитой конвекции. Изв. АН СССР, серия физики атмосферы и океана, т. 1, № 11.
- Копров Б. М. и Цванг Л. Р. 1965. Прямые измерения турбулентного потока тепла с борта самолета. Изв. АН СССР, серия физики атмосферы и океана, т. 1, № 6.
- Кочин Н. Е. 1938. Пространственная задача о волнах на поверхности раздела двух масс жидкости разной плотности, вызываемых неровностями дна. Труды ГГО, вып. 28.
- Крамер Г. 1948. Математические методы статистики. Изд. иностр. лит., М.
- Кремер С. И. 1954. Методика измерения микропульсаций скорости ветра и температуры в атмосфере. Труды Геофиз. ин-та АН СССР, № 24 (151).
- Курилова Ю. В. 1960. Некоторые особенности струйных течений над территорией СССР. Труды ЦАО, вып. 33.
- Лайхтман Д. Л. 1947. О волновых движениях на поверхности раздела в атмосфере. Труды ГГО, вып. 2 (64).
- Лайхтман Д. Л. 1961. Физика пограничного слоя атмосферы. Гидрометеонадат, Л.
- Лайхтман Д. Л., Альтер-Залик Ю. Ж. 1966. Об использовании аэрологических данных для определения болячки самолетов в свободной атмосфере. Изв. АН СССР, серия физики атмосферы и океана, т. 2, № 5.
- Лайхтман Д. Л., Вютнер Э. К. 1965. Основные критерии, определяющие интенсивность турбулентности в горном районе. Труды ГГО, вып. 171.
- Ламли Дж. Л. и Пановский Г. А. 1966. Структура атмосферной турбулентности. М., «Мир».
- Ландау Л. Д., Лифшиц Е. М. 1953. Механика сплошных сред. Гостехиздат, М.
- Литвинова В. Д., Силаева В. И. 1960. Результаты исследования вертикальных движений воздуха при полетах на свободных аэростатах. Труды ЦАО, вып. 34.
- Ляпин Е. С. 1948. О турбулентном перемешивании в атмосфере. Метеорология и гидрология, № 5.
- Матвеев Л. Т. 1958. Общий курс метеорологии (основы физики атмосферы). Ч. 1. Изд. ЛКВВИА им. А. Ф. Можайского.
- Матвеев Л. Т. 1961. Условия образования и эволюции облаков. Сб. «Исследование облаков, осадков и грозового электричества». Изд. АН СССР, М.
- Матвеев Л. Т. 1965. Основы общей метеорологии. Физика атмосферы. Гидрометеонадат, Л.
- Мельничук Ю. В. 1964. Некоторые вопросы измерения пульсаций ветра в тропосфере радиолокационным методом. Труды ЦАО, вып. 57.
- Мельничук Ю. В. 1966. Измерение турбулентности в осадках с помощью доплеровской радиолокационной станции. Изв. АН СССР, серия физики атмосферы и океана, т. 2, № 10.
- Минервин В. Е. 1966. Турбулентность в нижнем слое атмосферы и в облаках нижнего яруса. Труды ЦАО, вып. 71.
- Монин А. С. 1956. О макротурбулентном обмене в земной атмосфере. Изв. АН СССР, серия геофиз., № 4.
- Монин А. С. 1958. Структура атмосферной турбулентности. Теория вероятности и ее применение, т. 3, вып. 3.
- Монин А. С. 1962. О спектре турбулентности в температурно неоднородной среде. Изв. АН СССР, серия геофиз., № 3.

- Монин А. С. 1967. О влиянии температурной стратификации среды на турбулентность. Международный коллоквиум по тонкой структуре атмосферы. Изд. «Наука».
- Монин А. С., Обухов А. М. 1954. Основные закономерности турбулентного перемешивания в приземном слое атмосферы. Тр. Геофиз. ин-та АН СССР, № 24.
- Монин А. С., Яглом А. М. 1965 (ч. I), 1967 (ч. II). Статистическая гидромеханика. Ч. I. Изд. «Наука».
- Мусхелиши Ш. А. 1960. О возмущениях, порождаемых одиноким препятствием в поле горизонтальной составляющей скорости. Изв. АН СССР, сер. геофиз., № 10.
- Мусхелиши Ш. А. 1962. Волны препятствия в атмосфере. Гидрометеонадат, Л.
- Обухов А. М. 1941. О распределении энергии в спектре турбулентного потока. Изв. АН СССР, серия геофиз., № 4—5.
- Обухов А. М. 1946. Турбулентность в температурно неоднородной атмосфере. Труды Ин-та теорет. геофизики АН СССР, т. 1.
- Обухов А. М. 1955. К вопросу об оценке успешности альтернативных прогнозов. Изв. АН СССР, серия геофиз., № 4.
- Обухов А. М., Пинус Н. З. и Кречмер С. И. 1952. Результаты экспериментальных исследований микротурбулентности свободной атмосферы. Труды ЦАО, вып. 6.
- Озмидов Р. В. 1964. Некоторые данные о крупномасштабных характеристиках поля горизонтальных компонент скорости в океане. Изв. АН СССР, сер. геофиз., № 11.
- Панчев Ст. 1963. К вопросу о статистической структуре поля скорости ветра в свободной атмосфере. Метеорология и гидрология, № 8.
- Парчевский В. 1937. Планеристу о волновых движениях в атмосфере. Изд. ДОСААФ, М.
- Парчевский В. 1958. Исследование термических движений в атмосфере. Метеорология и гидрология, № 5.
- Пахомов Л. А. 1962. Самолетная аппаратура для измерений вектора ветра. Труды ЦАО, вып. 41.
- Пахомов Л. А. 1967. Характер поля ветра и температуры в окрестности верхней границы волнистых облаков. Труды ЦАО, вып. 79.
- Пахомов Л. А., Пинус Н. З. и Шметер С. М. 1960. Аэрологические исследования изменчивости коэффициента преломления атмосферы для ультракоротких радиоволн. Гидрометеонадат, М.
- Пацеева В. А. 1964. Исследование орографических возмущений атмосферы с помощью уравновешенных шаров-тонов. Труды ЦАО, вып. 59.
- Пекарис Е. М. 1965. Численный способ решения нелинейной задачи обтекания неровности земли воздушным потоком. Труды ММИ, вып. 6.
- Пекарис Е. М. 1966. Обтекание изолированного препятствия воздушным потоком (нелинейная задача). Метеорология и гидрология, № 10.
- Песков Б. Е. 1963. Некоторые особенности образования кучево-лождевых облаков и условия полета вблизи них. Метеорология и гидрология, № 6.
- Пинус Н. З. 1949. Об экспериментальном исследовании вертикальных движений в свободной атмосфере. Труды ЦАО, вып. 5.
- Пинус Н. З. 1962. Особенности вертикальных движений в свободной атмосфере. Труды ЦАО, вып. 6.
- Пинус Н. З. 1955. Об атмосферной турбулентности, вызывающей болтанку самолетов. Метеорология и гидрология, № 2.
- Пинус Н. З. 1956. К вопросу об оценке атмосферной турбулентности по интенсивности болтанки скоростных самолетов. Метеорология и гидрология, № 10.
- Пинус Н. З. 1957. Турбулентность, сопоставимая с размером самолета. Изв. АН СССР, серия геофиз., № 3.
- Пинус Н. З. 1960. Современное состояние вопроса о турбулентности свободной атмосферы, вызывающей болтанку самолетов. Труды ЦАО, вып. 34.
- Пинус Н. З. 1961. Тропапауза и уровень с максимальной скоростью ветра. Метеорология и гидрология, № 3.
- Пинус Н. З. 1962. Структура поля скорости ветра в верхней атмосфере и нижней стратосфере. Метеорология и гидрология, № 4.
- Пинус Н. З. 1963а. Статистические характеристики горизонтальной компоненты скорости ветра на высотах 6—12 км. Изв. АН СССР, серия геофиз., № 1.
- Пинус Н. З. 1963. Вертикальные движения в грозовых облаках. ДАН СССР, т. 150, № 4.
- Пинус Н. З. 1964. Некоторые результаты исследований мезо- и микроструктуры поля ветра на высотах 6—12 км. Труды ЦАО, вып. 53.
- Пинус Н. З. [и др.]. 1964. Основные принципы автоматизации обработки самолетной метеоинформации. Метеорология и гидрология, № 9.
- Пинус Н. З. 1966. Энергетические спектры пульсаций скорости ветра в свободной атмосфере. Метеорология и гидрология, № 4.

- Пинус Н. Э., Литвинова В. Д. 1962. Об интенсивности турбулентности в облаках. Изв. АН СССР, сер. геофиз., № 1.
- Пинус Н. Э., Литвинова В. Д. 1965. О структуре поля скоростей ветра в области струйных течений. Труды ЦАО, вып. 63.
- Пинус Н. Э., Шмелер С. М. 1958. Некоторые особенности турбулентности над горными районами. Труды ЦАО, вып. 24.
- Пинус Н. Э., Шмелер С. М. 1962. Атмосферная турбулентность, влияющая на полет самолетов. Гидрометеонадат, М.
- Пинус Н. Э., Щербакова Л. В. 1966. О структуре поля скорости ветра в термически стратифицированной атмосфере. Изв. АН СССР, серия физики атмосферы и океана, т. 2, вып. 11.
- Праудмен Дж. 1957. Динамическая океанография. Изд. иностр. лит., М.
- Пристли С. Х. Б. 1964. Турбулентный перенос в приземном слое атмосферы. Гидрометеонадат, Л.
- Пчелко И. Г. 1962. Аэронавигационные условия полетов самолетов в верхних слоях тропосферы и нижней стратосферы. Гидрометеонадат.
- Пчелко И. Г. 1966. Турбулентность при ясном небе. Метеорология и гидрология, № 12.
- Решикова А. А. 1960. Некоторые результаты исследования турбулентности на фронтах. Труды ЦАО, вып. 34.
- Решикова А. А. 1964. О турбулентности в струйных течениях при ясном небе. Труды ЦАО, вып. 54.
- Решикова А. А. 1965. Пространственное распределение орографических турбулентных зон на участке Адлер—Новороссийск во время борма. Труды ЦАО, вып. 63.
- Решикова А. А., Силваева В. И., Шмелер С. М. 1964. Турбулентность, вызывающая болтанку самолетов в зоне кучево-дождевых облаков. Труды ЦАО, вып. 53.
- Скацкий В. И. 1957. Электромеханический акселерограф с пьезокварцевым датчиком. Изв. АН СССР, сер. геофиз., № 3.
- Скворцов А. А. 1947. Об испарении и обмене в приземном слое атмосферы. Тр. ин-та энергет. АН Узб. ССР, вып. 1, Ташкент.
- Скворцов А. А. 1951. О тепловой коллекции и обмене в приземном слое атмосферы. Изв. АН СССР, сер. геофиз., № 6.
- Солодовников В. В. 1952. Введение в статистическую динамику систем автоматического управления. Гостехиздат, М.—Л.
- Солодовников В. В. 1954. Основы автоматического регулирования. Машизна.
- Сулаквелидзе Г. К., Бабилашвили А. Ш. и Лапчева В. Ф. 1965. Образование осадков и воздействие на градовые процессы. Гидрометеонадат, Л.
- Сытыва Н. В. 1937. Автономные дондлеровские наминационные приборы. Изд-во «Советское радио».
- Татарский В. И. 1967. Распространение волн в турбулентной атмосфере. М.
- Тверская Н. П. 1964. Турбулентный обмен в облаках вертикального развития. Труды ЛГМИ, вып. 22.
- Трубинов Б. Н. 1958. Пространственная задача обтекания возвышенности неограниченным сверху воздушным потоком. ДАН СССР, т. 129, № 4.
- Трубинов Б. Н. 1964. Исследования воздушных потоков над горными районами с учетом термической неоднородности подстилающей поверхности. Изв. АН СССР, сер. геофиз., № 2.
- Трубинов Б. Н. 1966. О переносе мезомасштабных тропосферных возмущений в верхние слои атмосферы. Труды ЦАО, вып. 69.
- Трубинов Б. Н. 1967. Некоторые вопросы теории свободной (ичейковой) и вынужденной конвекции. Труды ЦАО, вып. 75.
- Фишер Р. А. 1958. Статистические методы для исследователей. Госстатиздат, М.
- Химичи А. Я. 1938. Теория корреляции стационарных случайных процессов. УМН, вып. 5.
- Химичи И. О. 1963. Турбулентность. Физматгиз, М.
- Хргиан А. Х. 1954. Подветренные волны. Природа, № 8.
- Хргиан А. Х. 1958. Вертикальные движения атмосферы и ветер над горной страной. Труды ЦАО, вып. 24.
- Цванг Л. Р. 1962. Измерение турбулентных потоков тепла и спектров температурных пульсаций. Труды ИФА АН СССР, вып. 4.
- Цитович Т. А. 1939. К вопросу формирования подфронтальной части облачной системы теплого фронта. Труды ЦАО, вып. 30.
- Чернов Ю. В. 1965. Исследование восходящих потоков с помощью планетров. Труды ЦАО, вып. 63.
- Черныш В. И. 1965. Самолетный цифровой запоминающий метеорологический информации. Труды ЦАО, вып. 63.
- Чурминова М. П. 1950. О турбулентности в некоторые дни с кучевыми облаками. Труды ГГО, вып. 24 (86).

- Чурникова М. П. 1955. Некоторые характеристики турбулентности в дни со слоистой облачностью. Труды ГГО, вып. 54.
- Шинский Н. С. 1964. Облака, осадки, грозное электричество. Гидрометиздат, Л.
- Шметер С. М. 1957. Движение шар-зонда в ускоренном воздушном потоке. Труды ЦАО, вып. 22.
- Шметер С. М. 1957. О точности вычисления числа Ричардсона по данным радиозондовых наблюдений. Труды ЦАО, вып. 22.
- Шметер С. М. 1978. Об обтекании горных препятствий воздушными потоками. Труды ЦАО, вып. 24.
- Шметер С. М. 1960а. Некоторые характеристики турбулентности и поля температуры над горами. Метеорология и гидрология, № 3.
- Шметер С. М. 1960б. Турбулентность в облаках верхней тропосферы. Труды ЦАО, вып. 34.
- Шметер С. М. 1962. Поле ветра в окрестностях кучево-дождевых облаков. Метеорология и гидрология, № 11.
- Шметер С. М. 1963. Некоторые особенности структуры полей метеорологических элементов в зоне кучево-дождевых облаков. Труды ВГМС, т. 7.
- Шметер С. М. 1964. Стадии развития кучево-дождевых облаков и особенности распределения метеорологических параметров в их зоне. Труды ЦАО, вып. 53.
- Шметер С. М. 1966. Взаимодействие кучево-дождевых облаков с полем ветра в приземной атмосфере. Изв. АН СССР, сер. физики атмосферы и океана, т. 2, № 11.
- Шметер С. М. и Шур Г. Н. 1957. Электрометеорограф для самолетных исследований. Труды ЦАО, вып. 22.
- Шметер С. М., Спасаева В. И. 1966. Вертикальные потоки внутри кучево-дождевых облаков. Метеорология и гидрология, № 10.
- Шметер С. М., Шиндман В. А. 1966. Влияние турбулентности на вертикальный профиль ветра в облаках. Труды ЦАО, вып. 71.
- Шиндман В. А. 1961. О стационарных волнах в области тропопавза. Труды ГГО, вып. 107.
- Шур Г. Н. 1957. Определение вертикальных скоростей турбулентных порывов ветра при самолетных исследованиях. Труды ЦАО, вып. 22.
- Шур Г. Н. 1958. Метод и приборы для получения некоторых характеристик турбулентности атмосферы с самолета. Труды ЦАО, вып. 24.
- Шур Г. Н. 1959. Приборы для исследования спектра атмосферной турбулентности методом гармонического анализа с использованием магнитной памяти. Труды ЦАО, вып. 31.
- Шур Г. Н. 1962. Экспериментальные исследования энергетического спектра атмосферной турбулентности. Труды ЦАО, вып. 43.
- Шур Г. Н. 1964. Спектральная структура турбулентности по данным самолетных исследований. Труды ЦАО, вып. 53.
- Шур Г. Н. 1967. Спектр турбулентности устойчиво стратифицированной атмосферы. Труды ЦАО, вып. 78.
- Юдени М. И. 1946. Вопросы теории турбулентности и структуры ветра с приложением к задаче о колебаниях самолета. Труды НИИ ГГО, серия 1, вып. 35.
- Юргенсон А. П. 1960. Исследование структуры турбулентных движений, вызывающих болтанку современных самолетов. Метеорология и гидрология, № 10.
- Ackerman V. 1958. Turbulence around tropical cumuli. J. Met., vol. 5, No. 1.
- Anderson C. E. 1962. Observational evidence on the kinematics of growing cumulus and thunderstorm clouds. Trans. N. Y. Acad. Sci., ser. II, vol. 24, 8.
- Ball F. K. 1961. Viscous dissipation in the atmosphere. J. Met., vol. 18.
- Bannon J. K. 1951a. Meteorological aspects of turbulence affecting aircraft at high altitude. Prof. Notes of Met. Off., vol. 104, (4G-60).
- Bannon J. K. 1951b. Severe turbulence encountered by aircraft near jet-streams. Met. Mag., vol. 80, (3K-163).
- Bannon J. K. 1952. Weather systems associated with some occasions of severe turbulence at high altitude. Met. Mag., vol. 81.
- Batchelor J. K. 1954. Heat convection and buoyancy effects in fluids. Q. J. Roy. Met. Soc., vol. 80, No. 345.
- Berenger M. et Gerbier N. 1956. Les mouvements ondulatoires à St-Auban-sur-Durance (Basses-Alpes), première campagne d'études et de mesures. Monogr. 4 de la Met. Nat.
- Berenger M. et Heissat J. 1959. Contribution à l'étude statistique et météorologique de la turbulence. Monogr. 17 de la Meteor. Nationale.
- Berger F. B. 1959. Doppler radar navigation. Proc. Nat. Electr. Conf., vol. 14.
- Bindon H. H. 1951. Clear-air gusts in the upper troposphere over eastern Canada. Weather, 6 (3K-165).

- Blackman R. B. and Tukey J. W. 1958. The measurement of power spectra. Dover Publications Inc.
- Belgiano R. 1959. Turbulent spectra in a stably stratified atmosphere. *J. Geophys. Res.*, vol. 64.
- Belgiano R. 1962. Structure of turbulence in stratified media. *J. Geophys. Res.*, vol. 67, No. 8.
- Bovsheverov V. M., Gurvich A. S., Monin A. S. and Tsvang L. R. 1960. The direct measurements of the turbulent heat flux by means of an ultrasonic anemometer. Publ. IAMP, 12/6.
- Briggs B. A. 1961. Severe clear-air turbulence near the British Isles. *Met. Mag.*, vol. 90.
- Briggs J. and Roach W. T. 1963. Aircraft observations near jet-streams. *Q. J. Roy. Met. Soc.*, vol. 89.
- Brunledge K. C. and Clodman J. L. 1962. Model cross-sections across the jet-streams. *J. Appl. Met.*, vol. 3.
- Brunt D. 1937. Natural and artificial clouds. *Q. J. Roy. Met. Soc.*, vol. 63.
- Burns A. 1964. Power spectra of low level atmospheric turbulence measured from an aircraft. Ministry of Aviation, London, C. P. 7:3.
- Byers H. R. 1952. An example of a flight through thunderstorm updraft. *Bull. Am. Met. Soc.*, vol. 33.
- Byers H. R. and Braham R. R. 1948. Thunderstorm structure and circulation. *J. Met.*, vol. 3.
- Byers H. R. and Braham R. R. 1949. Thunderstorm. Wash.
- Chambers E. 1955. Clear-air turbulence and civil jet operations. *J. Roy. Aeron. Soc.*, vol. 59.
- Chandrasekhar S. 1953. The instability of a layer of fluid heated below and subject to Coriolis forces. I. *Proc. Roy. Soc. Ser. A*, vol. 217.
- Chandrasekhar S. 1955. The instability of a layer of fluid heated below and subject to Coriolis forces. II. *Proc. Roy. Soc. Ser. A*, vol. 231.
- Clem Le Roy H. 1957. Clear-air turbulence from 25 000 to 45 000 feet over the United States. Techn. Rept Air Weather Serv., 105-147.
- Clodman J. 1953. High level turbulence. *Met. Branch Dept of Transport, Toronto, TEC 100, CIR 2332.*
- Collis R. T. 1964. Lidar detection of CAT. *Astronautics and Aeronautics*, vol. 2, No. 12.
- Colson D. 1963. Analysis of clear-air turbulence for March 1962. *Monthly Wea Rev.*, vol. 91.
- Colson D. and Panofsky H. A. 1965. An index of clear-air turbulence. *Q. J. Roy. Met. Soc.*, vol. 91, No. 390.
- Cone C. D. 1962. Thermal soaring of birds. *American Scientist*, vol. 50.
- Cooke T. H. 1962. A smoke-trail technique for measuring wind (Plate III). *Q. J. Roy. Met. Soc.*, vol. 88, No. 375.
- Corby G. A. 1954. The airflow over mountain. *Q. J. Roy. Met. Soc.*, vol. 80, No. 346.
- Corby G. A. and Wallington C. E. 1956. Airflow over mountains: the lee-wave amplitude. *Q. J. Roy. Met. Soc.*, vol. 82.
- Crossly A. F. 1961. Ice accretion and turbulence on North Atlantic air routes. *Q. J. Roy. Met. Soc.*, vol. 87, No. 371.
- Dol K. 1962. Formation and movement of precipitation clouds. *Geophys. Mag.*, 31, 2.
- Ellison T. K. and Turner J. S. 1960. Mixing of dense fluid in a turbulent pipe flow, parts 1-2. *J. Fluid Mech.*, vol. 8, No. 4.
- Endlich R. M. and McLean C. S. 1957. The structure of the jet-streams. *J. Met.*, vol. 14.
- Endlich R. M. 1963. The detailed structure of the atmosphere in regions of clear-air turbulence. Final Rept, Contr. CWB-15424, Stanford Res. Inst., Cal.
- Endlich R. M. and Mancuso R. L. 1965. Objective analysis and forecasting of clear-air turbulence. Final Rept, Contr. CWB-10871, Stanford Res. Inst., Cal.
- Endlich R. M. and McLean C. S. 1965. Jet-stream structure over the central United States determined from aircraft observations. *J. Appl. Met.*, 4.
- Folta H. P. 1967. Prediction of clear-air turbulence. *Atm. Sci. Paper*, 106, Colorado State Univ.
- Förchtgott J. 1949. Wave streaming in the lee of mountain ridges. *Bull. Met. Czech.*, 3, Prague.
- Foster D. S. 1958. Thunderstorm gust compared with computed downdraft speeds. *Monthly Wea Rev.*, vol. 89.
- Frenzen P. 1962. On the origin of certain symmetrical patterns of atmospheric convection. *Tellus*, vol. 14.
- Fujita T. 1960. Mesometeorological study of pressure and wind fields beneath isolated radar echoes. *Proc. VIII Wea Radar Conf.*, Wash.
- Fujita T. 1963. Analytical mesometeorology: a review. *Met. Monogr.*, 5.
- Fujita T. and Arnold D. 1963. Development of a cumulonimbus under the influence of strong vertical shear. *Proc. X Wea Radar Conf.*, Wash.
- Georgii W. 1959. *Meteorologie und Navigation des Segelfluges*. Braunschweig.

- Georgii W. 1960. Physik des Jet-Stream. München.
- Georgii W. 1961. Scgelling in hohen Wellen. Flug-Revue, 5.
- Gerbler N. and Berenger M. 1961. Experimental studies of lee waves in the French Alps. Q. J. Roy. Met. Soc., vol. 87, 371.
- Gossard E. and Munk W. 1964. On gravity waves in the atmosphere. J. Met., vol. 11, No. 4.
- Hamel G. 1916. Spiralförmige Bewegungen zäher Flüssigkeiten Jahresber. d. deutsch. mathem. Ver., 25, 34.
- Haman K. 1962. On some causes of clear-air turbulence. Acta Geophys. Polonica, X, No. 4.
- Haurwitz B. 1947. Internal waves in the atmosphere and convective patterns. Ann. N. Y. Acad. Sci., vol. 48.
- Haurwitz B. 1951. The perturbation equations in meteorology. Compendium Met., Boston.
- Heisenberg W. 1946. Zur statistischen Theorie der Turbulenz. Z. Phys., Bd 124, H. 7/12.
- Hesse W. 1961. Handbuch der Aerologie. Leipzig.
- Hislop C. S. 1950. Gusts from a clear sky. Aircraft, Melbourne, vol. 29.
- Hislop C. S. 1951. Clear-air turbulence over Europe. J. Roy. Aeron. Soc., vol. 55.
- Holahan J. 1957. Doppler progress sets first pace for hardware development. Av. Age, October.
- Holmboe J. and Killeforth H. 1957. Investigations of mountain lee waves and the air flow over the Sierra Nevada. Final Rept. Contr. AF 19 (604)—728.
- Howells J. D. 1940. An approximate equation for the spectrum of a conserved scalar quantity in turbulent fluid. J. Fluid Mech., 9, No. 5.
- Hyde E. A. 1954. Air turbulence at high altitudes. A report by short Bros. and Harand test pilots, London.
- James D. G. 1953. Fluctuations of temperature below cumulus clouds. Q. J. Roy. Met. Soc., vol. 79, No. 371.
- Jones L. F. 1954. Five flights through a thunderstorm belt. Q. J. Roy. Met. Soc., vol. 80, No. 345.
- Jones D. C. E. 1954. Exceptionally severe clear-air turbulence and other phenomena on April 14. Met. Mag., vol. 84.
- Junge Chr. 1938. Turbulenzmessungen in den höheren Atmosphärenschichten. Ann. d. Hydrogr. und Marit. Met., LXVI, H. III.
- Kao S. K. and Woods H. D. 1964. Energy spectra of meso-scale turbulence along and across the jet-stream. J. Atm. Sci., vol. 21, No. 5.
- Kao S. K. and Sizoo A. H. 1966. Analysis of clear-air turbulence near the jet-stream. J. Geophys. Res., vol. 71, No. 16.
- Kao S. K. and Sands E. E. 1966. Energy spectra, mean and eddy kinetic energies of the atmosphere between surface and 30 kilometers. J. Geophys. Res., vol. 71, No. 22.
- King L. W. 1914. On the convection of heat from small cylinders in a stream of fluids. Phil. Trans. Roy. Soc., Ser. A, 214.
- Kuettner J. 1952. Note on high level turbulence encountered by a glider. Airforce Surveys in Geophy. 29.
- Kuettner J. 1958. The rotor flow in the lee of mountains. Schweiz. Aero-Revue, 33, Bern.
- Kuettner J. 1959. The band structure of the atmosphere. Tellus, vol. 11, No. 3.
- Lottau H. and Davidson E. 1957. Exploring the atmosphere's first mile. N. Y.
- Levine J. 1959. Spherical vortex theory of bubble-like motion in cumulus clouds. J. Met., vol. 16.
- Lhermitte R. M. 1962. Note of wind variability with Doppler radar. J. Atm. Sci., vol. 19, 243—246.
- Lira G. 1940. Ueber den Einfluss von Bodenerhebungen auf die Strömung einer stabilgeschichteten Atmosphäre. Beitr. Phys. frei. Atmos., Bd 20.
- Ludlam F. H. and Scorer R. S. 1953. Bubble theory of penetrative convection. Q. J. Roy. Met. Soc., vol. 79, No. 339.
- Ludlam F. H. 1962. Severe local storms: a review. Met. Monogr., vol. 5, 27.
- Ludlam F. H. 1963. Airflow in cumulonimbus. Atm. Turb. Relate Aircraft, London.
- Lumley J. L. 1964. The spectrum of nearly inertial turbulence in a stably stratified fluid. J. Atm. Sci., vol. 21, No. 1.
- Lumley J. L. and Pain E. R. 1966. One-dimensional spectra derived from an airborne hot-wire anemometer. Q. J. Roy. Met. Soc., vol. 92, No. 393.
- Mal S. 1930. Forms of stratified clouds. Beitr. Phys. frei. Atmos., Bd. 17.
- Malkus J. K. and Scorer R. S. 1955. The erosion of cumulus towers. J. Met., vol. 12.
- Malkus J. S. and Witt G. 1959. The evolution of a convective element; a numerical calculation. The Atmosphere and the Ocean in Motion, Sci. Contribut. to the Rossby Mem.
- Malkus J. S. and Riehl H. 1964. Cloud structure and distributions over the tropical Pacific Ocean. Berkeley.
- Mantila H. 1963. The structure of winds of the upper troposphere at meso-scale. J. Atm. Sci., vol. 20, 94.

- Naito K. 1960. The airflow over mountains. Tech. Note, 34, WMO, Geneva.
- Naito K. 1966. Internal gravity-shear waves in the troposphere. *Canadian J. Phys.*, vol. 44, Toronto.
- Newton Ch. W. and Newton H. R. 1959. Dynamical interaction between large convective clouds and environment with vertical shear. *J. Met.*, 16, vol. 5, 27.
- Notess C. B. 1957. A study of the nature of atmospheric turbulence based upon flight measurements of the gust velocity components. Cornell Aerolab. Rep. VC 901-F-1.
- Palm E. 1958. Two-dimensional and three-dimensional waves. *Geophys. Publ.*, Norv., XX, No. 3.
- Panofsky H. A. and McCormic R. A. 1954. Properties of spectra of atmospheric turbulence at 100 meters. *Q. J. Roy. Met. Soc.*, vol. 80, No. 346.
- Pallow A. and Southwell R. V. 1940. On maintained convective motion in a fluid heated from below. *Proc. Roy. Soc., A*, vol. 176, No. 906.
- Phillips O. M. 1965. On the Bolgiano and Lumley-Shur theories of the buoyancy subrange. *Fine-Scale Structure of the Atmosphere, Colloquium, Moscow.*
- Phillips O. M. 1967. The generation of clear air turbulence by the degradation of internal waves. (Перевод в сб. «Атмосферная турбулентность и распространение радиоволн». Труды Международного colloквиума. Изд. «Наука».)
- Pilsbury R. K. 1955. A preliminary analysis of standing-wave reports at Northolt during the winter of 1953-1954. *Met. Mag.*, 84.
- Press H., Schindler M. H. and Tompson J. K. 1953. Summary of pilot reports of clear-air turbulence at altitudes above 10000 feet. *Res. Met. Nat. Adv. Comm. Aeron.*, RMI, 52, L 36.
- Press H., Meadows M. T. and Hadlock J. 1958. A reevaluation of data on atmospheric turbulence and airplane gust loads for application in spectral calculations. NASA Report 1272.
- Priestley C. H. B. 1954. Convection from a large horizontal surface. *Austral. J. Phys.*, vol. 7, No. 1.
- Priestley C. H. B. 1955. Free and forced convection in the atmosphere near the ground. *Q. J. Roy. Met. Soc.*, vol. 81, No. 348.
- Queney P. 1936. Recherches relatives à l'influence du relief sur les éléments météorologiques. *La Météorologie*, 3 ser., N 4.
- Queney P. 1947. Theory of perturbations in stratified currents with application to airflow over mountain barriers. *Univ. Chicago, Dept. Met., Misc. Rept.*, 23.
- Queney P. 1941. Ondes de gravité produites dans un courant aérien par une petite chaîne de montagnes. *C. R. Acad. Sci.*
- Reiter E. R. 1961. *Meteorologie der Strahlströme (Jet-Streams)*. Vienna, Springer-Verlag.
- Reiter E. R. and Burns A. 1965. Atmospheric structure and clear-air turbulence. *International Colloquium on Fine-Scale Structure of Atmosphere, Moscow.*
- Reiter E. R. and Burns A. 1966. The structure of clear-air turbulence derived from "Topcat" aircraft measurements. *J. Atm. Sci.*, vol. 23, No. 2.
- Richardson L. F. 1920. The supply of energy from and to atmospheric eddies. *Proc. Roy. Soc., Ser. A*, vol. 97.
- Ridland D. M. 1964. The measured response of an aircraft to the vertical velocity component of atmospheric turbulence. *Aeronautical Res. Council, C. P.*, 708.
- Sasaki G. 1958. A theory and analysis of clear-air turbulence. *Texas, Agric. and Mech. College, Dept. of Oceanogr. and Met. Sci., Rept. I, Contr. AF 19 (604)-1965.*
- Scorer R. S. 1949. Theory of waves in the lee of mountains. *Q. J. Roy. Met. Soc.*, vol. 75.
- Scorer R. S. 1951. Clear-air turbulence over Europe. *Weather*, 6 (3K-177).
- Scorer R. S. 1953. Theory of airflow over mountains. II: the flow over a ridge. *Q. J. Roy. Met. Soc.*, vol. 79.
- Scorer R. S. 1956. Air flow over an isolated hill. *Q. J. Roy. Met. Soc.*, vol. 82.
- Scorer R. S. 1958. Experiments with convection bubbles. *Aero-Revue*, vol. 31, No. 8.
- Scorer R. S. and Ronne C. 1956. Experiment with convection bubbles. *Weather*, 11.
- Scorer R. S. 1957. Experiment on convection of isolated masses of buoyant fluid. *J. Fluid Mech.*, vol. 2.
- Störmer C. 1948. Mother-of-pearls clouds. *Weather*, No. 3.
- Sekera Z. 1948. Helmholtz waves in a linear temperature field with vertical wind shear. *J. Met.*, vol. 5, No. 3.
- Smith F. B. 1961. An analysis of vertical wind-fluctuations at heights between 500 and 5000 feet. *Q. J. Roy. Met. Soc.*, vol. 87, No. 372.
- Steiner R., Rhyne R. 1962. Some measured characteristics of severe storm turbulence. *National Sev. Storm Project, Report N 10.*

- Steiner R., Rhyne R. 1964. Atmospheric turbulence and airplane response in convective-type clouds. *Journ. Aircraft*, vol. 1, No. 1.
- Steiner R. A. 1965. Review of NASA high-altitude clear-air turbulence Sampling Programs. AIAA paper, 65-13.
- Sugimoto J. 1956. Effect of turbulence on aircraft operations. *J. Met. Res.*, Tokyo, 8.
- Taylor C. B. 1938. The spectrum of turbulence. *Proc. Roy. Soc. A164*, 476.
- Taylor J. 1965. Manual on aircraft loads. Pergamon Press.
- Tchen C. M. 1953. On the spectrum of energy in turbulent shear flow. *J. Res. Nat. Bur. Stand.*, vol. 50, No. 1.
- Tchen C. M. 1954. Transport processes as foundation of the Heisenberg and Obukhoff theories of turbulence. *Phys. Rev.*, vol. 93, No. 1.
- Van der Hoven J. 1957. Power spectrum of horizontal wind speed in the frequency range from 0.0007 to 900 cycles per hour. *J. Met.*, vol. 14, 2.
- Wan Chang Chin. 1960. The wind and temperature spectra of the upper troposphere and lower stratosphere. *J. Met.*, vol. 17, No. 1.
- Watson N. R. 1967. Some measurements of turbulence in altocumulus clouds. *Q. J. Roy. Met. Soc.*, vol. 93, No. 396, 227-237.
- Woodward B. 1959. The motion in and around isolated thermals. *Q. J. Roy. Met. Soc.*, vol. 85, No. 364.
- Würtele M. 1957. The three-dimensional lee wave. *Beitr. d. Phys. freie Atmosph.*, Bd 29.
- Yates A. H. 1953. Atmospheric convection; the structure of thermals below cloud base. *Quart. Journ. of Roy. Met. Soc.*, vol. 79, No. 341.
- Zierep J. 1957. Neue Forschungsergebnisse aus dem Gebiet der atmosphärischen Hinderniswellen. *Beitr. d. Phys. freie Atm.*, 29.
- Zierep J. 1959. Zur Theorie der Zellularkonvektion. III. *Beitr. d. Phys. freie Atm.*, Bd 32, H. 1/2.
- Zierep J. 1960. Zur Theorie der Zellularkonvektion. IV. *Beitr. d. Phys. freie Atm.*, Bd 32, H. 3/4.